Universitat Internacional de Catalunya
Facultat de Medicina i Ciències de la Salut
Departament de Ciències Bàsiques - Bioenginyeria

Tesis doctoral

A BIOENGINEERING APPROACH FOR CORNEAL ENDOTHELIAL REGENERATION

BEGOÑA MARIA BOSCH CANALS

A BIOENGINEERING APPROACH FOR CORNEAL ENDOTHELIAL REGENERATION

BEGOÑA MARIA BOSCH CANALS

PhD Thesis

Thesis supervisors: Dr Román Pérez, Dr Javier Gil and Dr Alfonso Sabater

Bioengineering Institute of Technology

Universitat Internacional de Catalunya

Barcelona, 2019

Abstract

Nowadays, there are approximately 10 million people worldwide with visual impairment due to corneal diseases. Currently, the main therapeutic solution is the transplant of a donor's cornea. The great majority of transplants is due to some failure in the inner layer of the cornea, which is called the corneal endothelium and this is mainly related with the inability of this layer to regenerate *in vivo*. However, transplants present several limitations such as the low number of healthy donors or immunological rejection by the patient.

In order to overcome these problems, several researchers have focused in culturing corneal endothelial cells (CEC) to subsequently replace non-functional CEC. However, cell therapy is still very recent and still presents a series of drawbacks. For instance, using animal CEC or cells from other patients has shown to lead into immunological rejection. In order to avoid this, it is possible to use stem cells from the same patient, which have the ability to differentiate into many cell types, including the corneal endothelium. Currently, the stem cells used to regenerate CEC are mainly pluripotent stem cells, either embryonic stem cells (ESC) or induced pluripotent stem cells (iPSC), which are derived from adult cells. Despite their great potential for treating diseases, these types of stem cells present major limitations such as the risk of teratoma formation. In addition, they present other disadvantages such as ethical problems associated with the use of ESCs, safety problems related to iPSC since they requires the use of virus for their production hence limiting its clinical application.

For this reason, and in order to solve the current problems in the regeneration of corneal endothelium, this thesis project uses dental pulp stem cells (DPSC) for the formation of CEC. DPSC are an accessible source derived from the same patient, avoiding possible future problems of rejection. In addition, the use of DPSC avoids the ethical and security problems associated with ESC and iPSC. Furthermore, DPSC and CEC have the same embryological origin, as they both arise from neural crest stem cells. In fact, DPSC express neural crest stem cells markers, which facilitates their differentiation into neural crest stem cells (NCSC), which is an intermediate step for the formation of CEC. Therefore, this thesis project uses a two-step protocol, where DPSC are differentiated into NCSC and, subsequently, NCSC are derived into CEC.

Because the use of cell therapies alone may present limited cell viability once it is injected, the field of tissue engineering is a new discipline that has appeared to overcome this limitation. Tissue engineering combines the use of cells, biomaterials and biological molecules. It has been demonstrated that the use of different topographies in cell culture modulates cell behavior, and may have an effect on their functionality, cell distribution or cell size. Therefore, this thesis project applies tissue engineering as another strategy for the generation of functional CEC with its characteristic phenotype and morphology. For doing this, we have mimicked the natural CEC environment by cultivating the cells on substrates with different curvatures, composition or topographies that are able to mimic those of the human eye.

In conclusion, this thesis project proposes the use of bioengineering, by differentiating CEC from stem cells derived from the patient and the use of biomaterials with different topographies and curvatures, for the regeneration of corneal endothelium.

Resumen

Actualmente, en el mundo hay aproximadamente 10 millones de personas con discapacidad visual debido a enfermedades corneales. La única solución terapéutica es el trasplante de córnea de un donante. La gran mayoría de trasplantes es debido a algún fallo en la capa más interna de la córnea, el endotelio corneal, ya que es la única capa de la córnea que no tiene la capacidad de regenerarse *in vivo*. Sin embargo, existen varios problemas asociados a este trasplante como el escaso número de donantes sanos o el rechazo inmunológico por parte del paciente.

Para intentar sustituir el trasplante, diversos investigadores han conseguido cultivar células de endotelio corneal (CEC) para reemplazar posteriormente las células endoteliales no-funcionales de córnea. No obstante, la terapia celular es todavía muy reciente y sigue presentando una serie de inconvenientes. Por ejemplo, muchos estudios realizados cultivan CEC de animales o utilizan células de otros pacientes que pueden llevar a rechazo inmunológico. Para evitarlo, algunos estudios utilizan células madre del propio paciente, que son capaces de diferenciarse a muchos tipos celulares, entre ellos, el endotelio corneal. Actualmente, las células madre utilizadas para formar células de endotelio corneal son principalmente las células madre pluripotentes, tanto de origen embrionario (ESC) como inducidas a partir de células adultas (iPSC). A pesar de los grandes avances, estos tipos de células madre presentan grandes limitaciones que son principalmente el riesgo de formación de teratomas y la probabilidad de rechazo inmunológico. Además, presentan otros inconvenientes como los problemas éticos que conlleva el uso de las ESC, los problemas de seguridad de las iPSC debido a que su obtención requiere el uso de virus y supone un problema para su aplicación clínica.

Por este motivo, y con el objetivo de intentar solventar los problemas actuales en la regeneración de endotelio corneal, este proyecto de tesis utiliza células madre de la pulpa dental (DPSC) para la formación de CEC. Las DPSC son fáciles de extraer y, al provenir del propio paciente, no presenta problemas de rechazo. Además, la utilización de las DPSC evita los problemas éticos y de seguridad de asociados a las ESC y las iPSC. Asimismo, las DPSC y las CEC ambas tienen el mismo origen y provienen de células de la cresta neural (NCSC). De hecho, las DPSC expresan marcadores de cresta neural, lo que facilita la diferenciación de

éstas a células de la cresta neural, que es un paso intermedio hasta la formación de CEC. Por ello, este proyecto de tesis se basa en un protocolo de dos etapas donde las DPSC son diferenciadas a NCSC y, posteriormente, las NCSC se diferencian a CEC.

Debido a las limitaciones que presentan las terapias celulares respecto a la viabilidad celular tras el trasplante, el mundo de la ingeniería de tejidos es una nueva disciplina que permite solucionar estas limitaciones. La ingeniería de tejidos combina el uso de células, biomateriales y moléculas biológicas. Se ha demostrado que el uso de diferentes topografías en el cultivo de células puede modular su comportamiento, lo que puede afectar en su funcionalidad, su distribución o su tamaño. Por ello, este proyecto de tesis aplica la ingeniería de tejido como otra estrategia para conseguir CEC funcionales con el fenotipo y la morfología adecuadas. Para ello, se ha intentado mimetizar el hábitat natural en el que se encuentran las células humanas. Esto se ha logrado cultivando las células sobre unos sustratos con diferentes curvaturas o topografías que mimeticen el ojo humano.

En conclusión, este proyecto de tesis propone el uso de la bioingeniería, mediante la diferenciación a CEC desde células madre del propio paciente y el uso de biomateriales con diferentes topografías y curvaturas, para la regeneración de endotelio corneal.

Thesis objectives

The aim of this thesis is to develop a strategy that may be used as a combination of a cell-based therapy using dental pulp stem cells (DPSC) with biomaterials for corneal endothelium regeneration. For this purpose, the objectives are divided into three main objectives:

1. To obtain Neural crest stem cells (NCSC) from DPSC as progenitor cells using different strategies
2. To find strategies to differentiate the produced NCSC into corneal endothelial cells (CEC)
3. To use biomaterials to mimic the substrates in which native CEC are found to improve their behavior and functionality.

The specific objectives are:

1. To obtain NCSC from DPSC as progenitor cells using different strategies
   1.1. To produce induced pluripotent stem cells (iPSC) from DPSC, as the gold standard for the production of NCSC are iPSC, and to characterize its genetic analysis.
   1.2. To differentiate DPSC and iPSC derived from DPSC directly into NCSC
   1.3. To find optimum conditions for the production of neurospheres in suspension for the formation of NCSC.
   1.4. To compare the differentiation process from DPSC to NCSC using adherent and suspension methods.
   1.5. To produce embryoid bodies as a pluripotent mimicking strategy to obtain NCSC.
2. To find strategies to differentiate the produced NCSC into CEC
   2.1. To use the direct differentiation of DPSC into CEC based on their common origin.
   2.2. To produce CEC from NCSC derived from DPSC
   2.3. To compare the use of different substrates for CEC maintenance
   2.4. To verify the optimum culture medium for the culture of CEC
3. To use biomaterials to mimic the substrates in which native CEC are found to improve their behavior and functionality.
   3.1. To find optimum conditions for the production of a clinically relevant implantable corneal endothelium mimicking film.

3.2. To produce and find the proper conditions for the production of clinically relevant platforms that mimic native environments for the successfully maintenance and differentiation of CEC phenotype mainly combining different topographies and curvatures.

3.3. To analyze cell morphology based on the different types of substrates of fibroblast like cells cultured on the different substrates

3.4. To visualize cell morphology of CEC cultured on substrates with different topographies and curvatures.

3.5. To analyze gene expression of the main CEC related markers when cultured on the different substrates.

Publications and conferences

Bosch BM, Gil FJ, Sabater AL, Perez RA. Corneal endothelial regeneration using biomimetic substrates (in preparation)

Fraioli R, Neubauer S, Rechenmacher F, **Bosch BM**, Dashnyam K, Kim J-H, et al. Control of stem cell response and bone growth on biomaterials by fully non-peptidic integrin selective ligands. Biomater Sci. 2019 Feb

Núñez-Toldrà R, Montori S, **Bosch B**, Hupa L, Atari M, Miettinen S. S53P4 Bioactive Glass inorganic ions for Vascularized Bone Tissue Engineering by DPPSC Co-cultures. Tissue Eng Part A. 2019 Jan 5

Bosch BM, Montori S, Sabater AL, Atari M. Dental pulp pluripotent-like stem cells as a new cell source for regenerative medicine in corneal endothelium therapy. *The Biology of Regenerative Medicine 2017,* 25-27th April 2017, Cambridge, UK (Poster presentation)

Table of contents

Chapter I: INTRODUCTION

Chapter I: Introduction

1. 1. Introduction

Throughout the years, science and technology have evolved at fascinating speeds that have allowed us having more commodities and technologies involved in our daily lives. Furthermore, these technologies, especially those linked to medical systems, have allowed us to increase, not only the life expectancy but also has allowed us improving the quality of life. The increase in the life expectancy has also allowed discovering new diseases that were unknown until very recently. For instance, cancer has been recently diagnosed as the cause of death of thousands of people, although up to now, its causes and possible treatments were unknown. Nevertheless, the combination of novel technologies and scientists have allowed fascinating discoveries that are saving the lives of many people.

Together with the appearance of new diseases, our tissues are increasing as well as the time in which they need to be functional. This means that tissues, with increasing age, reduce their properties, such as stiffness, elasticity or composition among others. The loss of their main properties are inherently bound with a loss of function. For instance, blood vessels that have lower elasticity are unable to properly pump the blood and hence need assistance in order to distribute the oxygen throughout the body. This generally happens with all our tissues as age is increased.

One of our main organ that is of great importance and provides us with one of the five senses is the eye, which provides the vision. The eye is composed of several parts and each one of them is in charge of a specific function in the perception of vision. It is a very complex organ, with very defined structure and architectures, presenting blood vessels, nerves and specialized cells. Similar to the blood vessels, the loss of the elasticity and the fact that some cells have very limited replicating capacity, reduce the self-healing capacity of the eye. For this purpose, ophthalmology is the area that is related to studying the eye and how to maintain its proper function. Nevertheless, in many situations, ophthalmology cannot prevent certain failures and diseases and for this reason, there is a need to produce materials that are able to regenerate or substitute the damaged parts. For this purpose, the appearance of bioengineering, which is able to replace a damaged tissue or stimulate the regeneration of the damaged tissue, is considered a very promising strategy to allow people that have suffered from certain eyes conditions, to improve their quality of vision.

1. 2. Eye structure

The eye is the organ responsible for the vision and consists of three layers: the outer, the middle and the inner, as shown in Figure 1.1 [1]. The outer layer contains the cornea and the sclera, which are responsible for the shape as well as supporting the ocular globe. The cornea consists of an anterior curved transparent layer that permits the light to enter inside the eye whereas the sclera is a posterior opaque sphere that maintains the ocular shape and offers resistance to any internal or external stimuli. Following the external layer is the middle layer mainly composed of the uvea, which consists of three areas: choroid, iris and ciliary bodies [1]. The choroid is the vascular part on the eye and provides nutrients and oxygen into the inner layer. The iris is a circular structure that gives the color of the eye and is responsible of the aperture of the pupil, controlling the amount of light that enters inside the eye. Finally, the ciliary bodies are composed of ciliary muscles, which continuously change the shape of the lens [1]. Followed by the middle layer is the final inner layer, where the retina is found, which is in the posterior part of the eye. This layer contains nerve cells and sensitive cells, named photoreceptors, which detects the light and colors and transmits the light signals into the brain by the optic nerve. The retina contains a small area known as macula that contains tightly packed photoreceptors, responsible of making highly detailed images. The eye is filled with transparent fluid divided in two sections: the anterior and the posterior segment. The anterior segment is composed of the aqueous humor and consists of the anterior chamber, which goes from the cornea to the iris, and the posterior chamber, which goes from the iris to the lens. The posterior segment goes from the lens to the retina and contains the vitreous humor. These segments present two main functions: to maintain the shape thanks to the generated pressure from the fluids and to transmit the light to the optic nerve [1].

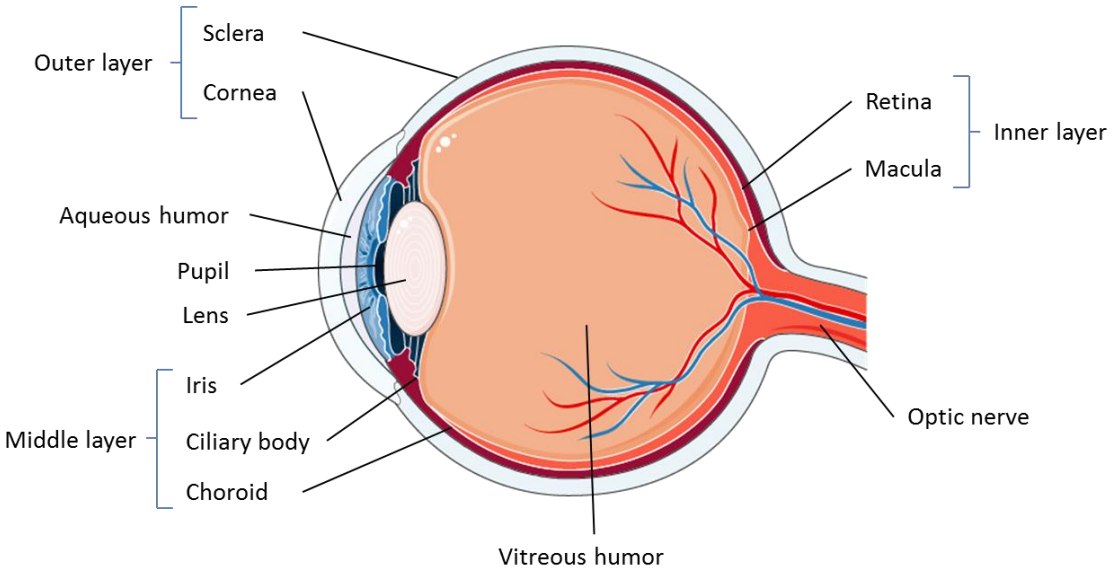

Figure 1.1. Scheme of the different structures of the human eye. The outer layer contains sclera and cornea, the middle layer iris, ciliary body and choroid, and the inner layer contains the retina. The eye contains aqueous humor and vitreous humor, separated by the iris.

1. 3. Eye diseases

As the eye is the only organ responsible for the vision, diseases affecting eye layers can end in visual impairment or blindness. Visual impairment is a decreased visual function, which is related to more difficulty in performing vision-related tasks and, subsequently, in a reduced vision-related quality of life [2,3]. Nowadays, the main diseases which causes blindness or visual impairment are refractive errors, cataract, glaucoma, age-related macular degeneration, diabetic retinopathy and corneal opacity diseases [4].

The refractive error is the most common eye condition of visual impairment and occurs when the shape of the cornea changes and the light cannot enter directly in the retina [5]. Refractive errors include hyperopia (farsightedness), myopia (nearsightedness) and astigmatism [6]. Nowadays, there are many treatments to correct these errors like corrective glasses, contact lenses or refractive surgery.

Cataracts is an opacification of the lens, which ends in blurry vision. The lens is mainly composed of water and proteins. Several factors such as age, UV irradiation or certain diseases (like diabetes) make proteins to aggregate and create insoluble forms that start making opaque the lens [7]. Fortunately, similar to the refractive errors, cataracts are

completely treatable. Moreover, it is an age-related disease as its incidence increases at the age of 50 [4].

Glaucoma occurs when excess of aqueous humor is present in the anterior chamber, which normally increases the intraocular pressure and progressively degenerates the optic nerve, causing an irreversible loss of vision [8]. Controlling and decreasing the intraocular pressure by medical treatments is used to prevent the apparition of glaucoma [9].

Age-related macular degeneration is a disease that damages the macula, which is the part of the retina with high photoreceptors density. This results in the loss of central vision and a highly decreased vision acuity, making patients not being able to do common activities such as reading or driving [10]. Nowadays, there are several efficient treatment for this disease, such as surgical or medical therapies [11].

Diabetic retinopathy is a disease present in patients affected with diabetes, which have high glucose levels in blood that damage the retinal microvasculature and can cause hemorrhages or occlusions, decreasing visual function [12]. Diabetic retinopathy only affects a small-proportion of global visual impairment or blindness and can be prevented with glucose blood controls [13].

Corneal opacity diseases are mainly Fuchs endothelial dystrophy and bullous keratopathy. These diseases affect the outer layer of the eye, which is not able to maintain the corneal transparency and, hence significantly reduce vision [14,15]. Nowadays, the only treatment for corneal blindness is corneal transplant from a human cadaveric donor. However, there is a global shortage of donors and this procedure has several complications, so other alternatives should be found [16,17].

Out of the different layers, we have focused on the cornea. Despite there are several eye related diseases, we believe that some of the current available treatments for some inner layers are currently the only viable options, such as several oral and liquid form drugs which overall may have a positive effect on the affected part of the eye. Hence, finding alternatives is sometimes difficult as the current surgery technologies may not allow for certain surgeries to be performed. For this reason, we believe that, on the one hand cornea is one of the most damaged tissues and, on the other hand, it is an easily accessible tissue, which allows certain manipulation and hence, improve the current available treatments for this purpose. From now on, we will focus on the structure of the cornea and how we can improve currents strategies and where the new strategies are stirring to.

1. 4. Corneal structure

The cornea is a transparent avascular wall on the eye and it is responsible of focusing the light that enters. Its thickness is around 500 µm and it contains three cellular layers (epithelium, stroma and endothelium) separated by two acellular membranes (Bowman's layer and the Descemet's membrane) [18]**.** The epithelial surface is a 50 µm thick stratified layer localized in the anterior part of the cornea and acts as a barrier to any external damage [19]. This layer harbors a stem cell population that makes the epithelium to be constantly self-renewed. The Bowman's layer is an acellular limiting membrane between the epithelium and the stroma. It is mainly composed of collagen I, III and V [20]. The stroma is the thickest part of the cornea, constituting 90% of corneal thickness, and it mainly contains a highly-organized extracellular matrix, mainly containing type I and keratocytes [21,22]. It provides structural strength and stability [18,19]**.** The Descemet's membrane is the basement of the corneal endothelial cells. Its thickness varies from 3 µm at birth to 10 µm in adults [23]. Lastly, the inner layer is the corneal endothelium, which is a thin monolayer of flat pentagonal and hexagonal cells in contact with the aqueous humor. Its main function is to maintain transparency by the regulation of the hydration between the corneal stroma and the anterior chamber [24]. Corneal structure can be observed in Figure 1.2.

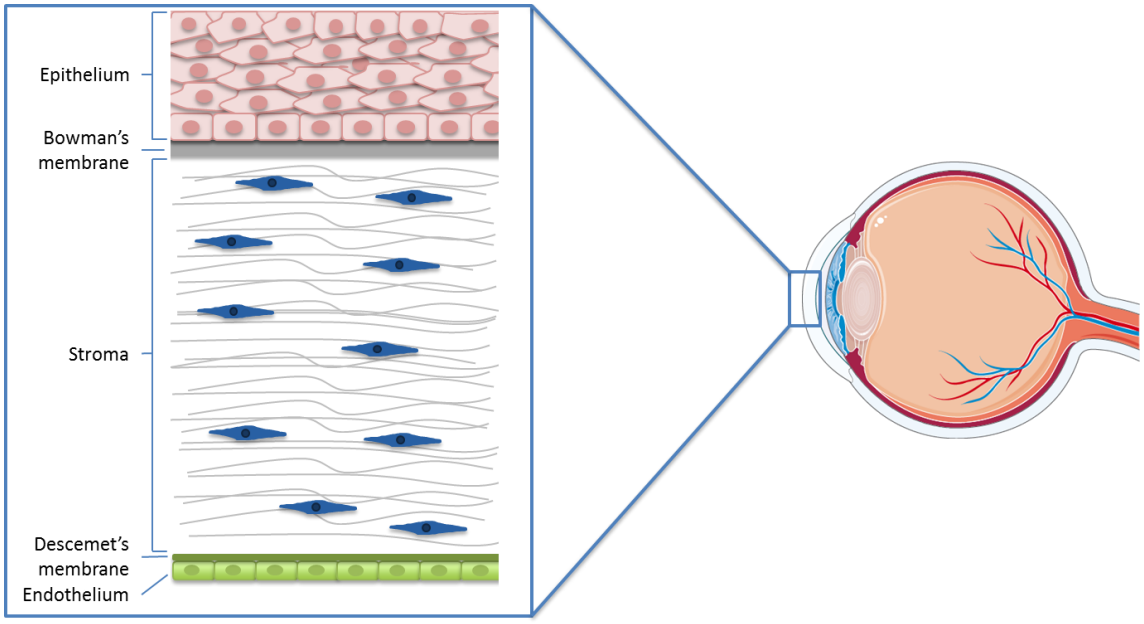

Figure 1.2. Corneal structure. The different layers consist of epithelium, Bowman's layer, stroma, Descemet's membrane and endothelium.

1. 5. Clinical need for corneal regeneration

Diseases affecting the cornea are the fifth leading cause of blindness and it affects more than 10 million people in the world today [25,26]. Nowadays, corneal transplant is the gold standard treatment for these diseases. In fact, it is the type of transplant most frequently performed worldwide [16].

An organ transplant is the replacement of a dysfunctional tissue or organ with a healthy one that can be from the same patient (autograft), from a human donor (allograft) or from an animal (xenograft). In the case of corneal transplant, corneas are derived from human cadaveric donors. Corneal transplant, named as keratoplasty, can be performed replacing the full cornea, known as penetrating keratoplasty (PK), or only the damaged corneal layers, known as partial thickness transplants [27]. PK replaces the five layers of the cornea whereas partial thickness transplants conserves the healthy and functional tissue from the cornea. Over the last decade, the number of PK has been decreasing and partial thickness transplants are the most selected option. In fact, according to the annual Eye Bank Association of America (EBAA) report from 2018, endothelial keratoplasties, which is performed due to corneal endothelium failure, was the most performed keratoplasty and represented more than 60% of all corneal transplants, which presented an increase of 4.6% from the previous year report [28]. The top indication for corneal transplant is related to a disease that affects the corneal endothelium, known as Fuchs dystrophy, which represent 39% of all transplants performed [16]. The next leading causes are keratoconus, which normally affects all corneal layers and represents 27% of the transplants, and infectious keratitis, affecting the epithelium (20%) [16].

All in all, surgical intervention is still a difficult option and this process faces many challenges such as a severe worldwide shortage of donors and graft rejection by the patient [29]. In fact, only 1 of 70 patients undergoes corneal transplant [16]. Overall, it seems that one of the most damaged tissues and vulnerable is the endothelium, as most of the cornea transplants performed are mainly due to its failure. Hence, to address this issue, it is necessary to find an alternative solution such as the development of an *in vitro* tissue construct for corneal endothelium regeneration.

1. 6. Corneal endothelium

1. 6. 1. Biology

The corneal endothelium consists of a single layer of arranged polygonal cells with a neural crest origin. This layer is located in the posterior part of the eye, between the corneal stroma and the anterior chamber. In humans and primates, the *in vivo* corneal endothelial cells (CEC) are in a non-proliferative state as they are arrested at the G1-phase due to strong contact inhibition, low concentration of growth factors that enhances mitosis and containing elevated amounts of reactive oxygen species as a result of the high exposure to light [21,30,31]. For this reason, newborns present a peak value of ~4000 cells/mm^2 of cell density but this value decreases as there is a rate of 0.6% of average cell density decline per year in a healthy cornea and the existing cells migrate and enlarge to replace the dead cells [32,33].

The basement of human CEC (HCEC) is the Descemet's membrane and it contains different proteins such as fibronectin, laminin or collagen [34]. Moreover, HCEC also interact with the corneal stroma, which is rich in chondroitin sulphate and collagen I [22]. Furthermore, the topography is also important, as the Descemet's membrane has a rough surface with elevations and pores in the nanoscale range [35].

1. 6. 2. Function

CEC play an essential role in the maintenance of corneal transparency through its barrier and the Na^+/K^+-ATPase pump functions that regulate corneal hydration [36]. An abnormal pump function results in an excess of fluid in the corneal stroma due to fluid absorption from the aqueous humor or secondary to epithelial or stroma injury. This excess of fluid in the cornea changes the composition of the proteins, which ends in corneal edema and, subsequently, in a decreased level of corneal transparency [36].

Moreover, as cornea is an avascular tissue, the corneal endothelium represents a nutritional gateway between the anterior chamber and the cornea. Mostly all the nutrients required for the cornea, which are in the aqueous humor, are transferred into the cornea through the pumps of CEC [37].

1. 7. Current strategies in corneal endothelial regeneration

1. 7. 1. Corneal endothelium transplant

If an irreversible damage occurs due to any trauma or disease, such as Fuchs dystrophy, *in vivo* CEC are not able to regenerate due to its non-proliferate state so corneal endothelial functions are lost, transparency is not maintained and edema appears. Subsequently, it can result in a pathological condition named as bullous keratopathy and a surgical treatment is needed in order to recover the corneal dysfunction [14].

Nowadays, transplant is the initial treatment for any corneal dysfunction. In 1905, the first full-thickness corneal transplant or penetrating keratoplasty (PK) was successfully performed for treating corneal endothelium failure. Although this technique improves the patient's vision, there are some problems associated as long recovery, refraction errors, rejection or the need of hard contact lenses [38]. For this reason, depending on the cellular layer that is damaged, partial keratoplasties are nowadays increasingly performed. Partial keratoplasties techniques are deep anterior lamellar keratoplasty (DALK) or endothelial keratoplasty (EK). On the one hand, DALK replaces the epithelium, bowman's layer and stroma. On the other hand, EK can selectively replace the posterior layer of endothelium and Descemet membrane, a graft of around 20 µm and being called Descemet Membrane endothelial keratoplasty (DMEK) and, in some cases, also part of the stroma, a thicker graft of 70 – 150 µm and named as Descemet stripping automated endothelial keratoplasty (DSAEK), as shown in Figure 1.3 [39].

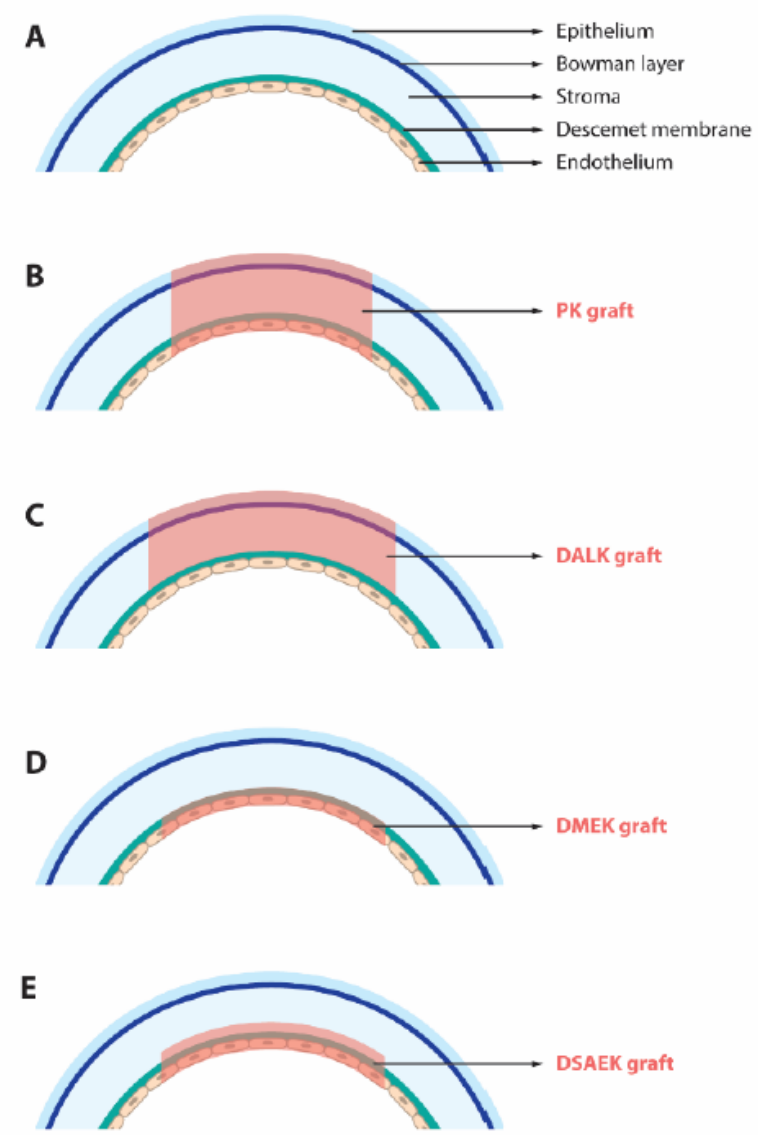

Figure 1.3. Corneal transplant. (A) Corneal layers and (B-E) different keratoplasty procedures: (B) penetrating keratoplasty or PK, (C) deep anterior lamellar keratoplasty or DALK, (D) Descemet Membrane endothelial keratoplasty or DMEK and (E) Descemet stripping automated endothelial keratoplasty or DSAEK. Modified from [39].

In sum, in comparison to PK, partial keratoplasty ends up in better vision, lower surgery complications and lower time of recovery [38]. However, corneal transplant still faces many limitations as immune rejection, difficulty of the surgery, invasive technique and secondary complications [40]. For this purpose, other strategies as drug therapy and cell-based strategies have recently become viable options.

1. 7. 2. Drug therapy

Innovative medical treatments using drugs like Rho-kinase (ROCK) inhibitors have been used for corneal endothelial dysfunction [41]. ROCK are proteins of the Rho pathway which regulates a variety of cellular functions as cell proliferation, migration and cell-size regulation [42]. Recently, Rho pathway has been shown to be involved in ocular diseases so ROCK inhibitors have been used a novel treatment in this field [43]. In fact, several studies have focused on the evaluation of ROCK inhibitors for corneal endothelial regeneration. Koizumi et al. demonstrated that the inhibition of ROCK signaling enhanced cell proliferation, which resulted in higher cell density with better CEC phenotype [44]. Okumura et al. studied the positive effect of a selective ROCK inhibitor in corneal thickness and in cell morphology, function and density, in *in vivo* rabbit and primate models [45–47]. Furthermore, Okumura et al. also showed that the application of a topic ROCK inhibitor ended in the recovery of corneal transparency in 3 patients that presented postoperative acute corneal endothelial decompensation [48].

1. 7. 3. Cell therapy strategies

Currently, the isolation, culture and differentiation of cells *in vitro* is a common strategy used in regenerative medicine. Cells are the basic element in all organs and tissues of an organism. Through its signals and molecular mechanisms, they are indispensable for the regeneration and healing processes. In regenerative medicine, two types of cells can be used: specialized cells or stem cells.

1. 7. 3. 1. Specialized cells

Specialized cells are mature cells that are present in any tissue and are responsible for their functionality. In the corneal endothelium, the only specialized cells that reside are CEC. Several groups have been able to isolate and expand HCEC from human cadaveric donors despite its *in vivo* non-proliferative state [49]. However, the use of these cells present some disadvantages like the global shortage of donors and the use of other human cells (allogeneic cells), which may end in immune rejection. Therefore, many investigators have focused on the generation of CEC from other sources that contain stem cells.

1. 7. 3. 2. Stem cells

Stem cells are defined by two main characteristics: self-renewal, which is done through cell division maintaining its undifferentiated state, and capacity of differentiation into a more specialized cell type. Thanks to these properties, stem cells are an excellent candidate for regenerative medicine.

As shown in Figure 1.4, stem cells can be divided by its differentiation potential [50]:

- **Totipotent Stem Cells**: they are also known as omnipotent stem cells as they have the ability to form embryonic and extra-embryonic cells. The zygote or fertilised egg, which is the most undifferendiated cell, and its first few cell divisions belong to this group.
- **Pluripotent Stem Cells**: they are descendants of totipotent cells and they present the ability of differentiation into any cellular type from the three germ layers (ectoderm, mesoderm and endoderm). This group includes embryonic stem cells (ESCs) and induced pluripotent stem cells (iPSC). On the one hand, ESCs are obtained from the inner cell mass of a 4-5 days human embryo blastocyst. On the other hand, iPSC are somatic cells that have been reprogrammed into a pluripotent state. This was discovered in 2006 by Takahashi and Yamanaka, who demonstrated that mouse embryonic fibroblasts could be transformed into pluripotent stem cells with four gene factors (Oct3/4, Sox2, c-Myc, and Klf4) [51]. For doing this, they introduced the specific transcription factors in the cell with a retrovirus and they found that mouse and also human iPSC were similar to ESC in morphology, gene expression, proliferation and teratoma formation [51,52]. Although they are used worldwide with excellent results, they present some safety and ethical concerns.
- **Multipotent Stem Cells**: this type of stem cells can only be differentiated into tissues from the same germ layer. The most common example of this kind of cells are the ones from the mesoderm, known as Mesenchymal Stem Cells (MSC). MSC can be found in different tissues like dental pulp, umbilical cord, bone or blood and they avoid ethical and safety problems, which are present in pluripotent cells. For this reason, they provide a new dimension in regenerative medicine.

- **Unipotent Stem Cells**: they can only form their own cell type but have the stem cell ability of self-renewal. An example of unipotent cells are the skin cells, which can replace the dead cells when a trauma occurs.

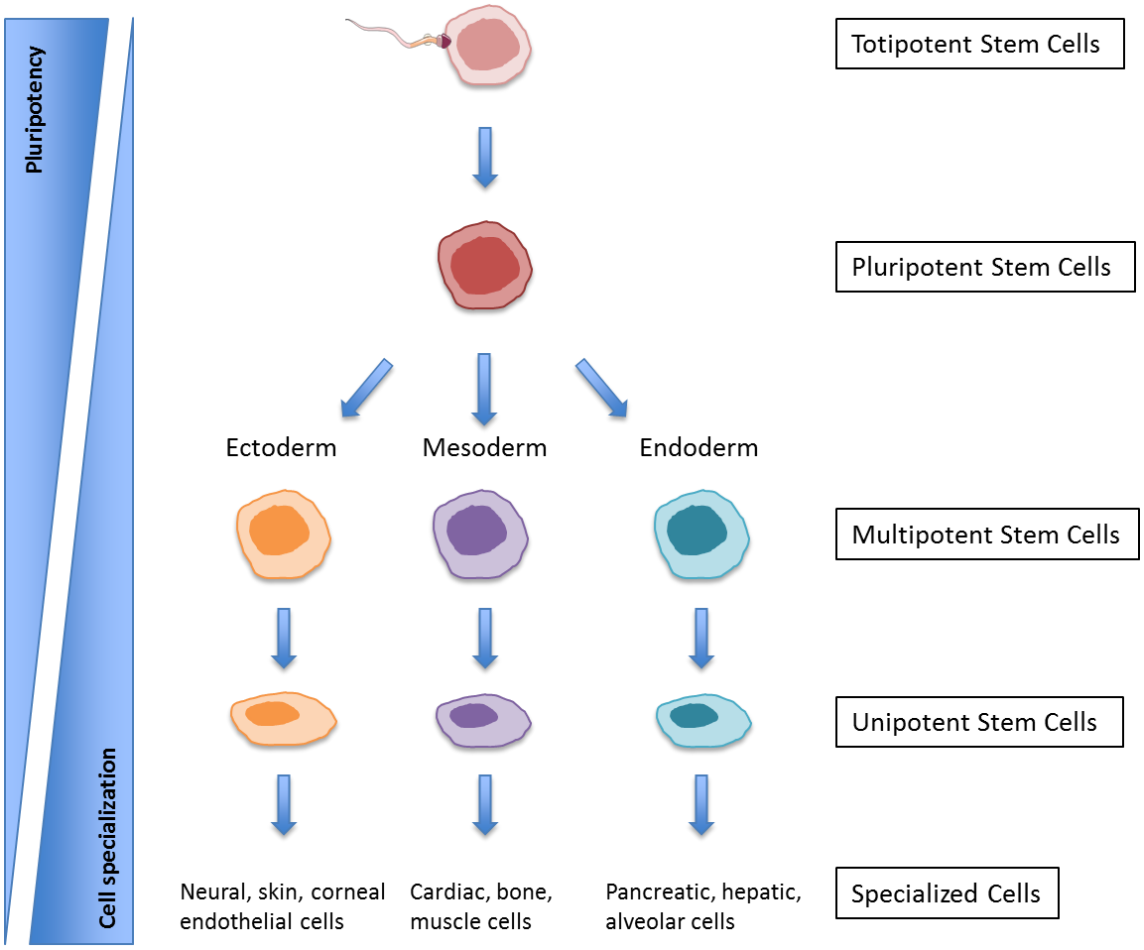

Figure 1.4. Stem cell hierarchy. Classification of stem cells depending on their pluripotency capacity and cell specialization.

1. 7. 3. 3. Producing specialized corneal endothelial cells

Corneal endothelial regeneration using cell therapies are based on the isolation and expansion of HCEC or the differentiation of stem cells into CEC.

It has been reported that the modulation of phosphatidylinositol 3-kinase (PI3K)/Akt and Smad2 signaling pathway promotes CEC proliferation and wound healing [53]. Therefore, different groups have evaluated the effect of different molecules which modulates this pathway in the culture medium.

On the one hand, epidermal growth factor (EGF), basic fibroblasts growth factor (bFGF) and transforming growth factor beta 2 (TGF- β2), which are present in the endothelium and the

aqueous humor, have been described to enhance *in vitro* cell migration, proliferation and corneal wound healing [54–58]. This can be explained as EGF and bFGF activates PI3K/Akt pathway which permits CEC to enter in the S-phase, a proliferative phase, of the cell cycle [59,60]. On the contrary, TGF-β2 suppresses cell proliferation but enhances cell migration and corneal endothelial wound healing activating Smad2 pathway.

On the other hand, it has been reported that insulin growth factor a (IGF-1), heregulin beta and activin A permits an upregulation of PI3K/Akt and Smad2 signaling pathways, which promotes CEC proliferation, migration and physiological functions. Furthermore, using these factors, corneal thickness was successfully recovered in a rabbit model [61].

Although culture components are indispensable for the correct formation and expansion of CEC, the culture system is also a very important factor to take into account. Cells can be cultured in adherent or in suspension conditions. Most cell types are cultured as a cell monolayer in adherent culture, using treated-culture plates to enhance its adhesion and proliferation. Cells can also be cultured in suspension conditions, which forms a 3D cell culture system that mimics the physiological tissue environment and permits a higher cell to cell interaction. It has been demonstrated that the formation of 3D aggregates in suspension culture of stem cells resembles an early-embryogenic process, known as gastrulation, which permits the formation of a more primitive stage of differentiation and, subsequently, higher differentiation potential [62,63].

1. 8. Mid-term and future strategies in corneal endothelial regeneration

1. 8. 1. Biomaterials and tissue engineering

A biomaterial is any natural or synthesized substance used to replace or restore damaged or dysfunctional tissue. Biomaterials are made to mimic the *in vivo* cell micro and nanoenvironment and have to be compatible with biological systems. Moreover, they can incorporate small molecules, drugs or genetic material in order to modify cell behavior or help to differentiate them into a specific cell type. For these reasons, biomaterials have always had a huge effect on medicine. In fact, over 2,000 years ago the first biomaterials were used in dentistry and ophthalmology as gold or wooden teeth and glass eyes [64]. Nowadays, new biomaterials that serve as a scaffold for cells *in vitro* and *in vivo* are

constantly being developed. For this, there is a wide variety of biomaterials with different structures and functions depending on their composition or morphology [65].

1. 8. 1. 1. Composition

- **Ceramics:** Ceramics or bioceramics are inorganic and non-metallic materials. The main bioceramic is composed of calcium phosphate, which includes hydroxyapatite carbon, β-tricalcium phosphate and biphasic calcium phosphate [66]. This type of material is very biocompatible with cells and tissues. Ceramics are strong in compression and highly inert, as they have minimal effects with their surroundings. In consequence, they present low toxicity and inflammatory response. Bioceramics are widely used in bone regeneration [67].
- **Metallic:** metal-based constructs are widely used thanks to its excellent physical properties, as they are strong, tough and ductile. They also present the ability to promote cell and tissue proliferation [66]. A very common metal used is titanium, which is very biocompatible and presents a high mechanical strength and corrosion resistance. However, it is expensive, difficult to make and may corrode [66].
- **Polymers:** These materials are extensively used in tissue engineering due to its excellent properties. They can be chemically functionalized and present unique characteristics as biodegradation, biocompatibility and intrinsic biological domains. They can be classified depending on their origin, a synthetic or natural source [65,66].
    - **Synthetic polymers:** these polymers are made of diverse monomers of different lengths. There is a huge variety of synthetic polymers which can be designed depending on the needs. For this reason, they offer the required mechanical and physicochemical properties as tensile strength, stiffness and biodegradation. Normally, synthetic polymers are cheap as they can be easily fabricated in huge quantities. A very common example is poly(lactic acid) (PLA), which is approved by the US Food and Drug Administration (FDA) [65].
    - **Natural polymers:** these materials are present in organism membranes and in tissue extracellular matrices (ECM) and include proteins and polysaccharides. Due to their natural origin, they offer great advantages like biocompatibility and binding domains. These domains help in cell attachment and

differentiation as they recognize the natural substrate [65]. For corneal regeneration, collagen is the most important protein as it is the principal component of the cornea. All in all, diverse natural scaffolds have been used in this field [24].

- **Composites:** the union of minimum two distinct materials forms composites. This combination results in an enhancement of physical or biological properties. For example, collagen and chitosan together have been determined to enhance the optical transparency and mechanical strength in membranes for corneal tissue engineering [68].
- **Decellularized matrices:** a native matrix is the best environment for cellular ingrowth. For this, the isolation of a tissue and the removal of its cellular content results in an excellent biomimetic scaffold for the adhesion, proliferation and differentiation of cells. The decellularization process leaves only the components of the native matrix with its natural micro- and nanotopography. Moreover, this decellularized matrix can be modified in order to increase desired properties as biocompatibility, biodegradability or non-immunogenicity [69]. All in all, they present low availability from human sources [65].

1. 8. 1. 2. Morphology

- **Porous/Fibrous scaffolds:** these scaffolds are the most extensively utilized in tissue engineering. The porosity mimics the native ECM and enables the passage of nutrients and signals, which enhances cell proliferation. This pattern, shown in Figure 1.5, can be achieved through several techniques like 3D printing, solvent-casting or freeze-drying. This results in a great diversity of the pore structure [65].
- **Microparticles and nanoparticles:** these scaffolds are normally used for the controlled release of biomolecules due to its micro and nanosize (Figure 1.5). The use of these particles present several advantages as ease of fabrication, size and morphology control and controlled physicochemical characteristics [70]. The development of micro and nanocarries which allows the incorporation of cells, growth factors or drugs present an innovative technique as a drug delivery system [71].

- **Hydrogels:** they are three-dimensional polymeric networks full of aqueous medium [72]. They possess unique properties due to its softness, which gives them the ability to incorporate cells and molecules and to adopt different shapes. In addition, the release of bioactive molecules can be easily controlled [73]. The first hydrogels were for contact lens applications and were developed by Wichterle et al. in 1960 [74]. Nowadays, hydrogels are globally being studied and are used in a broad range of applications. Recently, researchers have developed bio-inks, composed of an hydrogel and cells, which can be used with 3D bioprinters and form tissue constructs [75]. In this technique, the use of hydrogels offer excellent characteristics, as they do not only serve as a matrix for cells, but they also preserve the printed shape, present stability and the desired mechanical properties, are non-cytotoxic, maintain cell viability and is an easy-handling technique [76].

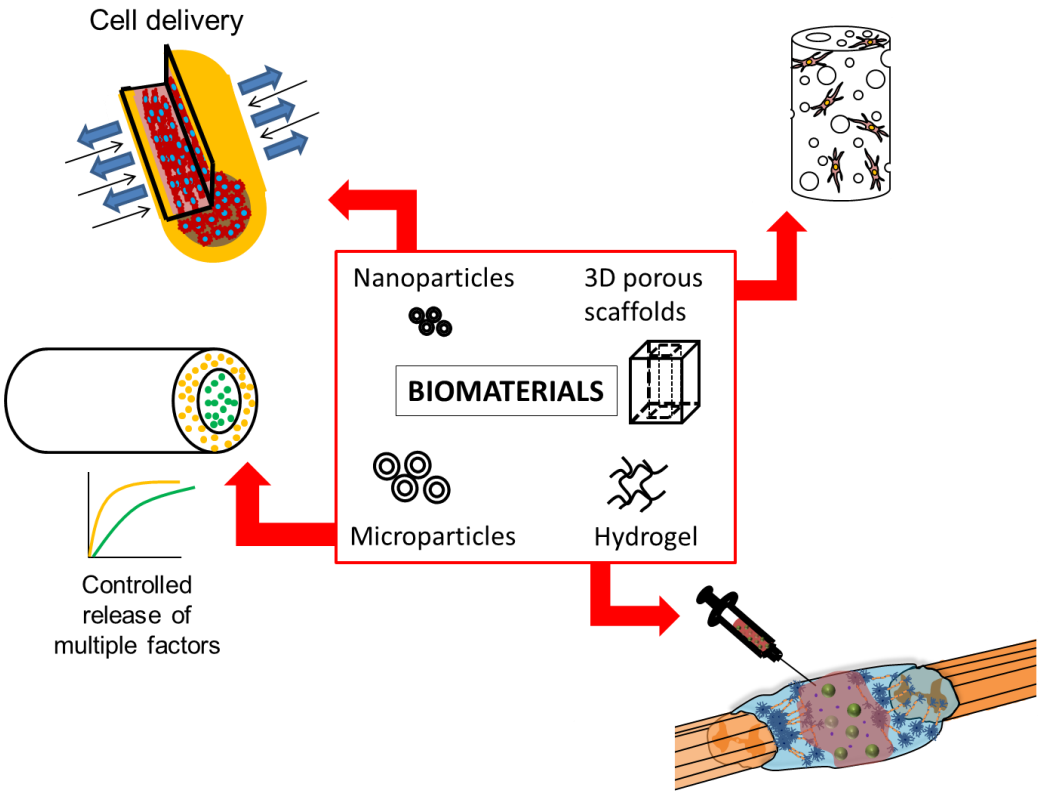

Figure 1.5. Biomaterials for tissue engineering. Different structures based on its morphology as nanoparticles, microparticles, porous scaffolds and hydrogels.

1. 8. 2. Biomaterials and tissue engineering for corneal endothelial regeneration

There are a few groups who have used biomaterials for corneal endothelial regeneration. Mainly, different artificial or decellularized matrices have been developed to serve as a culture coating in order to enhance the proliferation of CEC. Initially, cultured animal CECs were seeded on gelatin membranes [77,78] and on denuded Descemet membranes [79–81]. Later, cultured HCEC sheets appeared using different coatings as human corneas without endothelium [82,83] or denuded Descemet membrane from a second donor [84]. Moreover, other native biomaterials have been used as CEC culture coating like amniotic membrane [85], collagen sheets [86,87], corneal stromal discs [88], a thermoresponsive polymer poly(N-isopropylacrylamide) (PNIPAAm) [89,90] and coating with different components as fibronectin, albumin and collagen [47,91].

Furthermore, mainly two techniques have been performed in rabbits and monkeys from cultured CEC, which are cell injection [47,86] and transplantation of a cell sheet [78,80,85,87–90,92,93]. On the one hand, injection of CEC into the anterior chamber is a minimally invasive method to recover CEC as corneal transplantation is not needed, but it presents some limitations as the difficulty of attachment of the cells into the corneal endothelium [86]. Furthermore, their viability after injection is completely unknown. For this reason, this group overcame this problem by adding ferromagnetic particles and improved cellular attachment using a magnetic source [94]. Later, Shao et al. also used the cell injection technique by injecting endothelial progenitor cells from umbilical cord blood (UCB EPC) labeled with immunomagnetic nanoparticles and demonstrated that cells migrated to the corneal endothelium using magnet attraction [95]. Although their results determined that labeled cells ended in better visual acuity and corneal thickness than non-labeled group, corneas did not become fully transparent.

Besides from cell injection, the most performed technique for CEC transplantation is the use of cell sheets. For example, Mimura et al. cultured CEC and after reaching cell confluence, they were detached and cultured in collagen sheet which was centrifuged to ensure its cell attachment, which was ultimately transplanted [87]. They showed that cells exhibited its characteristic morphology and expressed the main CEC markers. Furthermore, corneal transparency and thickness was recovered after transplantation [87]. Similar results were obtained by Honda et al. which used a stromal disc as a cell carrier [88]. Another strategy was the use of thermoresponsive polymers, which are able to coat the surface of a substrate

with a polymer such as PNIPAAm that can allow the detachment of cells by decreasing the temperature to 20ºC [89,90]. These studies showed that cells exhibited its characteristic morphology and expressed the main CEC markers. Furthermore, corneal transparency and thickness was recovered after transplantation [89,90]. However, cell sheets were cultured in flat conditions and its transplantation to the cornea, which is a curved structure, ended in the formation of wrinkles which could lead to cell detachment [88]. Interestingly, some groups improved this technique by culturing monkey and human CEC in curved conditions [92,93]. They demonstrated that transplantation of a curved carrier could be performed without the formation of wrinkles and corneal transparency was restored. However, the follow-up study was only for 2 or 4 weeks so long-term evaluation could not be achieved [92,93].

In the last years, many advances in corneal endothelial regeneration have been accomplished (summarized in table 1.1). The main goal has been the achievement of the integration of CEC-derived from stem cells with bioengineering and biomaterials. It has been generally accepted that cells alone may have difficulties in surviving and hence, the use of these technologies may provide substrates that will allow improving the efficiency of the implanted cells. In fact, Shao et al. transplanted CEC-derived from human fetal bone marrow using a porcine corneal acellular matrix as a cell carrier. Their results indicated that cells presented its typical morphology, expressed the characteristic markers and could recover corneal transparency 28 days after transplantation [96]. Similar results were obtained by other group which successfully transplanted a decellularized porcine corneal matrix with CECs-derived from hESC [97]. However, transplanted corneas could not achieve absolutely transparency as the carrier was not able to degrade and could lead to immune rejection. Furthermore, recent studies transplanted CEC-derived from murine skin derived precursors (SKP) and from human umbilical cord in a rabbit model of bullous keratopathy and was able to recover corneal transparency and thickness [91,98]. However, these studies used rabbit models and, unlike humans or primates, rabbit corneal endothelial cells have the ability to proliferate in vivo. For this reason, further studies should be performed using animal models that could resemble human corneal physiology.

Year	Author	Cell culture coating	CEC source	Technique	Transplantation
1979	Gospodarowicz et al. [78]	Gelatin	BCEC	Cell sheet	Cat
1986	Insler and Lopez [80]	Denuded Descemet Membrane	HCEC	Cell sheet	Monkey
2004	Ishino et al. [85]	Collagen IV	HCEC	Cell sheet	Rabbit
2004	Mimura et al. [87]	Bovine ECM	HCEC	Cell sheet	Rabbit
2005	Mimura et al. [86]	Poly-lysine + Fibronectin	HCEC	Cell injection	Rabbit
2005	Mimura et al. [94]	NS	RCEC	Cell injection	Rabbit
2006	Sumide et al. [90]	Collagen IV and PNIPAAm	HCEC	Cell sheet	Rabbit
2007	Lai et al. [89]	PNIPAAm	HCEC	Cell sheet	Rabbit
2009	Honda et al. [88]	Corneal stromal disc	HCEC	Cell sheet	Rabbit
2011	Shao et al. [96]	Porcine DCM	BM-EPC	Cell sheet	Cat
2012	Okumura et al. [47]	FNC	RCEC and MCEC	Cell injection	Rabbit and monkey
2014	Zhang et al. [97]	Porcine DCM	ESC	Cell sheet	Rabbit
2014	Kimoto et al. [92]	Gelatin hydrogel	MCEC	Cell sheet	Monkey
2015	Shao et al. [95]	Collagen I	UCB-EPC	Cell injection	Rabbit
2017	Inagaki et al. [98]	Gelatin and type I atellocolagen	Murine SKP	Cell sheet	Rabbit
2017	Yoshida et al. [93]	Porcine collagen-vitrigel	HCEC	Cell sheet	Rabbit
2018	Yamashita et al. [91]	FNC/Collagen I	hUC	Cell sheet	Rabbit

Table 1.1. Tissue engineering in corneal endothelial regeneration. ECM: Extracellular matrix; NS: Not specified; PNIPAAm: Poly(N-isopropylacrylamide); DCM: Decellularized matrix; FNC: fibronectin, albumin and collagen mix; BCEC: bovine corneal endothelial cells; HCEC: human CEC; BM-EPC: bone marrow-derived endothelial progenitor cells; RCEC: rabbit CEC; MCEC: monkey CEC; ESC: embryonic stem cells; UCB-EPC: umbilical cord blood endothelial progenitor cells; SKP: skin-derived precursors; hUC: human umbilical cord

1.9. References

[1] C.E. Willoughby, D. Ponzin, S. Ferrari, A. Lobo, K. Landau, Y. Omidi, Anatomy and physiology of the human eye: Effects of mucopolysaccharidoses disease on structure and function - a review, Clin. Exp. Ophthalmol. 38 (2010) 2–11. doi:10.1111/j.1442-9071.2010.02363.x.

[2] H.T. V Vu, J.E. Keeffe, C.A. McCarty, H.R. Taylor, Impact of unilateral and bilateral vision loss on quality of life, Br. J. Ophthalmol. 89 (2005) 360. doi:10.1136/BJO.2004.047498.

[3] K. Adigun, T.S. Oluleye, M.M. Ladipo, S.A. Olowookere, Quality of life in patients with visual impairment in Ibadan: a clinical study in primary care, J. Multidiscip. Healthc. 7 (2014) 173. doi:10.2147/JMDH.S51359.

[4] S.R. Flaxman, R.R.A. Bourne, S. Resnikoff, E. Al, Global causes of blindness and distance vision impairment 1990–2020: a systematic review and meta-analysis, Lancet Glob. Heal. 5 (2017) e1221–e1234. doi:10.1016/S2214-109X(17)30393-5.

[5] Q. Zhang, Genetics of refraction and Myopia, in: Prog. Mol. Biol. Transl. Sci., Academic Press, 2015: pp. 269–279. doi:10.1016/bs.pmbts.2015.05.007.

[6] D.M. Costakos, Eye Disorders, in: Nelson Pediatr. Symptom-Based Diagnosis, Elsevier, 2018: p. 563–593.e2. doi:10.1016/B978-0-323-39956-2.00032-7.

[7] K.L. Moreau, J.A. King, Protein misfolding and aggregation in cataract disease and prospects for prevention, Trends Mol. Med. 18 (2012) 273–282. doi:10.1016/j.molmed.2012.03.005.

[8] J.L. Wiggs, Glaucoma, Emery Rimoin's Princ. Pract. Med. Genet. (2013) 1–15. doi:10.1016/B978-0-12-383834-6.00144-0.

[9] M. V. Boland, A.-M. Ervin, D.S. Friedman, H.D. Jampel, B.S. Hawkins, D. Vollenweider, Y. Chelladurai, D. Ward, C. Suarez-Cuervo, K.A. Robinson, Comparative Effectiveness of Treatments for Open-Angle Glaucoma: A Systematic Review for the U.S. Preventive Services Task Force, Ann. Intern. Med. 158 (2013) 271. doi:10.7326/0003-4819-158-4-201302190-00008.

[10] L.S. Lim, P. Mitchell, J.M. Seddon, F.G. Holz, T.Y. Wong, Age-related macular degeneration, Lancet. 379 (2012) 1728–1738. doi:10.1016/S0140-6736(12)60282-7.

[11] M. Khan, K. Agarwal, M. Loutfi, A. Kamal, Present and possible therapies for age-related macular degeneration., ISRN Ophthalmol. (2014) 608390.

doi:10.1155/2014/608390.

[12] P.H. Scanlon, Diabetic retinopathy, Medicine (Baltimore). 43 (2015) 13–19. doi:10.1016/J.MPMED.2014.10.009.

[13] C.-H. Zhu, S.-S. Zhang, Y. Kong, Y.-F. Bi, L. Wang, Q. Zhang, Effects of intensive control of blood glucose and blood pressure on microvascular complications in patients with type II diabetes mellitus., Int. J. Ophthalmol. 6 (2013) 141–5. doi:10.3980/j.issn.2222-3959.2013.02.06.

[14] N. Morishige, K.H. Sonoda, Bullous keratopathy as a progressive disease: Evidence from clinical and laboratory imaging studies, Cornea. 32 (2013) S77–S83. doi:10.1097/ICO.0b013e3182a1bc65.

[15] S.E. Wilson, W.M. Bourne, Fuchs' dystrophy., Cornea. 7 (1988) 2–18.

[16] P. Gain, R. Jullienne, Z. He, M. Aldossary, S. Acquart, F. Cognasse, G. Thuret, Global survey of corneal transplantation and eye banking, JAMA Ophthalmol. 134 (2016) 167–173. doi:10.1001/jamaophthalmol.2015.4776.

[17] A.L. Yu, M. Kaiser, M. Schaumberger, E. Messmer, D. Kook, U. Welge-Lussen, Perioperative and postoperative risk factors for corneal graft failure., Clin. Ophthalmol. 8 (2014) 1641–7. doi:10.2147/OPTH.S65412.

[18] J. Zavala, G. Ló Pez Jaime, C.R. Barrientos, J. Valdez-Garcia, Corneal endothelium: developmental strategies for regeneration, Eye. 27 (2013). doi:10.1038/eye.2013.15.

[19] M. Yoshihara, H. Ohmiya, S. Hara, S. Kawasaki, Y. Hayashizaki, M. Itoh, H. Kawaji, M. Tsujikawa, K. Nishida, Discovery of molecular markers to discriminate corneal endothelial cells in the human body., PLoS One. 10 (2015) e0117581. doi:10.1371/journal.pone.0117581.

[20] S.E. Wilson, J.W. Hong, Bowman's layer structure and function: critical or dispensable to corneal function? A hypothesis., Cornea. 19 (2000) 417–20.

[21] Y. Liu, H. Sun, M. Hu, M. Zhu, S. Tighe, S. Chen, Y. Zhang, C. Su, S. Cai, P. Guo, Human Corneal Endothelial Cells Expanded *In Vitro* Are a Powerful Resource for Tissue Engineering, Int. J. Med. Sci. 14 (2017) 128–135. doi:10.7150/ijms.17624.

[22] D.W. DelMonte, T. Kim, Anatomy and physiology of the cornea, J. Cataract Refract. Surg. 37 (2011) 588–598. doi:10.1016/J.JCRS.2010.12.037.

[23] M. Ali, V. Raghunathan, J.Y. Li, C.J. Murphy, S.M. Thomasy, Biomechanical relationships between the corneal endothelium and Descemet's membrane, Exp. Eye

Res. 152 (2016) 57–70. doi:10.1016/j.exer.2016.09.004.

[24] T. Mimura, S. Yamagami, S. Amano, Corneal endothelial regeneration and tissue engineering, Prog. Retin. Eye Res. 35 (2013) 1–17. doi:10.1016/j.preteyeres.2013.01.003.

[25] P.M. Mathews, K. Lindsley, A.J. Aldave, E.K. Akpek, Etiology of Global Corneal Blindness and Current Practices of Corneal Transplantation : A Focused Review, Cornea 2018. 37 (2018) 1–6. doi:10.1097/ICO.0000000000001666.

[26] J.P. Whitcher, M. Srinivasan, M.P. Upadhyay, Corneal blindness: A global perspective, Bull. World Health Organ. 79 (2001) 214–221. doi:10.1111/ceo.12330.

[27] G.E. Boynton, M.A. Woodward, Evolving Techniques in Corneal Transplantation, Curr. Surg. Reports. 3 (2015). doi:10.1007/s40137-014-0079-5.

[28] Eye Bank Association of America, (n.d.). https://restoresight.org/eye-bank-association-america/ (accessed May 14, 2019).

[29] J. Navaratnam, T.P. Utheim, V.K. Rajasekhar, A. Shahdadfar, Substrates for Expansion of Corneal Endothelial Cells towards Bioengineering of Human Corneal Endothelium., J. Funct. Biomater. 6 (2015) 917–45. doi:10.3390/jfb6030917.

[30] N.C. Joyce, C.C. Zhu, D.L. Harris, Relationship among oxidative stress, dna damage, and proliferative capacity in human corneal endothelium, Investig. Ophthalmol. Vis. Sci. 50 (2009) 2116–2122. doi:10.1167/iovs.08-3007.

[31] N.C. Joyce, D.L. Harris, D.M. Mello, Mechanisms of mitotic inhibition in corneal endothelium: Contact inhibition and TGF-b2, Investig. Ophthalmol. Vis. Sci. 43 (2002) 2152–2159.

[32] U. Elbaz, K. Mireskandari, N. Tehrani, C. Shen, M.S. Khan, S. Williams, A. Ali, Corneal Endothelial Cell Density in Children: Normative Data From Birth to 5 Years Old, Am. J. Ophthalmol. 173 (2017) 134–138. doi:10.1016/J.AJO.2016.09.036.

[33] W.M. Bourne, L.R. Nelson, D.O. Hodge, Central corneal endothelial cell changes over a ten-year period., Invest. Ophthalmol. Vis. Sci. 38 (1997) 779–782.

[34] A. Kabosova, D.T. Azar, G.A. Bannikov, K.P. Campbell, M. Durbeej, R.F. Ghohestani, J.C.R. Jones, M.C. Kenney, M. Koch, Y. Ninomiya, B.L. Patton, M. Paulsson, Y. Sado, E.H. Sage, T. Sasaki, L.M. Sorokin, M.F. Steiner-Champliaud, T.T. Sun, N. SundarRaj, R. Timpl, I. Virtanen, A. V. Ljubimov, Compositional differences between infant and adult human corneal basement membranes, Investig. Ophthalmol. Vis. Sci. 48 (2007) 4989–

4999. doi:10.1167/iovs.07-0654.

[35] S. Koo, R. Muhammad, G.S.L. Peh, J.S. Mehta, E.K.F. Yim, Micro- and nanotopography with extracellular matrix coating modulate human corneal endothelial cell behavior, Acta Biomater. 10 (2014) 1975–1984. doi:10.1016/J.ACTBIO.2014.01.015.

[36] P. Labelle, The Eye, in: Pathol. Basis Vet. Dis. Expert Consult, Mosby, (2016): p. 1265–1318.e1. doi:10.1016/B978-0-323-35775-3.00021-7.

[37] J.A. Bonanno, Molecular mechanisms underlying the corneal endothelial pump., Exp. Eye Res. 95 (2012) 2–7. doi:10.1016/j.exer.2011.06.004.

[38] B. Van den Bogerd, S.N. Dhubhghaill, C. Koppen, M.J. Tassignon, N. Zakaria, A review of the evidence for in vivo corneal endothelial regeneration, Surv. Ophthalmol. 63 (2017) 149–165. doi:10.1016/j.survophthal.2017.07.004.

[39] W. Zhong, M. Montana, S.M. Santosa, I.D. Isjwara, Y.H. Huang, K.Y. Han, C. O'Neil, A. Wang, M.S. Cortina, J. de la Cruz, Q. Zhou, M.I. Rosenblatt, J.H. Chang, D.T. Azar, Angiogenesis and lymphangiogenesis in corneal transplantation–A review, Surv. Ophthalmol. 63 (2018) 453–479. doi:10.1016/j.survophthal.2017.12.008.

[40] D.T.H. Tan, J.K.G. Dart, E.J. Holland, S. Kinoshita, Corneal transplantation, Lancet. 379 (2012) 1749–1761. doi:10.1016/S0140-6736(12)60437-1.

[41] S.B. Han, Y.-C. Liu, K. Mohamed-Noriega, J.S. Mehta, Application of Novel Drugs for Corneal Cell Regeneration., J. Ophthalmol. (2018) 1215868. doi:10.1155/2018/1215868.

[42] K. Riento, A.J. Ridley, Rocks: Multifunctional kinases in cell behaviour, Nat. Rev. Mol. Cell Biol. 4 (2003) 446–456. doi:10.1038/nrm1128.

[43] R. Nourinia, S. Nakao, S. Zandi, S. Safi, A. Hafezi-Moghadam, H. Ahmadieh, ROCK inhibitors for the treatment of ocular diseases, Br. J. Ophthalmol. 102 (2018) 1–5. doi:10.1136/bjophthalmol-2017-310378.

[44] N. Koizumi, N. Okumura, M. Ueno, S. Kinoshita, New therapeutic modality for corneal endothelial disease using Rho-associated kinase inhibitor eye drops, Cornea (2014): pp. S25–S31. doi:10.1097/ICO.0000000000000240.

[45] N. Okumura, N. Koizumi, E.D.P. Kay, M. Ueno, Y. Sakamoto, S. Nakamura, J. Hamuro, S. Kinoshita, The ROCK inhibitor eye drop accelerates corneal endothelium wound healing, Investig. Ophthalmol. Vis. Sci. 54 (2013) 2439–2502. doi:10.1167/iovs.12-11320.

[46] N. Okumura, Y. Okazaki, R. Inoue, K. Kakutani, S. Nakano, S. Kinoshita, N. Koizumi, Effect of the rho-associated kinase inhibitor eye drop (Ripasudil) on corneal endothelial wound healing, Investig. Ophthalmol. Vis. Sci. 57 (2016) 1284–1292. doi:10.1167/iovs.15-18586.

[47] N. Okumura, N. Koizumi, M. Ueno, Y. Sakamoto, H. Takahashi, H. Tsuchiya, J. Hamuro, S. Kinoshita, ROCK inhibitor converts corneal endothelial cells into a phenotype capable of regenerating in vivo endothelial tissue, Am. J. Pathol. 181 (2012) 268–277. doi:10.1016/j.ajpath.2012.03.033.

[48] N. Okumura, S. Kinoshita, N. Koizumi, Application of Rho Kinase Inhibitors for the Treatment of Corneal Endothelial Diseases, J. Ophthalmol. 2017 (2017) 1–8. doi:10.1155/2017/2646904.

[49] M. Parekh, S. Ferrari, C. Sheridan, S. Kaye, S. Ahmad, Concise Review: An Update on the Culture of Human Corneal Endothelial Cells for Transplantation, Stem Cells Transl. Med. 5 (2015) 258–264. doi:10.5966/sctm.2015-0181.

[50] D. Ilic, J.M. Polak, Stem cells in regenerative medicine: Introduction:, Br. Med. Bull. 98 (2011) 117–126. doi:10.1093/bmb/ldr012.

[51] K. Takahashi, S. Yamanaka, Induction of pluripotent stem cells from mouse embryonic and adult fibroblast cultures by defined factors., Cell. 126 (2006) 663–76. doi:10.1016/j.cell.2006.07.024.

[52] K. Takahashi, K. Tanabe, M. Ohnuki, M. Narita, T. Ichisaka, K. Tomoda, S. Yamanaka, Induction of Pluripotent Stem Cells from Adult Human Fibroblasts by Defined Factors, Cell. 131 (2007) 861–872. doi:10.1016/j.cell.2007.11.019.

[53] K.W. Kim, S.H. Park, S.J. Lee, J.C. Kim, Ribonuclease 5 facilitates corneal endothelial wound healing via activation of PI3-kinase/Akt pathway, Sci. Rep. 6 (2016) 31162. doi:10.1038/srep31162.

[54] M.B. Grant, P.T. Khaw, G.S. Schultz, J.L. Adams, R.W. Shimizu, Effects of epidermal growth factor, fibroblast growth factor, and transforming growth factor-beta on corneal cell chemotaxis., Invest. Ophthalmol. Vis. Sci. 33 (1992) 3292–301.

[55] S.K. Nayak, P.S. Binder, The Growth of Endothelium from Human Corneal Rims in Tissue Culture, Invest. Ophthalmol. Vis. Sci. 25 (1984) 1213–1216.

[56] V.P. Hoppenreijs, E. Pels, G.F. Vrensen, J. Oosting, W.F. Treffers, Effects of human epidermal growth factor on endothelial wound healing of human corneas., Invest.

Ophthalmol. Vis. Sci. 33 (1992) 1946–57.

[57] V.P. Hoppenreijs, E. Pels, G.F. Vrensen, W.F. Treffers, Basic fibroblast growth factor stimulates corneal endothelial cell growth and endothelial wound healing of human corneas., Invest. Ophthalmol. Vis. Sci. 35 (1994) 931–44.

[58] P.G. Woost, M.M. Jumblatt, R.A. Eiferman, G.S. Schultz, Growth factors and corneal endothelial cells: I. Stimulation of bovine corneal endothelial cell DNA synthesis by defined growth factors., Cornea. 11 (1992) 1–10.

[59] W. Zhang, J. Chen, Y. Fu, X. Fan, The signaling pathway involved in the proliferation of corneal endothelial cells, J. Recept. Signal Transduct. 35 (2015) 585–591. doi:10.3109/10799893.2015.1026445.

[60] M.E. Díaz, L. González, J.G. Miquet, C.S. Martínez, A.I. Sotelo, A. Bartke, D. Turyn, Growth hormone modulation of EGF-induced PI3K-Akt pathway in mice liver, Cell. Signal. 24 (2012) 514–523. doi:10.1016/j.cellsig.2011.10.001.

[61] A.L. Sabater, E.J. Andreu, M. García-Guzmán, T. López, G. Abizanda, V.L. Perez, J. Moreno-Montañés, F. Prósper, Combined PI3K/Akt and Smad2 activation promotes corneal endothelial cell proliferation, Investig. Ophthalmol. Vis. Sci. 58 (2017) 745–754. doi:10.1167/iovs.16-20817.

[62] A. Stolzing, E. Bauer, A. Scutt, Suspension Cultures of Bone-Marrow-Derived Mesenchymal Stem Cells: Effects of Donor Age and Glucose Level, Stem Cells Dev. 21 (2012) 2718–2723. doi:10.1089/scd.2011.0406.

[63] M. Baker, Embryoid bodies get organized, Nat. Reports Stem Cells. (2008). doi:10.1038/stemcells.2008.146.

[64] R. Langer, D.A. Tirrell, Designing materials for biology and medicine, Nature. 428 (2004) 487–492. doi:10.1038/nature02388.

[65] R.A. Perez, C.R. Jung, H.W. Kim, Biomaterials and Culture Technologies for Regenerative Therapy of Liver Tissue, Adv. Healthc. Mater. 6 (2017) 1600791. doi:10.1002/adhm.201600791.

[66] E.J. Lee, F.K. Kasper, A.G. Mikos, Biomaterials for tissue engineering., Ann. Biomed. Eng. 42 (2014) 323–37. doi:10.1007/s10439-013-0859-6.

[67] H. Bakht Khosh Hagh, F. Farshi Azhar, Reinforcing materials for polymeric tissue engineering scaffolds: A review, J. Biomed. Mater. Res. Part B Appl. Biomater. (2018). doi:10.1002/jbm.b.34248.

[68] W. Li, Y. Long, Y. Liu, K. Long, S. Liu, Z. Wang, Y. Wang, L. Ren, Fabrication and characterization of chitosan–collagen crosslinked membranes for corneal tissue engineering, J. Biomater. Sci. Polym. Ed. 25 (2014) 1962–1972. doi:10.1080/09205063.2014.965996.

[69] D. Rana, H. Zreiqat, N. Benkirane-Jessel, S. Ramakrishna, M. Ramalingam, Development of decellularized scaffolds for stem cell-driven tissue engineering, J. Tissue Eng. Regen. Med. 11 (2017) 942–965. doi:10.1002/term.2061.

[70] C. Berkland, K. (Kevin) Kim, D.W. Pack, PLG Microsphere Size Controls Drug Release Rate Through Several Competing Factors, Pharm. Res. 20 (2003) 1055–1062. doi:10.1023/A:1024466407849.

[71] B. Dhandayuthapani, Y. Yoshida, T. Maekawa, D.S. Kumar, Polymeric scaffolds in tissue engineering application: A review, Int. J. Polym. Sci. 2011 (2011) 1–19. doi:10.1155/2011/290602.

[72] E.M. Ahmed, Hydrogel: Preparation, characterization, and applications: A review, J. Adv. Res. 6 (2015) 105–121. doi:10.1016/j.jare.2013.07.006.

[73] J.L. Drury, D.J. Mooney, Hydrogels for tissue engineering: Scaffold design variables and applications, Biomaterials. 24 (2003) 4337–4351. doi:10.1016/S0142-9612(03)00340-5.

[74] O. Wichterle, D. Lím, Hydrophilic Gels for Biological Use, Nature. 185 (1960) 117–118. doi:10.1038/185117a0.

[75] T.K. Merceron, S. V. Murphy, Hydrogels for 3D Bioprinting Applications, Essentials 3D Biofabrication Transl. (2015) 249–270. doi:10.1016/B978-0-12-800972-7.00014-1.

[76] I.M. El-Sherbiny, M.H. Yacoub, Hydrogel scaffolds for tissue engineering: Progress and challenges, Glob. Cardiol. Sci. Pract. 2013 (2013) 38. doi:10.5339/gcsp.2013.38.

[77] J.P. McCulley, D.M. Maurice, B.D. Schwartz, Corneal Endothelial Transplantation, Ophthalmology. 87 (1980) 194–201. doi:10.1016/S0161-6420(80)35259-7.

[78] D. Gospodarowicz, G. Greenburg, J. Alvarado, Transplantation of Cultured Bovine Corneal Endothelial Cells to Species With Nonregenerative Endothelium: The Cat as an Experimental Model, Arch. Ophthalmol. 97 (1979) 2163–2169. doi:10.1001/archopht.1979.01020020481016.

[79] M.M. Jumblatt, D.M. Maurice, J.P. McCulley, Transplantation of tissue-cultured corneal endothelium, Investig. Ophthalmol. Vis. Sci. 17 (1978) 1135–1141.

doi:10.1097/00003226-198706010-00062.

[80] M.S. Insler, J.G. Lopez, Transplantation of cultured human neonatal corneal endothelium, Curr. Eye Res. 5 (1986) 967–972. doi:10.3109/02713688608995178.

[81] D. Gospodarowicz, G. Greenburg, The coating of bovine and rabbit corneas denuded of their endothelium with bovine corneal endothelial cells, Exp. Eye Res. 28 (1979) 249–265. doi:10.1016/0014-4835(79)90087-3.

[82] M. Böhnke, P. Eggli, K. Engelmann, Transplantation of cultured adult human or porcine corneal endothelial cells onto human recipients in vitro. Part II: Evaluation in the scanning electron microscope, Cornea. 18 (1999) 207–213. doi:10.1097/00003226-199903000-00011.

[83] S. Amano, Transplantation of cultured human corneal endothelial cells., Cornea. 22 (2003) S66–S74. doi:10.1097/00003226-200310001-00010.

[84] K.H. Chen, D. Azar, N.C. Joyce, Transplantation of adult human corneal endothelium ex vivo: a morphologic study., Cornea. 20 (2001) 731–7.

[85] Y. Ishino, Y. Sano, T. Nakamura, C.J. Connon, H. Rigby, N.J. Fullwood, S. Kinoshita, Amniotic membrane as a carrier for cultivated human corneal endothelial cell transplantation., Invest. Ophthalmol. Vis. Sci. 45 (2004) 800–6.

[86] T. Mimura, S. Yokoo, M. Araie, S. Amano, S. Yamagami, Treatment of rabbit bullous keratopathy with precursors derived from cultured human corneal endothelium, Investig. Ophthalmol. Vis. Sci. 46 (2005) 3637–3644. doi:10.1167/iovs.05-0462.

[87] T. Mimura, S. Yamagami, S. Yokoo, T. Usui, K. Tanaka, S. Hattori, S. Irie, K. Miyata, M. Araie, S. Amano, Cultured human corneal endothelial cell transplantation with a collagen sheet in a rabbit model, Investig. Ophthalmol. Vis. Sci. 45 (2004) 2992–2997. doi:10.1167/iovs.03-1174.

[88] N. Honda, T. Mimura, T. Usui, S. Amano, Descemet stripping automated endothelial keratoplasty using cultured corneal endothelial cells in a rabbit model., Arch. Ophthalmol. 127 (2009) 1321–6. doi:10.1001/archophthalmol.2009.253.

[89] J. Lai, K. Chen, G. Hsiue, Tissue-engineered Human Corneal Endothelial Cell Sheet Transplantation in a Rabbit Model Using Functional Biomaterials, Transplantation. 84 (2007) 1222–1232. doi:10.1097/01.tp.0000287336.09848.39.

[90] T. Sumide, K. Nishida, M. Yamato, T. Ide, Y. Hayashida, K. Watanabe, J. Yang, C. Kohno, A. Kikuchi, N. Maeda, H. Watanabe, T. Okano, Y. Tano, Functional human

corneal endothelial cell sheets harvested from temperature-responsive culture surfaces, FASEB J. 20 (2006) 392–394. doi:10.1096/fj.04-3035fje.

[91] K. Yamashita, E. Inagaki, S. Hatou, K. Higa, A. Ogawa, H. Miyashita, K. Tsubota, S. Shimmura, Corneal endothelial regeneration using mesenchymal stem cell derived from human umbilical cord, Stem Cells Dev. 27 (2018). doi:10.1089/scd.2017.0297.

[92] M. Kimoto, N. Shima, M. Yamaguchi, Y. Hiraoka, S. Amano, S. Yamagami, Development of a bioengineered corneal endothelial cell sheet to fit the corneal curvature, Investig. Ophthalmol. Vis. Sci. 55 (2014) 2337–2343. doi:10.1167/iovs.13-13167.

[93] J. Yoshida, S. Yokoo, A. Oshikata-Miyazaki, S. Amano, T. Takezawa, S. Yamagami, Transplantation of Human Corneal Endothelial Cells Cultured on Bio-Engineered Collagen Vitrigel in a Rabbit Model of Corneal Endothelial Dysfunction, Curr. Eye Res. 42 (2017) 1–6. doi:10.1080/02713683.2017.1351568.

[94] T. Mimura, S. Yamagami, T. Usui, Y. Ishii, K. Ono, S. Yokoo, H. Funatsu, M. Araie, S. Amano, Long-term outcome of iron-endocytosing cultured corneal endothelial cell transplantation with magnetic attraction, Exp. Eye Res. 80 (2005) 149–157. doi:10.1016/j.exer.2004.08.021.

[95] C. Shao, J. Chen, P. Chen, M. Zhu, Q. Yao, P. Gu, Y. Fu, X. Fan, Targeted transplantation of human umbilical cord blood endothelial progenitor cells with immunomagnetic nanoparticles to repair corneal endothelium defect., Stem Cells Dev. 24 (2015) 756–67. doi:10.1089/scd.2014.0255.

[96] C. Shao, Y. Fu, W. Lu, X. Fan, Bone marrow-derived endothelial progenitor cells: A promising therapeutic alternative for corneal endothelial dysfunction, Cells Tissues Organs. 193 (2011) 253–263. doi:10.1159/000319797.

[97] K. Zhang, K. Pang, X. Wu, Isolation and Transplantation of Corneal Endothelial Cell–Like Cells Derived from In-Vitro-Differentiated Human Embryonic Stem Cells, Stem Cells Dev. 23 (2014) 1340–1354. doi:10.1089/scd.2013.0510.

[98] E. Inagaki, S. Hatou, K. Higa, S. Yoshida, S. Shibata, H. Okano, K. Tsubota, S. Shimmura, Skin-Derived Precursors as a Source of Progenitors for Corneal Endothelial Regeneration., Stem Cells Transl. Med. 6 (2017) 788–798. doi:10.1002/sctm.16-0162.

Chapter II: DIFFERENT PATHWAY STRATEGIES FOR THE CONVERSION OF STEM CELLS INTO CORNEAL ENDOTHELIAL CELLS

Chapter II: Different pathway strategies for the conversion of stem cells into corneal endothelial cells

2.1. Introduction

Human corneal endothelial cells (HCEC) cannot divide *in vivo* as they are arrested in the G1-phase of the cell cycle, which results in a non-proliferative state [1]. Therefore, a significant loss of these cells results in corneal clouding and permanent loss of visual acuity. Nowadays, corneal transplantation is the main treatment for corneal endothelial diseases. However, there is a global shortage of corneal donors [2]. Therefore, cell therapy is needed in order to overcome this problem.

Massive production of HCEC from a small number of healthy and qualified donor tissues remains a challenge due to the limited regenerative capacity of HCEC [3]. In addition, cells from older donors grow slower, exhibit more heterogeneity and are more prone to senescence compared to those from younger donors [4,5]. Hence, producing a sufficient number of HCEC with the adequate phenotype and in large quantities remains a challenge.

For this reason, as a possible solution to this challenge, other cell sources with an undifferentiated phenotype may be used to promote the differentiation of stem cells into specific lineages related to corneal endothelial like cells. In this sense, cells such as fetal bone marrow-derived endothelial progenitor cells [6], cornea-derived precursors [7], embryonic stem cells (ESC) [8–10] and skin-derived precursors [11] have been differentiated into CEC. In general, defined protocols allowed the successful differentiation of the different stem cells, allowing the expression of the typical CEC markers and presenting similar morphology to native cells. To investigate its visual acuity, various groups transplanted these cells onto animal models and confirmed that transplanted corneas were able to maintain transparency and corneal thickness [6–8]. However, these methods presented some limitations as the need of an invasive technique and immune rejection [6–11]. Furthermore, the use of ESC has the implications of deeps ethical issues and their use should therefore be restricted [8–10].

Interestingly, recent strategies have been based on the replication of the natural formation of HCEC during embryogenesis. Among the different cell types, some stem cells have been

shown to have similar origin to that of HCEC. Of special interest are the NCSC, which have their origin in the neural crest (NC). NC is a transient group of cells generated during early development that give rise to a great diversity of cell lineages, such as HCEC [12,13]. The NC harbors a migratory and multipotent population of cells with high migration and self-renewal capacity [14]. Therefore, due to these characteristics, they are referred as neural crest stem cells (NCSC) [15–21]. Hence, a recent and powerful strategy has been based on the natural plasticity of CEC, which encouraged researchers to mimic the embryonic development of CEC by performing a two-step differentiation protocol [9,10]. First, cells were differentiated into neural crest stem cells (NCSC), and second, NCSC were differentiated into CEC. Differentiated CEC were able to express functional markers and similar morphology to native CEC. Nowadays, different strategies to generate NCSC from human ESC [21–24], induced pluripotent stem cells (iPSC) [17,25–27], skin [28] and gut [29] have been reported. Despite of the common strategies, different overall behaviors were observed depending on the cell origin. In the case of pluripotent stem cells, mainly ESC and iPSC, the differentiation process successfully generated NCSC and showed its differentiation potential into several cell types such as neurons, adipogenic, chondrogenic, osteogenic and smooth muscle cells. Surprisingly, for more specialized cells, such as mouse skin and gut cells, it was shown that cells were able to differentiate into NCSC and express NCSC typical markers, but they did not show a multipotential differentiation ability, as NCSC-derived cells were not able to form neurons [28,29].

Although these methods had promising results, they also presented a series of disadvantages such as ethical problems, immune reaction, bio-safety problems, long period of formation, potential genomic instability, teratoma formation or the need of an invasive and difficult technique for the isolation of adult cells [17,21–26,28,29].

Due to the great cost and limitations for the production of NCSC from the previously described cells, we have considered a novel cell source for their production. In this sense, dental pulp stem cells (DPSC), which like CEC derive from a cranial NC lineage, may be easily obtained using a non-invasive isolation technique that does not involve ethical issues [30]. DPSC present multi-lineage differentiation capacity and have successfully been differentiated into several cell types including bone, endothelial, hepatic and neural-like tissues and have been used in several clinical studies [31–39]. Moreover, DPSC have been

used for corneal regeneration [40,41]. More specifically, a previous report demonstrated that DPSC seeded on a contact lens and transferred into a human donor cornea were able to transdifferentiate and to regenerate corneal epithelium [41]. Another assay determined that DPSC could be differentiated into corneal stromal cells (keratocytes), as they both arise from NC, and differentiated cells expressed typical markers of keratocytes. Then, keratocytes-derived from DPSC were injected into a mouse cornea, showing the formation of functional keratocytes, which were able to maintain corneal transparency [40].

Therefore, as CEC and DPSC share the same embryonic origin, in this chapter we aimed to determine if DPSC could be differentiated into NCSC, which could be later differentiated into CEC.

2. 2. Materials & Methods

2.2.1. Cell culture

In this chapter, we were interested in studying the different possible pathways by which we can obtain NCSC that can be then successfully differentiated into CEC. For this purpose, our experimental tests and our hypothesis are based on the use of DPSC. Since the gold standard for the production of the NCSC are the iPSC, our intention is to compare the reprogramming of DPSC to fibroblasts, and to then compare the results with the direct conversion of the DPSC into NCSC. A scheme of the different cell types used are shown in Figure 2.1.

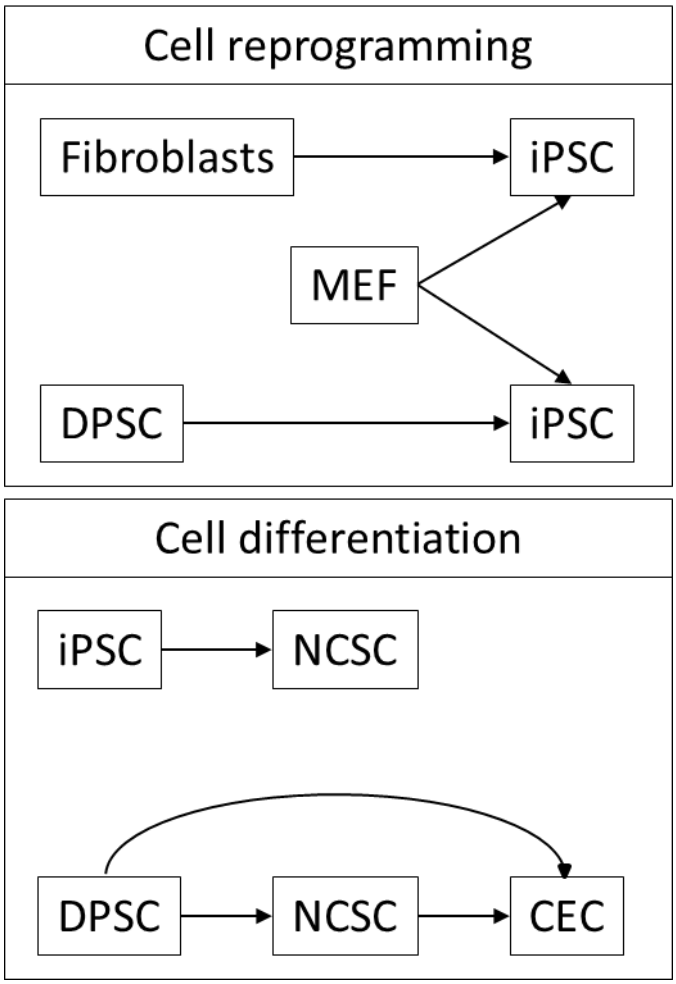

Figure 2.1. Scheme of the different cell types used for cell reprogramming and cell differentiation. Abbreviations: iPSC = induced pluripotent stem cells; MEF = mitotically inactivated mouse embryonic fibroblasts; DPSC = dental pulp stem cells; NCSC = neural crest stem cells; CEC = corneal endothelial cells.

For this purpose, we will initially describe how to culture both the DSPC and the fibroblasts, followed by their induction into iPSC and how this can be compared to the production of NCSC from DPSC. Finally, we will analyze different strategies that will guide the produced NCSC into CEC. Different cell culture media were used depending on the cell type, which are summarized in table 2.1.

Cell type	Medium Name	Components
DPSC	DPSC expansion	- DMEM HG - 10% FBS - 1% GlutaMAX - 1% P/S
Fibroblasts	Fibroblasts expansion	- DMEM HG

		- 10% FBS - 1% GlutaMAX - 1% P/S
	MEF expansion	- DMEM HG - 10% FBS - 0.1 mM MEM NEAA - 1% GlutaMAX - 1% P/S
iPSC	Reprogramming medium	- DMEM/F-12 - 20% KSR - 0.1 mM MEM NEAA - 1% GlutaMAX - 0.1 mM β-mercaptoethanol - 1% P/S - 4 ng/mL bFGF
	mTeSR-E8	Unknown (commercial)
	StemPro hESC SFM	Unknown (commercial)
CEC	CEC expansion	- DMEM HG - 10% FBS - 2 ng/mL bFGF - 0.1 mM β -mercaptoethanol - 1% GlutaMAX - 10 ng/mL heregulin beta - 10 ng/mL activin A - 200 ng/mL IGF-I - 1% P/S
	CEC commercial medium	NS (Celprogen serum-free medium)

Table 2.1. Cell culture media components of different cell types. Abbreviations: DPSC = dental pulp stem cells; iPSC = induced pluripotent stem cells; CEC = corneal endothelial cells; MEF = mouse embryonic fibroblasts; VTN = vitronectin; DMEM = dulbecco's modified Eagle's medium high glucose; FBS = fetal bovine serum; P/S = penicillin-streptomycin; KSR = knockout serum replacement; NEAA = non-essential aminoacids; bFGF = basic fibroblast growth factor; IGF-I: insulin growth factor 1; NS = not specified.

2.2.1.1. Dental Pulp Stem Cells

All experiments were performed with ethics approval from the Research Ethical Committee from the *Universitat Internacional de Catalunya*, under the project code BIO-ELB-2013-03 (supplementary data).

For the isolation of DPSC, healthy human third molars were extracted for orthodontic and prophylactic reason from 10 patients with ages between 14 and 18 years old. The teeth were then washed with a gauze soaked in 70% ethanol, followed by a second wash with

distilled water. The apices were opened fracturing the teeth and the dental pulp was extracted using a sterile nerve-puller file 15 and forceps. The dental pulp was then placed in falcon tubes that contained 1X phosphate-buffered saline (PBS) (Sigma-Aldrich) with 5% of 0.25% trypsin-EDTA (Thermo Fisher Scientific) and 1% Penicillin-Streptomycin (Thermo Fisher Scientific).

Samples were transferred to the laboratory and they were digested with 3 mg/mL collagenase type 1 (Sigma-Aldrich) at 37ºC for 60 minutes. Disaggregated dental pulps were washed twice with PBS and the tissue extracts were then cultured in DPSC expansion medium in culture flasks, at 37ºC in a 5% CO_2 incubator. The medium was changed every 2-3 days. When the cells reached 70% confluence, they were detached using TrypLE™ Express Enzyme (Thermo Fisher Scientific) and re-plated at a cell density of 2 x 10^3 cells/cm^2 or used for experiments.

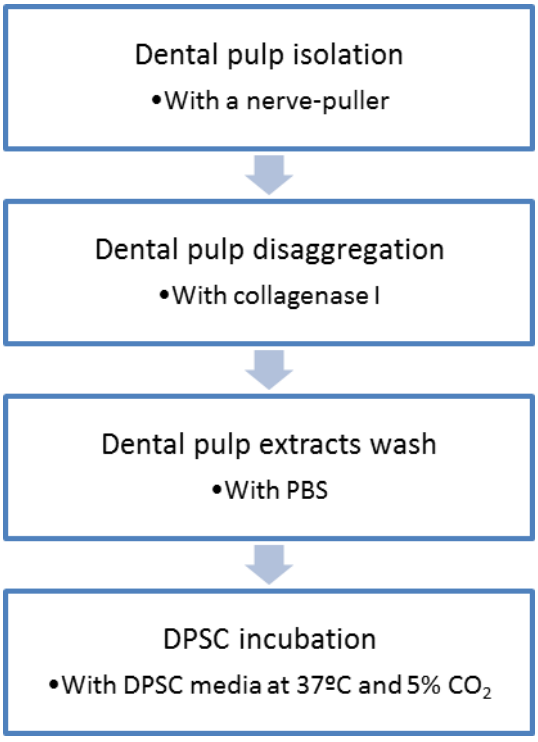

Figure 2.2. Flow chart of DPSC isolation. Initially, dental pulp is extracted from third molars with a nerve-puller. Then, disaggregation occurs and dental pulp extracts are washed twice with PBS. Finally, DPSC are plated in culture flasks and incubated at 37ºC, 5% CO_2, for at least one week.

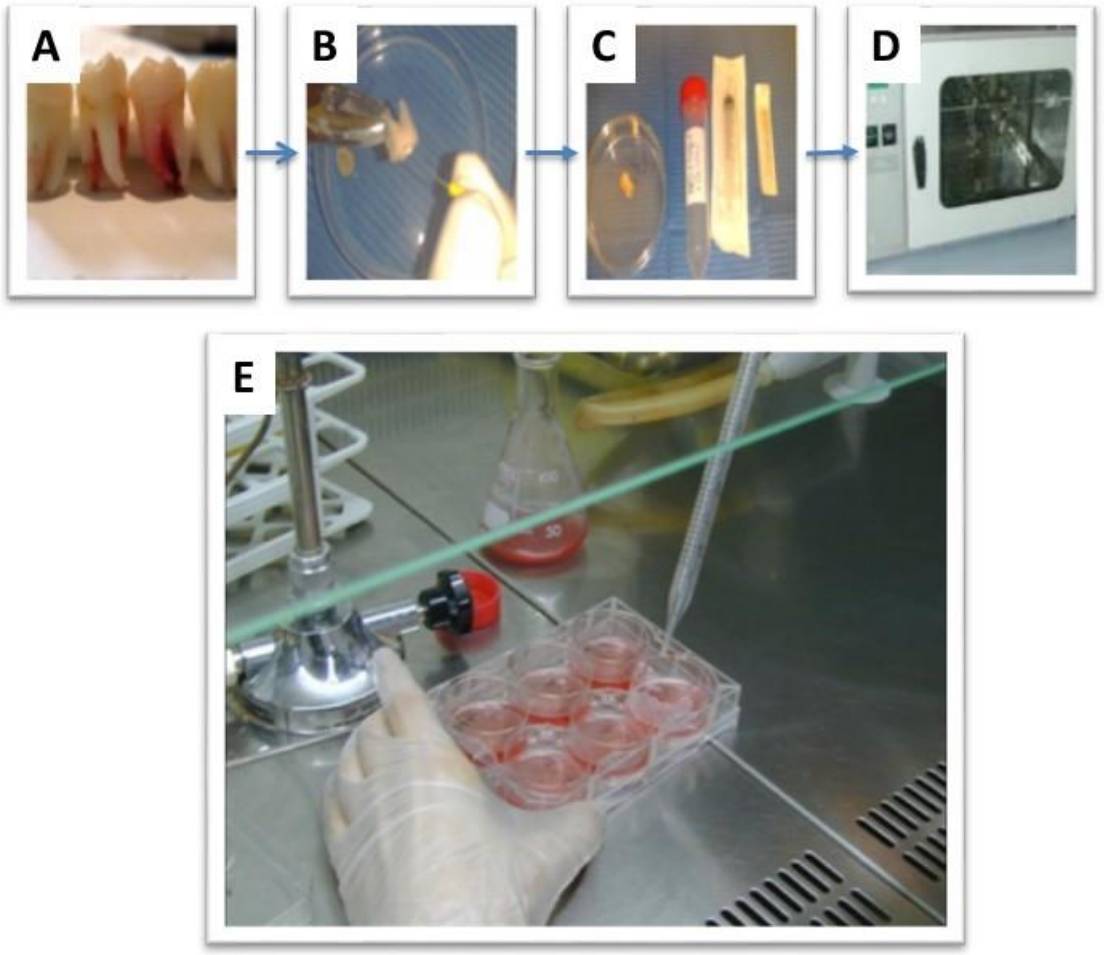

Figure 2.3. Scheme of DPSC isolation. A) Third molars were extracted for prophylactic reasons. B) Dental pulp tissue was extracted with a nerve-puller. C) Dental pulp disaggregation with collagenase IV and extracts were washed with PBS. D) Dental pulp extracts were cultured at 37ºC in 5%CO_2 incubator. E) Media is changed 3 days post-isolation.

2.2.1.2. Human fibroblasts

Human dermal fibroblasts (kindly donated by the Center for Applied Medical Research, University of Navarra) were expanded for the generation of iPSC. They were cultured in fibroblast expansion medium and the medium was changed every 2-3 days. When the cells reached 80% confluence, they were detached using TrypLE™ Express Enzyme (Thermo Fisher Scientific) and re-plated at a cell density of 3 x 10^3 cells/cm^2 or used for experiments.

2.2.1.3. Induced pluripotent stem cells production

IPSC are generally made from fibroblasts, since it is an easily accessible cell type that can be obtained in high cell populations and proliferates at high rates. These fibroblasts need to be

reprogrammed by the induction of the Yamanaka factors into iPSC. Since this is the gold standard procedure, and taking into account that we are using DPSC for the direct conversion into NCSC, we were interested in comparing the induction with the Yamanaka factors using both populations, fibroblasts and DPSC.

Step 1: Transduction efficiency of the reprogramming system

Four donors of DPSC and fibroblasts (as a positive control) were used for the formation of iPSC, as shown in table 2.2.

DONOR	AGE	GENDER	THIRD MOLAR
DPSC 1	14	Female	18, 28, 38, 48
DPSC 2	16	Female	18, 28, 38, 48
DPSC 3	16	Male	38
DPSC 4	16	Male	38,48

Table 2.2. DPSC donor information. Specifications of age, gender and extracted third molar, being 18 superior right, 28 superior left, 38 inferior left and 48 inferior right.

Cells were reprogrammed using the CytoTune ™ Reprogramming System (Non-integrating Viral Vector) [42]. This system uses non-integrative vectors based on the Sendai virus, which remains on the cytoplasm of the host cells. This guarantees their safety and applicability since they can be eliminated from cells with the successive passages. The vectors used in the kit express the four Yamanaka factors (Oct4, Sox2, Klf4, and c-MYC) necessary for the reprogramming of any somatic cell to iPSC [43]. Before starting the reprogramming experiment, the efficiency of transduction of DPSC was validated. Therefore, the reprogramming kit contains a vector which integrates emerald green fluorescent protein (EmGFP). This fluorescent vector is necessary for the subsequent analysis of the process efficiency by a fluorescence microscopy.

Transduction efficiency

Firstly, the appropriate virus volume needed for the reprogramming was tested for DPSC cells with the CytoTune™ -EmGFP Sendai Fluorescence Reporter. For this reason, three multiplicities of infections (MOI), which corresponds to the ratio of virus per cell, were

tested: 1, 3 and 9. Moreover, diverse cell densities were also studied: 100 (low), 500 (medium) and 1000 (high) cells/cm^2. The titer of virus was lot-dependent.

$$Volume\ of\ virus\ (\mu L) = \frac{MOI\ \left(\frac{CIU}{cell}\right) x\ number\ of\ cells}{titer\ of\ virus\ \left(\frac{CIU}{cell}\right) x\ 10^{-3}(\frac{mL}{\mu L})}$$

To begin, DPSC cells were seeded 6 days before transduction on the different densities. For transduction efficiency, 48 hours post-transduction the expression of EmGFP of all the conditions was observed by fluorescence microscopy (JuLI, NanoEnTek Inc.). Non-transduced DPSC cells were used as negative control.

Step 2: Cell culture on vitronectin or feeder layer substrates

The cell reprogramming step needs to be performed on a substratum that enhances iPSC production and maintenance. In this sense, two viable options exists, being the production vitronectin (VTN)-coated well plates or a feeder layer.

Vitronectin coated well plates

The VTN-coated well plates were prepared as manufacturer's indications using a 250 µg/ml solution of Vitronectin XF (STEMCELL Technologies). Briefly, the commercial VTN solution was diluted with CellAdhere dilution buffer (STEMCELL Technologies) to obtain a final concentration of 10 µg/ml. Diluted VTN was used to coat Non-Tissue Culture-Treated 6-well Plates (STEMCELL Technologies) and left for 2 hours drying at room temperature. Then, excess of VTN was collected and well plates were gently washed with CellAdhere dilution buffer. Finally, cell medium was added to the plates.

Mitotically inactivated mouse embryonic fibroblasts

The mitotically inactivated mouse embryonic fibroblasts (MEF) were used as a feeder layer in pluripotent cultures and is necessary for the maintenance of undifferentiated iPSC cells. For this reason, mitomycin C was used to mitotically inactivate MEF as it inhibits cell proliferation, so cells remain viable but cannot replicate. Briefly, for the preparation of inactivated MEF, the cell line SNL 76/7 was used (Cell Biolabs) and cultured as indicated in the commercial protocol. Cells were cultured with MEF expansion medium and when cells reached 95% confluence, they were detached with 0.25% trypsin-EDTA (Thermo Fisher

Scientific) and they were transferred to tissue culture flasks at a density of 2 x 10^4 cells/cm^2 and placed in a 5% CO_2 incubator at 37ºC. To mitotically inactivate MEF, cells were cultured until they reached 90% of confluence. Cells were washed with PBS and 10 µg/mL mitomycin C (Sigma-Aldrich), which was resuspended in DMEM, was added. After 2 hours of incubation, cells were washed three times with PBS and mitomycin-treated SNL were detached and used for experiments.

DPSC of four patients at passage 5 and fibroblasts at passage 14 were plated in a 6-well plate at a cell density of 1000 cells/cm^2. After 6 days, the transduction of the four Yamanaka factors was performed. 24 hours after the transduction, the medium was replaced with fresh media to remove the reprogramming vector. The media was then changed every other day for both conditions. Seven days after the transduction, the transduced cells were plated on mitotically inactivated MEF dishes or in VTN-coated dishes in their medium.

Step 3: Colony picking

The day after, the medium was replaced with iPSC reprogramming medium and was changed every other day. After 14 days colonies started to emerge and, finally, 4 weeks after iPSC colonies were picked for their expansion. To detach iPSC colonies, collagenase type IV (Thermo Fisher Scientific) was added and when the edges of the colonies started to detach, collagenase was removed and fresh media was added. Then, single colonies were picked, slightly broken with a micropipette and re-plated in a 48 and 24-well plate. Moreover, colonies were passaged at a split ratio of 1:4 when 70-80% of the culture dish was covered or when colonies were larger than 700 µm.

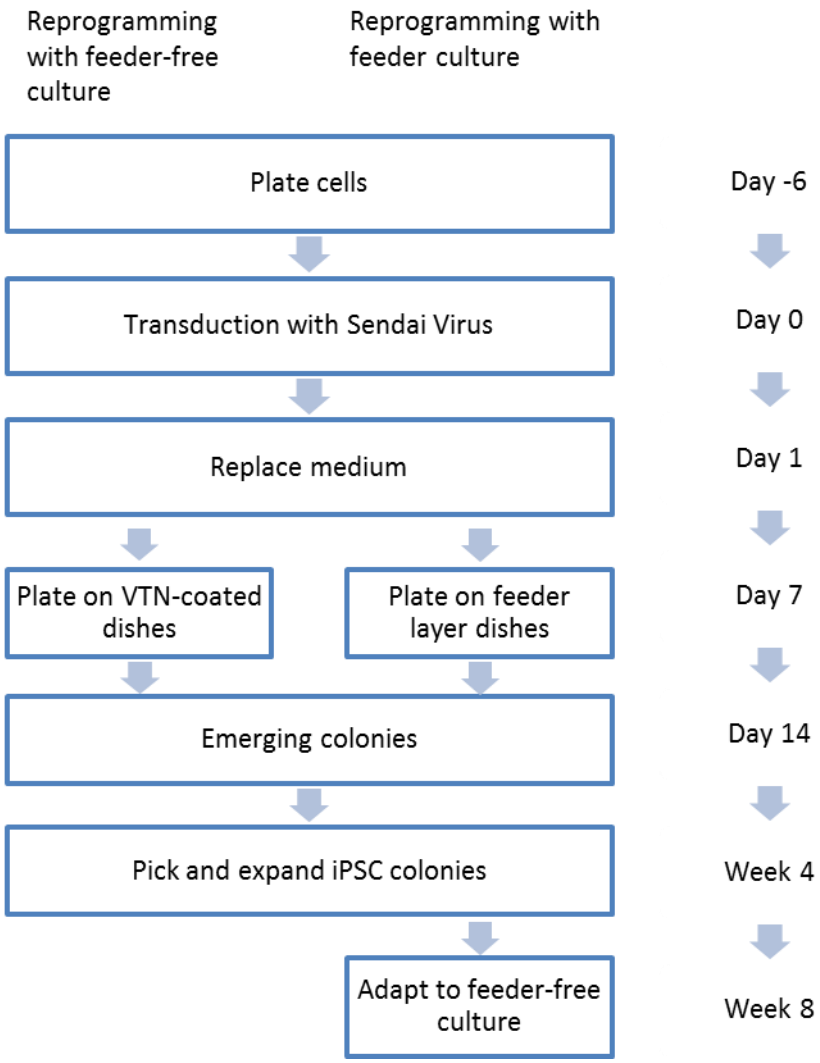

Figure 2.4. Flow chart of the cell reprogramming protocol. Firstly, cells were plated 6 days prior to transduction. Then, Sendai virus containing the four Yamanaka factors were added. 24 hours later, medium was fully replaced. 7 days post-transduction, transduced cells were plated on MEF or VTN-coated dishes. At day 14, colonies started to emerge. 4 weeks after transduction, colonies were passaged and expanded. Finally, 8 weeks later, iPSC cultured in feeder layers were adapted to feeder-free conditions.

Step 4: Adaptation to feeder free conditions (only MEF cultured iPSC)

Selected iPSC colonies initially cultured with feeder cells, after its optimization and expansion, were transferred to a feeder-free culture to obtain a consistent and a more reproducible cell population for future applications. For the adaptation to feeder-free and xeno-free conditions two different commercial coatings were used: Geltrex (Thermo Fisher Scientific) and Vitronectin (VTN) (STEMCELL technologies). This adaptation also required the use of xeno-free commercial media, named as fresh medium, and consisted of StemPro hESC SFM (Thermo Fisher Scientific) and mTeSR-E8 (STEMCELL technologies), respectively.

Prior to cell detachment, the new well plates were treated with Geltrex and VTN. In order to prepare the Geltrex well plates, Geltrex solution, which was at 15 mg/mL, was diluted with DMEM/F-12 to obtain a final concentration of 150 µg/mL. Diluted Geltrex was added to the dishes and incubated at 37ºC for one hour. Then, dishes were kept at room temperature for one hour and excess volume was gently aspirated. Then, cells with culture medium were added to the dishes. VTN was performed as previously described for the direct reprogramming process on feeder free culture.

For doing this, iPSC cells were detached as described above with collagenase IV and iPSC colonies were carefully picked, avoiding the edges to prevent fibroblast contamination, and small cell clumps were transferred into Geltrex and VTN-coated dishes. The medium was replaced in a progressive manner to increase the adaptation efficiency:

Day 1: 100% mitotically inactivated MEF expansion conditioned medium (MEF-CM)

Day 2: 75% MEF-CM + 25% fresh medium

Day 3: 50% MEF-CM + 50% fresh medium

Day 4: 25% MEF-CM + 75% fresh medium

Day 5: 100% fresh medium

2.2.1.4 Corneal endothelial cells

CEC were used for two main purposes. On the one hand, cells were used as conditioned cell culture media for the successful differentiation of NCSC into HCEC. On the other hand, cells were as well used as control populations to determine whether the final cell differentiation was successfully achieved. For this purpose, two different cell sources were used for the HCEC culture: isolate HCEC from donors and commercially available HCEC.

Isolation of human Corneal Endothelial Cells

All studies were adhered to the Declaration of Helsinki. Six human donor corneoscleral rims, non-transplantable for clinical reasons, were obtained from the Florida Lions Eye Bank (Miami, USA). Donor corneas were maintained in corneal preservation medium (Optisol) at 4ºC for less than 7 days before cell culture. Briefly, full cornea was rinsed with PBS. The iris was removed with tweezers to avoid contaminations from other cell types. Then, the

Descemet's membrane perimeter was delimitated with an 8-mm trephine. Finally, the Descemet's membrane with the corneal endothelium was gently removed with tweezers and digested at 37 ºC for 15 hours with 1 mg/mL of collagenase A (Roche) in CEC expansion medium as described by Sabater et al. [44]. Culture medium was changed every 2-3 days.

Commercial Corneal Endothelial Cells

Human Corneal Endothelial Primary cell culture was purchased from Celprogen and cultured as manufacturer's indications. Shortly, frozen vial was centrifuged at 100g for 7 minutes and resuspended in commercial medium. All cells were plated in a T25 pre-coated culture flask (Celprogen) and incubated at 37ºC, 5% CO_2. Medium was changed every 24-48 hours. When 95%cell confluence was reached, cells were detached using Cell Dissociation Media Xeno Free (Celprogen) and centrifuged. Then, cells were re-plated in pre-coated culture flasks at a cell density of 1 x 10^4 cells/cm^2 or used for further experiments.

2.2.2. Cell differentiation

To induce DPSC differentiation into CEC, different induction methods were evaluated. The common strategies in all of them is that initially pluripotent cells need to be derived into NCSC, which can then be differentiated into CEC [9,10,45].

Based on previous works and based on the fact that dental pulp stem cells have the same origin as NCSC, we have designed different strategies. No previous work has directly obtained NCSC or HCEC from DPSC and hence this work may represent a great novelty, since it may reduce the cost and the time. We have adapted similar protocols used for other cell types to these cells to validate our different strategies. On the one hand, we have designed different pathways for the production of NCSC derived from DPSC. On the other hand, once these NCSC were successfully induced, we designed two different pathways to form the final HCEC. A summary of the proposed pathways compared to the existing gold standard are shown in Figure 2.5.

First Step: NCSC induction methods

1. Adherent culture [17].
2. Neurosphere formation (in suspension method). It is hypothesized that suspension culture may enhance NCSC formation. For this purpose, initially a suspension

induction methods was initially tested (2.1), followed by an adherent culture system (2.2) [20,26].

3. Embryoid body formation. The third induction method was to generate more undifferentiated cells by the formation of embryoid bodies (EB), which is a cell culture system that mimics early human embryogenesis [46]. The intention was to increase the levels of pluripotency by enhancing the cell to cell interactions and to hence mimic more the iPSC cells in order to enhance the differentiation into the neurospheres. Later, EB were differentiated into NCSC on suspension culture.

Second step: CEC induction methods

A. One-step or direct differentiation. CEC differentiation from DPSC using a protocol which had been previously reported to generate *in vitro* CEC [47].

B. Two-step differentiation. CEC differentiation from NCSC-derived from DPSC. This is the first attempt, as previous research has mainly been based on the generation of CEC from NCSC-derived from pluripotent stem cells [10,48].

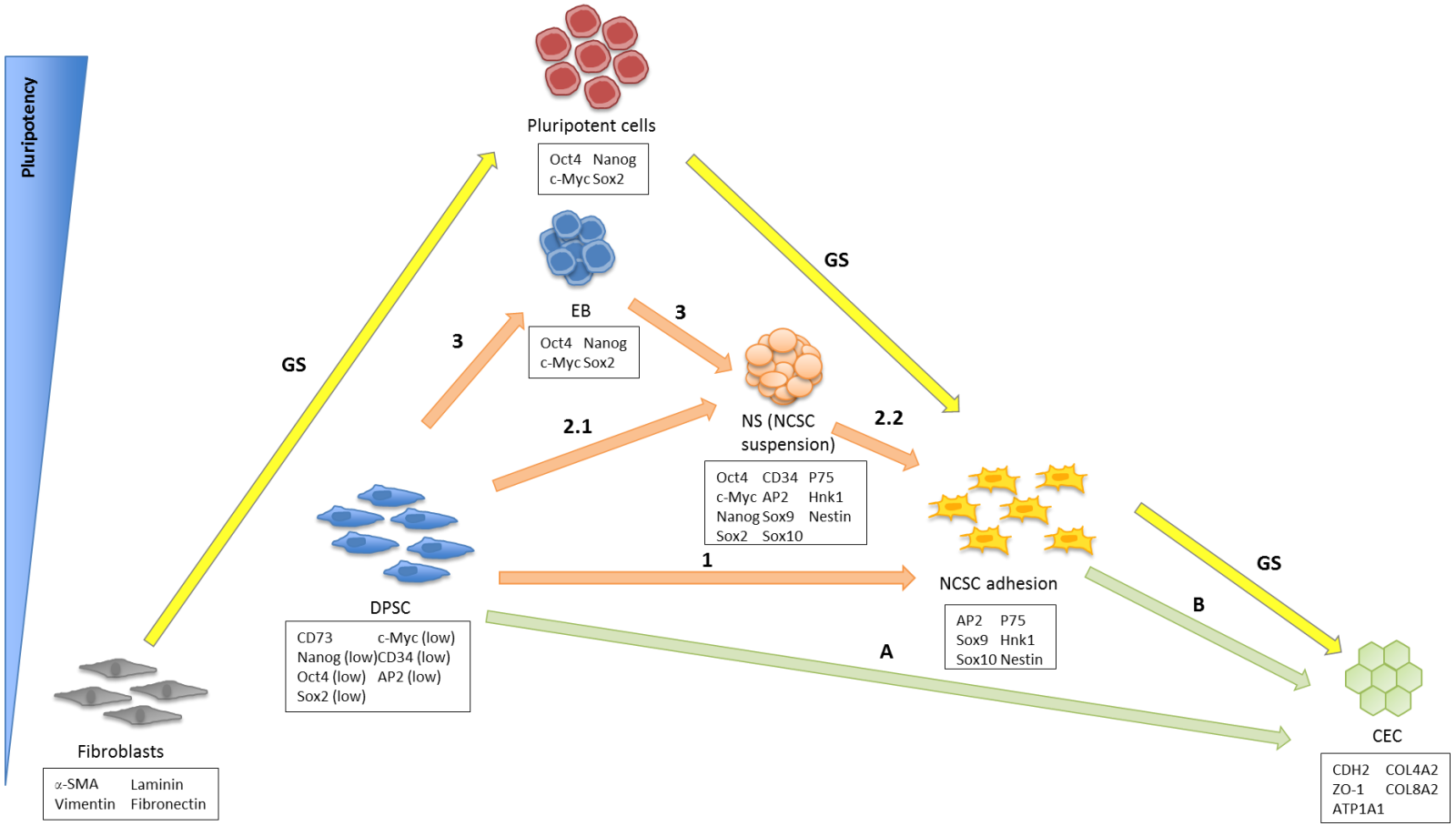

Figure 2.5. Scheme of CEC differentiation process from DPSC. DPSC were differentiated into NCSC trying 3 induction methods (orange arrows).DPSC were differentiated into CEC using 2 induction methods (green arrows). The GS for the generation of CEC uses NCSC differentiated from pluripotent cells obtained from fibroblasts (yellow arrow). Main characteristic markers are shown for each cell type [14,16,22,24,25,67–69,71–73]. Abbreviations: GS = gold standard; DPSC = dental pulp stem cells; EB = embryoid bodies; NS = neurospheres; NCSC = neural crest stem cells; CEC = corneal endothelial cells.

For the generation of NCSC and CEC, different culture media were used depending on the differentiation process. Table 2.3 summarizes the components of these differentiation culture media.

Differentiation	Medium name	Components
NCSC	Induction medium	- DMEM-F12 - 1X B-27 supplement - 1X N-2 supplement - 20 ng/mL EGF - 20 ng/mL bFGF - 5 ng/mL heparin - 2 mM Ala-Glu
CEC	One-step differentiation medium A1	- MEM - 1% BSA - 1 µM RA - 1 ng/mL TGF-β2 - 10 µM ROCK inhibitor
	One-step differentiation medium A2	- MEM - 1% BSA - 1 µM GSK3 inhibitor - 40 ng/mL bFGF - 10 µM ROCK inhibitor.
	Two-step differentiation medium B1	Conditioned medium from Commercial CEC
	Two-step differentiation medium B2	Conditioned medium from isolated CEC

Table 2.3. Neural crest stem cells (NCSC) and corneal endothelial cell (CEC) differentiation media. Abbreviations: DMEM = Dulbecco's modified Eagle's medium; EGF = epidermal growth factor; bFGF = basic fibroblast growth factor; Ala-Glu = L-alanyl-L-glutamine; BSA = bovine serum albumin; RA = retinoic acid; TGF-β2 = transforming growth factor - β2; GSK3 = glycogen synthase kinase 3.

2.2.2.1. Neural crest stem cells differentiation

To induce DPSC differentiation into NCSC different strategies were evaluated.

Adherent culture

Our first strategy for NCSC differentiation was modified from the protocol of Menendez et al. [17], which cultured iPSC in a NC induction medium on adherent plates. Therefore, iPSC reprogrammed from DPSC were used as a positive control. Once DPSC differentiation to NCSC showed similar results to iPSC, further experiments were only performed with DPSC.

Initially, DPSC at passage 7 and different cell densities (0.5 x 10^3 cells/cm^2; 0.5 x 10^4 cells/cm^2; 10^4 cells/cm^2 and 2 x 10^4 cells/cm^2) were used for the differentiation to NCSC. Cells were cultured in NCSC induction medium for 21 days. Culture medium was changed every 2-3 days. Total RNA was extracted for further analysis. A scheme can be observed at Figure 2.6. Cell differentiation and gene expression analysis will be explained in the following section 2.2.3.

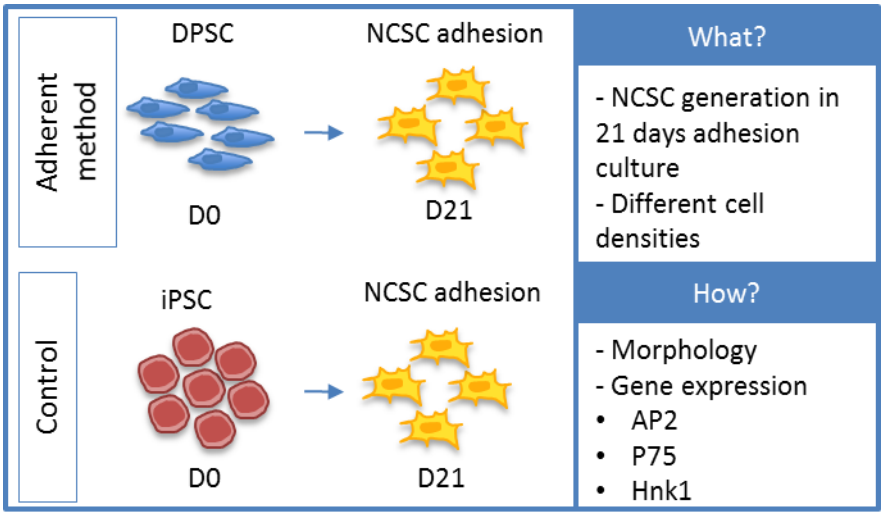

Figure 2.6. Scheme of NCSC adherent method. On the left, diagram of the experimental design. On the top right, hypothesis and experimental conditions. On the bottom right, confirmation analysis performed for NCSC differentiation.

Neurospheres formation (suspension method)

Induction of NCSC from DPSC cells can also be done through the formation of floating clusters named as neurospheres (NS) in suspension culture, followed by an adhesion culture phase. Previous researchers have described similar strategy using different cell types [20,26]. DPSC and iPSC-derived from DPSC were cultured with NC induction medium at a cell density of 2 x 10^4 cells/well in suspension in 24-well plates (Greiner) for 10 days to form NS. At day 10, NS were transferred to 6-well plates pre-coated with 5 µg/mL fibronectin (Thermo Fisher Scientific), where cells were able to attach, using the same NC induction medium for 4 more days. A scheme can be observed in Figure 2.7.

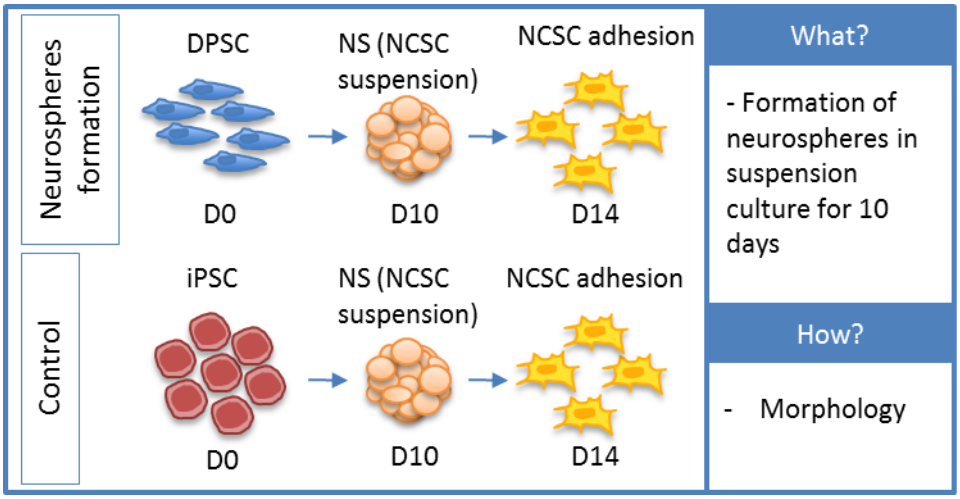

Figure 2.7. Scheme of neurospheres formation method. On the left, diagram of the experimental design. On the top right, hypothesis. On the bottom right, confirmation analysis performed for NCSC differentiation.

Since NS were formed at lower time points and in order to analyze their ability to increase the NCSC gene expression in the suspension system, DPSC were cultured in NC induction medium on ultra-low adhesion 24-well plates (Corning). As NS were formed from day 1 of differentiation, cells were cultured for 4 days to reduce the time and cost associated to the differentiation process. Based on preliminary results, iPSC were not use for further experiments. For analysis, protein and RNA of NS were analyzed every day to determine the optimal day of differentiation, as shown in Figure 2.8.

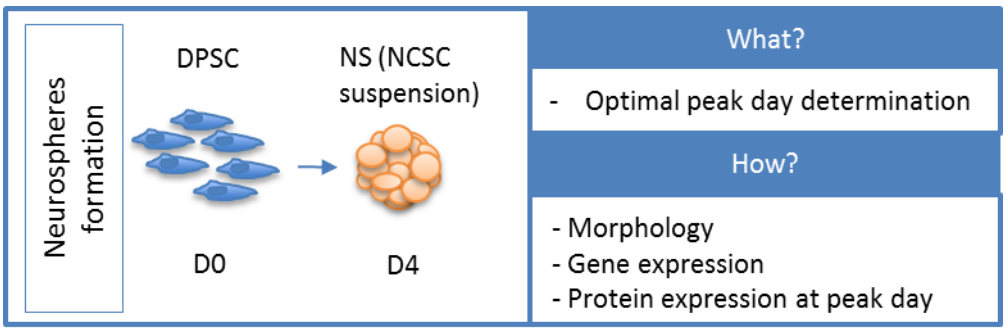

Figure 2.8. Scheme of neurospheres formation method for the optimal day determination. On the left, diagram of the experimental design. On the top right, experimental conditions. On the bottom right, confirmation analysis performed for NCSC differentiation.

Once optimal peak day was determined, NS were plated and expanded in adhesion conditions in order to obtain high amounts of NCSC for the differentiation into CEC. Therefore, DPSC were cultured in suspension culture with NC induction medium for 4 days

to form NS. Then, NS were plated in fibronectin-coated dishes and cultured in NC induction medium for 15 days more. A diagram can be observed in Figure 2.9. Finally, RNA and protein expression was observed at 0, 4, 12, 15 and 19 days of differentiation.

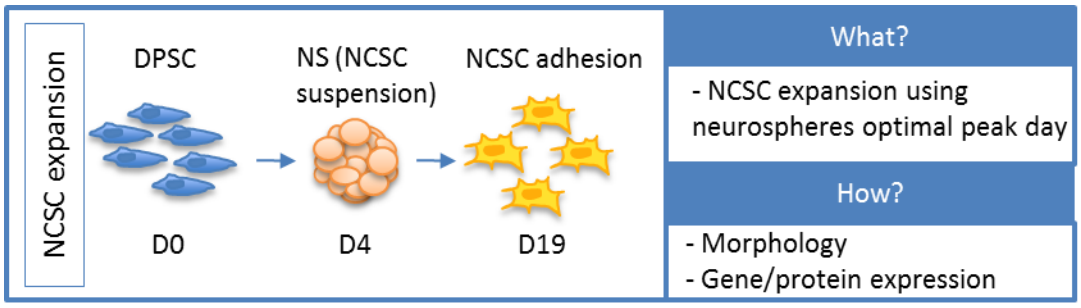

Figure 2.9. Scheme of NCSC expansion, using the optimal peak day. On the left, diagram of the experimental design. On the top right, experimental conditions. On the bottom right, confirmation analysis performed for NCSC differentiation.

Embryoid body formation

Brickman et al. reported that the formation of embryoid bodies (EB) spontaneously stimulated a process known as gastrulation, which occurs during the first week of human embryogenesis [49]. Based on a previous protocol, our next hypothesis was that the formation of EB should enhance the differentiation process [16].

Therefore, DPSC were cultured in AggreWell™ plates (STEMCELL technologies) with DPSC medium for 10 days for EB formation. Then, EB were transferred to 24-well ultra-low adhesion plates and were cultured in NC induction medium for 4 days. The results were compared to the suspension method to obtain the NS at 4 days. Finally, total RNA was analyzed to confirm the differentiation process, as shown in Figure 2.10.

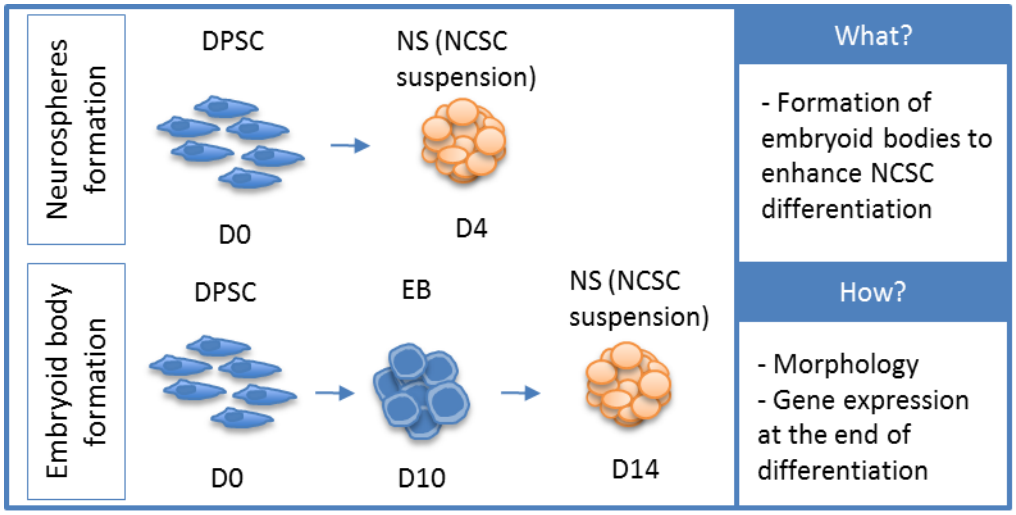

Figure 2.10. Scheme of neurospheres formation and embryoid body formation method. On the left, diagram of the experimental design. On the top right, hypothesis. On the bottom right, confirmation analysis performed for NCSC differentiation.

2.2.2.2. Corneal endothelial cell differentiation

Diverse induction methods were tried for the generation of *in vitro* CEC. Therefore, different culture media and initial cell type were used during the optimization process.

One-step differentiation of selected DPSC populations

Hatou et al. successfully generated CEC from corneal-stromal progenitor cells [7]. Therefore, as corneal stromal cells and DPSC present the same embryonic origin [13], our first strategy was to perform a direct differentiation from DPSC into CEC. As previous reports used defined and non-defined media for the differentiation process, we tried both media for the formation of CEC with optimal characteristics [6,45,47].

To begin, we used a defined differentiation medium which had been previously described to generate CEC from corneal stromal cells [47]. Prior to cell differentiation, we separated a population of DPSC that was CD73-negative, as it has been previously reported that CD73-negative population enhanced the functional expression and hexagonal morphology of CEC during HCEC culture [50]. For this, MiniMACS™ columns (Miltenyi Biotec) were used. These columns contain a powerful magnet that retains labeled cells with specific MACS MicroBeads (Miltenyi Biotec). Cells were separated following the manufacturer's protocol. Briefly, 1 x 10^6 cells were centrifuged at 300g for 10 minutes and resuspended with 98 µL of buffer (1X PBS, 0.5% BSA and 2 mM EDTA) and 2 µL of antibody CD73-PE MACS MicroBeads

(Miltenyi Biotec). Cells were incubated at 4ºC in the dark for 10 minutes. Then, cells were washed with buffer solution, followed by resuspension in 500 µL of buffer. Cells were finally separated through a MS Column. The MS Column was washed three times with buffer solution and all the flow-through were collected for unlabeled cells (CD73-negative). Finally, the MS Column was removed from the magnetic field of MACS Separator and placed on a new collection tube. The MS Column was washed with 1 mL of buffer and labeled cells (CD73-positive) were collected. Cell separation was confirmed by analysis with a flow cytometer (FACS).

For CEC one-step differentiation process, a modification of a previous protocol [47], which generated HCEC from corneal stromal cells, was used. This protocol contained two induction media, the first medium (A1) induced NCSC formation and the second medium (A2) generated CEC. Briefly, selected cells were first cultured with the induction medium A1 for 2 or 5 days at a cell density of 1.5 x 10^4 cells/cm^2. Then, the medium was changed every 2-3 days until day 14 of differentiation with CEC induction medium A2. In parallel, selected DPSC were cultured for 14 days with only differentiation medium A2. One-step differentiation is shown in Figure 2.11.

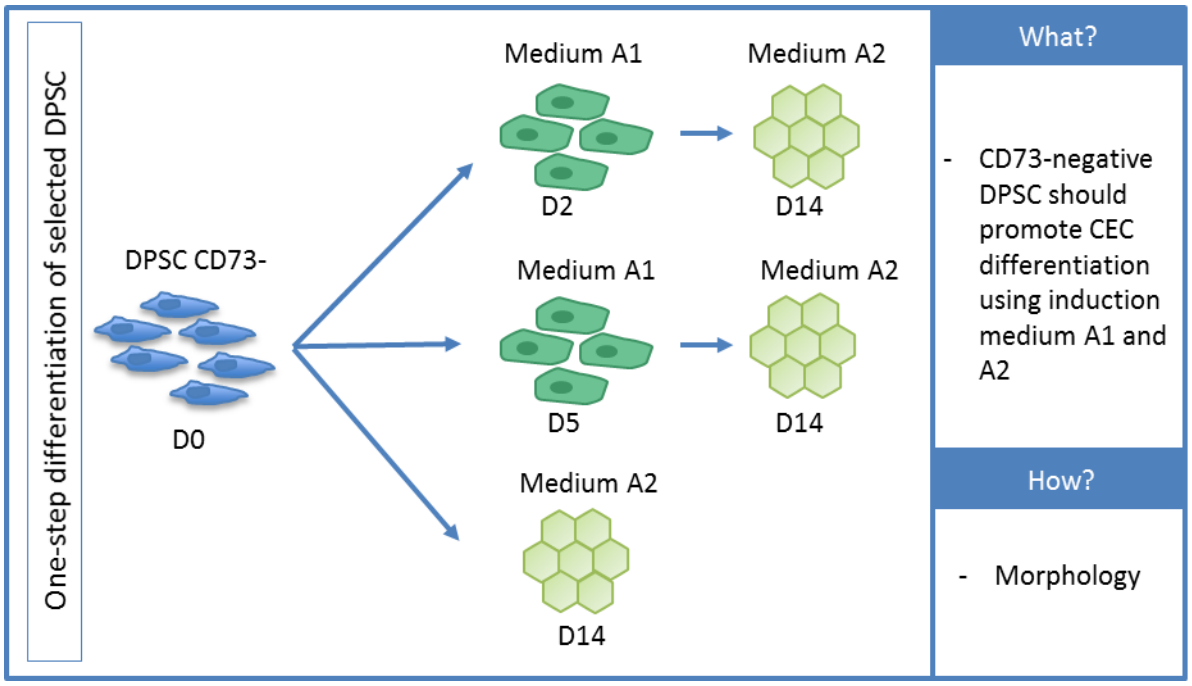

Figure 2. 11. Scheme of CEC induction method A. On the left, diagram of the experimental design. On the top right, hypothesis. On the bottom right, confirmation analysis performed for CEC differentiation.

Two-step differentiation

Previous reports have demonstrated that conditioned medium (Figure 2.14) enhanced cell differentiation [6,45]. Moreover, as CEC arises from NC during embryogenesis, some investigators generated CEC from NCSC [10,48]. Therefore, next induction method was to differentiate NCSC-derived from DPSC into CEC using two conditioned media, one from commercial HCEC and a second one from isolated HCEC. A scheme of the conditioned medium system can be observed in Figure 2.12.

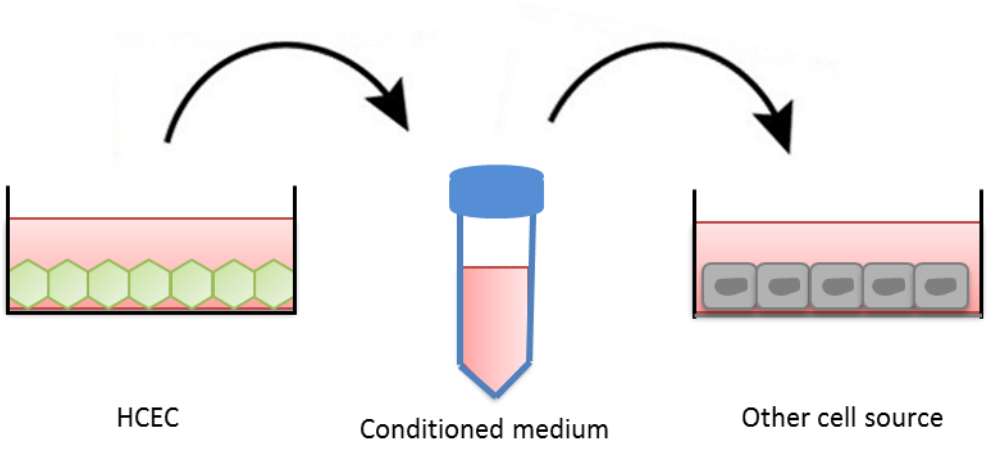

Figure 2. 12. Diagram showing HCEC conditioned medium system.

For the differentiation process, NCSC-derived from DPSC were cultured for 15 days in commercial conditioned medium (B1) or isolated conditioned medium (B2). Total RNA was isolated at days 0 and 15 of differentiation. A diagram of the differentiation is shown in Figure 2.13.

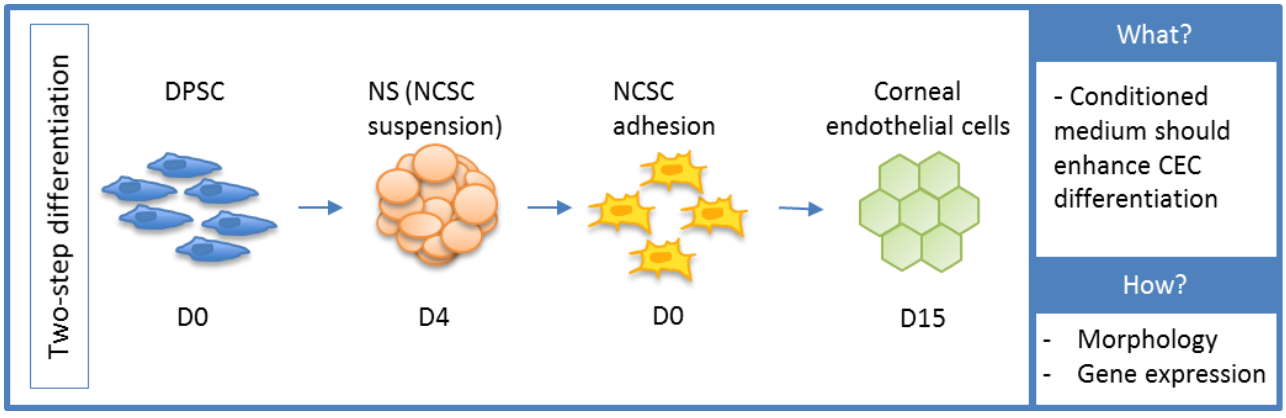

Figure 2. 13. Scheme of CEC two-step differentiation method using conditioned medium. On the left, diagram of the experimental design. On the top right, hypothesis. On the bottom right, confirmation analysis performed for CEC differentiation.

Commercial conditioned medium

Commercial CEC were cultured as described in section 2.2.1.5 and when cells reached 90% of confluence, conditioned medium was collected and stored at -20ºC. CEC differentiation medium B1 contained 50% of filtered (0.45 µm) conditioned medium to remove dead cells and 50% of fresh Celprogen medium, supplemented with 50 ng/mL bFGF and 10 µM of ROCK inhibitor.

Isolated conditioned medium

A conditioned medium from isolated HCEC was provided by the Bascom Palmer Eye Institute, University of Miami Miller School of Medicine. Firstly, human CEC were isolated from donor corneas and cultured with CEC medium, as described at section 2.2.1.5. Conditioned media was collected every 2-3 days and stored at -20ºC. Finally, CEC differentiation medium B2 was composed of 50% of filtered (0.45 µm) conditioned medium and 50% of fresh CEC expansion medium, supplemented with 50 ng/mL bFGF and 10 µM of ROCK inhibitor.

2.2.3. Cell analysis and characterization

2.2.3.1. Cell morphology imaging

As initial characterization technique, once cell culture end points were reached, cellular morphology was performed. For this purpose, samples were fixed with 4% paraformaldehyde (Sigma-Aldrich) for 20 minutes at room temperature. Then, cells were washed with PBS twice and permeabilized with 0.3% Saponin for 10 minutes at room temperature. At this stage, cells were observed by optimal microscopy (Olympus CKX41, Nikon) to observe the overall cell morphology and to verify their correct proliferation rate.

After this stage, immunofluorescence (IF) assay was performed, for which cells were washed three times with PBS, followed by blocking with Image-iT FX Signal Enhancer (Thermo Fisher Scientific) for 30 minutes at room temperature. After two washes with PBS, the primary antibodies (Table 2.4.) were added and incubated overnight, at 4ºC in the dark. Samples

were then washed twice with PBS and secondary antibody, in the case it was required, was added and incubated for one hour at room temperature in the dark. After two washes, cells were then counterstained with 1 μg/mL 4',6-diamidino-2-phenylindole (DAPI) for 5 minutes and then rinse twice with PBS. Then, samples were observed using an inverted fluorescence microscope with an epifluorescence attachment (Eclipse TS100; Nikon).

For the specific case of the NS, a slightly different protocol was used. For this purpose, NS were firstly embedded with O.C.T. Compound (Sakura) and frozen at -20ºC overnight and then at -80ºC for at least 24 hours. After, samples were cryosectioned (Cryotome SME, Thermo) and kept on super frost slides. The immunofluorescence staining was performed as described in the previous paragraph. For negative control, PBS was used instead the primary antibody.

Primary Antibody Against	Company	Cat. Number	Dilution	Secondary Antibody (dilution)
p75	Advanced Targeting Systems	AB-N07	1:200	Alexa Fluor 488 anti-mouse IgG (1:250)
Nestin	Merck Millipore	AB5922	1:1000	Alexa Fluor 555 anti-rabbit IgG (1:250)
Sox10	Chemicon, Millipore	AB5727	1:100	Alexa Fluor 555 anti-rabbit IgG (1:250)
Oct4	Santa Cruz Biotechnologies	sc-5279	1:100	Alexa Fluor 488 anti-mouse IgG (1:250)
Nanog	Genetex	GTX100863	1:100	Alexa Fluor 555 anti-rabbit IgG (1:250)

Table 2.4. List of antibodies used for immunofluorescence assays.

2.2.3.2. Genetic Stability by CGH

The genetic stability of iPSC cells was analyzed by short-Comparative Genomic Hybridization (short-CGH). Cell reprogramming is a process that may result in DNA damage and, subsequently, may end in genetic alterations or instability [51,52]. The detection of this instability is necessary for safety reasons with respect to tumorigenicity. This technique shows the detection of any chromosome difference between a sample DNA and a reference DNA in fragments larger than 10 Mb. Short-CGH was performed as described in Rius et al. [53] at the *Universitat Autònoma of Barcelona* (UAB).

Briefly, 15-20 single cells of each sample of iPSC were amplified with degenerate oligonucleotide-primed PCR (DOP-PCR). Afterwards, amplification products of the whole

genome were fluorescently labeled, in red for test samples DNA and in green for control reference DNA. Then, samples and reference DNA were mixed in equimolar proportions and precipitated with ethanol. Lastly, the hybridization was done with a normal male (46, XY) metaphase chromosome and the capture of 12 metaphases per sample was performed with an epifluorescence microscope. Finally, these captures were analyzed using Isis CGH software (Meta Systems).

2.2.3.3. Flow cytometry

One of our hypothesis was that the differentiation into CEC cells, using CD37-negative cells could provide an enhanced pathway for its proper differentiation. In order to confirm that our previous separation method was able to separate both cell population depending on the CD73 marker, fluorescence-activated cell sorting (FACS) was used to detect the different cell populations marked with the specific antibody. Briefly, cells were detached and the cell pellet was washed with PBS to avoid medium contamination. Then, at least 3 x 10^5 cells were blocked for 10 minutes at 4ºC in dark. The blocking was performed with anti-human phycoerythrin (PE)-conjugated anti-CD73 (Miltenyi Biotec) in a solution with PBS, 0.5% BSA and 2mM EDTA at a pH=7.2. Finally, cells were washed with PBS and 2% FBS before its measurement with a flow cytometer (FACS Calibur, BD Biosciences). Analysis was performed with WinMDI 2.8 software. IgG and non-stained cells were used as positive and negative control respectively.

The flow cytometer was as well used for the purpose of detecting the percentage of populations expressing a determined protein. In the case of iPSC generation, transduced cells already expressed a fluorochrome, the Emerald Green Fluorescent Protein (EmGFP), which was present in the vector. For this reason, the percentage of transduced cells (cells with EmGFP expression) was measured with a flow cytometer. The protocol used was similar as the protocol explained in the previous paragraph. Non-transduced cells were used as negative control.

2.2.3.4. Quantitative Real Time – Polymerase Chain Reaction (qPCR)

In order to verify the proper differentiation and that the different induction methods, gene expression was analyzed at each end time points as described in the previous section. Gene expression was analyzed by quantitative real time – polymerase chain reaction (qPCR). Shortly, total RNA was isolated using NucleoSpin RNA kit (Macherey-Nagel) including DNAse

treatment following the manufacturer's instructions. One µg of RNA with a ratio of intensities at the wavelengths of 260/280 nm between 1.8-2 was then reversed transcribed into cDNA using Transcriptor First Strand cDNA Synthesis Kit (Roche) according to the manufacturer's recommendations. Specific primers (Table 2.5) and FastStart Universal SYBR Green Master (Roche) were used to amplify the desired cDNA. Finally, the amplifications were performed in a CFX96 Real-Time PCR Detection System (Bio-Rad) for quantitative Real-Time PCR.

Gene	Primer	Sequence (5' -3')	Accession Number
Oct4	Forward	AGCGAACCAGTATCGAGAAC	NM_002701
	Reverse	TTACAGAACCACACTCGGAC	
Nanog	Forward	TGAACCTCAGCTACAAACAG	NM_024865
	Reverse	TGGTGGTAGGAAGAGTAAAG	
Sox2	Forward	GCCGAGTGGAAACTTTTGTCG	NM_003106
	Reverse	GGCAGCGTGTACTTATCCTTCT	
c-MYC	Forward	GGCTCCTGGCAAAAGGTCA	NM_002467
	Reverse	CTGCGTAGTTGTGCTGATGT	
Nestin	Forward	CTGCTACCCTTGAGACACCTG	NM_006617
	Reverse	GGGCTCTGATCTCTGCATCTAC	
p75	Forward	CCTACGGCTACTACCAGGATG	NM_002507
	Reverse	CACACGGTGTTCTGCTTGT	
Sox9	Forward	AGCGAACGCACATCAAGAC	NM_000346
	Reverse	CTGTAGGCGATCTGTTGGGG	
AP2	Forward	AGGTCAATCTCCCTACACGAG	NM_003220
	Reverse	GGAGTAAGGATCTTGCGACTGG	
CHD7	Forward	TGATGAGTCTTTTTGGCGAGG	NM_017780
	Reverse	CTGGATTTTCCGGGTAACCAC	
Sox10	Forward	CTGGACACTAAACCCCTGCC	NM_006941
	Reverse	CATGTGGACTGGGCTGCAGAC	
CD73	Forward	CCAGTACCAGGGCACTATCTG	NM_002526
	Reverse	TGGCTCGATCAGTCCTTCCA	
CD34	Forward	CTACAACACCTAGTACCCTTGGA	NM_001025109
	Reverse	GGTGAACACTGTGCTGATTACA	
ATP1A1	Forward	TGTGATTCTGGCTGAGAACG	NM_001160234
	Reverse	TGCTCATAGGTCCACTGCTG	
COL4A2	Forward	TAAGGGTGAAAAGGGTGACG	NM_001846
	Reverse	ACTGATCTGGGTGGAAGGTG	
COL8A2	Forward	GAACTGGACGGTTCTGTGGT	NM_003759
	Reverse	AATTGCCGAAAGAGCTTGAA	
CDH2	Forward	CCTGGAACGCAGTGTACAGA	NM_001792
	Reverse	TGGTTTGACCACGGTGACTA	
ZO-1	Forward	AGTTTGGCAGCAAGAGATGG	NM_001355015

	Reverse	GCTGTCAGAAAGATCAGGGA	
GAPDH	Forward	CTGGTAAAGTGGATATTGTTGCCAT	NM_002046
	Reverse	TGGAATCATATTGGAACATGTAAACC	
b-ACTIN	Forward	AGAGCTACGAGCTGCCTGAC	NM_001101
	Reverse	AGCACTGTGTTGGCGTACAG	

Table 2.5. List of primers used for cDNA amplification in quantitative RT-PCR.

2.2.3.5. Statistical analysis

Mann-Whitney U-test was carried out to reveal significant differences. Differences were considered statistically significant with P value of less than 0.05. The data are presented as mean ± standard deviation.

GraphPad Prism version 6 (GraphPad Software Inc.) was used to graph the data and statistical analyses were performed using Statistical Package for the Social Sciences (SPSS) 21 (IBM).

2.3 Results and discussion

2.3.1. Induced pluripotent stem cell generation

2.3.1.1. Transduction efficiency

As an initial experiment, DPSC were reprogrammed with three different multiplicities of infections (MOI) and three cell densities. As shown in Figure 2.14, when cells were cultured in low cell density, EmGFP expression was only observed in the highest level of MOI. On the other hand, at medium and high cell density, EmGFP expression (in green) was present in the three levels of MOI. In the case of medium cell density, the expression of EmGFP increased as the multiplicity of infection was also increased. All in all, at the highest cell density there were no differences between the medium and highest MOI, although at the lowest MOI the expression of EmGFP was lower. As expected, the negative control showed no expression as no transduction had been performed. For this reason, in order to use the less quantity of virus and to reduce costs, the multiplicity of 3 and highest cell density were chosen for the generation of iPSC.

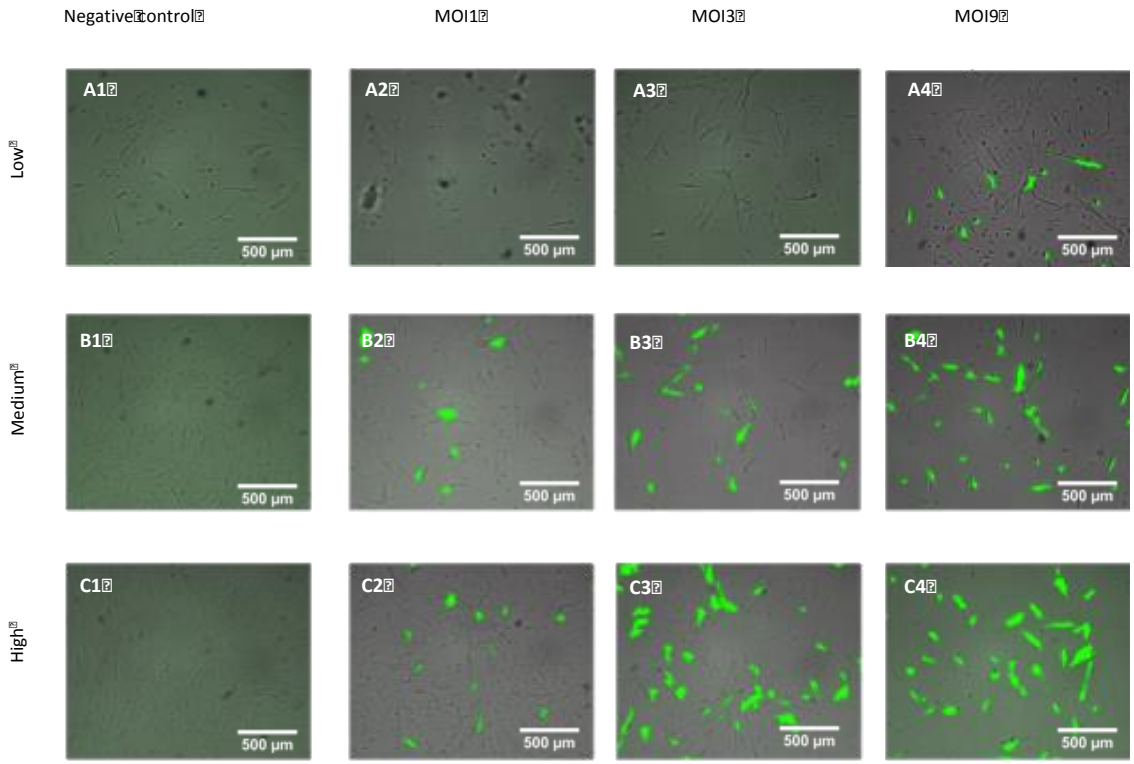

Figure 2. 14. EmGFP expression 48 hours post-transduction analyzed by fluorescence microscopy. Images of non-transduced (A1,B1,C1) and transduced (A2-A4,B2-B4,C2-C4) cells with three different MOI (1, 3 and 9). Three cell densities: low (A1-A4), medium (B1-B4) and high (C1-C4). Scale bars: 500 µm.

2.3.1.2. Cell reprogramming

Two days post-transduction of DPSC and fibroblast cells (positive control), EmGFP expression was observed in all transduced-cells by fluorescence microscopy (Figure 2.15). There was no expression in non-transduced cells, used as a negative control. Moreover, DPSC2 and 3 presented a very low cell density.

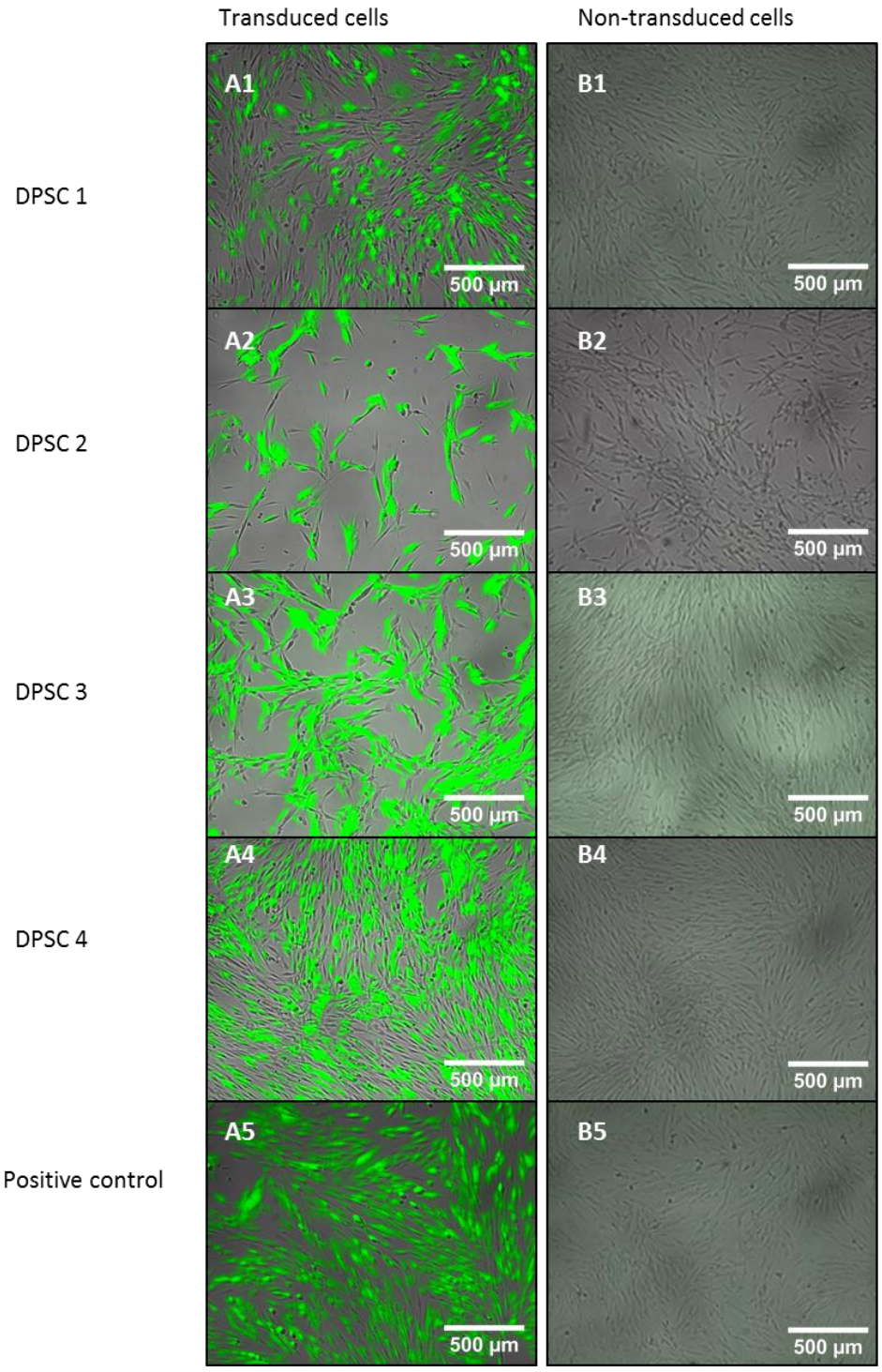

Figure 2.15. EmGFP expression 48 hours post-transduction of DPSC and positive control cells, observed by fluorescence microscopy. EmGFP expression of transduced (A1-A5) and non-transduced cells (B1-B5). Scale bars: 500 µm

In order to confirm the transduction efficiency, at day 6 post-transduction, cells were sorted using a flow cytometer by their EmGFP expression. The results showed that 3 out of 4 samples expressed very high levels of transduction, as shown by the expression of EmGFP

(DPSC2: 94.06%; DPSC3: 95.98%; DPSC4: 98.05%), which was very similar to the positive control (fibroblasts), which expressed 98.37% (Figure 2.16). Only in one of the cases, the results showed a lower transduction efficiency, as shown by the lower levels of EmGFP expression (DPSC1: 61.55%).

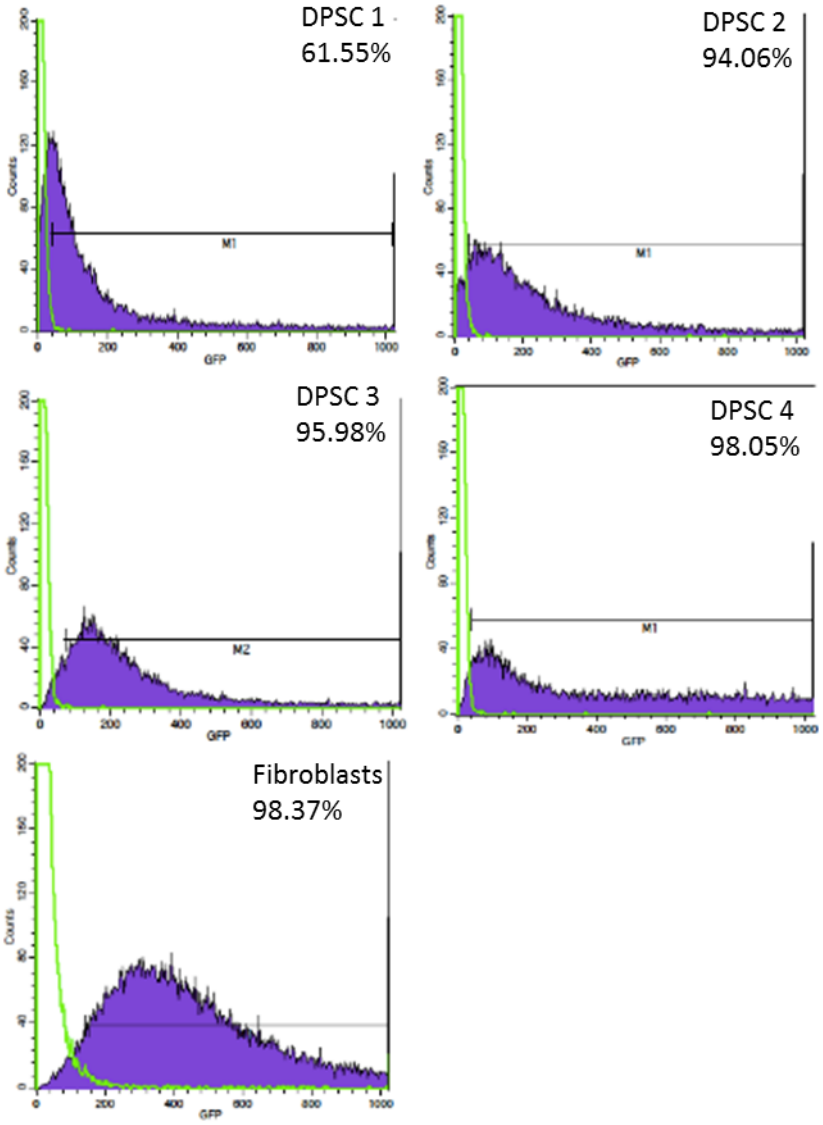

Figure 2.16. Transduction efficiency at day 6 post-transduction analyzed by FACS.

One week post-transduction, as shown in Figure 2.17, transduced-cells became larger and more aggregated, showing typical morphologies of iPSC, in comparison with non-transduced cells, which exhibited a spindle-like morphology. Furthermore, the number of cells in transduced-cells was lower than non-transduced cells. This is mainly related with the fact that virus transduction can result in more than 50% of cytotoxicity. It is also interesting to highlight the differences shown between the DPSC1 group and the other DPSC groups. As

was seen in the previous transduction efficiency section, this group presented lower levels of transduction. As can be seen in Figure 2.17, the number of cells appeared to be significantly higher than in the other DPSC groups, showing similar values to the non-transduced cells. Furthermore, cells also had a tendency to aggregate, but this was smaller than in the other DPSC groups.

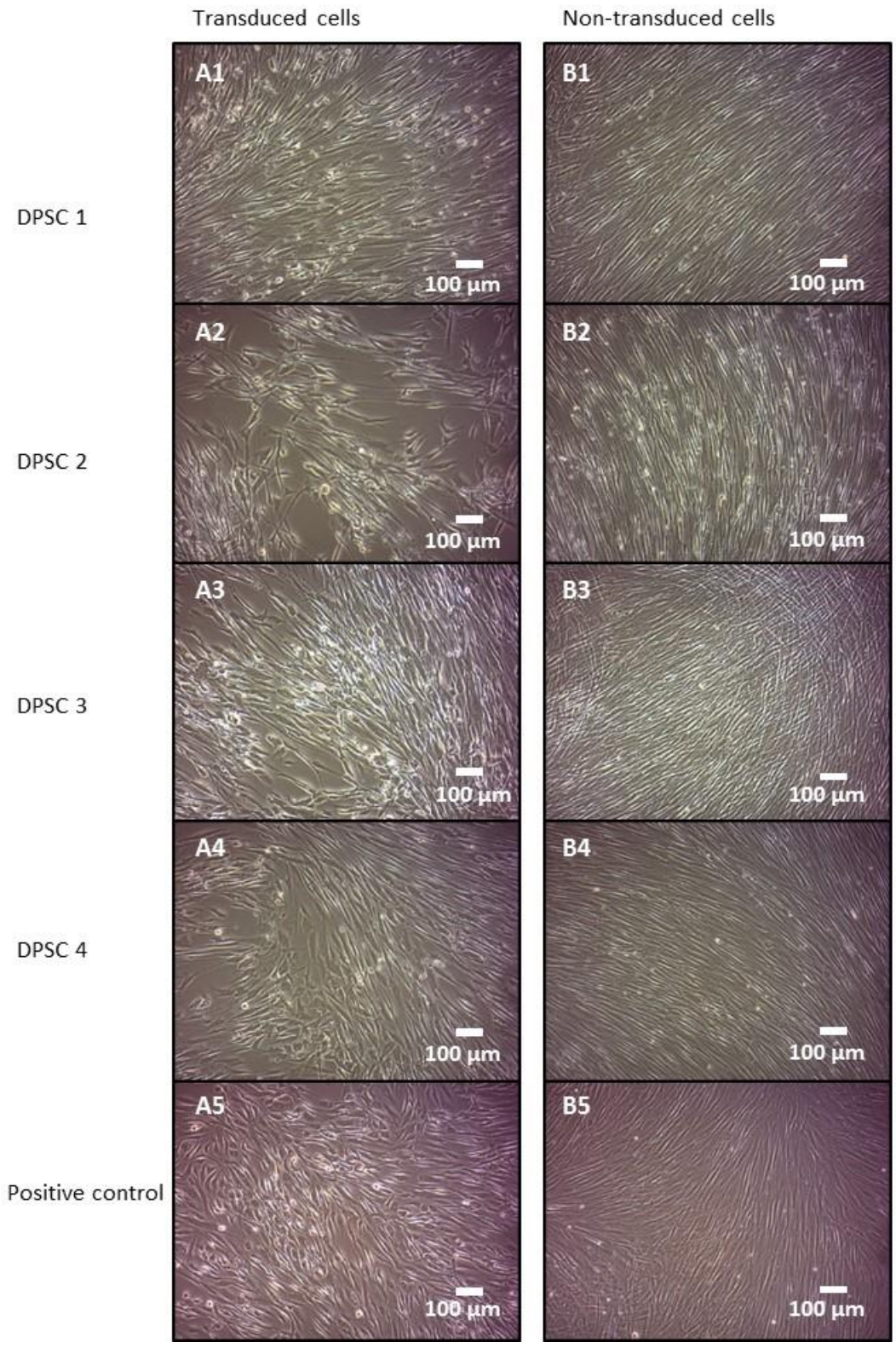

Figure 2.17. DPSC and positive control (fibroblasts) at day 7 post-transduction. Transduced cells (A1-A5) and non-transduced cells (B1-B5) were cultured in DPSC or fibroblast medium. Scale bars: 100 µm.

2.3.1.3. Culture optimization: feeder or feeder-free culture?

After three weeks of cell expansion, as expected, the fibroblasts (positive control) were able to form colonies in feeder conditions (Figure 2.18), validating our protocols and procedures. Interestingly, DPSC cells were able as well to form for colonies, although this was only observed for the DPSC1, 3 and 4 groups. Surprisingly, the DPSC 1 group that presented lower rates of transduction efficiency showed very similar results to DPSC 3 and 4.

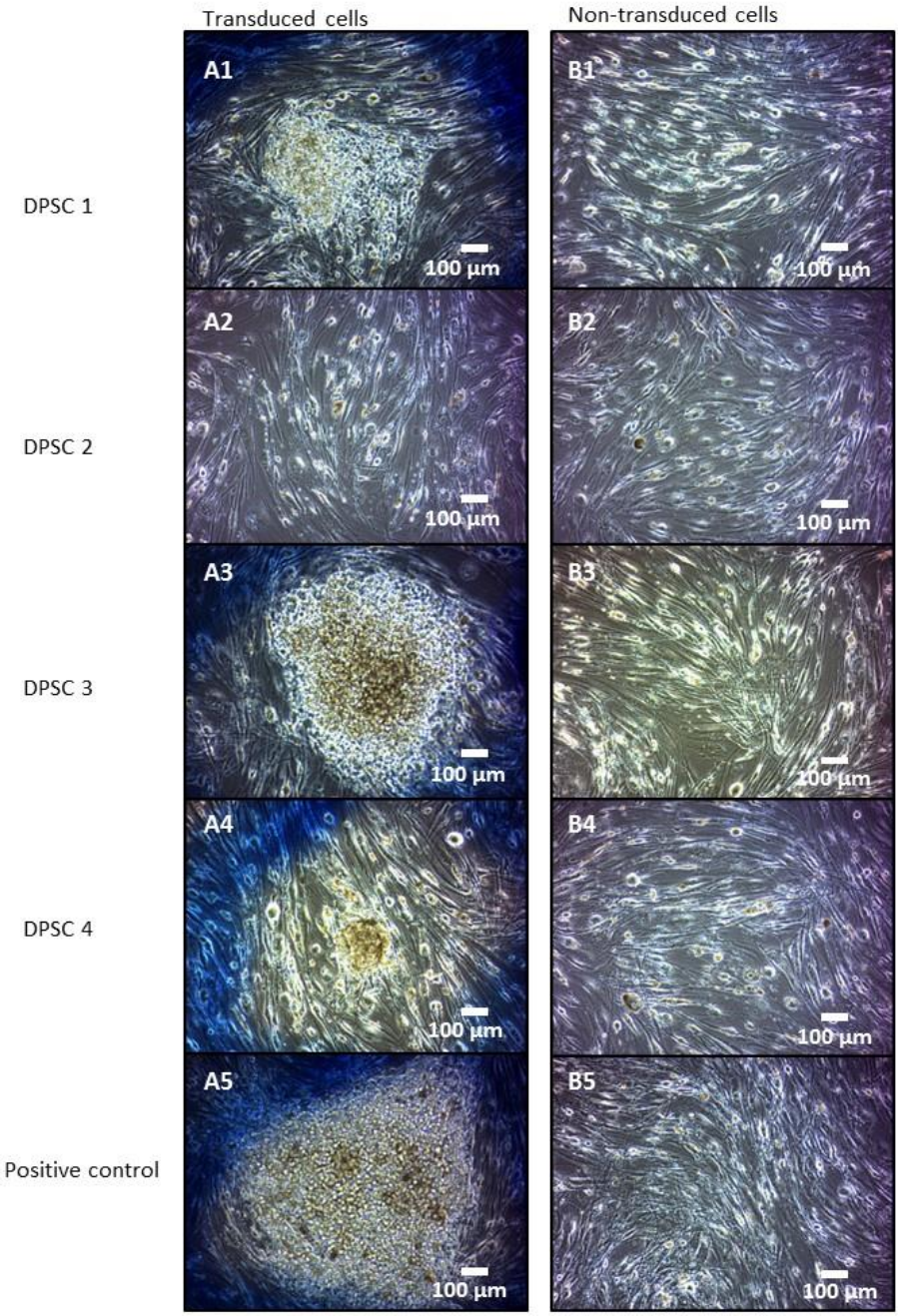

Figure 2.18. iPSC colonies formation from DPSC and positive control (fibroblasts) 3 weeks post-transduction. Transduced cells (A1-A5) and non-transduced cells (B1-B5) were cultured in iPSC medium in feeder conditions. Scale bars: 100 µm

We then repeated the same procedure on feeder free conditions, using VTN as the coating matrix (Figure 2.19). As expected, the fibroblasts (positive control) were able to form colonies, although colonies tended to have a significantly smaller size. Furthermore, none of the DPSC cells were able to form iPSC colonies. Therefore, since at least in the feeder conditions the different experimental groups were able to form the colonies except for the DPSC2, this group was not further used.

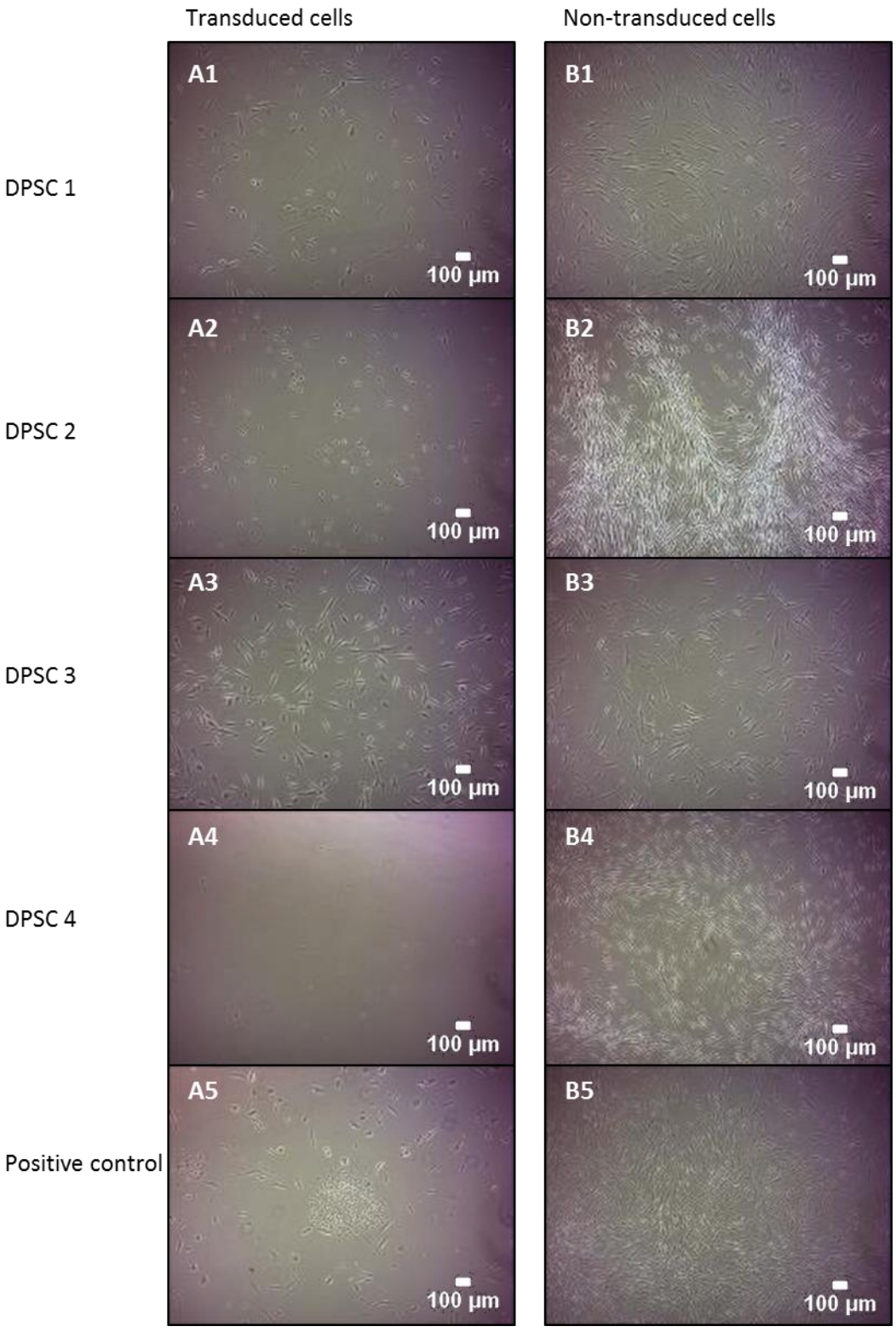

Figure 2.19. IPSC colonies formation from DPSC and positive control (fibroblasts) 3 weeks post-transduction. Transduced cells (A1-A5) and non-transduced cells (B1-B5) were cultured in iPSC medium in feeder-free conditions. Scale bars: 100 µm

In order to avoid the contamination of reprogrammed cells with fibroblasts when using feeder conditions, reprogrammed cells need to be transferred into feeder-free conditions. For this purpose and to ensure which coating material was optimum for the transfer of selected colonies from feeder conditions to feeder-free conditions, we compared the feeder conditions with two different feeder-free substrates: Geltrex and VTN. As can be observed in the microscopy images (Figure 2.20), only some cells of the colonies presented the flatter cobblestone-like characterized morphology of pluripotent stem cells. These cells were amplified and, the iPSC colonies in feeder conditions were finally transferred into Geltrex- and VTN-coated dishes (feeder-free dishes). In all the conditions, iPSC on VTN-coated dishes exhibited more pluripotent characteristic properties as cobblestone-like colonies and individual cells inside the colony with a high nuclear to cytoplasm ratio. In contrast, Geltrex presented some surrounding cells that presented different morphologies, which could be estimated to the fibroblasts from the feeder layer. For this reason, the culture and expansion of iPSC was performed on VTN-coated dishes.

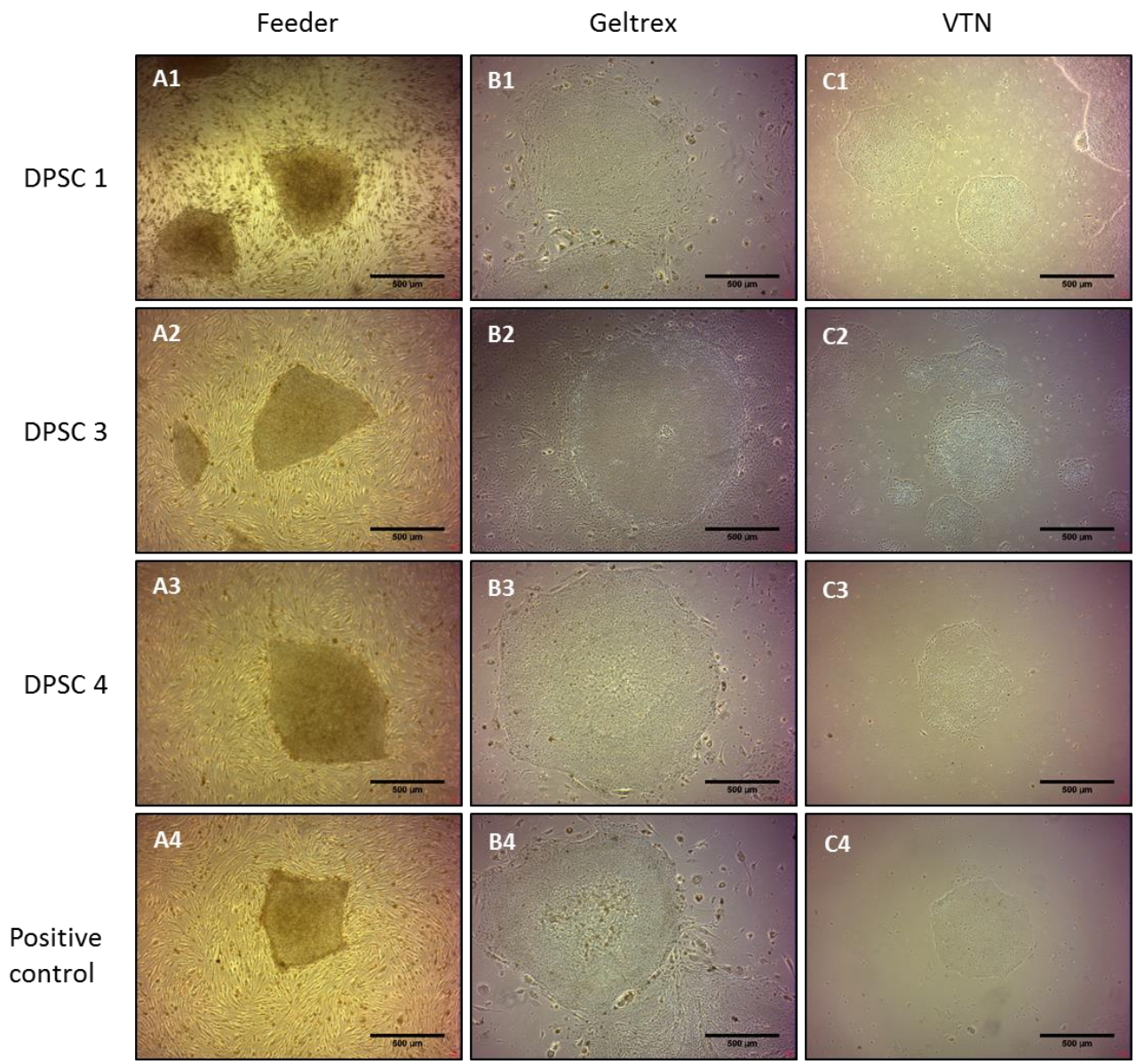

Figure 2.20. Culture adaptation from feeder to feeder-free conditions of iPSC generated from DPSC and positive control (fibroblasts). IPSC colonies cultured on feeder conditions (A1-A4). IPSC colonies cultured in Geltrex-coated dishes (B1-B4). IPSC colonies cultured in VTN-coated dishes (C1-C4). Scale bars: 500 µm

2.3.1.4. IPSC characterization

In order to confirm the successful reprogramming into iPSC, DPSC were characterized by its gene expression before and after the transduction. Fibroblasts and iPSC-derived from fibroblast were used as a positive control. Two different pluripotent markers (Nanog and Oct4) were analyzed by quantitative PCR and the fold gene expression of all samples was compared to fibroblast before the transduction. The expression of both pluripotent genes showed that all cells presented an up-regulation in Nanog and Oct4 after cell reprogramming, confirming that they were iPSC (Figure 2.21). Surprisingly, iPSC derived

from DPSC presented significantly higher levels of Nanog and Oct4 than the positive control (iPSC from fibroblasts). In all cases, the levels of expression were two orders of magnitude higher than their respective non-reprogrammed cells, implying its successful reprogramming into iPSC.

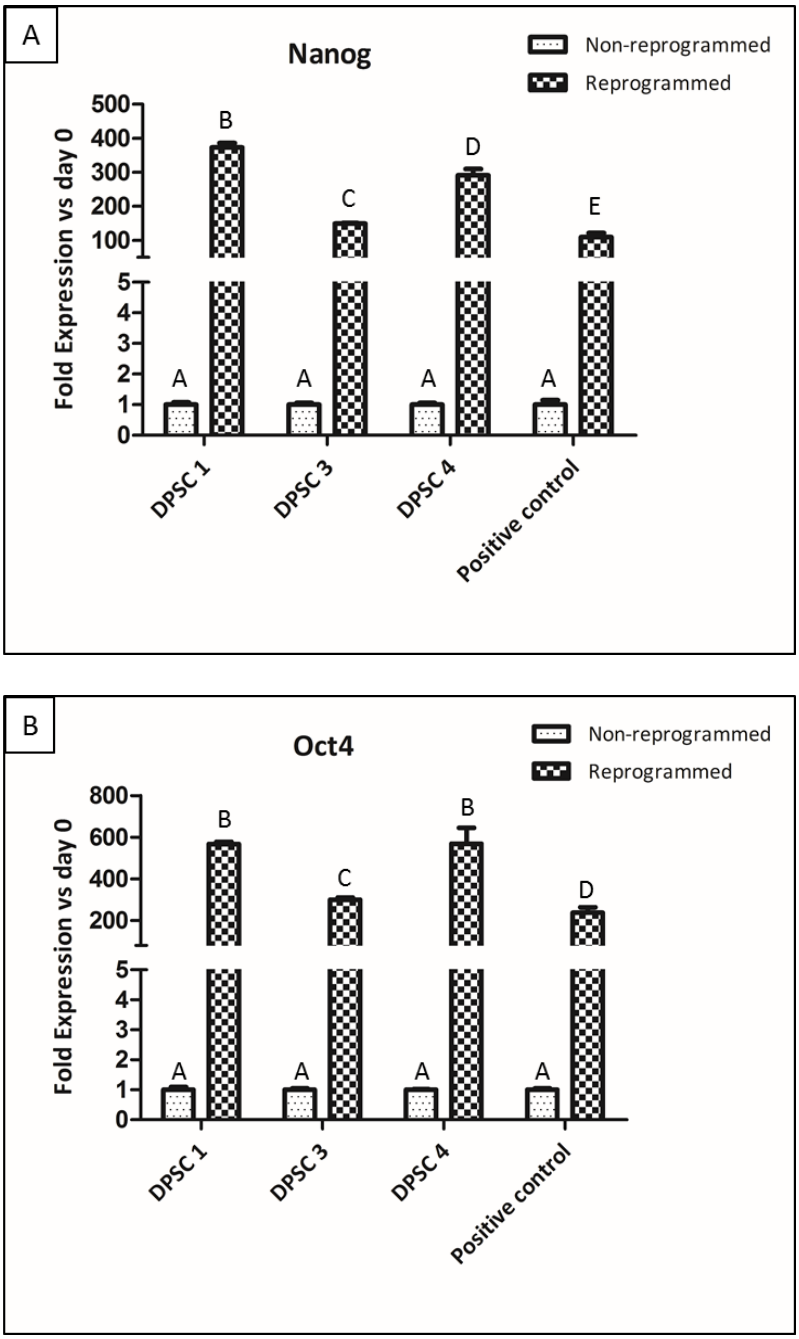

*Figure 2.21. IPSC gene expression characterization. Relative mRNA expression in DPSC and fibroblasts (positive control), before and after cell reprogramming. Pluripotent expression of Nanog (A) and Oct4 (B) by quantitative RT-PCR. *Different letter denotes significant differences. Same letter denotes non-significant differences.*

Finally, as shown in Figure 2.22, the genetic stability was also examined in iPSC cells in order to confirm that there were no genetic mutations throughout the reprogramming process. This process was performed by short-CGH in the best colonies of iPSC derived from DPSC, which were DPSC 1 and 3. Results showed that iPSC presented a normal karyotype, without any chromosome structural alterations and normal number of chromosomes (no presence of any aneuploidy).

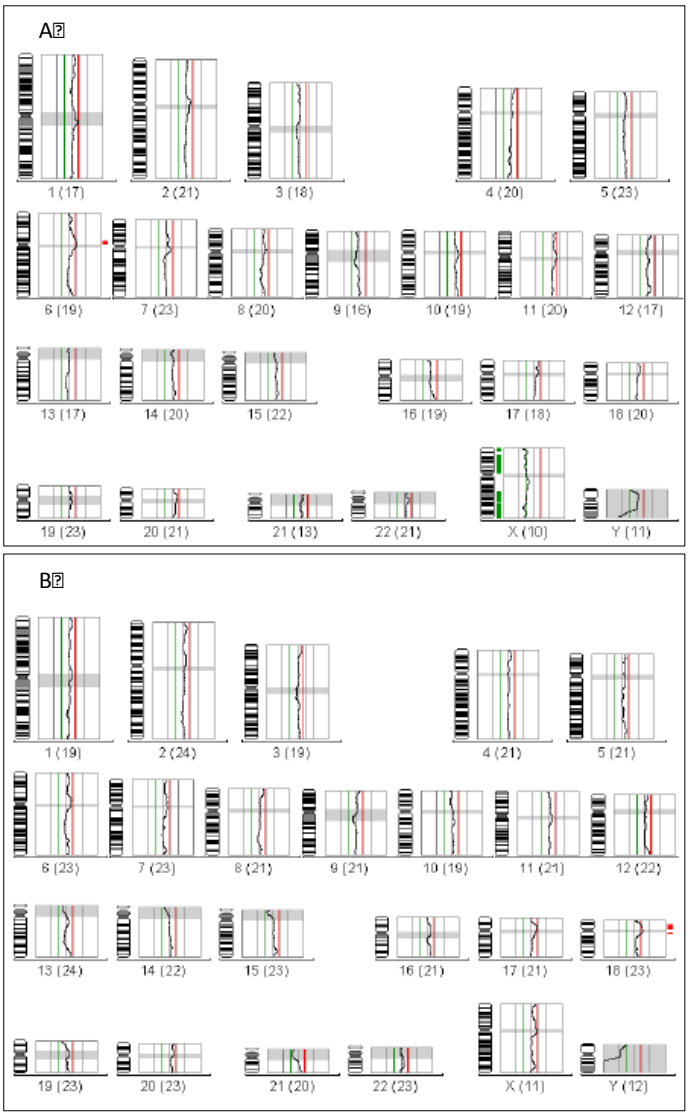

Figure 2.22. Genetic stability of iPSC from DPSC. Short-CGH summary from iPSC reprogrammed from DPSC 1 (A) (N=2, n=15) and DPSC 3 (B) (N=2, n=20). For the analysis, 47, XXY control samples (green) and iPSC samples (red) were co-hybridized onto 46, XY metaphases (n=12).

2.3.2. Neural crest stem cell differentiation

2.3.2.1 Adherent culture

To begin, DPSC and iPSC from DPSC were used for NCSC differentiation. Both populations were cultured for 21 days in NC induction medium in three cell densities: 0.5 x 10^4(low), 10^4 (medium) and 2 x 10^4 (high) cells/cm^2. Microscope images show that there were no differences in the three cell densities tested. IPSC cells had the typical stellate morphology of NCSC (Figure 2.23). Furthermore, in the three cell densities, iPSC cells started to detach at day 14 due to high cell density.

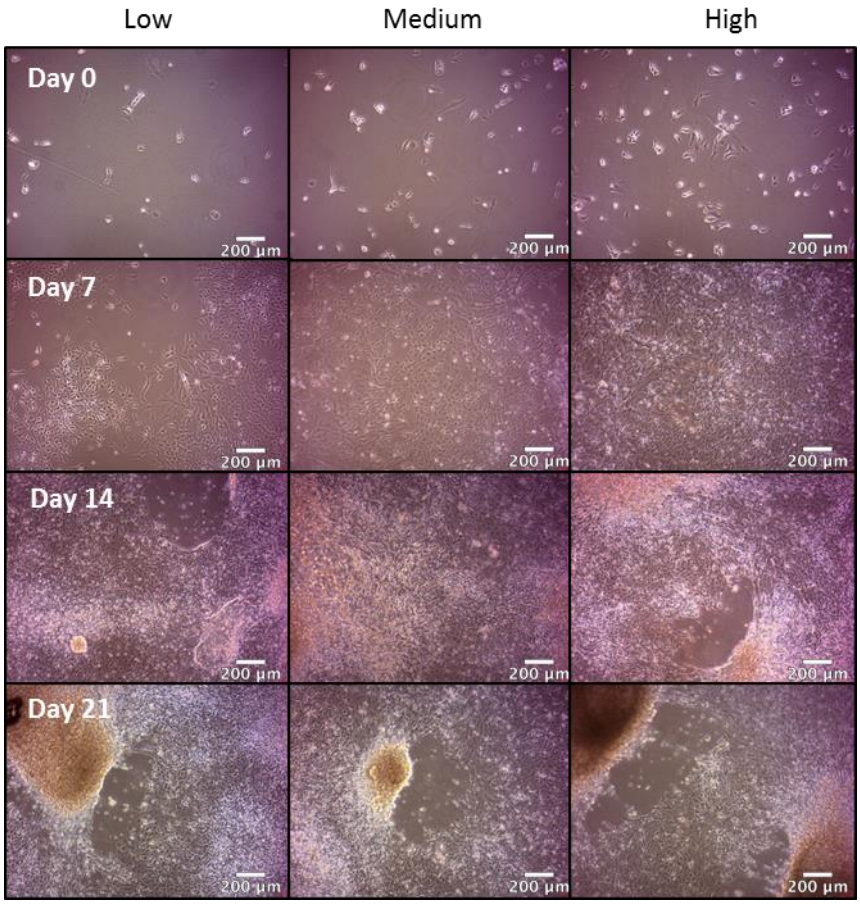

Figure 2.23. NCSC differentiation using an adherent culture method from positive control (iPSC). Microscopy images of cell morphology at days 0, 7, 14 and 21 of NCSC differentiation at three cell densities (low, medium and high). Scale bars: 200 µm.

On the other hand, as shown in Figure 2.24, DPSC became elongated with an spindle shape morphology and presented very high cell density in all conditions. In this case, cells were not detached from the culture plates.

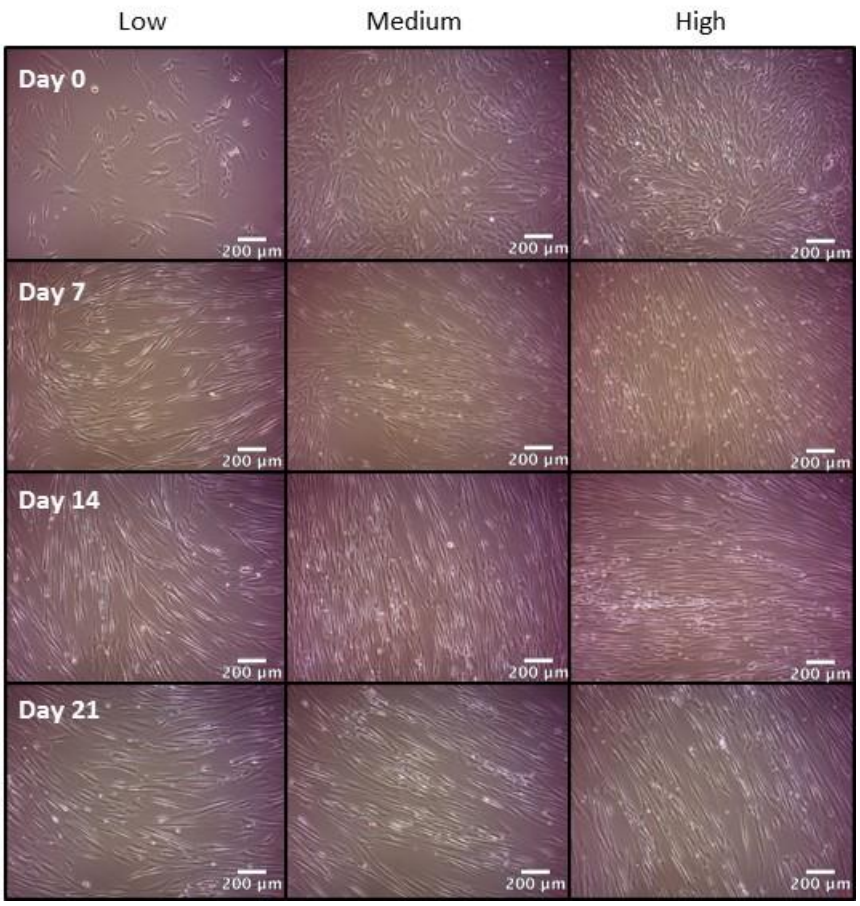

Figure 2.24. NCSC differentiation using an adherent culture method from DPSC. Microscopy images of cell morphology at days 0, 7, 14 and 21 of NCSC differentiation at three cell densities (low, medium and high). Scale bars: 200 µm.

Aiming to characterize NCSC markers, gene expression was examined by quantitative RT-PCR at day 21 of differentiation for the low cell density, which was the only condition in which not all cells had detached from the well plate. As shown in Figure 2.25, all analyzed NCSC genes levels were significantly up-regulated in differentiated cells compared with undifferentiated cells (day 0). More specifically, NCSC-derived from iPSC exhibited higher levels of AP2 (Figure 2.25 A) in contrast to NCSC-derived from DPSC which presented higher levels of Hnk1 (Figure 2.25 B).

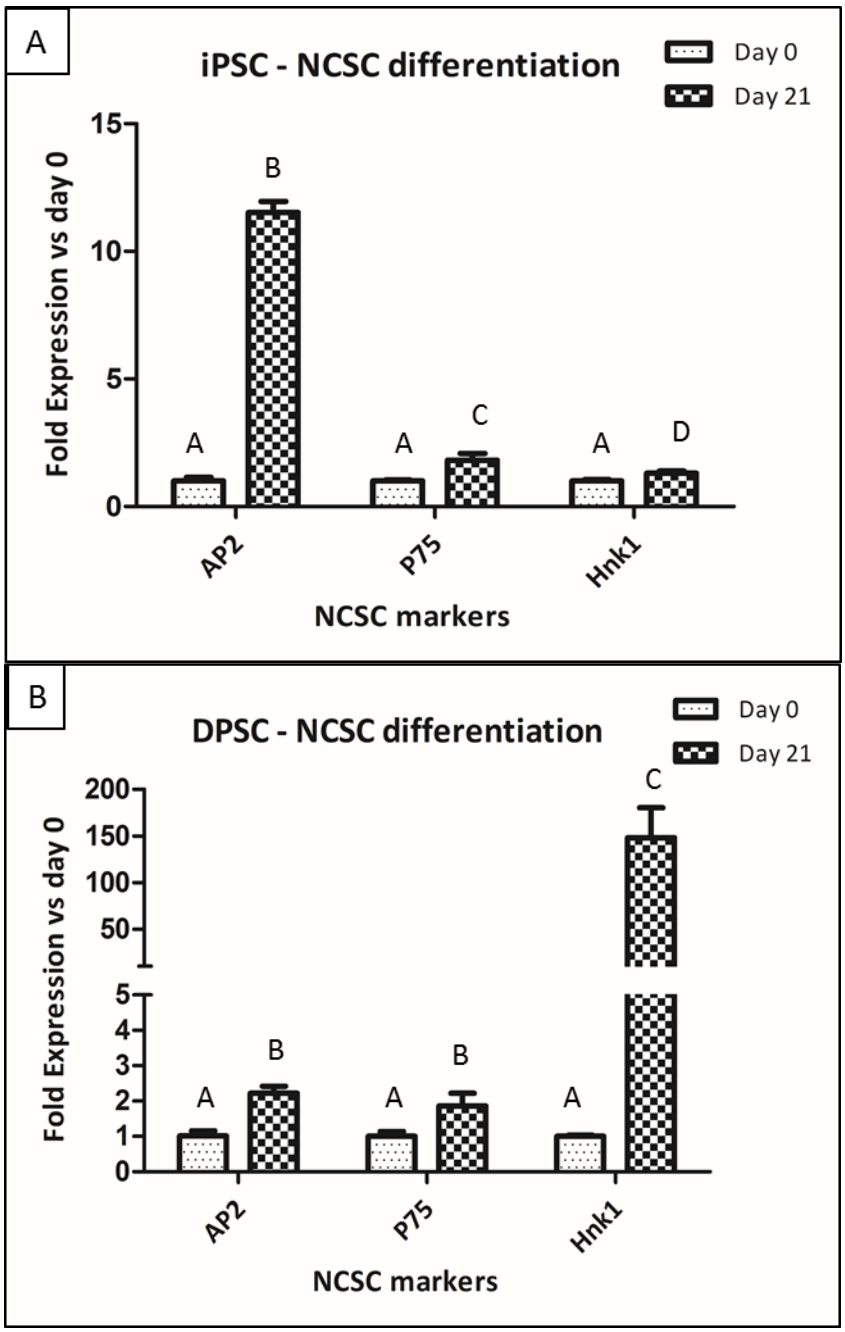

*Figure 2.25. NCSC differentiation using an adherent culture method. Relative mRNA expression in iPSC (positive control) (A) and DPSC (B), at days 0 and 21 of NCSC differentiation. NCSC expression of AP2, p75 and Hnk1 by quantitative RT-PCR. *Different letter denotes significant differences. Same letter denotes non-significant differences.*

Despite the low cell density showed promising results, we decreased the cell density one order of magnitude in order to prevent cell detachment. Furthermore, in order to study the optimum peak time of differentiation, we analyzed the gene expression at different time points of the differentiation. Regarding the cell morphology, NCSC-derived from iPSC presented a characteristic stellate morphology at day 7, while DPSC maintained an

elongated spindle shape (Figure 2.26). This trend continued similar in both cases until day 21, only showing increased cell number. In general, cell proliferation was visually observed to be very similar.

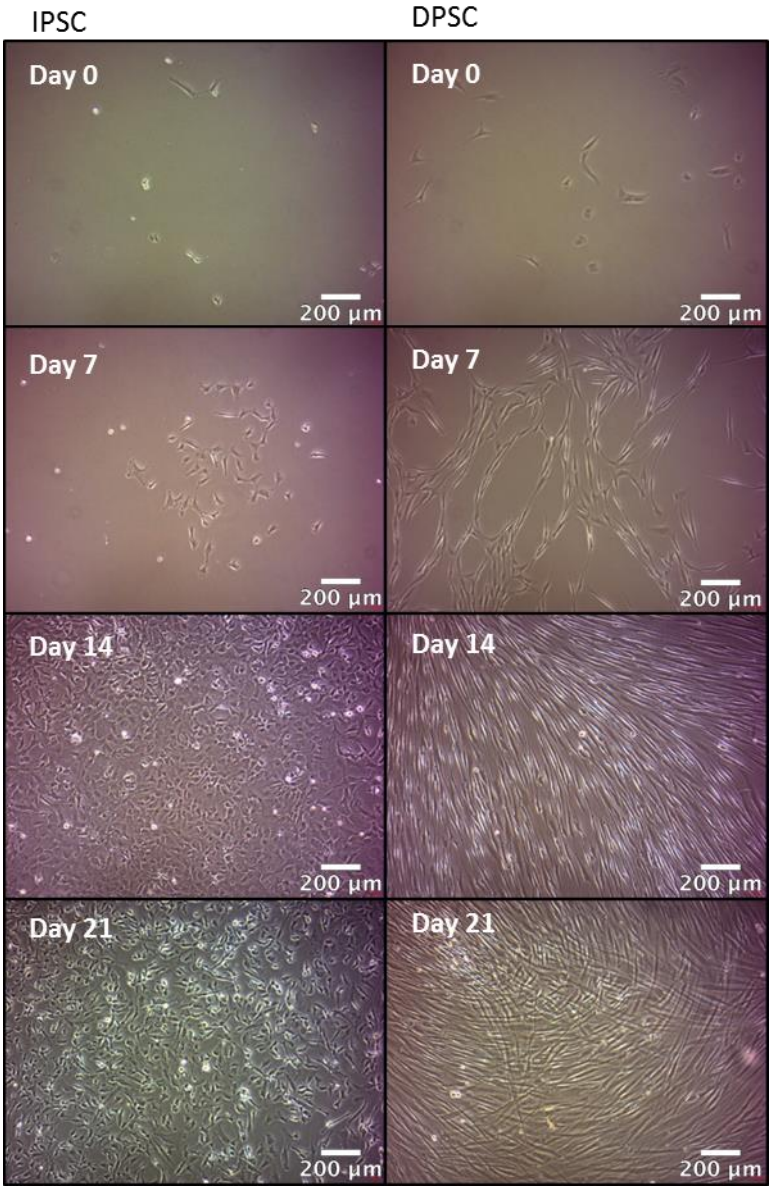

Figure 2. 26. NCSC differentiation using an adherent culture method from iPSC (positive control) and DPSC. Microscopy images of cell morphology at days 0, 7, 14 and 21 of NCSC differentiation. Scale bars: 200 µm.

Aiming to analyze the gene expression, surprisingly in the case of NCSC-derived from iPSC the NCSC markers AP2 and p75 decreased throughout the different days of differentiation, reaching its lower value at 14 days, which tended to further increase at 21 days (Figure 2.27 A). Nevertheless, the values tended to decrease respect its initial cell culture. Different trend was observed for the NCSC obtained directly from DPSC. As shown in Figure 2.27 B,

NCSC-derived from DPSC presented an increase on the AP2 expression at day 14, reducing afterwards its value at day 21. The levels at 14 days increased 8-fold respect to its initial seeding, while the increase was approximately 4-fold after at 21 days respect the initial seeding. However, the expression of p75 was maintained low during the differentiation process.

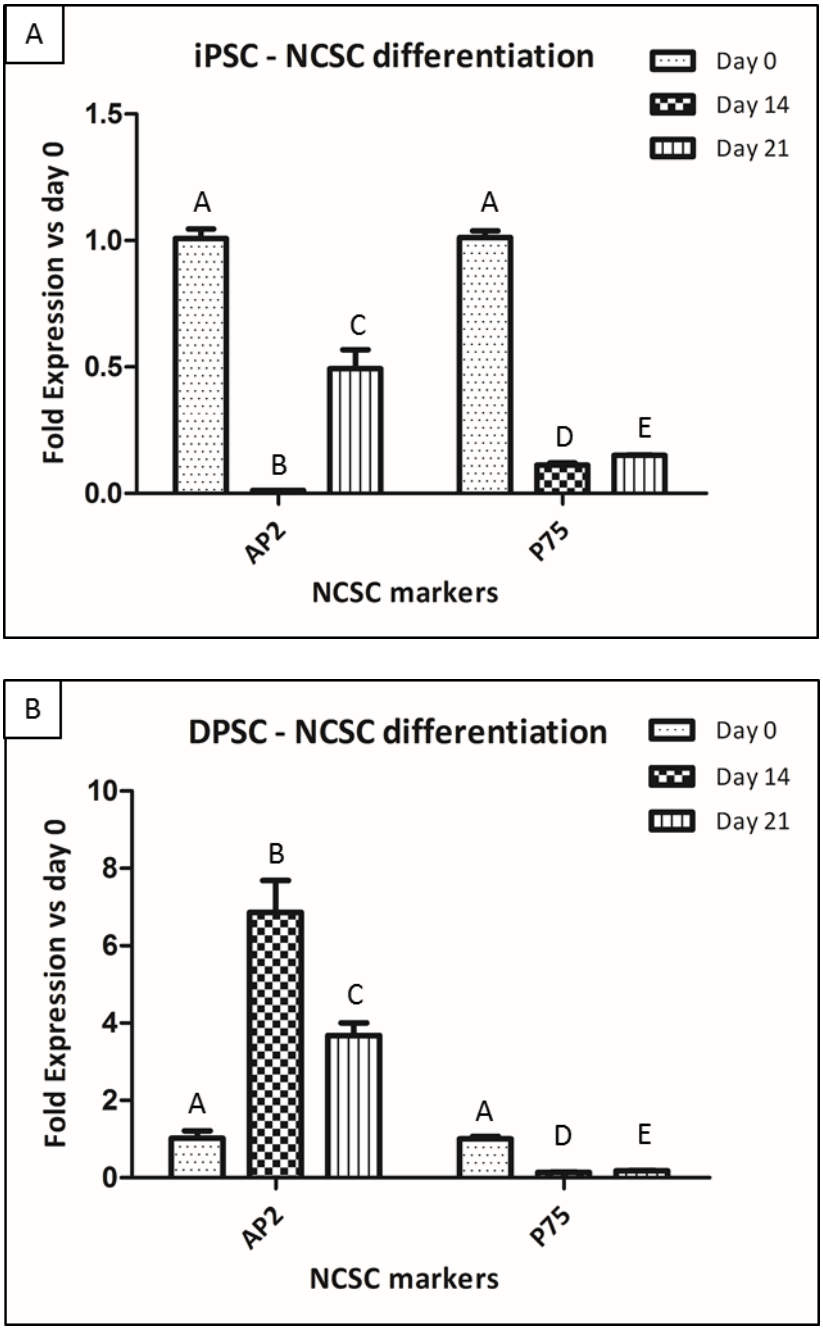

*Figure 2.27. NCSC differentiation using an adherent culture method. Relative mRNA expression in iPSC (positive control) (A) and DPSC (B), at days 0, 14 and 21 of NCSC differentiation. NCSC expression of AP2 and p75 by quantitative RT-PCR. * Different letter denotes significant differences. Same letter denotes non-significant differences.*

2.3.2.2. Neurospheres formation

Suspension culture allows cell to cell interactions, which helps in the induction of NCSC. For this reason, the second induction method consisted of a first stage on suspension culture and then an adherent culture in fibronectin-coated plates.

Regarding cell morphology, when iPSC were cultured in NC induction medium they were able to form NS in suspension culture after 10 days (Figure 2.28). NS number decreased after 14 days since their maintenance was jeopardized with every cell culture media change and taking into account that the number of initially formed NS formed were low, the chances of survival were very low. In contrast, when using DPSC, some cell aggregates were formed at day 10 in suspension culture. Nevertheless, due to the small number of NS formed, their maintenance was jeopardized with every cell culture media change. One surprising fact found in both cases was that, despite the cell cultures plates were purchased as suspension culture well plates, the formed NS tended to attach to the bottom of the well plate, hence reducing our initial hypothesis of having a suspension cell culture and providing the adequate environment for the cell to cell interaction.

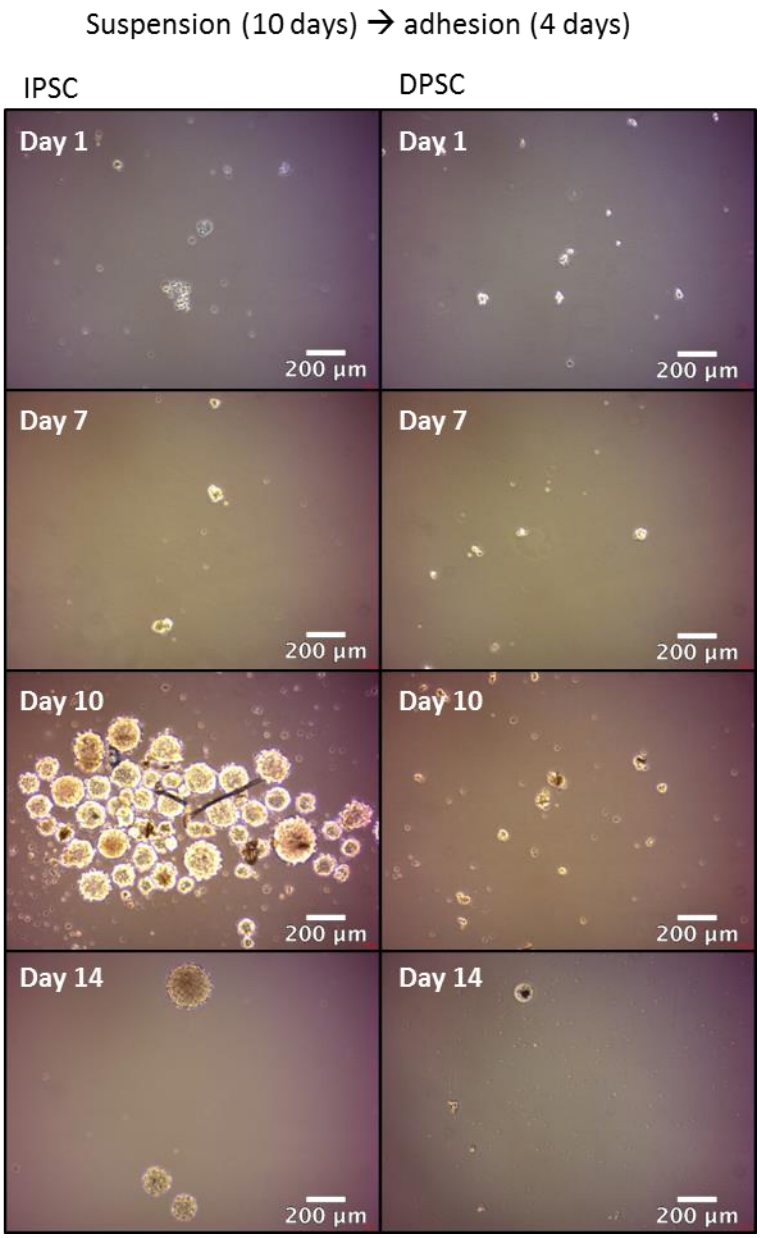

Figure 2.28. NCSC differentiation using neurospheres formation method. Cells were cultured for 10 days in suspension and 4 days in adhesion conditions. Microscope images of cell morphology at days 1, 7, 10 and 14 of NCSC differentiation from iPSC (positive control) and DPSC. Scale bars: 200 µm.

Due to the above mentioned problems, we sought for different well plates for our specific cell types and the desired suspension system and found that well plates Corning 3473 seemed highly recommended for our purpose. In this case, since the NS were already obtained for the iPSC, we performed the experiment merely with the DPSC. Furthermore, since the amount of NS jeopardized at longer time points was very high, we also optimized the time point at which the NS obtained the highest expression of NCSC markers. NS were cultured up to 4 days and their gene expression and morphology were analyzed at each day.

As shown in Figure 2. 29, microscope images revealed that NS formation started at day 1 of differentiation and that the sphere diameter increased every day until day 4. Total RNA was analyzed every day until day 4 of differentiation.

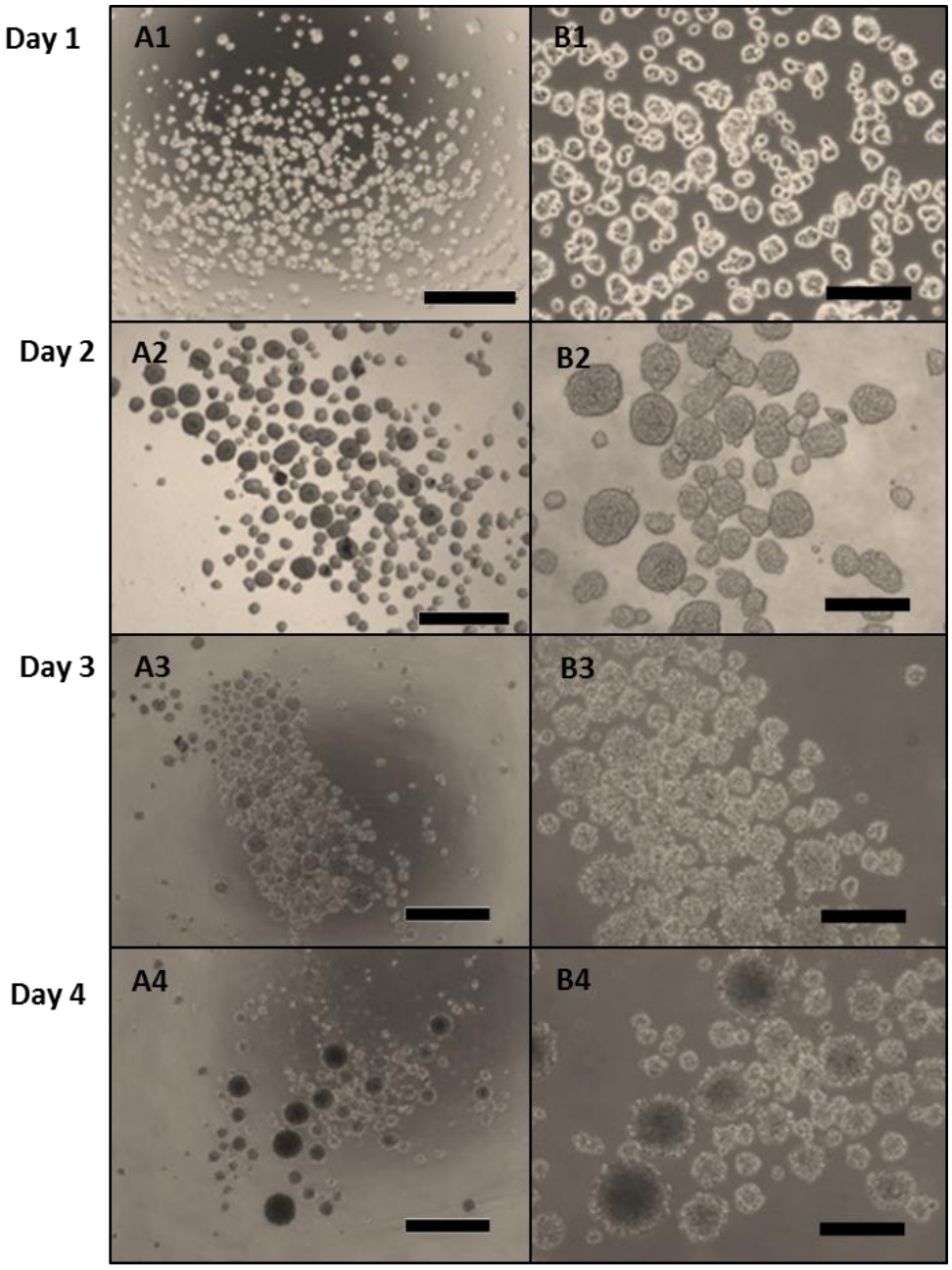

Figure 2.29. NCSC differentiation using neurospheres formation method from DPSC. Microscope images of cell morphology at days 1, 2, 3, 4 and 5 of NCSC differentiation in suspension culture. Scale bars: 500 µm (A1-A4) and 250 µm (B1-B4)

The results obtained by qPCR showed that most genes were induced to their highest expression levels at day 4 of differentiation (Figure 2.30). The early transcription factor AP2

and early marker Sox9 exhibited its peak level at day 3 while, NCSC markers CHD7 and p75 and the neural marker Nestin presented the highest expression level at day 4 (Figure 2.30).

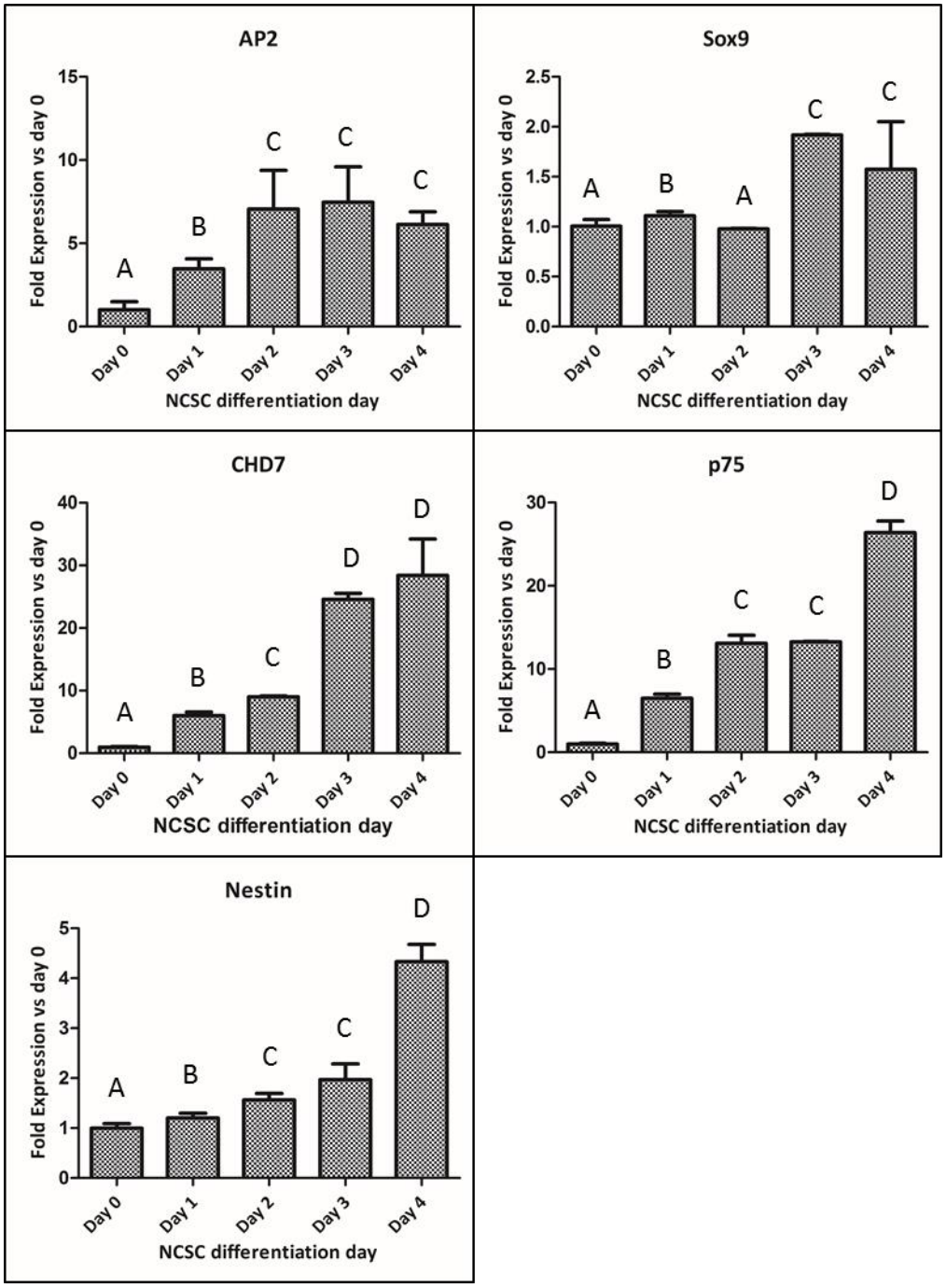

*Figure 2.30. Neurospheres gene expression. Relative mRNA expression in DPSC at days 0, 1, 2, 3 and 4 of NCSC differentiation in suspension culture. NCSC expression (AP2, Sox9, CHD7 and p75) and neural marker Nestin analyzed by quantitative RT-PCR. * Different letter denotes significant differences. Same letter denotes non-significant differences.*

Moreover, as shown in Figure 2.31, the expression of pluripotent markers Oct4, Nanog, Sox2 and c-MYC presented its peak day at day 4, presenting a significant increase with time. Moreover, the expression of the progenitor or early human marker CD34 highly increased throughout NCSC differentiation days. Finally, also directly related with the decrease of the mesenchymal markers, the mesenchymal marker CD73 decreased through the differentiation days.

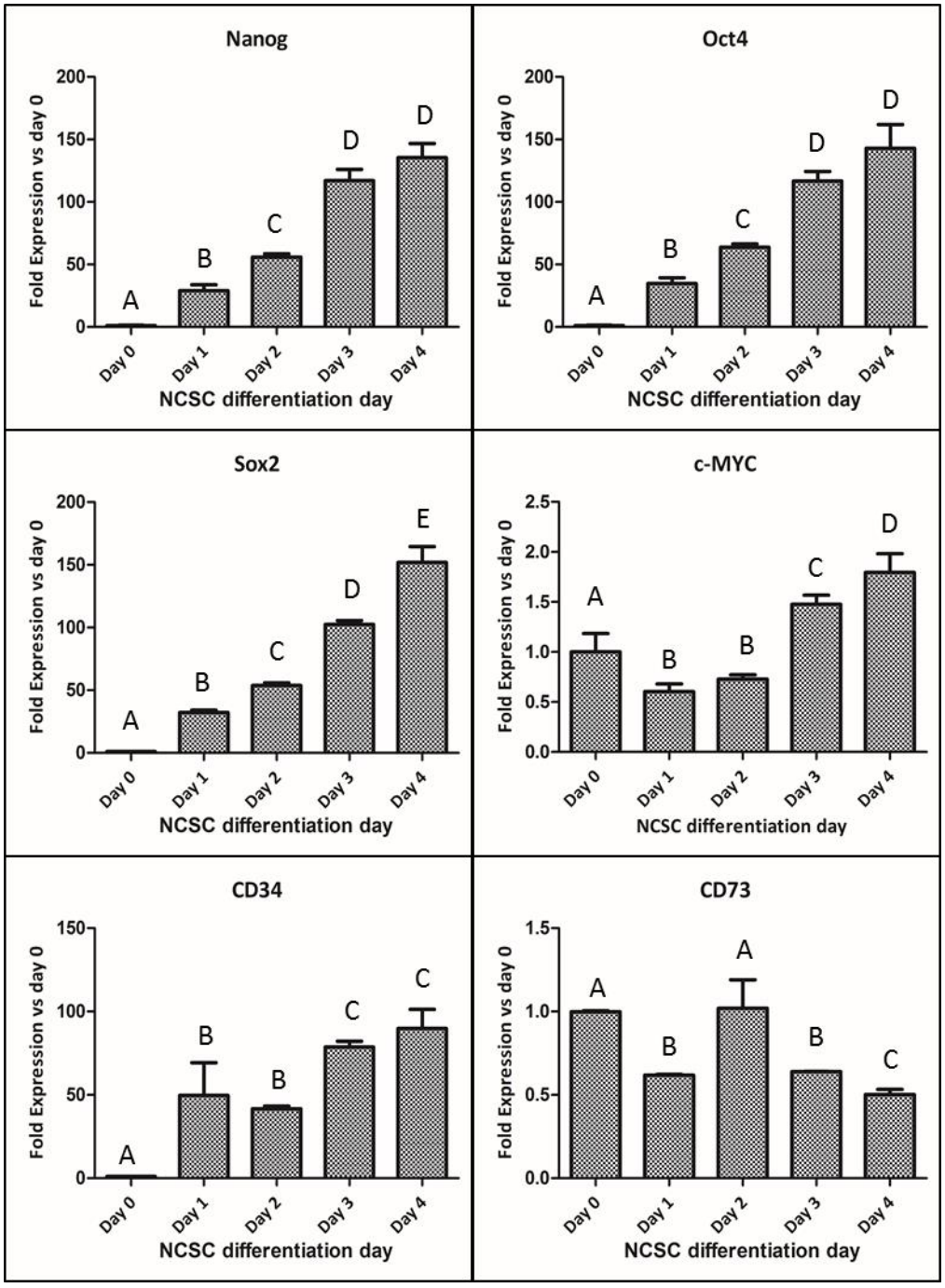

*Figure 2.31. Neurospheres gene expression. Relative mRNA expression in DPSC at days 0, 1, 2, 3 and 4 of NCSC differentiation in suspension culture. Pluripotent expression (Sox2, Oct4, Nanog, c-MYC), progenitor/early human marker (CD34) and mesenchymal marker (CD73) analyzed by quantitative RT-PCR. * Different letter denotes significant differences. Same letter denotes non-significant differences.*

To finally confirm the results of the increased NCSC markers, we performed an IF assay in which the NS at day 4 were analyzed for the expression of p75 (Figure 2.32). Results confirmed the expression of the early NCSC marker, p75, in the NS at day 4. Other NS control groups could not be used as control since the NS formation leads to the increased levels of p75. The staining of DPSC cells at day 0 in which no NS induction was performed, did not show any levels of expression of p75 by IF.

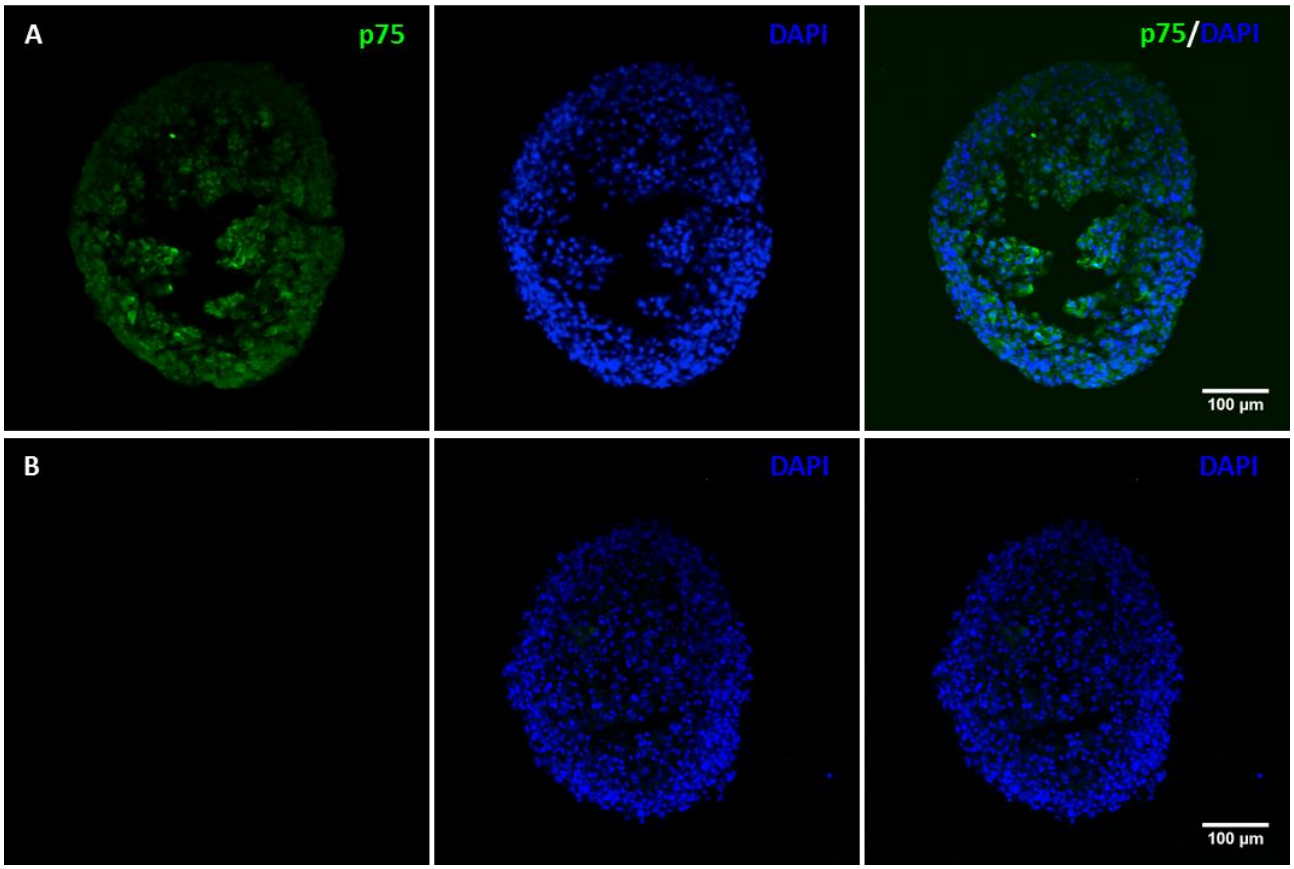

Figure 2.32. Neurosphere protein expression. A) NCSC marker p75 (green) and nuclear marker DAPI (blue) was analyzed in a neurosphere at day 4 of NCSC differentiation by immunofluorescence assay. B) Negative control of the assay. Scale bar: 100 µm.

Neural crest stem cells expansion

Once optimal peak day was determined, NS were plated on adherent conditions for 15 more days for the generation of larger amounts of NCSC. Optical microscopy images show that NS

were formed at day 4 (Figure 2.33 A1 – A2). The cells were then left on the coated fibronectin dishes and cells tended to attach, allowing the migration of the NCSC into the Petri dish, slowly allowing cells to migrate into the dish and disrupting the original NS morphology. The NS were still observed at day 12, although their morphology completely disappeared at 15 and 19 days. Cells were finally allowed to expand and reach confluence for a total of 19 days (Figure 2.33).

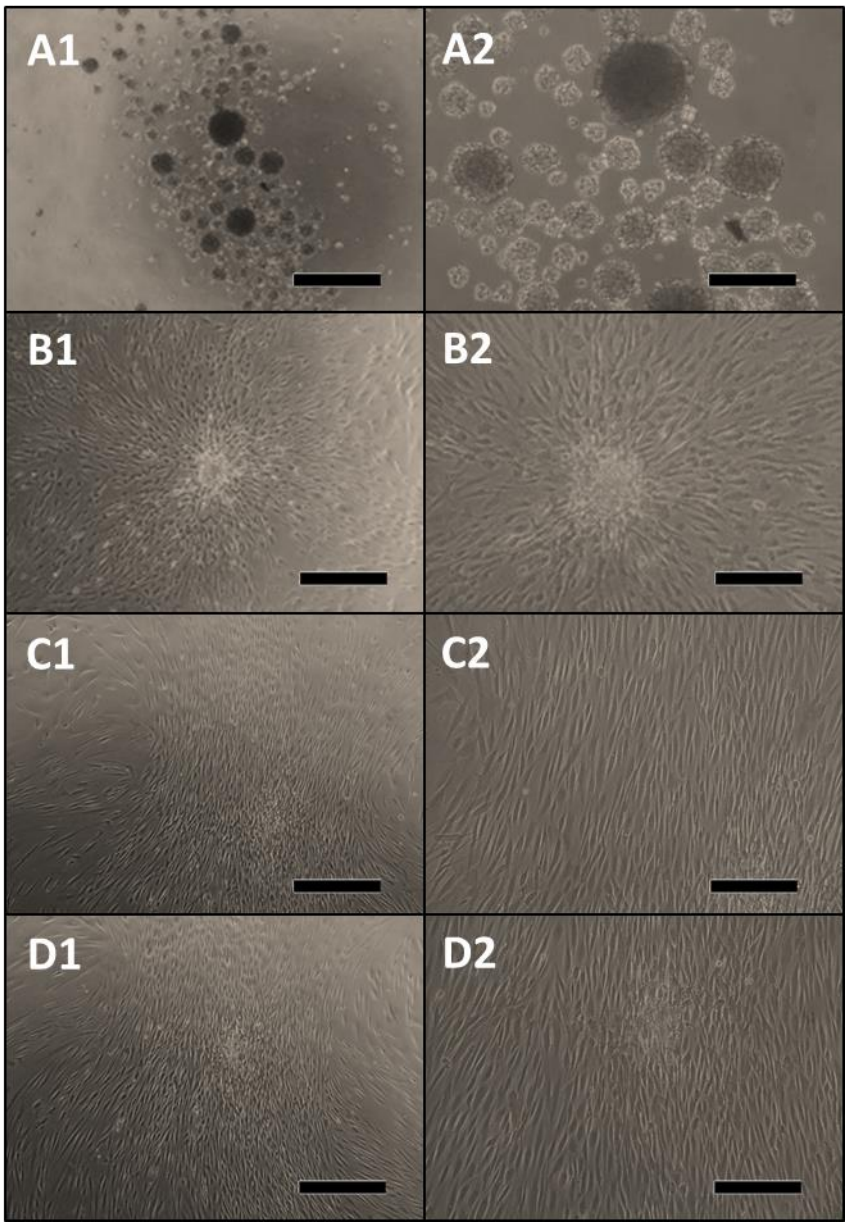

Figure 2.33. NCSC differentiation in suspension and adhesion culture. Microscope images of cell morphology of the NCSC differentiation from DPSC. DPSC-derived NCSC in suspension (A1-A2) at day 4 and in adhesion at days 12 (B1-B2), 15 (C1-C2) and 19 (D1-D2). Scale bars: 500 µm (A1-D1) and 200 µm (A2-D2).

Regarding the gene expression, pluripotent markers (Oct4, Nanog and Sox2) were significantly highly up-regulated at day 4 of NS formation but their expression decreased during adhesion culture (Figure 2.34).

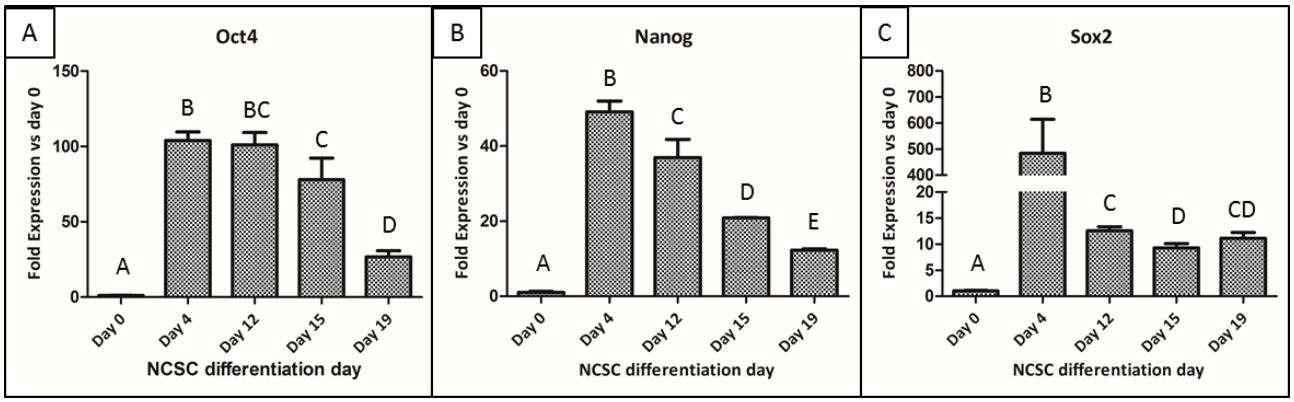

*Figure 2.34. NCSC expansion gene expression. Relative mRNA expression in DPSC at days 0, 4, 12, 15 and 19 of NCSC differentiation in suspension culture. Pluripotent expression of Oct4 (A), Nanog (B) and Sox2 (C) analyzed by quantitative RT-PCR. * Different letter denotes significant differences. Same letter denotes non-significant differences.*

As can be observed in Figure 2.35 A, similar behavior was observed for the Sox10 marker, which is related to NCSC, showing a decreased expression after cells started attaching on the coated Petri dish. On the other hand, p75, which is expressed in progenitor and migrating NC cells, increased throughout the 19 days of NC induction and expansion (Figure 2.35 B). Moreover, the expression of the neural marker Nestin was also increased during NS formation but it was down-regulated when cells were cultured in fibronectin-coated dishes (Figure 2.35 C).

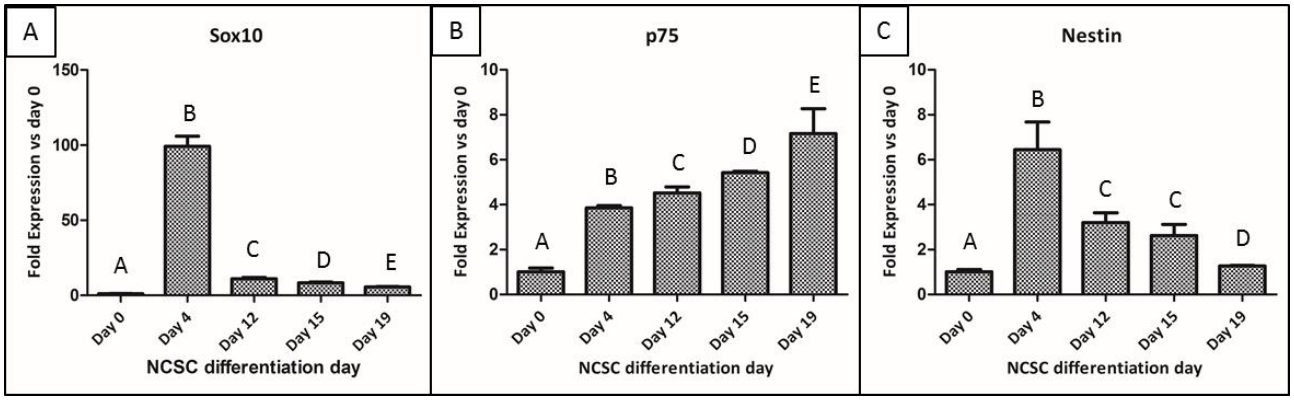

Figure 2.35. NCSC expansion gene expression. Relative mRNA expression in DPSC at days 0, 4, 12, 15 and 19 of NCSC differentiation in suspension culture. NCSC marker Sox10 (A), and p75 (B), and neural marker Nestin (C)

*analyzed by quantitative RT-PCR. * Different letter denotes significant differences. Same letter denotes non-significant differences.*

To further characterize the differentiation process, immunostaining of NS and migrating NCSC cells was performed. As shown in Figure 2.36, Nestin, Oct4, Nanog, Sox10 and p75 were present in NS.

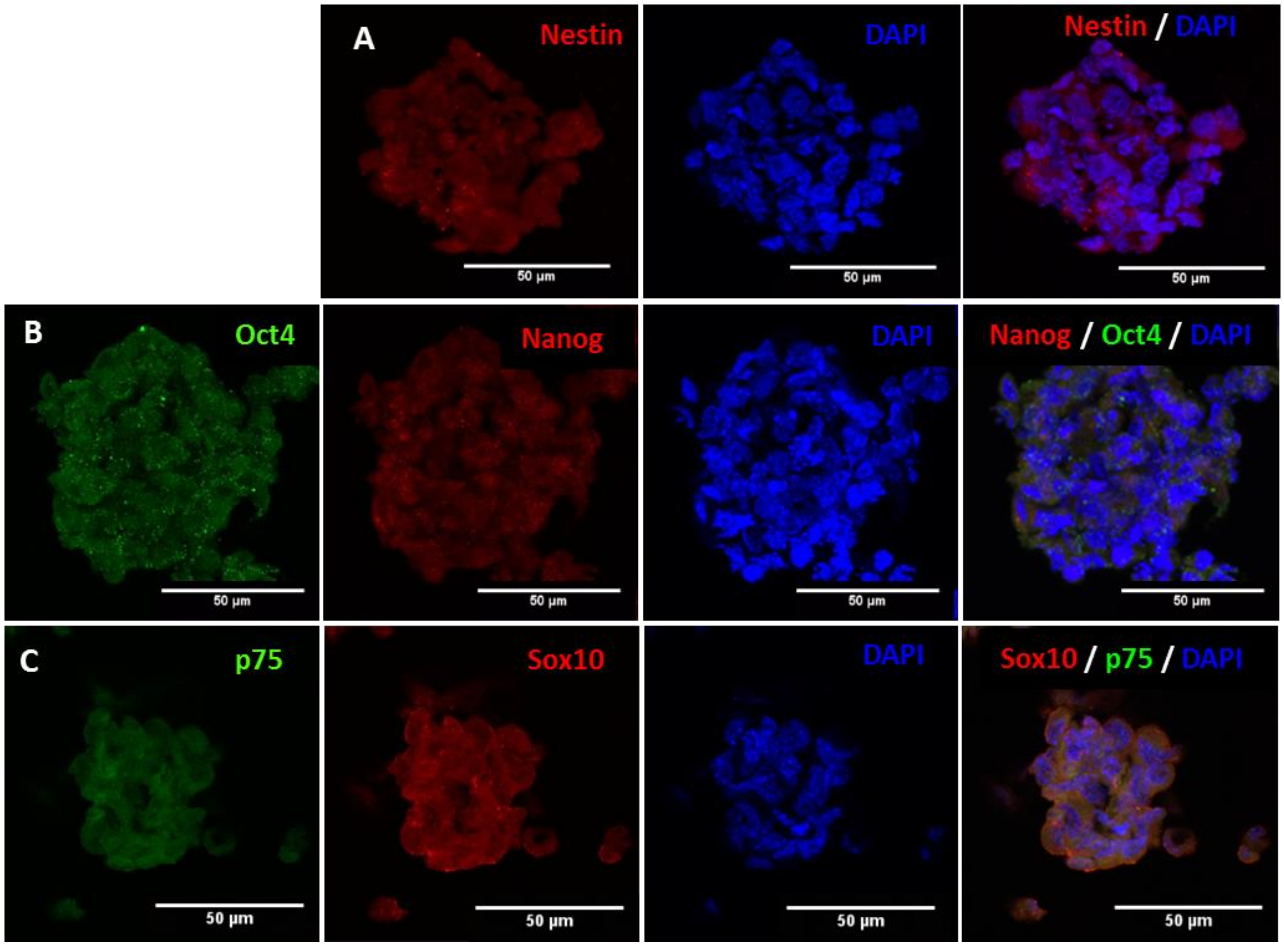

Figure 2.36. Neurospheres protein expression at day 4 of NCSC differentiation by immunofluorescence assay. A) Neural marker Nestin (red) and nuclear marker DAPI (blue). B) Pluripotent markers Oct4 (green) and Nanog (red), and nuclear marker DAPI (blue). C) NCSC marker p75 (green), NCSC marker Sox10 (red) and nuclear marker DAPI (blue). Scale bars: 50 µm.

Regarding adhesion culture, immunofluorescence revealed the presence of p75 as well as some Nestin and Oct4 positive cells (Figure 2.37), similar to qPCR results.

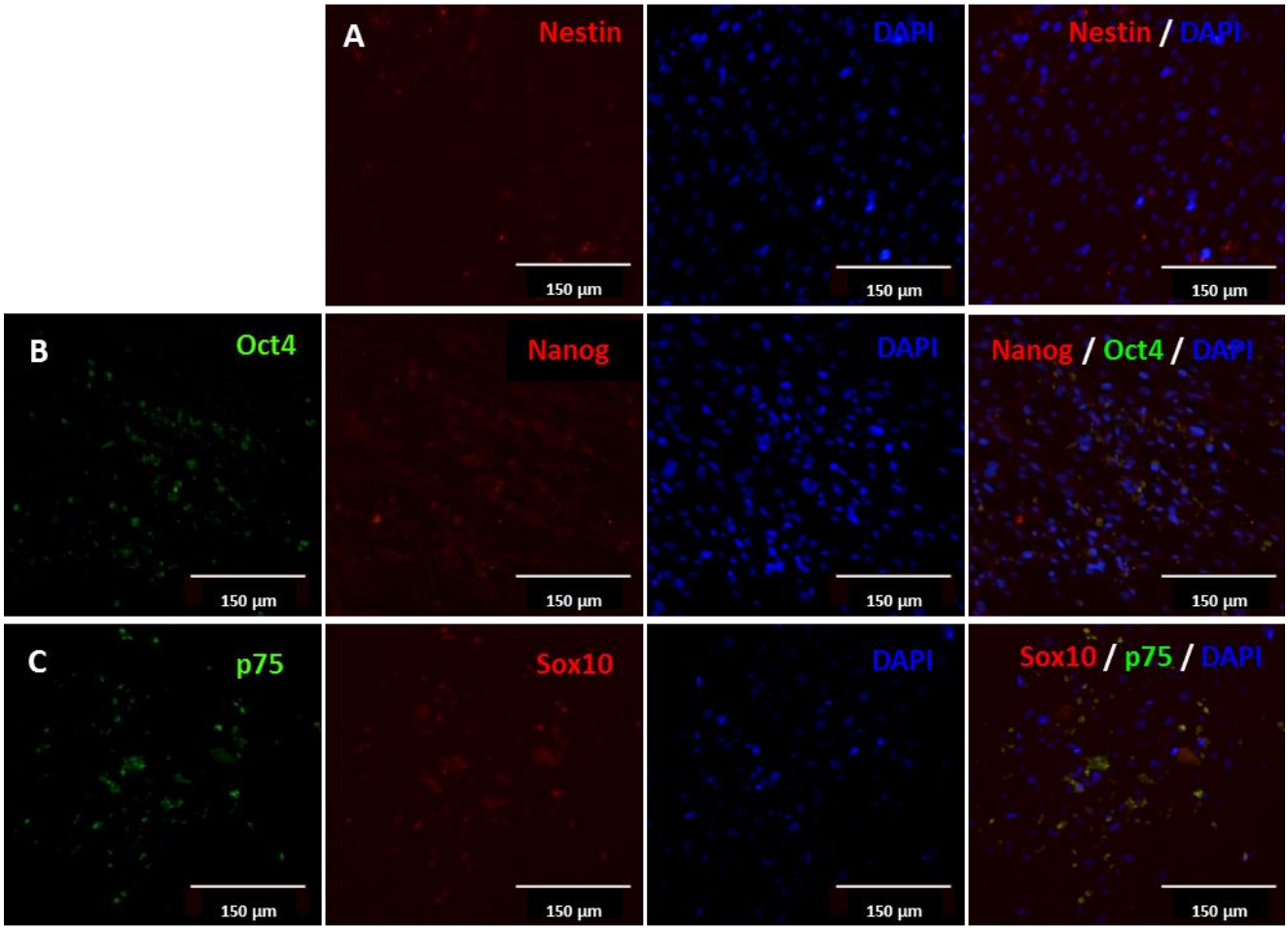

Figure 2. 37. NCSC protein expression at day 19 of NCSC differentiation by immunofluorescence assay. A) Neural marker Nestin (red) and nuclear marker DAPI (blue). B) Pluripotent markers Oct4 (green) and Nanog (red), and nuclear marker DAPI (blue). C) NC marker p75 (green), NCSC marker Sox10 (red) and nuclear marker DAPI (blue). Scale bars: 150 µm.

2.3.2.3. Embryoid bodies formation

The last NCSC induction method was to form EB from DPSC, which should facilitate the differentiation. As mentioned before, it was expected that the enhancement of the pluripotent like status prior to the formation of the NS could allow similar behavior as that of iPSC and hence increase the neural phenotype of the formed NS. EB were formed in Aggrewell plates (Fig. 2.38 A1-A2) and cultured in NCSC induction medium for NS formation (Fig 2.38 A3-A4). In parallel, NS formation method was performed as a control (Figure 2.38 B).

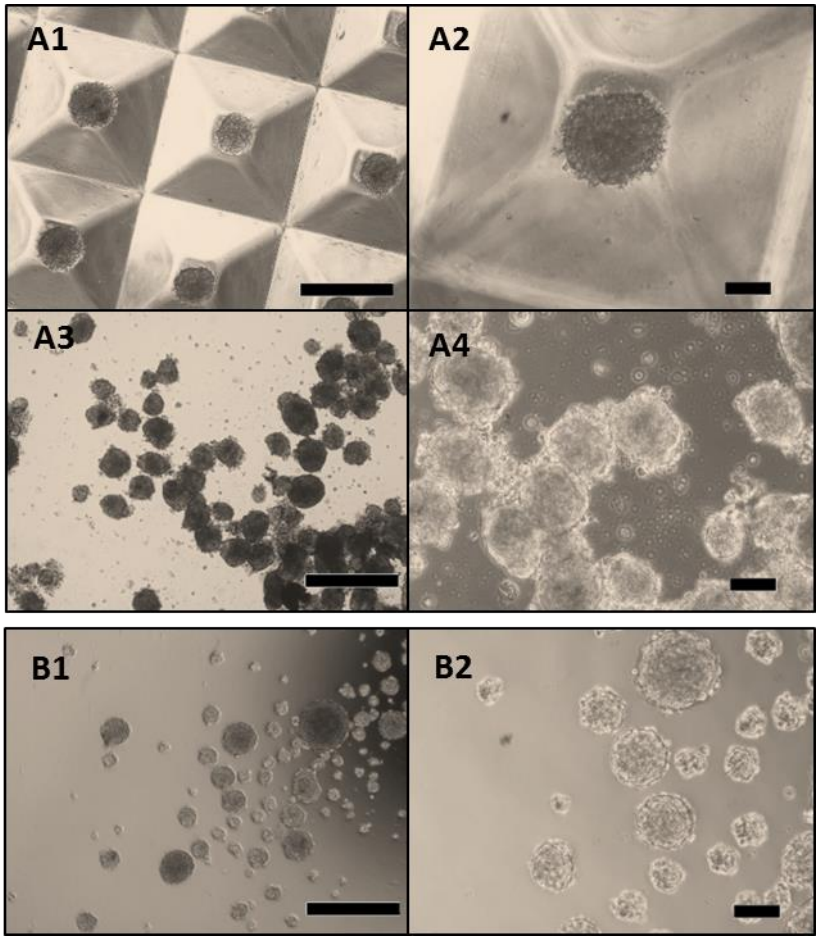

Figure 2.38. NCSC differentiation with and without EB formation. Microscope images of cell morphology from NCSC differentiation via EB (A) or without EB formation (B). EB formation in AggreWell plates (A1-A2). NCSC differentiation from EB (A3-A4). NCSC differentiation from DPSC (B1-B2). Scale bars: 500 µm (A1, A3, B1) and 100 µm (A2, A4, B2).

We then compared the gene expression with the previously described method of NS formation. In order to understand the results, it has to be taken into account that for EB formation, the time taken was 10 day for the EB, followed by 4 days of NS formation. Nevertheless, for the direct NS formation, the time taken was 4 days in suspension culture. Regarding gene expression (Figure 2.39) of AP2, it was highly up-regulated at the end of differentiation after using the EB method compared to the direct NS formation. Interestingly, when using the direct NS formation method, the levels of expression of AP2 were two orders of magnitude higher than day 0. However, p75 expression was significantly decreased in both methods.

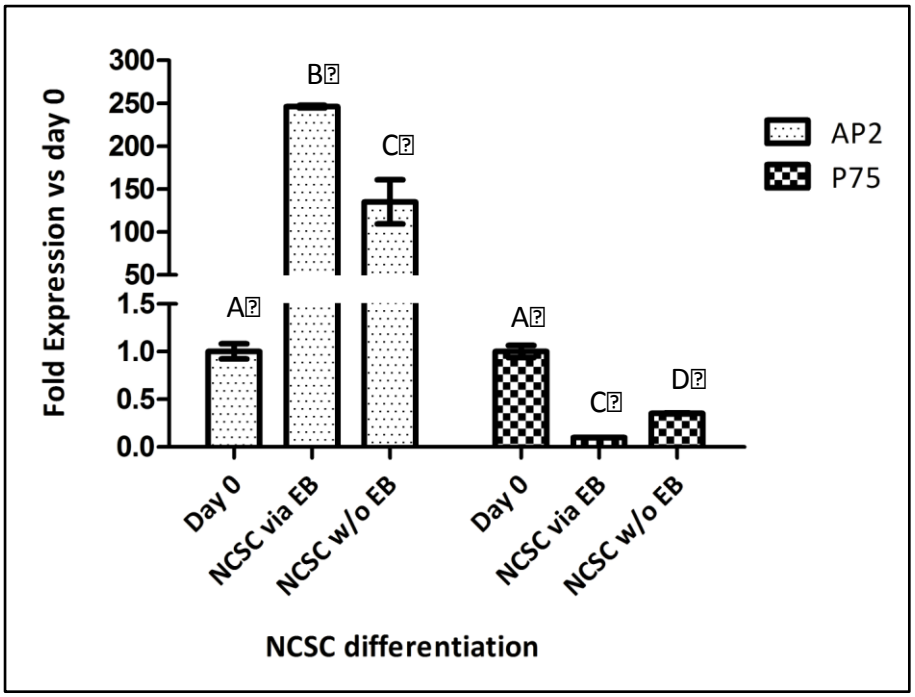

*Figure 2.39. Gene expression of NCSC differentiation with and without (w/o) EB formation. Relative mRNA expression in DPSC at days 0 and last day of NCSC differentiation with and without (w/o) EB formation. Expression of early AP2 and late p75 NCSC markers analyzed by quantitative RT-PCR. * Different letter denotes significant differences. Same letter denotes non-significant differences.*

2.3.3. Corneal endothelial cell differentiation

2.3.3.1. One-step differentiation

For CEC differentiation, we first separated DPSC population using MACS columns with labeled Microbeads against CD73. Therefore, positive DPSC (CD73-positive) were labeled while negative cells (CD73-negative) were non-labeled. For confirming a correct separation, FACS was performed in both populations. Graphics show that positive cells (M1) are on the right while negative cells are on the left. As Figure 2.40 shows, all positive cells were labeled with CD73 antibody (Figure 2.40 A) and nearly all the cells were correctly separated, as 99,78% of negative cells were non-labeled (Figure 2.40 B).

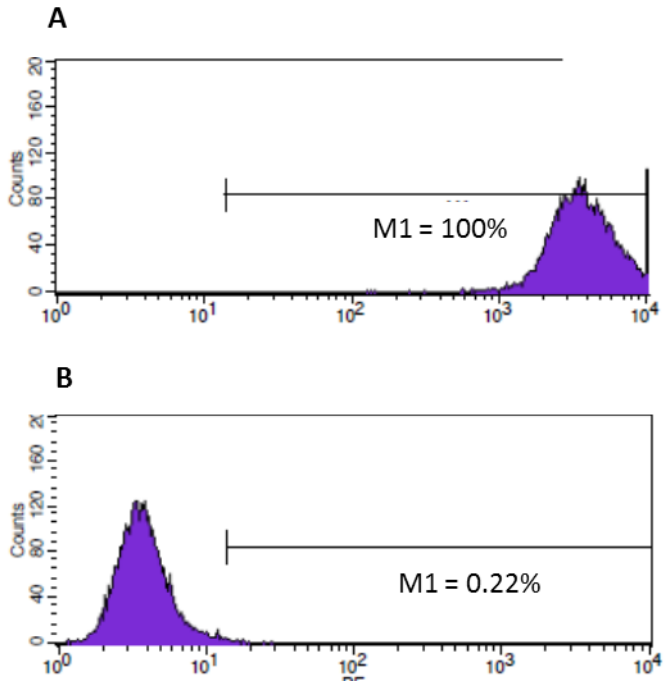

Figure 2. 40. DPSC separated with Microbeads against CD73. A) Positive population and B) negative population analyzed by FACS. M1=labeled cells.

Furthermore, both populations of DPSC were analyzed by its gene expression for NCSC markers (Figure 2.41). Results showed that AP2 and p75 were significantly increased in negative CD73 cells compared to positive cells.

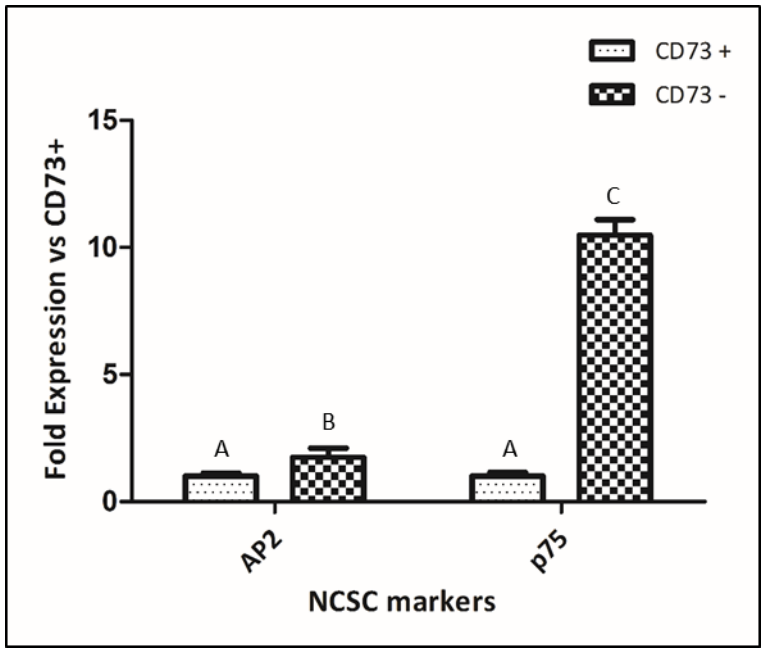

*Figure 2. 41. DPSC separated with Microbeads against CD73. Fold gene expression compared to positive cells of NCSC markers (AP2 and p75) in positive (CD73+) and negative (CD73-) cells analyzed by quantitative PCR. * Different letter denotes significant differences. Same letter denotes non-significant differences.*

Finally, negative DPSC population (CD73-negative) was cultured in a defined cultured medium, which consisted of CEC media A1 (for 2 or 5 days) and then CEC media A2. As microscope images show in Figure 2.42, in all conditions cells were not able to survive and at day 14 all cells were dead (rounded floating cells). In fact, at day 2, few cells were attached and presented an elongated morphology. Then, at day 5, nearly all the cells were rounded, which is indicative of cell death.

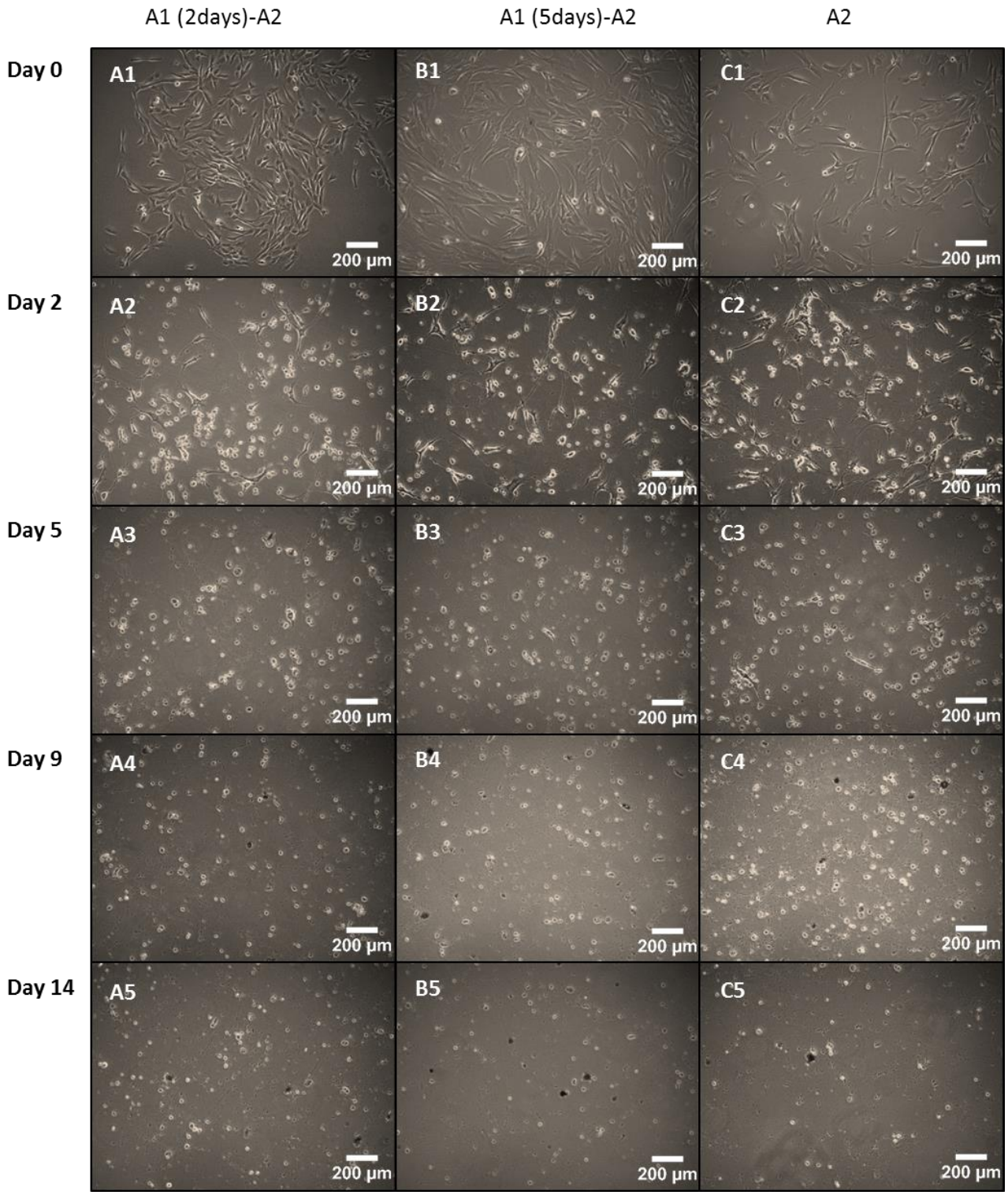

Figure 2. 42. One-step differentiation into CEC from CD73-negative DPSC at days 0, 2, 5, 9 and 14. A1-A5) Cells cultured in CEC media A1 for 2 days and then CEC media A2. B1-B5) Cells cultured in CEC media A1 for 5 days and then CEC media A2. C1-C5) Cells cultured in CEC media A2 for 14 days. Scale bars: 200 µm.

Despite the efforts to separate the cells that had no presence of the CD73 marker, results showed no sign of cellular activity. Hence, our initial hypothesis for the direct conversion

was not successful. For this purpose, we then analyzed other possible strategies for the conversion of CEC from NCSC-derived from DPSC using conditioned medium. Despite the following strategy will require a two-step process, we hypothesize that it will be a less aggressive strategy.

2.3.3.2. Two-step differentiation

The two-step differentiation process used conditioned medium from commercial or isolated HCEC for the differentiation of NCSC-derived from DPSC into CEC.

Commercial conditioned medium

Induction method B1 used commercial conditioned medium (Celprogen) collected from commercial CEC at cell culture confluence of 90%.

As shown in Figure 2.43, NCSC from attached NS were used as day 5 of CEC differentiation from DPSC. Cells were cultured for up to 19 days. Initially, at days 12 and 16 cells presented a more polygonal morphology, which is characteristic of CEC. However, at day 19, cells started to form a cell network.

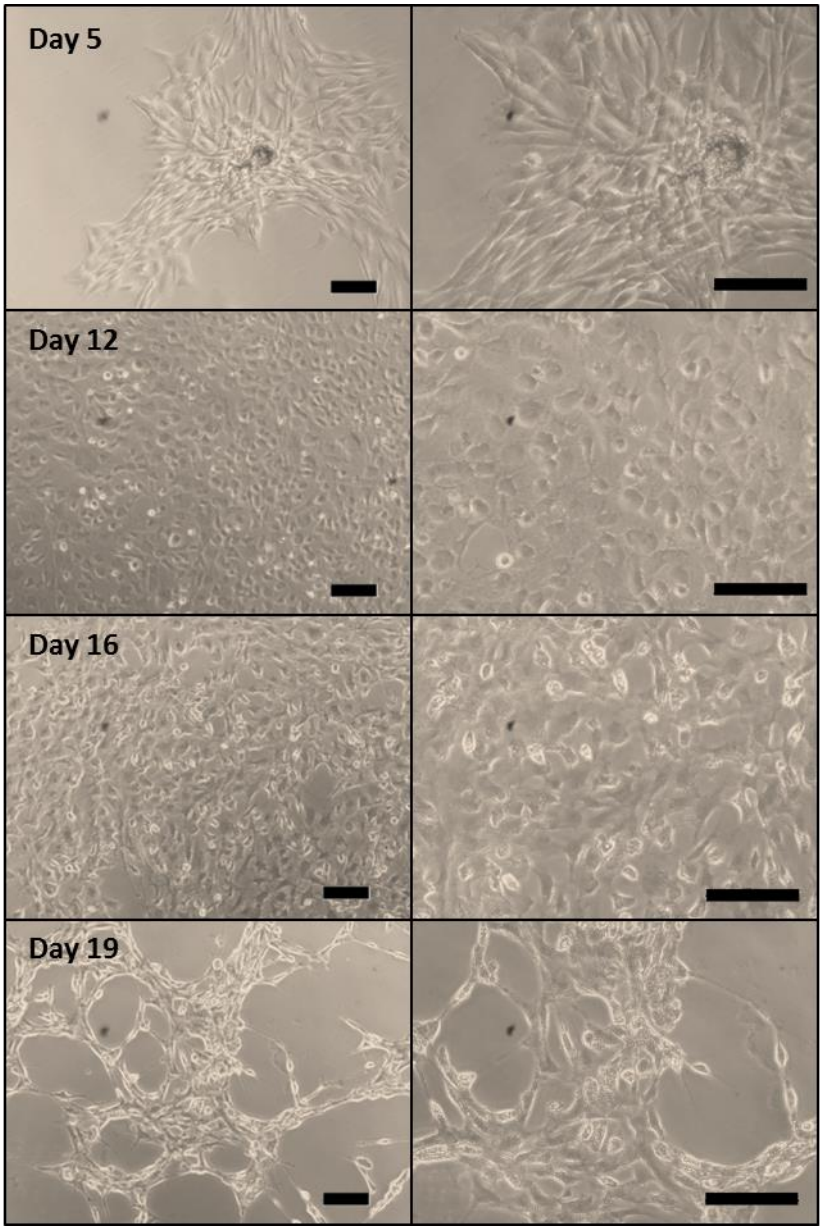

Figure 2. 43. Two-step differentiation into CEC using commercial conditioned medium B1at days 5, 12, 16 and 19. Scale bars: 100 µm

Regarding gene expression, compared to NCSC, characteristic CEC markers CDH2 and ZO-1 were significantly up-regulated during the differentiation process (Figure 2.44 A-B). Furthermore, as shown in Figure 2.44 C, the pump function marker ATP1A1 showed a significantly increased gene expression at the end of differentiation. Finally, characteristic CEC markers COL4A2 and COL8A2 also presented higher expression at day 19 (Figure 2.44 D-E). In general, as expected, values were lower than the positive control, which were the commercial CEC.

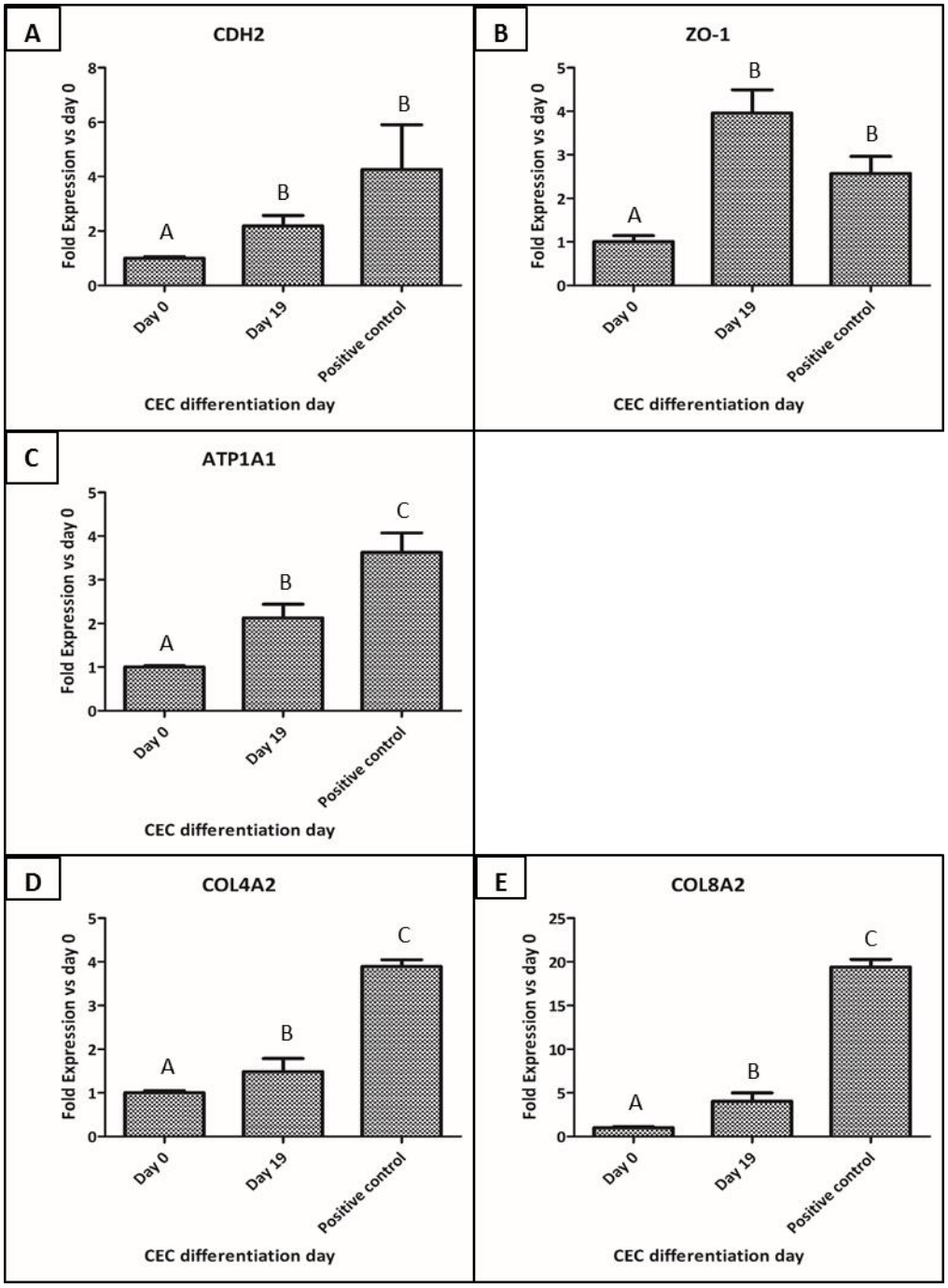

*Figure 2. 44. Two-step differentiation into CEC using commercial conditioned medium B1. Fold gene expression compared to day 0 of cell to cell contact markers (CDH2 and ZO-1), pump function marker (ATP1A1) and extracellular components (COL4A2 and COL8A2) at days 0 and 19 of CEC differentiation from DPSC. Analysis performed by quantitative PCR. * Different letter denotes significant differences. Same letter denotes non-significant differences.*

Isolated conditioned medium

Firstly, isolated corneal endothelium was cultured with its Descemet's membrane for 20 days in culture wells. Microscope images show the characteristic polygonal morphology of CEC during all culture days (Figure 2.45). Moreover, lower magnification images show how stripped Descemet's membrane presented large fragments throughout its culture. Conditioned medium collected from primary culture of CEC with its Descemet's membrane was used for the formation of CEC induction medium B2.

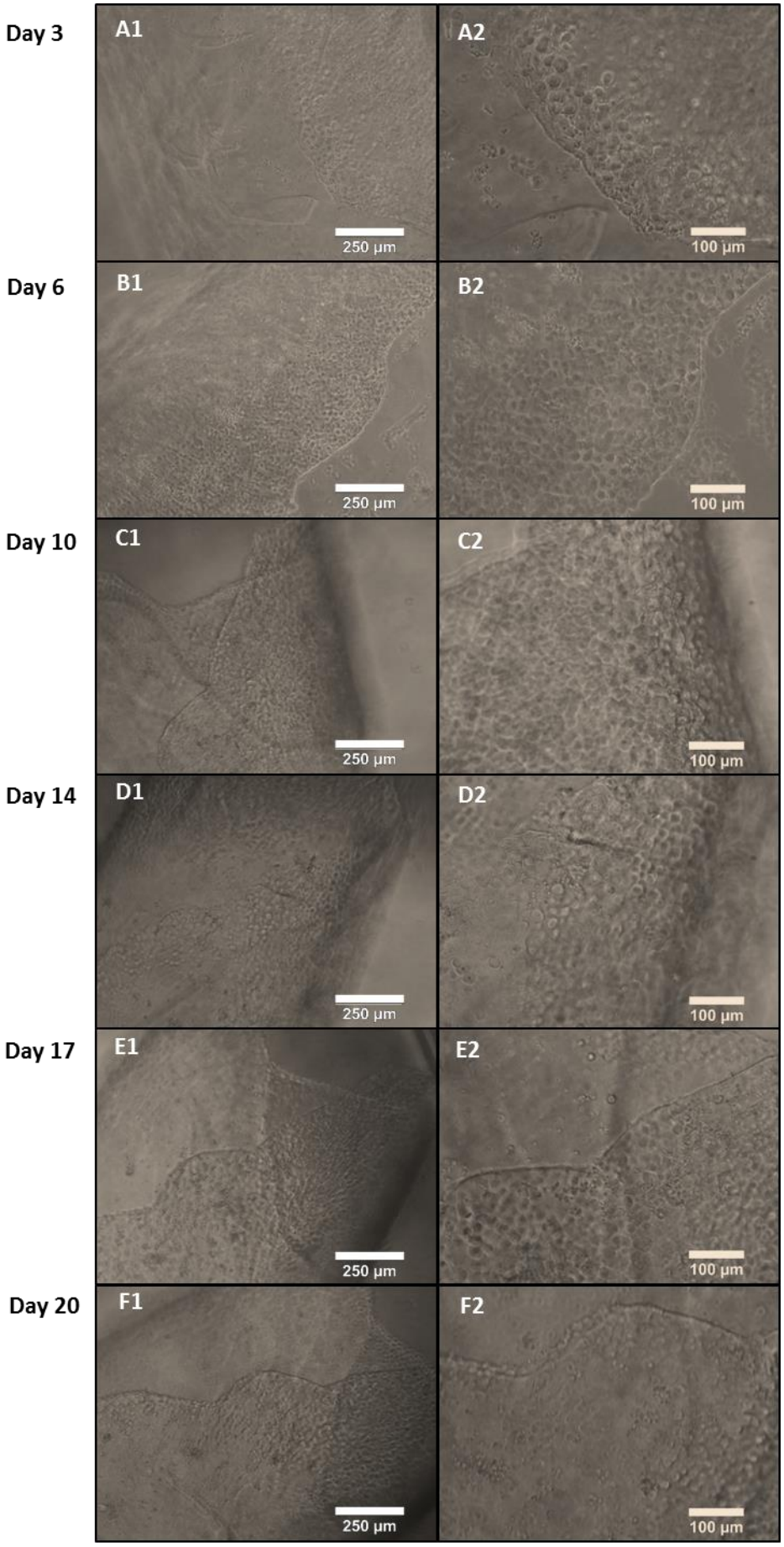
Day 3
A1
250 µm
A2
100 µm
Day 6
B1
250 µm
B2
100 µm
Day 10
C1
250 µm
C2
100 µm
Day 14
D1
250 µm
D2
100 µm
Day 17
E1
250 µm
E2
100 µm
Day 20
F1
250 µm
F2
100 µm

Figure 2. 45. Isolation of human corneal endothelium with its Descemet's membrane. Microscope images of human corneal endothelium at days 3, 6, 10, 14, 17 and 20 of cell culture in CEC medium. Scale bars: 250 µm (A1-F1) and 100 µm (A2-F2).

Then, conditioned medium B2, from isolated CEC, was used for CEC differentiation from NCSC-derived from DPSC.

Microscopy images (Figure 2.46) showed that NCSC-derived from DPSC started to emerge from NS on adherent dishes. Day 5 of the differentiation was taken at the time point in which the NS were cultured on the Petri dish. Then, cells were re-plated at a very high cell density for CEC differentiation. Images showed that at day 12, cells already started to present the characteristic polygonal morphology of CEC. However, at day 19 of the differentiation, due to the cell confluence, cells mostly exhibited the polygonal morphology, although some more elongated cells could be visualized.

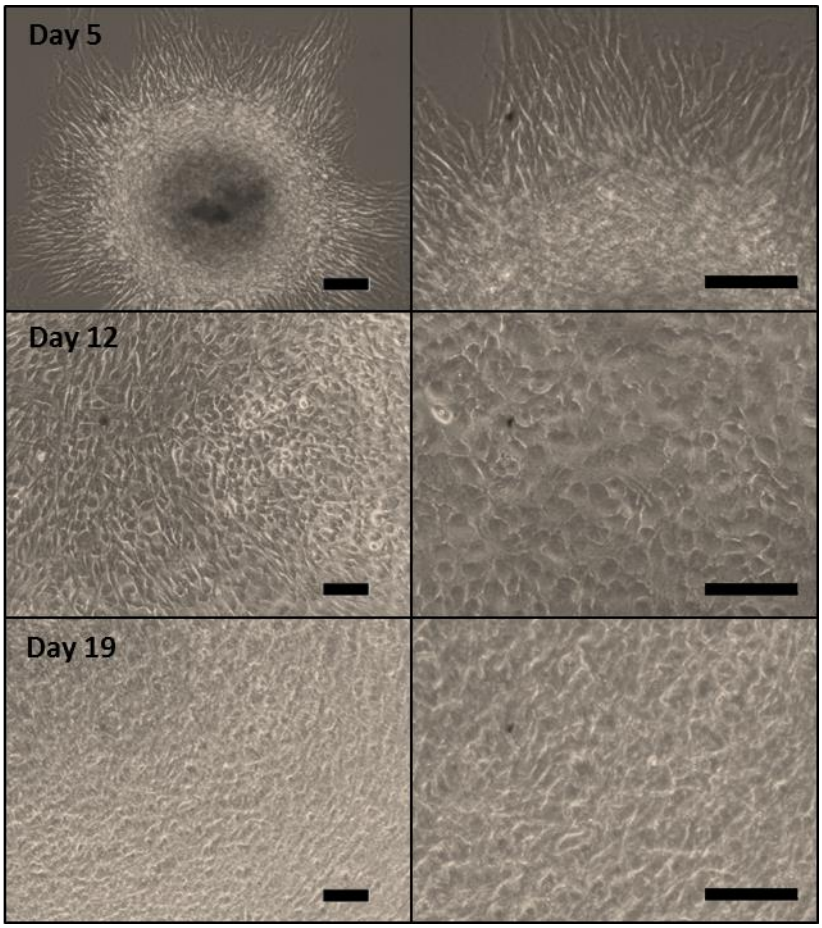

Figure 2. 46. Two-step differentiation into CEC using isolated conditioned medium B2. Microscope images at days 5, 12 and 19 of CEC differentiation from DPSC. Scale bars: 100 µm.

Regarding gene expression (Figure 2.47), we compared the values of different genes during the differentiation compared to the control cells, which were CEC from isolated donor corneas. The early CEC marker CDH2 decreased its expression during the differentiation process (Fig. 2.47 A). The expression of the cell to cell contact marker ZO-1 showed a significantly up-regulation at days 12 and 19 of the differentiation, showing similar values to that of control samples (Fig. 2.47 B). However, the pump function ATP1A1 expression showed a significantly progressive increase in the differentiation process (Fig. 2.47 C). Lastly, extracellular matrix components were analyzed, showing that COL4A2 and COL8A2 gene expression showed an up-regulation at days 12 and 19 of differentiation compared to undifferentiated DPSC (Fig. 2.47 D-E). As in previous differentiation, mostly all CEC markers, except ZO-1, from differentiated cells showed decreased levels compared to the control, which were CEC from isolated corneas.

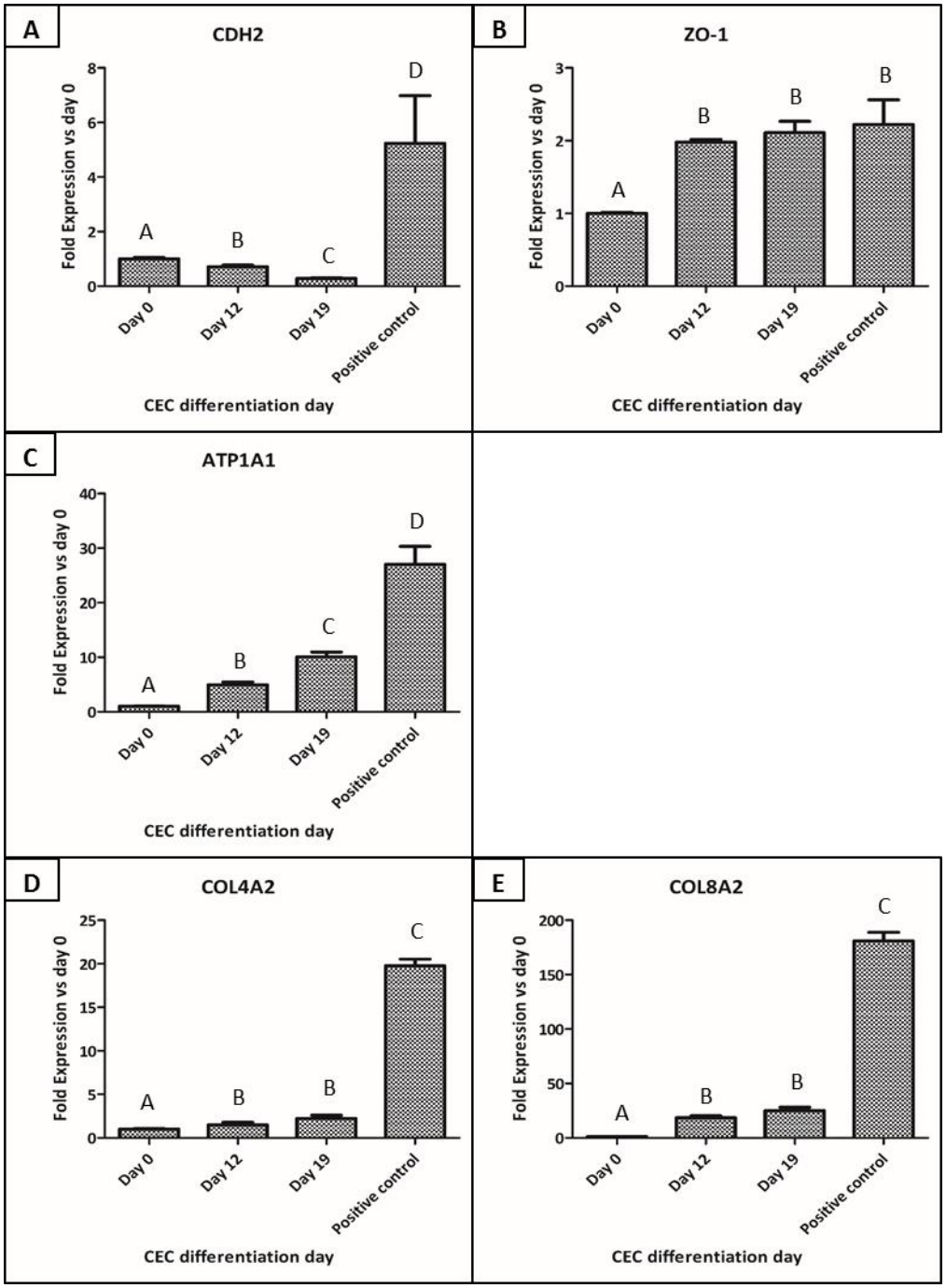

*Figure 2. 47. Two-step differentiation into CEC using isolated conditioned medium B2. Fold gene expression compared to day 0 of cell to cell contact markers CDH2 (A) and ZO-1 (B), pump function marker ATP1A1 (C) and extracellular components COL4A2 (D) and COL8A2 (E) at days 0, 12 and 19 of CEC differentiation. Analysis performed by quantitative PCR. * Different letter denotes significant differences. Same letter denotes non-significant differences.*

2.4. Discussion

Nowadays, the formation of patient-derived CEC *in vitro* is necessary to overcome actual problems such as shortage of cornea donors, immune rejection or safety problems, among others [2,8–10]. Therefore, the aim of this chapter was to investigate the feasibility of obtaining CEC from patient DPSC.

Firstly, DPSC were isolated from third molars of different patients. This represents a very accessible source, which is normally extracted for prophylactic causes. Furthermore, these cells exhibit potential self-renewal properties and also present similar characteristics to neural crest progenitor or stem cells due to their NC origin [30]. In the same way, CEC also arise from NC during embryogenesis [13]. Therefore, we hypothesized that CEC differentiation could be performed from DPSC. For doing this, a two-step protocol was used where first DPSC were differentiated into NCSC and then, NCSC-derived from DPSC were differentiated into CEC.

2.4.1. Induced pluripotent stem cells

Previous investigators used iPSC cells as the cell source for their NCSC differentiation [17,25,26]. Therefore, our positive control for the differentiation process were iPSC-derived from DPSC. For this reason, the first step was to transform DPSC into iPSC with a commercial kit. This process is performed by genetically modifying adult cells with the four Yamanaka factors (Oct3/4, Klf4, Sox2 and c-MYC) [54]. This results in the generation of cells with a pluripotent stem cell-like state similar to embryonic stem cells (ESC). There are different methods for transfecting cells with these four factors, such as integrative and non-integrative virus or with non-viral strategies such as chemical defined factors, among others [55]. We used a commercial kit (CytoTune™-iPS 2.0 Sendai Reprogramming Kit) that uses a non-integrative method using Sendai Virus (SeV). This process guarantees a safe and efficient form of introducing the Yamanaka factors in the cells without integrating the vector into the host cell and without altering its genetic information. This process has already been validated for different cell types, although the most commonly used cell source have been fibroblasts, which were used as a positive control in our experiment [17].

Initially, we were interested in studying the cell reprogramming efficiency of the described method and for this purpose iPSC colony formation was evaluated in feeder conditions. The

results showed that in general the different groups were able to efficiently transfect cells. Nevertheless, an anomaly was observed, showing that for instance, group DPSC 2 presented a very high transduction efficiency (Figure 2.16), but these cells were not able to form colonies. However, the DPSC 1 group, which presented a lower value of transfection, being near 64%, was able to form iPSC colonies (Figure 2.18). These results confirmed that cell reprogramming is age and sex-dependent, as donor from DPSC 1 was the youngest one (14-year-old woman), DPSC 2 was a 16-year-old woman and DPSC 3 and 4 were 16-year-old men. Moreover, our results also showed that transduction and reprogramming efficiency are not related. This is in line with a previous study which reported that reprogramming efficiency is age and donor-dependent [56]. Nevertheless, the overall results showed promising abilities of the DPSC to be reprogrammed into iPSC.

As described earlier, these results were obtained from feeder conditions. Interestingly, colonies were only able to grow in feeder conditions (Figure 2.18). This can be explained as feeder cells secrete factors and provide an extracellular matrix for cells that help in the maintenance of normal karyotype and in the maintenance of an undifferentiated state provided by the cellular contact [57]. However, the development of a feeder-free and xeno-free culture is necessary for future human therapeutic applications. Therefore, it is important to adapt iPSC to a feeder-free culture. Furthermore, feeder-free conditions also present some advantages as they are easier to culture, there is no need to pre-seed feeder cells and they are more reproducible, as there is no risk of fibroblast contamination with stem cells [58]. Therefore, iPSC colonies were adapted to feeder-free conditions. For this purpose, different routinely used substrates mimicking feeder layers were used to grow iPSC: Geltrex, which is a commercially available reduced growth factor basement membrane extract, and VTN, which is a matrix protein extracted from blood plasma. Although cells exhibited similar characteristic morphology in both substrates, colonies on Geltrex-coated dishes exhibited a more irregular morphology and also presented possible contamination of differentiated cells (Figure 2.20). These results are in line with a previous report which determined that iPSC seeded on VTN-coated dishes presented higher cell proliferation and cell survival and presented the characteristic morphology compared to iPSC cultured on Matrigel, which is generated from the same basement membrane as Geltrex [59,60]. Actually, some of the recent research is striving into comparing feeder and feeder-free

cultures of iPSC showing that, when the proper culture media is used, feeder-free conditions, such as Matrigel, provide similar results to the culture using feeder layer without jeopardizing the risk of fibroblast contamination [61]. For these reasons, VTN-coated dishes were used for further experiments.

Finally, in order to confirm the cell reprogramming process, gene expression was analyzed (Figure 2.21). Our results showed that iPSC-derived from DPSC exhibited significantly higher expression of both pluripotent markers (Oct4 and Nanog) compared to the positive control (iPSC-derived from fibroblasts). This can be explained as DPSC are isolated from third molars, which are the last teeth to develop. Furthermore, it has also been previously hypothesized that the epigenetic conformation of mesenchymal like stem cells probably decrease the barriers for cellular reprogramming, hence increasing efficiency and the rate of iPSC production compared to fibroblasts [58]. The fact that these type of cells endogenously already express some of the pluripotent markers, increases the chances of reprogramming [62]. In our case, due to its late development, DPSC present a stem/progenitor cell population and slightly expresses various pluripotent markers [63,64] in contrast to fibroblasts, which are differentiated cells. In fact, despite fibroblasts have been established as the gold standard for reprogramming, these have only been widely studied as a cell source to analyze iPSC production mechanisms. Therefore, our results are consistent with a previous study which evaluated the formation of iPSC from adipose tissue-derived mesenchymal stem cells and determined that endogenous low-level pluripotent expression of Oct4, Sox2, Klf4, and c-Myc enhanced cellular reprogramming [65]. Therefore, cell reprogramming to iPSC seems to be easily performed and with higher pluripotent levels in the case of DPSC than with fibroblasts.

2.4.2. Neural crest stem cells differentiation

NCSC represent a key cell source for many applications in tissue engineering due to its presence in neural and non-neural tissues like smooth muscle, bone and cornea [30], among others. In fact, due to its broad developmental potential, NC is often referred as the “fourth germ layer”, in addition to mesoderm, ectoderm and endoderm [3]. However, human NC cannot be studied due to ethical and technical problems as NC is only generated within the embryo during first weeks of embryogenesis [16]. Therefore, it is of great interest to

develop a protocol for obtaining NCSC from other sources. In this chapter, three methods were evaluated for the generation of NCSC.

As shown in Figure 2.49, different markers are implicated during the differentiation into NCSC. It has been reported that NCSC present stemness properties [14,66]. Our results showed that the expression of pluripotent markers such as Oct4, Sox2, Nanog and c-MYC and the early human marker CD34 increased during the beginning of the process, which is in agreement with previous results [67–69]. Moreover, the expression of the mesenchymal marker CD73, which has been described to be expressed in DPSC, decreases during the differentiation process [70]. Previous studies described that during NCSC differentiation, early inductive signals help the expression of transcription factors such as AP2, which activates the expression of NCSC genes as Sox9 and Sox10 [14,24,71,72]. Moreover, it has also been described that p75, CHD7 and Hnk1 are expressed in progenitor and migrating NCSC [22,24,25]. Furthermore, it has also been reported that the neural stem cell marker Nestin is expressed during NCSC differentiation [16,22,24,73].

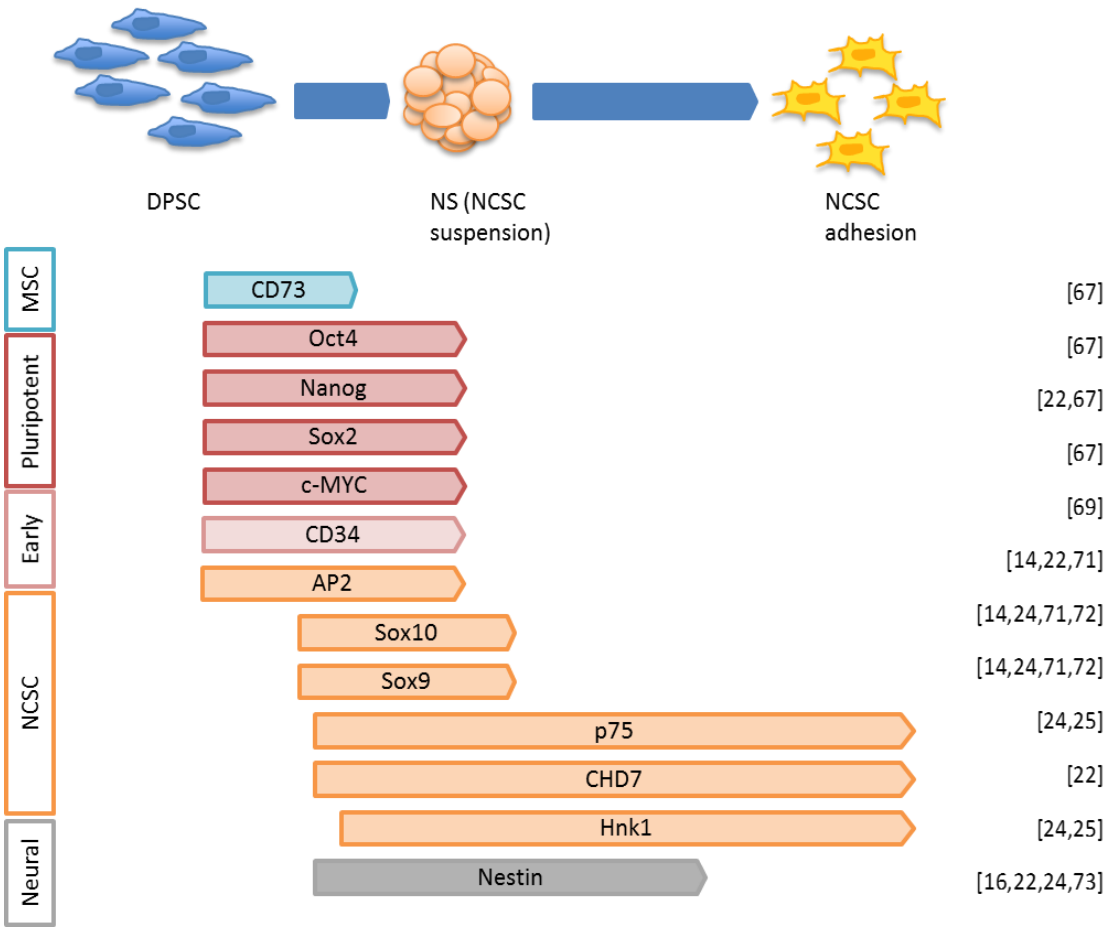

Figure 2.49. Summary of NCSC differentiation and expansion from DPSC. Expression of mesenchymal marker (CD73), pluripotency markers (Oct4, Nanog, Sox2 and c-MYC), human early or progenitor marker (CD34), NCSC markers (AP2, Sox9, Sox10, p75, Hnk1, CHD7) and neural marker (Nestin) during the differentiation process.

2.4.2.1. Adherent method

In this chapter, different methods were tried for an efficient generation of NCSC. Firstly, an adhesion culture based on a previous protocol [17] was used for the formation of NCSC. As expected, when the cell density was high, our results showed that AP2, P75 and Hnk1 exhibited higher levels at the end of the differentiation (Figure 2.25). AP2 is an early NCSC transcription factor, whereas p75 is a mid-term differentiation marker and Hnk1 mid-late term differentiation marker. When comparing the results between the iPSC differentiation and the direct DPSC differentiation into NCSC, we saw that the levels of the early maker AP2 showed significantly higher levels in the iPSC differentiation than in the DPSC differentiation. This could be related with the fact that iPSC presented a more undifferentiated phenotype whereas DPSC actually have some common markers with NCSC.

In other words, DPSC are able to express NCSC makers without any induction. For this reason, it is hypothesized that iPSC took longer time for the complete differentiation, hence only expressing the early marker AP2, whereas DPSC was already in the mid-term process of the differentiation and hence showed lower levels of AP2 and p75, but expressed significantly higher levels of the mid-late term marker Hnk1. On the one hand, iPSC cells are in a pluripotent state so during NCSC differentiation we expected to present at first higher expression of early NCSC transcription factors such as AP2 [54]. On the other hand, DPSC are derived from the NC, and as shown by Janebodin et al., undifferentiated DPSC already express some NCSC characteristic cell markers [64]. For this reason, we expected that at the end of differentiation they expressed late NCSC markers such as Hnk1.

Regarding cell density, iPSC started to detach from the plates after 14 days of differentiation, as shown in Figure 2.26. Therefore, we reduced the seeding cell density in order to overcome this problem. Our results showed that a reduction in the seeding cell density was able to decrease cell detachment, even after 3 weeks in culture (Figure 2.26). Moreover, only in the positive control differentiation, cells exhibited its characteristic stellate morphology, as in previous differentiations [22,26,74]. Regarding the gene expression, in the positive control the gene expression only increased for the mid-term NCSC marker P75 (Figure 2.27). Although differentiated DPSC did not present NCSC typical morphology, surprisingly the gene expression of NCSC marker AP2 was up-regulated. One possible explanation of the slightly different behavior when the cell density was decreased in order of magnitude is related with the cell to cell interactions that are produced in the cell culture [75]. For the higher cell density, we expected to have higher cell to cell interactions, hence decreasing the cell to matrix interactions and hence mimicking a similar trend to those observed with the NS [75]. Nevertheless, when the cell density was decreased, the levels of cell to cell interactions was decreased and the cell to matrix interactions was increased, also reducing the signaling between cells and hence become distant from the NS like behavior. This made the differentiation markers have a different trend, showing lower levels of iPSC for the AP2 throughout the 21 days of differentiation. Nevertheless, DPSC showed increasing levels of AP2 levels after 14 days, which ultimately decreased at 21 days. Our hypothesis was that no significant markers could be expressed for the differentiation of iPSC, but these levels were expressed for the DPSC, clearly showing

that the differentiation had started for the DPSC cells. Furthermore, the differentiation seemed to end in the initial stage as the levels of the mid-term marker p75 were low in all cases.

2.4.2.2. Neurosphere formation

Other studies have reported that suspension conditions also induced NCSC differentiation [20,26]. Therefore, our next hypothesis was that the formation of floating clusters named as NS should enhance the differentiation process. It has been previously reported that the cell to cell contact may enhance the pluripotent like status an hence allow a better development similar to that of embryonic development and hence enhanced the neural differentiation [26]. The process was performed for both the iPSC and for the DPSC, showing that only iPSC were able to successfully form the NS. DPSC showed the formation of cell aggregates (Figure 2.28), as they could not be considered NS, since it has been previously described that NS are generally in the range of sizes between 100 and 200 microns [76]. Cell aggregates could be of interest, but we hypothesized that the smaller size would lead to decreased cell to cell contact and hence interfere with the expected higher pluripotency. Furthermore, the NS like clusters tended to attached on the well plate in the iPSC, which lead to the conclusion that the well plates were not adequate for this type of culture. Once again, the fact that the cell to cell contact was decreased and the cell to matrix contact was increased, the pluripotent markers were inherently decreased as was previously seen [77]. In the previous study, the comparison between a cell to cell contact and a cell to matrix contact was analyzed based on its pluripotent markers expression, confirming that pluripotent markers progressively decreased when cell to matrix contact increased [77]. For this purpose, we changed the cell culture plates and performed similar experimental plan only using DPSC, as iPSC had already somehow worked. In addition, we believed that prolonged culture times jeopardized the NS formation and its survival, as it is known that as the NS size increases, the chances of oxygen and nutrient diffusion into the central cells is decreased [76]. For this purpose, we expected reducing the culture time points to avoid presenting NS with sizes beyond 250 microns, as is it known that diffusion of nutrients and oxygen above 300 microns is very limited [76]. For this purpose, we then determined the optimal peak day for NCSC induction.

We examined NCSC differentiation based on mRNA expression, which showed that early NCSC markers AP2 and Sox9 had its higher expression before day 4 (Figure 2.30).

Furthermore, NCSC markers p75 and CHD7 showed its peak expression at day 4, which is in line with previous reports that determined that p75 and CHD7 are necessary for the formation of migratory NCSC [22]. Neural marker Nestin also increased during the differentiation process, which had been previously determined [16,73]. On the other hand, as reported in a previous study, the expression of the mesenchymal marker CD73 decreased through the differentiation process [15].

Moreover, suspension culture allows cell to cell interactions, which supports the induction of progenitor or stem cells [20]. In fact, it has been demonstrated that suspension culture and the formation of three-dimensional aggregates recapitulates early embryogenesis as they spontaneously begin gastrulation [46]. Further, previous reports showed that neural crest stem or progenitor cells present "stemness" properties [14,66]. This could explain the increased gene expression of pluripotent (Oct4, Sox2, Nanog and c-MYC) and progenitor or early human stem cell marker (CD34) during first days of NCSC differentiation (Figure 2.31).

Finally, as shown in Figure 2.32, we were able to confirm by immunofluorescence assay that NCSC marker p75 was expressed in the periphery of the NS. Previous studies reported as well similar results, showing as well the expression in the periphery of the NS [21].

Neural crest stem cell expansion

As corneal endothelial cell (CEC) differentiation requires a starting high cell density, an expansion of the NS in adhesion conditions was performed. As Le Douarin et al. reported that migrating NCSC give rise to a variety of differentiated phenotypes, including cardiac cells, gut cells, pigment cells, smooth muscle cells, odontoblasts, endocrine cells , neurons and glial cells, among others, NCSC characterization was confirmed on different days of cell expansion [78]. As shown in Figures 2.34-2.37, our results show that expansion of NS in adhesion conditions decreased the expression of NCSC markers. In fact, the early NCSC marker Sox10 was highly expressed in suspension conditions and its expression dramatically decreased in adhesion conditions. These results initially seemed contradictory, as previous results have shown that Sox10 seemed to be expressed at higher rates in migrating adherent cells compared to the NS [15]. This could be explained by the difference in size of the NS. In our case, the NS size was in the size range between 100 and 200 microns, whereas in the previous paper the NS size ranged 1000 microns. This expanded size

probably decreased the chances of survival in the center of the NS, creating hypoxia conditions and stimulating cells to migrate out of the NS. Previous results showed NS in sizes range similar to our results, showing that normal NS were in the range of few hundreds of microns [76,79–83]. Nestin, which has also been reported to be present during NCSC differentiation [73], decreased its level of expression in expanded cells. However, mRNA and protein expression of mid-late NCSC marker P75, increased through the 19 days of NCSC induction and expansion. As was previously seen, it was expected that the levels of p75 increased as this marker is related to migrating cells [21]. Finally, as shown in Figure 2.34-2.37 and related with the fact that in adhesion, cell to matrix interactions were enhanced and the cell to cell contact was decreased we expected a decrease in the pluripotent markers. As expected, protein and mRNA expression of pluripotent markers increased during suspension culture but when NS were cultured in adhesion conditions its levels decreased, as confirmed by previous reports [22,67].

2.4.2.3. Embryoid body formation

In the third and final strategy, which was very related to the second strategy, we intended forming EB, which are slightly different to NS, despite both of them enhance the cell to cell contact. The main differences between both of them was the induction medium used, as the EB medium tended to increase more pluripotent markers than the medium used for NS formation, which tended to increase the levels of neural crest markers. It has been reported that EB, which are cell aggregates from pluripotent cells, can be differentiated to any cell type. Therefore, we hypothesized that EB formation, should facilitate NCSC induction. It was previously shown that higher NCSC markers were observed when embryoid bodies were formed [16,84,85].

Our results showed that, although NCSC marker AP2 expression was higher when EB formation was induced, the differentiation using NS directly also presented very high levels of AP2 expression (Figure 2.39). Nevertheless, the levels of p75 were decreased. It has to be considered that AP2 is an early marker, whereas p75 is a mid-stage maker. The fact that the levels of AP2 are higher for the EB pathway compared to the NS formation and that these values are opposite for the mid stage marker p75 could lead to a possible conclusion that the differentiation is accelerated for the NS formation. Furthermore, it has to be taken into account that the time taken to achieve each culture is significantly different taking 14 days

for the EB route and only 4 days for the NS route. Hence, this new alternative is clearly showing an economic and timeless strategy to obtain similar results. Therefore, we determined that NCSC differentiation via EB formation was not required and DPSC cells could be directly differentiated to NCSC after 4 days of suspension culture.

2.4.3. Corneal endothelial cell differentiation

The aim of this chapter was to generate CEC using a two-step protocol, where DPSC were differentiated into NCSC and then to CEC. In fact, different groups have already generated CEC using a NC induction step protocols [7,9,10,86]. Nevertheless, the routes to achieve the NCSC are based on pluripotent cells such as embryonic stem cells and iPSC. Once the first step of the differentiation process was optimized and confirmed, differentiation from NCSC-derived from DPSC into CEC was attempted by different strategies. Each strategy was evaluated by the expression of different CEC gene markers. As there are different markers for the characterization of HCEC, we selected the expression of markers that are implied on cell functionality and extracellular components secreted by CEC.

As shown in Figure 2.51, firstly, cell to cell contact markers are expressed, like the tight junction ZO-1 and N-cadherin (CDH2), which acts as cell barrier [11]. Then, cells start to differentiate and they become functional, expressing Na^+/K^+-ATPase α1-subunit (ATP1A1), which is the main pump transporter of excess fluid from the cornea [87]. This is consistent with a previous study which determined that ZO-1 tight junction is expressed earlier than pump function ATP1A1 [88]. Finally, CEC secrete collagen type IV and VIII, as COL4A2 and COL8A2, which are components of the Descemet's membrane [89–91] For this reason, the gene expression of CDH2, ZO-1, ATP1A1, COL4A2 and COL8A2 was analyzed for CEC characterization.

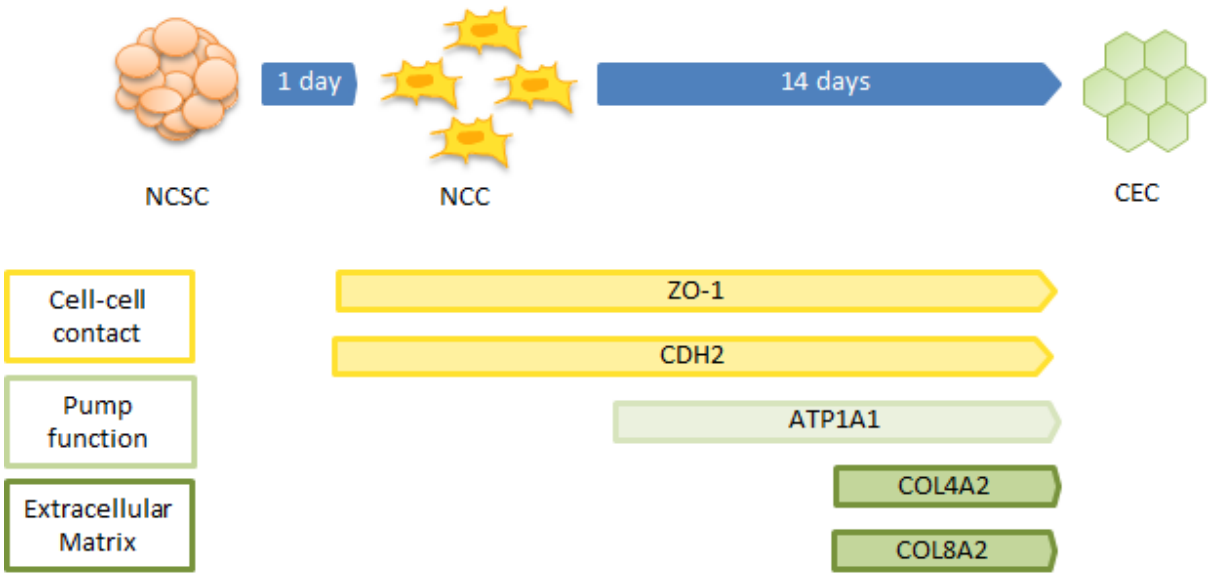

Figure 2.51. Summary of CEC differentiation from NCSC. Expression of cell-cell contact markers (ZO-1 and CDH2), pump function marker (ATP1A1) and extracellular matrix components (COL4A2 and COL8A2) during the differentiation process.

2.4.3.1. One-step differentiation

In order to understand this first mechanism of differentiation into CEC, it is important to initially understand how CEC are formed in natural environments. Corneal endothelium embryogenesis starts when mesenchyme cells are connected to adjacent cells through bands of tight junction complexes and a monolayer of cells is formed. Later, mesenchymal cells start to differentiate and form CEC. Finally, CEC secrete collagen and form the Descemet's membrane [92,93]. Therefore, we hypothesized that CEC differentiation should present the same evolution.

Our first induction method was to perform a direct differentiation from DPSC, as DPSC and CEC have the same embryological origin and DPSC already present NCSC characteristics [30,64]. Previous studies have confirmed that CD73-negative cells presented hexagonal morphology and high expression of characteristic CEC markers [50]. For this reason, DPSC were successfully separated against CD73 antibody (Figure 2.40).

Once CD73-negative population was expanded and characterized, CEC differentiation was performed based on a previous protocol where human iPSC and corneal stromal cells were differentiated into CEC [47]. However, our results showed that CD73-negative DPSC were

not able to survive when they were cultured on this differentiation medium (Figure 2.42). The differentiation medium contained transforming growth factor-beta 2 and a glycogen synthase kinase inhibitor (GSK3 inhibitor), which had been already described to induce NCSC formation by activating Smad3 and Wnt pathway [9,94]. Despite of the culture media used, cells were not able to survive. This could be related with the fact that CD73 is related to cellular multiresistence so CD73-negative cells are more sensitive [95]. Furthermore, the fast reduction of their stemness probably reduced the cell to cell contact which deemed cells into an unresponsive status in which cells were not able to poorly communicate and hence started decreasing their metabolic activity. Perhaps, a more progressive induction of the cell population with defined culture media into a CD73-negative population would have increased the chances of cell survival. This confirmed that, although CD73-negative DPSC population already expressed some NCSC markers, direct differentiation using defined culture medium was not able to generate CEC.

2. 4. 3. 2. Two-step differentiation

As our initial results showed that defined medium was not able to differentiate DPSC into CEC, we then used a non-defined medium. Previous studies revealed that the formation of functional CEC from pluripotent stem cells and adult stem cells could be performed using co-culture systems or conditioned medium [6,11,45,96]. In fact, it has been described that *in vitro* cells secrete paracrine signals and soluble factors to cell media and create a microenvironment which mimics *in vivo* effects [96,97]. Therefore, the second strategy was to perform CEC differentiation from NCSC-derived from DPSC, using conditioned medium from CEC. As described earlier, two possible culture media were used.

Commercial conditioned medium

Firstly, commercial conditioned medium B1 was used. NCSC with its characteristic morphology were plated at a high cell density for CEC differentiation. As shown in Figure 2.43, at day 12 and 16 of CEC differentiation a monolayer of polygonal cells was formed. These images may indicate the formation of CEC, as they exhibit its characteristic morphology. However, at day 19 elongated cells started to appear, which may indicate that CEC started to become more fibroblastic cells. These results can be explained as the composition of the commercial conditioned medium B1 is unknown and it may contain

some factors such as vascular endothelial growth factor or fibroblast growth factor which can lead to the formation of corneal fibroblasts and form cell networks [98–100]. On the one hand, the cell morphology was clearly indicating that the cells were not behaving as normal HCEC, showing an elongated morphology. This could be ascribed to the endothelial to mesenchymal transition (EndMT), which is a variant of the epithelial to mesenchymal transition [101]. This is mainly related with the fact that CEC are in a non-proliferative state *in vivo* and in order to achieve a proliferative status *in vitro*, cells needed to be treated with specific cell culture media. In this sense, the addition of growth factors as well as the disruption of cell to cell contacts has allowed this proliferative status, but at the same time the phenotype expression has been postulated to change into a fibroblastic type [102–105]. A possible triggering stimuli could be provided by the cell culture media, as was previously postulated that the triggering factors for the transition from a rather endothelial phenotype to a fibroblastic phenotype could be TGF-β1-2-3, IL-1β, FGF-2 and Cx43 [100]. It was shown that the commercial cell culture media presented some of these factors, such as FGF2 and could therefore be postulated as one of the reasons for the change in phenotype. In order to understand more their characteristics, we analyzed CEC markers, which showed a higher gene expression at the end of the differentiation process (Figure 2.44). The values were in general lower than the controls and only presented a slight increase compared to the NCSC cells, therefore possibly demonstrating that the CEC phenotype was only slightly achieved. Further experiments should be performed analyzing the fibroblastic genes in order to verify the hypothesis. Furthermore, further experiments should study the use of specific media that limit the use of specific growth factors involved in the transition from endothelial to fibroblastic cells. These results indicate that conditioned medium enhanced CEC differentiation but some factors seemed to differentiate cells into corneal fibroblasts.

Isolated conditioned medium

In order to prevent corneal fibroblast contamination, last strategy for CEC differentiation was to use conditioned medium B2, which was collected from freshly isolated human corneal endothelium. For this reason, corneal endothelium with its Descemet's membrane was isolated from human donor corneas that were unable to be transplanted due to positive serology or history of cancer. Corneal endothelium with Descemet's membrane

were cultured for 20 days and cells exhibited its typical polygonal/hexagonal morphology during all the culture [93].

For the generation of patient-derived CEC with CEC conditioned medium B2 from isolated CEC, NCSC-derived from DPSC were differentiated into CEC.

Focusing on the microscope images, as expected, NCSC-derived from DPSC started to become polygonal-shaped at day 12 of differentiation and was maintained until the end of differentiation (Figure 2.46). Aiming to characterize CEC differentiation, gene expression revealed a higher expression in characteristic early CEC markers as tight junction ZO-1, pump function ATP1A1 and late CEC markers COL4A2 and COL8A2, as expected (Figure 2.47). The results showed significantly higher values compared to the use of commercially available culture medium, hence indicating the great potential of the conditioned medium produced by the native CEC. This reveals the importance of cross-talks between different cell types [106,107]. Despite NCSC and CEC do not simultaneously exist during embryogenesis, during the development it is expected that some singular moments in which both of them co-exist is possible and hence stimulate the formation of CEC [108]. Unexpectedly, CDH2 was down-regulated during the differentiation process. It could be hypothesized that CDH2 is a rather early marker and hence its expression was not significant since the conditioned medium was a very strong inducer of CEC and somehow was able to push cells into the CEC faster than the commercially available culture media [109]. This would also be related with the fact that the other mid-late markers increase their values significantly compared to the use of commercial media. Further assays should be performed in order to optimize and characterize the formation of CEC from NCSC. All in all, this chapter presents an efficient and simple protocol for the generation of NCSC from patient cells, which can be used for the generation of CEC. The formation of patient-derived CEC would overcome actual problems of corneal endothelium regeneration.

2. 5. Conclusions

In the present study, initial assays determined that iPSC could be generated from DPSC obtaining better results compared to fibroblasts, which are the most common cells used for reprogramming. Moreover, results have shown that DPSC can be successfully differentiated into NCSC using the neurospheres method in a similar way to iPSC. The differentiated cells

presented self-renewal and multipotency abilities and expressed typical NCSC markers. Moreover, NCSC-derived from DPSC were able to generate CEC, which exhibited its characteristic hexagonal morphology and presented an up-regulation in the expression of CEC markers at the end of the differentiation. All in all, this chapter presents an efficient and simple protocol for the generation of NCSC from patient cells, which can be used for the generation of CEC. The formation of patient-derived CEC would overcome actual problems of corneal endothelial regeneration.

2. 6. References

[1] N.C. Joyce, Proliferative capacity of corneal endothelial cells, Exp. Eye Res. 95 (2012) 16–23. doi:10.1016/j.exer.2011.08.014.

[2] J. Navaratnam, T.P. Utheim, V.K. Rajasekhar, A. Shahdadfar, Substrates for Expansion of Corneal Endothelial Cells towards Bioengineering of Human Corneal Endothelium., J. Funct. Biomater. 6 (2015) 917–45. doi:10.3390/jfb6030917.

[3] K.R. Katikireddy, T. Schmedt, M.O. Price, F.W. Price, U. V Jurkunas, Existence of Neural Crest-Derived Progenitor Cells in Normal and Fuchs Endothelial Dystrophy Corneal Endothelium., Am. J. Pathol. 186 (2016) 2736–50. doi:10.1016/j.ajpath.2016.06.011.

[4] K. Miyata, J. Drake, Y. Osakabe, Y. Hosokawa, D. Hwang, K. Soya, T. Oshika, S. Amano, Effect of donor age on morphologic variation of cultured human corneal endothelial cells., Cornea. 20 (2001) 59–63.

[5] T. Senoo, N.C. Joyce, Cell cycle kinetics in corneal endothelium from old and young donors., Invest. Ophthalmol. Vis. Sci. 41 (2000) 660–7.

[6] C. Shao, Y. Fu, W. Lu, X. Fan, Bone marrow-derived endothelial progenitor cells: A promising therapeutic alternative for corneal endothelial dysfunction, Cells Tissues Organs. 193 (2011) 253–263. doi:10.1159/000319797.

[7] S. Hatou, S. Yoshida, K. Higa, H. Miyashita, E. Inagaki, H. Okano, K. Tsubota, S. Shimmura, Functional Corneal Endothelium Derived from Corneal Stroma Stem Cells of Neural Crest Origin by Retinoic Acid and Wnt/b-Catenin Signaling, Stem Cells Dev. 22 (2013) 828–39. doi:10.1089/scd.2012.0286.

[8] K. Zhang, K. Pang, X. Wu, Isolation and Transplantation of Corneal Endothelial Cell–Like Cells Derived from In-Vitro-Differentiated Human Embryonic Stem Cells, Stem Cells Dev. 23 (2014) 1340–1354. doi:10.1089/scd.2013.0510.

[9] K.L. McCabe, N.J. Kunzevitzky, B.P. Chiswell, X. Xia, J.L. Goldberg, R. Lanza, Efficient generation of human embryonic stem cell-derived corneal endothelial cells by directed differentiation, PLoS One. 10 (2015) 1–24. doi:10.1371/journal.pone.0145266.

[10] Q. Song, S. Yuan, Q. An, Y. Chen, F.F. Mao, Y. Liu, Q. Liu, G. Fan, Directed differentiation of human embryonic stem cells to corneal endothelial cell-like cells: A transcriptomic analysis, Exp. Eye Res. 151 (2016) 107–114. doi:10.1016/j.exer.2016.08.004.

[11] L. Shen, P. Sun, C. Zhang, L. Yang, L. Du, X. Wu, Therapy of corneal endothelial dysfunction with corneal endothelial cell-like cells derived from skin-derived precursors, Sci. Rep. 7 (2017) 13400. doi:10.1038/s41598-017-13787-1.

[12] T. Kunisada, K.I. Tezulka, H. Aoki, T. Motohashi, The stemness of neural crest cells and their derivatives, Birth Defects Res. Part C - Embryo Today Rev. 102 (2014) 251–262. doi:10.1002/bdrc.21079.

[13] P.Y. Lwigale, Corneal Development: Different Cells from a Common Progenitor, in: Prog. Mol. Biol. Transl. Sci., Academic Press, (2015) 43–59. doi:10.1016/bs.pmbts.2015.04.003.

[14] J.A. Liu, M. Cheung, Neural crest stem cells and their potential therapeutic applications, Dev. Biol. 419 (2016) 199–216. doi:10.1016/j.ydbio.2016.09.006.

[15] C.L. Curchoe, J. Maurer, S.J. McKeown, G. Cattarossi, F. Cimadamore, M. Nilbratt, E.Y. Snyder, M. Bronner-Fraser, A. V Terskikh, Early acquisition of neural crest competence during hESCs neuralization., PLoS One. 5 (2010) e13890. doi:10.1371/journal.pone.0013890.

[16] Q. Liu, S.C. Spusta, R. Mi, R.N.T. Lassiter, M.R. Stark, A. Höke, M.S. Rao, X. Zeng, Human neural crest stem cells derived from human ESCs and induced pluripotent stem cells: induction, maintenance, and differentiation into functional schwann cells., Stem Cells Transl. Med. 1 (2012) 266–78. doi:10.5966/sctm.2011-0042.

[17] L. Menendez, M.J. Kulik, A.T. Page, S.S. Park, J.D. Lauderdale, M.L. Cunningham, S. Dalton, Directed differentiation of human pluripotent cells to neural crest stem cells., Nat. Protoc. 8 (2013) 203–12. doi:10.1038/nprot.2012.156.

[18] W. Xu, Y. Wang, E. Liu, Y. Sun, Z. Luo, Z. Xu, W. Liu, L. Zhong, Y. Lv, A. Wang, Z. Tang, S. Li, L. Yang, Human iPSC-Derived Neural Crest Stem Cells Promote Tendon Repair in a Rat Patellar Tendon Window Defect Model, Tissue Eng. Part A. 19 (2013) 2439–2451.

doi:10.1089/ten.tea.2012.0453.

[19] M. Sakaue, M. Sieber-Blum, Human epidermal neural crest stem cells as a source of Schwann cells, Development. 142 (2015) 3188–3197. doi:10.1242/dev.123034.

[20] S. Abe, S. Yamaguchi, Y. Sato, K. Harada, Sphere-Derived Multipotent Progenitor Cells Obtained From Human Oral Mucosa Are Enriched in Neural Crest Cells., Stem Cells Transl. Med. 5 (2016) 117–28. doi:10.5966/sctm.2015-0111.

[21] G. Lee, H. Kim, Y. Elkabetz, G. Al Shamy, G. Panagiotakos, T. Barberi, V. Tabar, L. Studer, Isolation and directed differentiation of neural crest stem cells derived from human embryonic stem cells, Nat. Biotechnol. 25 (2007) 1468–1475. doi:10.1038/nbt1365.

[22] R. Bajpai, D.A. Chen, A. Rada-Iglesias, J. Zhang, Y. Xiong, J. Helms, C.P. Chang, Y. Zhao, T. Swigut, J. Wysocka, CHD7 cooperates with PBAF to control multipotent neural crest formation, Nature. 463 (2010) 958–962. doi:10.1038/nature08733.

[23] G. Lee, S.M. Chambers, M.J. Tomishima, L. Studer, Derivation of neural crest cells from human pluripotent stem cells, Nat Protoc. 5 (2010) 688–701. doi:10.1038/nprot.2010.35.

[24] X. Jiang, Y. Gwye, S.J. McKeown, M. Bronner-Fraser, C. Lutzko, E.R. Lawlor, Isolation and characterization of neural crest stem cells derived from in vitro-differentiated human embryonic stem cells., Stem Cells Dev. 18 (2009) 1059–1070. doi:10.1089/scd.2008.0362.

[25] A. Tomokiyo, K. Hynes, J. Ng, D. Menicanin, E. Camp, A. Arthur, S. Gronthos, P. Mark Bartold, Generation of Neural Crest-Like Cells From Human Periodontal Ligament Cell-Derived Induced Pluripotent Stem Cells, J. Cell. Physiol. 232 (2017) 402–416. doi:10.1002/jcp.25437.

[26] E. Kawano, T. Toriumi, S. Iguchi, D. Suzuki, S. Sato, M. Honda, Induction of neural crest cells from human dental pulp-derived induced pluripotent stem cells., Biomed. Res. 38 (2017) 135–147. doi:10.2220/biomedres.38.135.

[27] K. Lin, L. Xia, H. Li, X. Jiang, H. Pan, Y. Xu, W.W. Lu, Z. Zhang, J. Chang, Enhanced

osteoporotic bone regeneration by strontium-substituted calcium silicate bioactive ceramics, Biomaterials. 34 (2013) 10028–10042. doi:10.1016/j.biomaterials.2013.09.056.

[28] C.E. Wong, C. Paratore, M.T. Dours-Zimmermann, A. Rochat, T. Pietri, U. Suter, D.R. Zimmermann, S. Dufour, J.P. Thiery, D. Meijer, F. Beermann, Y. Barrandon, L. Sommer, Neural crest-derived cells with stem cell features can be traced back to multiple lineages in the adult skin, J. Cell Biol. 175 (2006) 1005–1015. doi:10.1083/jcb.200606062.

[29] G.M. Kruger, J.T. Mosher, S. Bixby, N. Joseph, T. Iwashita, S.J. Morrison, Neural crest stem cells persist in the adult gut but undergo changes in self-renewal, neuronal subtype potential, and factor responsiveness., Neuron. 35 (2002) 657–69.

[30] A. Achilleos, P.A. Trainor, Neural crest stem cells: discovery, properties and potential for therapy., Cell Res. 22 (2012) 288–304. doi:10.1038/cr.2012.11.

[31] J. Yu, H. He, C. Tang, G. Zhang, Y. Li, R. Wang, J. Shi, Y. Jin, Differentiation potential of STRO-1+ dental pulp stem cells changes during cell passaging., BMC Cell Biol. 11 (2010) 32. doi:10.1186/1471-2121-11-32.

[32] F. Ferro, R. Spelat, C.S. Baheney, Dental pulp stem cell (DPSC) isolation, characterization, and differentiation, in: Methods Mol. Biol., (2014) 91–115. doi:10.1007/978-1-4939-1435-7_8.

[33] K. Yusa, O. Yamamoto, H. Takano, M. Fukuda, M. Iino, Zinc-modified titanium surface enhances osteoblast differentiation of dental pulp stem cells in vitro., Sci. Rep. 6 (2016) 29462. doi:10.1038/srep29462.

[34] W. Zhang, X.F. Walboomers, T.H. Van Kuppevelt, W.F. Daamen, P.A. Van Damme, Z. Bian, J.A. Jansen, In vivo evaluation of human dental pulp stem cells differentiated towards multiple lineages, J. Tissue Eng. Regen. Med. 2 (2008) 117–125. doi:10.1002/term.71.

[35] M. Nakashima, K. Iohara, M. Murakami, H. Nakamura, Y. Sato, Y. Ariji, K. Matsushita, Pulp regeneration by transplantation of dental pulp stem cells in pulpitis: a pilot clinical study, Stem Cell Res. Ther. 8 (2017) 61. doi:10.1186/s13287-017-0506-5.

[36] M. Nakashima, K. Iohara, Recent Progress in Translation from Bench to a Pilot Clinical Study on Total Pulp Regeneration, J. Endod. 43 (2017) S82–S86. doi:10.1016/j.joen.2017.06.014.

[37] M. Aimetti, F. Ferrarotti, M. Gamba, M. Giraudi, F. Romano, Regenerative Treatment of Periodontal Intrabony Defects Using Autologous Dental Pulp Stem Cells: A 1-Year Follow-Up Case Series, Int. J. Periodontics Restorative Dent. 38 (2017) 51–58. doi:10.11607/prd.3425.

[38] R. d'Aquino, A. De Rosa, V. Lanza, V. Tirino, L. Laino, A. Graziano, V. Desiderio, G. Laino, G. Papaccio, Human mandible bone defect repair by the grafting of dental pulp stem/progenitor cells and collagen sponge biocomplexes., Eur. Cell. Mater. 18 (2009) 75–83.

[39] A. Giuliani, A. Manescu, M. Langer, F. Rustichelli, V. Desiderio, F. Paino, A. De Rosa, L. Laino, R. D'Aquino, V. Tirino, G. Papaccio, Three years after transplants in human mandibles, histological and in-line holotomography revealed that stem cells regenerated a compact rather than a spongy bone: biological and clinical implications., Stem Cells Transl. Med. 2 (2013) 316–24. doi:10.5966/sctm.2012-0136.

[40] F.N. Syed-Picard, Y. Du, K.L. Lathrop, M.M. Mann, M.L. Funderburgh, J.L. Funderburgh, Dental Pulp Stem Cells: A New Cellular Resource for Corneal Stromal Regeneration, Stem Cells Transl. Med. 4 (2015) 276–285. doi:10.5966/sctm.2014-0115.

[41] E. Kushnerev, S.G. Shawcross, S. Sothirachagan, F. Carley, A. Brahma, J.M. Yates, M.C. Hillarby, Regeneration of corneal epithelium with dental pulp stem cells using a contact lens delivery system, Investig. Ophthalmol. Vis. Sci. 57 (2016) 5192–5199. doi:10.1167/iovs.15-17953.

[42] S.P. Medvedev, A.I. Shevchenko, S.M. Zakian, Induced Pluripotent Stem Cells: Problems and Advantages when Applying them in Regenerative Medicine., Acta Naturae. 2 (2010) 18–28.

[43] K. Takahashi, S. Yamanaka, Induction of pluripotent stem cells from mouse embryonic and adult fibroblast cultures by defined factors., Cell. 126 (2006) 663–76.

doi:10.1016/j.cell.2006.07.024.

[44] A.L. Sabater, E.J. Andreu, M. García-Guzmán, T. López, G. Abizanda, V.L. Perez, J. Moreno-Montañés, F. Prósper, Combined PI3K/Akt and Smad2 activation promotes corneal endothelial cell proliferation, Investig. Ophthalmol. Vis. Sci. 58 (2017) 745–754. doi:10.1167/iovs.16-20817.

[45] P. Chen, J. Chen, C. Shao, C.Y. Li, Y.D. Zhang, W.J. Lu, Y. Fu, P. Gu, X. Fan, Treatment with retinoic acid and lens epithelial cell-conditioned medium in vitro directed the differentiation of pluripotent stem cells towards corneal endothelial cell-like cells, Exp. Ther. Med. 9 (2015) 351–360. doi:10.3892/etm.2014.2103.

[46] M. Baker, Embryoid bodies get organized, Nat. Reports Stem Cells. (2008). doi:10.1038/stemcells.2008.146.

[47] S. Shimmura, S. Hatou, K. Tsubota, S. Yoshida, Method for producing corneal endothelial cell, 2014.

[48] M.D. Wagoner, L.R. Bohrer, B.T. Aldrich, M.A. Greiner, R.F. Mullins, K.S. Worthington, B.A. Tucker, L.A. Wiley, Feeder-free differentiation of cells exhibiting characteristics of corneal endothelium from human induced pluripotent stem cells., Biol. Open. (2018) bio.032102. doi:10.1242/bio.032102.

[49] J.M. Brickman, P. Serup, Properties of embryoid bodies, Wiley Interdiscip. Rev. Dev. Biol. 6 (2017) e259. doi:10.1002/wdev.259.

[50] N. Okumura, H. Hirano, R. Numata, M. Nakahara, M. Ueno, J. Hamuro, S. Kinoshita, N. Koizumi, Cell surface markers of functional phenotypic corneal endothelial cells, Investig. Ophthalmol. Vis. Sci. 55 (2014) 7610–7618. doi:10.1167/iovs.14-14980.

[51] M. Yoshihara, Y. Hayashizaki, Y. Murakawa, Genomic Instability of iPSCs: Challenges Towards Their Clinical Applications, Stem Cell Rev. 13 (2017) 7. doi:10.1007/S12015-016-9680-6.

[52] A. Gore, Z. Li, H.-L. Fung, J.E. Young, S. Agarwal, J. Antosiewicz-Bourget, I. Canto, A. Giorgetti, M.A. Israel, E. Kiskinis, J.-H. Lee, Y.-H. Loh, P.D. Manos, N. Montserrat, A.D. Panopoulos, S. Ruiz, M.L. Wilbert, J. Yu, E.F. Kirkness, J.C. Izpisua Belmonte, D.J. Rossi,

J.A. Thomson, K. Eggan, G.Q. Daley, L.S.B. Goldstein, K. Zhang, Somatic coding mutations in human induced pluripotent stem cells., Nature. 471 (2011) 63–7. doi:10.1038/nature09805.

[53] M. Rius, A. Obradors, G. Daina, J. Cuzzi, L. Marqus, G. Calderón, E. Velilla, O. Martínez-Passarell, M. Oliver-Bonet, J. Benet, J. Navarro, Reliability of short comparative genomic hybridization in fibroblasts and blastomeres for a comprehensive aneuploidy screening: First clinical application, Hum. Reprod. 25 (2010) 1824–1835. doi:10.1093/humrep/deq118.

[54] K. Takahashi, K. Tanabe, M. Ohnuki, M. Narita, T. Ichisaka, K. Tomoda, S. Yamanaka, Induction of Pluripotent Stem Cells from Adult Human Fibroblasts by Defined Factors, Cell. 131 (2007) 861–872. doi:10.1016/j.cell.2007.11.019.

[55] N. Malik, M.S. Rao, A review of the methods for human iPSC derivation, in: Methods Mol. Biol., NIH Public Access (2013) 23–33. doi:10.1007/978-1-62703-348-0_3.

[56] Y. Oda, Y. Yoshimura, H. Ohnishi, M. Tadokoro, Y. Katsube, M. Sasao, Y. Kubo, K. Hattori, S. Saito, K. Horimoto, S. Yuba, H. Ohgushi, Induction of pluripotent stem cells from human third molar mesenchymal stromal cells., J. Biol. Chem. 285 (2010) 29270–8. doi:10.1074/jbc.M109.055889.

[57] S. Llames, E. García-Pérez, Á. Meana, F. Larcher, M. del Río, Feeder Layer Cell Actions and Applications., Tissue Eng. Part B. Rev. 21 (2015) 345–53. doi:10.1089/ten.TEB.2014.0547.

[58] N. Sun, N.J. Panetta, D.M. Gupta, K.D. Wilson, A. Lee, F. Jia, S. Hu, A.M. Cherry, R.C. Robbins, M.T. Longaker, J.C. Wu, Feeder-free derivation of induced pluripotent stem cells from adult human adipose stem cells., Proc. Natl. Acad. Sci. U. S. A. 106 (2009) 15720–5. doi:10.1073/pnas.0908450106.

[59] G. Chen, D.R. Gulbranson, Z. Hou, J.M. Bolin, V. Ruotti, M.D. Probasco, K. Smuga-Otto, S.E. Howden, N.R. Diol, N.E. Propson, R. Wagner, G.O. Lee, J. Antosiewicz-Bourget, J.M.C. Teng, J.A. Thomson, Chemically defined conditions for human iPSC derivation and culture., Nat. Methods. 8 (2011) 424–9. doi:10.1038/nmeth.1593.

[60] T. Salo, M. Sutinen, E. Hoque Apu, E. Sundquist, N.K. Cervigne, C.E. de Oliveira, S.U.

Akram, S. Ohlmeier, F. Suomi, L. Eklund, P. Juusela, P. Åström, C.C. Bitu, M. Santala, K. Savolainen, J. Korvala, A.F. Paes Leme, R.D. Coletta, A novel human leiomyoma tissue derived matrix for cell culture studies, BMC Cancer. 15 (2015) 981. doi:10.1186/s12885-015-1944-z.

[61] P. Ghasemi-Dehkordi, M. Allahbakhshian-Farsani, N. Abdian, A. Mirzaeian, J. Saffari-Chaleshtori, F. Heybati, G. Mardani, A. Karimi-Taghanaki, A. Doosti, M.-S. Jami, M. Abolhasani, M. Hashemzadeh-Chaleshtori, Comparison between the cultures of human induced pluripotent stem cells (hiPSCs) on feeder-and serum-free system (Matrigel matrix), MEF and HDF feeder cell lines, J. Cell Commun. Signal. 9 (2015) 233. doi:10.1007/S12079-015-0289-3.

[62] J.B. Kim, H. Zaehres, M.J. Araúzo-Bravo, H.R. Schöler, Generation of induced pluripotent stem cells from neural stem cells, Nat. Protoc. 4 (2009) 1464–1470. doi:10.1038/nprot.2009.173.

[63] G.T.-J. Huang, T. Yamaza, L.D. Shea, F. Djouad, N.Z. Kuhn, R.S. Tuan, S. Shi, Stem/Progenitor Cell–Mediated De Novo Regeneration of Dental Pulp with Newly Deposited Continuous Layer of Dentin in an In Vivo Model, Tissue Eng. Part A. 16 (2010) 605–615. doi:10.1089/ten.tea.2009.0518.

[64] K. Janebodin, O. V Horst, N. Ieronimakis, G. Balasundaram, K. Reesukumal, B. Pratumvinit, M. Reyes, Isolation and characterization of neural crest-derived stem cells from dental pulp of neonatal mice, PLoS One. 6 (2011) e27526. doi:10.1371/journal.pone.0027526.

[65] M.-J. Chen, Y. Lu, T. Hamazaki, H.-Y. Tsai, K. Erger, T. Conlon, A.S. Elshikha, H. Li, A. Srivastava, C. Yao, M. Brantly, V. Chiodo, W. Hauswirth, N. Terada, S. Song, Reprogramming adipose tissue-derived mesenchymal stem cells into pluripotent stem cells by a mutant adeno-associated viral vector., Hum. Gene Ther. Methods. 25 (2014) 72–82. doi:10.1089/hgtb.2013.011.

[66] S. Thomas, M. Thomas, P. Wincker, C. Babarit, P. Xu, M.C. Speer, A. Munnich, S. Lyonnet, M. Vekemans, H.C. Etchevers, Human neural crest cells display molecular and phenotypic hallmarks of stem cells., Hum. Mol. Genet. 17 (2008) 3411–25.

doi:10.1093/hmg/ddn235.

[67] E. Buitrago-Delgado, K. Nordin, A. Rao, L. Geary, C. LaBonne, Shared regulatory programs suggest retention of blastula-stage potential in neural crest cells, Science 348 (2015) 1332–1335. doi:10.1126/science.aaa3655.

[68] L.E. Sidney, M.J. Branch, S.E. Dunphy, H.S. Dua, A. Hopkinson, Concise review: Evidence for CD34 as a common marker for diverse progenitors, Stem Cells. 32 (2014) 1380–1389. doi:10.1002/stem.1661.

[69] S.S. Joshi, B. Tandukar, L. Pan, J.M. Huang, F. Livak, B.J. Smith, T. Hodges, A.A. Mahurkar, T.J. Hornyak, CD34 defines melanocyte stem cell subpopulations with distinct regenerative properties, PLOS Genet. 15 (2019) e1008034. doi:10.1371/journal.pgen.1008034.

[70] P.D. Potdar, Y.D. Jethmalani, Human dental pulp stem cells: Applications in future regenerative medicine., World J. Stem Cells. 7 (2015) 839–51. doi:10.4252/wjsc.v7.i5.839.

[71] E. Van Otterloo, W. Li, A. Garnett, M. Cattell, D.M. Medeiros, R.A. Cornell, R. Geisler, P. Haffter, R.N. Kelsh, Novel Tfap2-mediated control of soxE expression facilitated the evolutionary emergence of the neural crest., Development. 139 (2012) 720–30. doi:10.1242/dev.071308.

[72] P. Betancur, M. Bronner-Fraser, T. Sauka-Spengler, Genomic code for Sox10 activation reveals a key regulatory enhancer for cranial neural crest., Proc. Natl. Acad. Sci. U. S. A. 107 (2010) 3570–5. doi:10.1073/pnas.0906596107.

[73] S. Abe, K. Hamada, M. Miura, S. Yamaguchi, Neural crest stem cell property of apical pulp cells derived from human developing tooth, Cell Biol. Int. 36 (2012) 927–936. doi:10.1042/CBI20110506.

[74] R.B. Bressan, F.R. Melo, P.A. Almeida, D.A. Bittencourt, S. Visoni, T.S. Jeremias, A.P. Costa, R.B. Leal, A.G. Trentin, EGF-FGF2 stimulates the proliferation and improves the neuronal commitment of mouse epidermal neural crest stem cells (EPI-NCSCs), Exp. Cell Res. 327 (2014) 37–47. doi:10.1016/j.yexcr.2014.05.020.

[75] Q. Jiao, X. Li, J. An, Z. Zhang, X. Chen, J. Tan, P. Zhang, H. Lu, Y. Liu, Cell-Cell Connection Enhances Proliferation and Neuronal Differentiation of Rat Embryonic Neural Stem/Progenitor Cells, Front. Cell. Neurosci. 11 (2017) 200. doi:10.3389/fncel.2017.00200.

[76] F. Xiong, H. Gao, Y. Zhen, X. Chen, W. Lin, J. Shen, Y. Yan, X. Wang, M. Liu, Y. Gao, Optimal time for passaging neurospheres based on primary neural stem cell cultures, Cytotechnology. 63 (2011) 621–631. doi:10.1007/s10616-011-9379-0.

[77] Y. Elkabetz, G. Panagiotakos, G. Al Shamy, N.D. Socci, V. Tabar, L. Studer, Human ES cell-derived neural rosettes reveal a functionally distinct early neural stem cell stage, Genes Dev. 22 (2008) 152–165. doi:10.1101/gad.1616208.

[78] N.M. Le Douarin, E. Dupin, Multipotentiality of the neural crest, Curr. Opin. Genet. Dev. 13 (2003) 529–536. doi:10.1016/j.gde.2003.08.002.

[79] E. Binder, D. Natarajan, J. Cooper, R. Kronfli, M. Cananzi, J.-M. Delalande, C. McCann, A.J. Burns, N. Thapar, Enteric neurospheres are not specific to neural crest cultures: implications for neural stem cell therapies., PLoS One. 10 (2015) e0119467. doi:10.1371/journal.pone.0119467.

[80] K.-L. Mung, Y.-P. Tsui, E.W.-Y. Tai, Y.-S. Chan, D.K.-Y. Shum, G.K.-H. Shea, Rapid and efficient generation of neural progenitors from adult bone marrow stromal cells by hypoxic preconditioning, Stem Cell Res. Ther. 7 (2016) 146. doi:10.1186/s13287-016-0409-x.

[81] B. Jevans, C.J. McCann, N. Thapar, A.J. Burns, Transplanted enteric neural stem cells integrate within the developing chick spinal cord: implications for spinal cord repair, J. Anat. 233 (2018) 592–606. doi:10.1111/joa.12880.

[82] M. V Covey, J.W. Streb, R. Spektor, N. Ballas, REST regulates the pool size of the different neural lineages by restricting the generation of neurons and oligodendrocytes from neural stem/progenitor cells., Development. 139 (2012) 2878–90. doi:10.1242/dev.074765.

[83] N.A. Mundell, P.A. Labosky, Neural crest stem cell multipotency requires Foxd3 to maintain neural potential and repress mesenchymal fates, Development. 138 (2011)

641. doi:10.1242/DEV.054718.

[84] J. Itskovitz-Eldor, M. Schuldiner, D. Karsenti, A. Eden, O. Yanuka, M. Amit, H. Soreq, N. Benvenisty, Differentiation of human embryonic stem cells into embryoid bodies compromising the three embryonic germ layers., Mol. Med. 6 (2000) 88–95.

[85] Y. Zhou, M.L. Snead, Derivation of cranial neural crest-like cells from human embryonic stem cells., Biochem. Biophys. Res. Commun. 376 (2008) 542–7. doi:10.1016/j.bbrc.2008.09.032.

[86] E. Inagaki, S. Hatou, K. Higa, S. Yoshida, S. Shibata, H. Okano, K. Tsubota, S. Shimmura, Skin-Derived Precursors as a Source of Progenitors for Corneal Endothelial Regeneration., Stem Cells Transl. Med. 6 (2017) 788–798. doi:10.1002/sctm.16-0162.

[87] C.C. Lachaud, F. Soria, N. Escacena, E. Quesada-Hernández, A. Hmadcha, J. Alió, B. Soria, Mesothelial cells: A cellular surrogate for tissue engineering of corneal endothelium, Investig. Ophthalmol. Vis. Sci. 55 (2014) 5967–5978. doi:10.1167/iovs.14-14706.

[88] Y. Chen, K. Huang, M.N. Nakatsu, Z. Xue, S.X. Deng, G. Fan, Identification of novel molecular markers through transcriptomic analysis in human fetal and adult corneal endothelial cells, Hum. Mol. Genet. 22 (2013) 1271–1279. doi:10.1093/hmg/dds527.

[89] J.M. Fitch, D.E. Birk, C. Linsenmayer, T.F. Linsenmayer, The spatial organization of Descemet's membrane-associated type IV collagen in the avian cornea., J. Cell Biol. 110 (1990) 1457–68.

[90] S. Biswas, F.L. Munier, J. Yardley, N. Hart-Holden, R. Perveen, P. Cousin, J.E. Sutphin, B. Noble, M. Batterbury, C. Kielty, A. Hackett, R. Bonshek, A. Ridgway, D. McLeod, V.C. Sheffield, E.M. Stone, D.F. Schorderet, G.C. Black, Missense mutations in COL8A2, the gene encoding the alpha2 chain of type VIII collagen, cause two forms of corneal endothelial dystrophy., Hum. Mol. Genet. 10 (2001) 2415–23.

[91] D.W. DelMonte, T. Kim, Anatomy and physiology of the cornea, J. Cataract Refract. Surg. 37 (2011) 588–598. doi:10.1016/J.JCRS.2010.12.037.

[92] A. Cvekl, E.R. Tamm, Anterior eye development and ocular mesenchyme: new insights

from mouse models and human diseases., Bioessays. 26 (2004) 374–86. doi:10.1002/bies.20009.

[93] A.O. Eghrari, S.A. Riazuddin, J.D. Gottsch, Overview of the Cornea: Structure, Function, and Development, in: Prog. Mol. Biol. Transl. Sci., Academic Press (2015) 7–23. doi:10.1016/bs.pmbts.2015.04.001.

[94] L. Menendez, T.A. YatsYatskievych, P.B. Antin, S. Dalton, Wnt signaling and a Smad pathway blockade direct the differentiation of human pluripotent stem cells to multipotent neural crest cells, Proc. Natl. Acad. Sci. 108 (2011) 19240–19245. doi:10.1073/pnas.1207810109.

[95] A. Mikhailov, A. Sokolovskaya, G.G. Yegutkin, H. Amdahl, A. West, H. Yagita, R. Lahesmaa, L.F. Thompson, S. Jalkanen, D. Blokhin, J.E. Eriksson, CD73 participates in cellular multiresistance program and protects against TRAIL-induced apoptosis., J. Immunol. 181 (2008) 464–75. doi:10.4049/jimmunol.181.1.464.

[96] N.C. Joyce, D.L. Harris, V. Markov, Z. Zhang, B. Saitta, Potential of human umbilical cord blood mesenchymal stem cells to heal damaged corneal endothelium., Mol. Vis. 18 (2012) 547–64.

[97] J. Renaud, M.-G. Martinoli, Development of an Insert Co-culture System of Two Cellular Types in the Absence of Cell-Cell Contact, J. Vis. Exp. (2016). doi:10.3791/54356.

[98] A. Berthaut, P. Mirshahi, N. Benabbou, D. Azzazene, C. Bordu, A. Therwath, J. Legeais, M. Mirshahi, Vascular endothelial growth factor receptor-1 (VEGFR-1) expression in human corneal fibroblast decreased with age., Mol. Vis. 15 (2009) 1997–2007.

[99] O. Maltseva, P. Folger, D. Zekaria, S. Petridou, S.K. Masur, Fibroblast growth factor reversal of the corneal myofibroblast phenotype., Invest. Ophthalmol. Vis. Sci. 42 (2001) 2490–5.

[100] O. Roy, V.B. Leclerc, J.M. Bourget, M. Thériault, S. Proulx, Understanding the process of corneal endothelial morphological change in vitro, Investig. Ophthalmol. Vis. Sci. 56 (2015) 1228–1237. doi:10.1167/iovs.14-16166.

[101] S. Piera-Velazquez, Z. Li, S.A. Jimenez, Role of endothelial-mesenchymal transition (EndoMT) in the pathogenesis of fibrotic disorders., Am. J. Pathol. 179 (2011) 1074–80. doi:10.1016/j.ajpath.2011.06.001.

[102] N. Okumura, E.D.P. Kay, M. Nakahara, J. Hamuro, S. Kinoshita, N. Koizumi, Inhibition of TGF-β Signaling Enables Human Corneal Endothelial Cell Expansion In Vitro for Use in Regenerative Medicine, PLoS One. 8 (2013) e58000. doi:10.1371/journal.pone.0058000.

[103] K. Engelmann, P. Friedl, Optimization of culture conditions for human corneal endothelial cells, Vitr. Cell. Dev. Biol. 25 (1989) 1065–1072. doi:10.1007/BF02624143.

[104] K. Engelmann, J. Bednarz, M. Valtink, Prospects for endothelial transplantation., Exp. Eye Res. 78 (2004) 573–8.

[105] C. Zhu, N.C. Joyce, Proliferative response of corneal endothelial cells from young and older donors., Invest. Ophthalmol. Vis. Sci. 45 (2004) 1743–51.

[106] R.S. Lindoso, F. Collino, S. Bruno, D.S. Araujo, J.F. Sant'Anna, C. Tetta, P. Provero, P.J. Quesenberry, A. Vieyra, M. Einicker-Lamas, G. Camussi, Extracellular vesicles released from mesenchymal stromal cells modulate miRNA in renal tubular cells and inhibit ATP depletion injury., Stem Cells Dev. 23 (2014) 1809–19. doi:10.1089/scd.2013.0618.

[107] T.J. Morrison, M. V Jackson, E.K. Cunningham, A. Kissenpfennig, D.F. McAuley, C.M. O'Kane, A.D. Krasnodembskaya, Mesenchymal stromal cells modulate macrophages in clinically relevant lung injury models by extracellular vesicle mitochondrial transfer, Am. J. Respir. Crit. Care Med. 196 (2017) 1275–1286. doi:10.1164/rccm.201701-0170OC.

[108] J. Graw, Eye development, 2010. doi:10.1016/S0070-2153(10)90010-0.

[109] P.Y. Lwigale, P.A. Cressy, M. Bronner-Fraser, Corneal keratocytes retain neural crest progenitor cell properties, Dev. Biol. 288 (2005) 284–293. doi:10.1016/J.YDBIO.2005.09.046.

Chapter III: MODULATING CORNEAL ENDOTHELIAL CELL RESPONSE WITH CORNEAL MIMICKING SUBSTRATES

Chapter III: Modulating corneal endothelial cell response with corneal mimicking substrates

3. 1. Introduction

The extracellular matrix (ECM) is a well-organized network composed of different materials and topographies depending on the tissue or organ [1]. It provides structural and mechanical support and directs cell attachment, proliferation and differentiation [1]. For this reason, extensive amounts of research have focused on the fabrication of substrates that resemble the ECM properties to enhance *in vitro* cell growth, function and differentiation [2–5]. The ECM can be mimicked by different strategies, which are mainly related to the physical properties, the chemical properties, its architecture or the external modulation. While the physical properties mainly take into account the structural aspects, such as the elastic modulus, the surface topography or its degradation properties, the chemical aspects deal with the presence of functional groups, the incorporation of releasable biologically active molecules or even the presence of ionic component that may have therapeutic activities [6,7]. Another relevant aspect is how its architecture is able to mimic the natural tissue that needs to be mimicked. In this sense, replicating the complex hierarchical structure of natural tissues is vastly complicated, but some attempts have been made that are very relevant for successful tissue regeneration [6,8].

These substrates may be generally described as biomaterials that can be conformed into different shapes and morphologies [9]. Generally, for the regeneration of a tissue that has been removed and needs to be replaced, scaffolds are generally used. These scaffolds are generally considered as macroporous structures with pores in the range of hundreds of microns that will allow cell colonization and hence guide tissue regeneration [10]. Nevertheless, some tissues do not need to fill and empty void and scaffolds are not necessary. In this case, such as in the case of corneal tissues, substrates in the form of films or directly having cell sheets are relevant for the purpose [11]. While mimicking the 3D architecture is a very promising strategy, combinatorial approaches in which the physical and the chemical properties of the substrates can also be tuned is of great need for future successful tissue regeneration.

As mentioned earlier the microstructures, such as the topography, may have a critical role in guiding cellular behaviors. In this sense, previous studies showed that micron-sized topographies were able to guide different cellular types into enhanced cellular behaviors [12]. The most common method for the generation of micro- and nanopatterned substrates is lithography [13–17]. Lithography can form three-dimensional (3D) and curved structures and its mechanism is based on printing of the master, molding and embossing [18]. This represents a rapidly, high quality and efficiently technique that is available worldwide [18,19].

For example, some groups as Lunova et al. concluded that topographically patterned substrates could control hepatic cell growth, size and morphology [20]. Therefore, they cultured cells on silicon micropatterned substrates with different geometric forms (circles, squares and stripped pillars) and different spacing distances between pillars. They concluded that patterned substrates decreased cell size and modulated cell shape. They also determined that spacing distance of 50 µm enhanced growth kinetics [20]. Hu et al. demonstrated that micro-wavy patterns helped on the adhesion and cell survival rate of aortic endothelial cells [21]. They evaluated cell behavior on 20 µm micro-grooved and micro-wavy patterned PDMS substrates and determined that cells were aligned through the channels of the wave. Further, cells presented stronger cell adhesion in micro-wavy substrates [21]. Moreover, the use of nanopatterned structures helped on the osteogenic differentiation of mesenchymal stem cells, as de Peppo et al. evaluated [14]. For this purpose, they seeded cells on titanium-coated substrates with hemi-spheres nanostructures of different diameters and determined that 100 nm and 200 nm patterns presented higher levels of characteristic osteogenic markers after 2 weeks of culture [14]. More specifically, the effect of *in vitro* microenvironments for corneal endothelium tissue engineering has also been studied. Previous reports determined that patterned substrates in the form of concentric circles, wells and pillars enhanced human corneal endothelial cell (HCEC) proliferation, morphology and function [15–17]. The enhanced results were based on higher proliferation rates, a more polygonal typical shape and higher protein and gene expression levels of the two main HCEC markers in patterned surfaces [15–17]. However, these previously presented works based on the lithography technique require a very specific set-up and its preparation is time consuming with an elevated cost [18,22]. Furthermore, this

technology uses photopolymerizable polymers that are generally not implantable and hence with limited clinical translation. Moreover, the technology is generally based on a 2D approach and scaling the nanotopographies into a 3D system still remains a challenge.

For this reason, 3D printing may be thought of an alternative for the formation of complex patterned structures. This technology permits the formation of very low-cost and fast complex prototypes for numerous applications [23]. Taking into account the intrinsic porosities created with the layer by layer deposition of the fused deposition modeling (FDM), and using the obtained structures as molds, by simply performing an indirect replication of the molds with a biocompatible and ECM mimicking material, the topography can easily be replicated [24]. Furthermore, the ability to displace the printed platform in the Z direction allows creating more complex structures, such as convex or concave structures [24]. In this sense, the replicating material was based on a hydrogel based material which resembles the chemical composition of native ECM [25]. The substrates have two possible clinical translation scenarios. On the one hand, it may allow the formation of a bulky hydrogel on top of which the cells can be seeded, allowing cells to migrate, adhere, proliferate and differentiate depending on the substrate. The overall idea is that once the cells have been cultured for a determined period of time, these may form cell sheets that can be easily removed. These cells have been previously prepared and have been detached from substrates using thermoresponsive polymer substrates [26,27]. On the other hand, the molds can also be covered with a certain hydrogel solution and allowed to dry until obtaining a thin film which could eventually be seeded with cells and allow its direct implantation after cell proliferation [11,28].

Taking into account that the corneal tissues have the native curvature of eyes, we hypothesized that culturing cells in a curved pattern could resemble the natural conditions in which corneal endothelial cells (CEC) are found and hence contribute to a better cell behavior. Actually, it has been previously observed that different cellular types have been cultured on curved substrates and that these curvatures were able to significantly affect its phenotypes. For example, Shen et al. demonstrated that the effect of curvature increased renal function [29]. Furthermore, Yoshida et al. demonstrated that human corneal endothelial cell (HCEC) could be cultured on a porcine-derived scaffold with spherical

curvature, similar to the cornea [30]. In this study, cells were regularly distributed despite the curvature of the scaffold. However, phenotypic analyses were not performed.

Hence, in this chapter we combined for the first time the formation of curved substrates with specific topographies using native corneal tissues mimicking materials. Initially we studied the feasibility of generating curved and micropatterned structures using a conventional 3D printer for corneal endothelium tissue engineering. We hypothesized that the generation of a substrate that mimicked native ECM with curved morphologies and with specified microtopographies that could modify cell phenotype could have a beneficial effect on CEC behavior.

3. 2. Materials & Methods

3. 2. 1. Fabrication of implantable based films and platforms

The films and platforms were fabricated using collagen type I, which were shaped into the proper morphology with the help of designed plastic molds.

3. 2. 1. 1. Mold design and fabrication

Mold design

The anatomical eye model was extracted from a previous study [31] and the different concave, convex and flat molds were designed (Figure 3.1) using the software SolidWorks 2018 SP5 (Dassault Systèmes). The final dimensions were 11 mm of corneal diameter and a value of sagittal height of 2 mm [31]. The resulting molds were exported as an STL file and, subsequently, the g-code for 3D printing was generated using the software Simplify3D v4.1 (Simplify3D) where the different layer heights (LH) were determined.

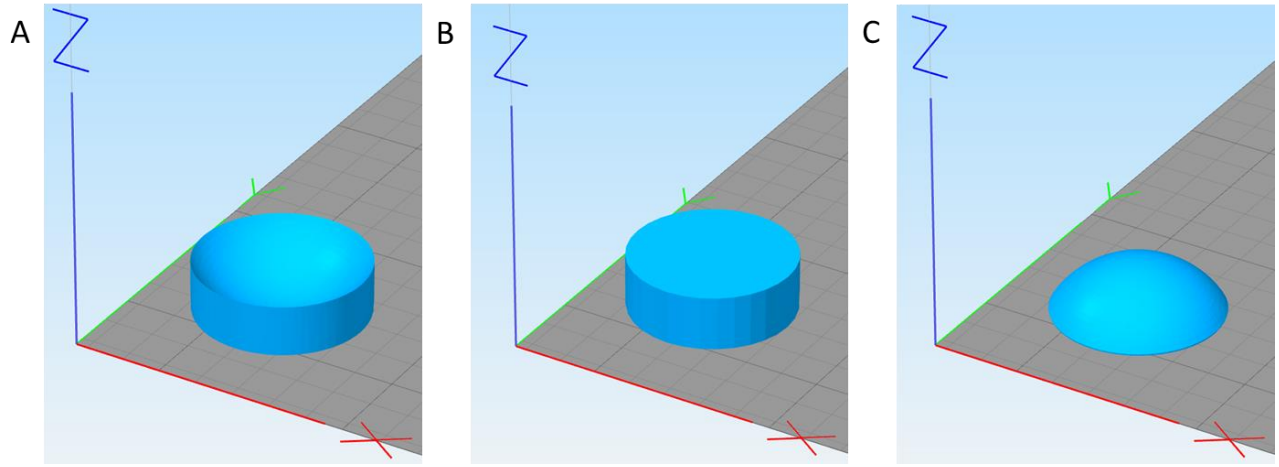

Figure 3.1. Digital corneal molds imported to the 3D printer software Simplyfy3D. A preview of the concave (A), flat (B) and convex (C) molds are displayed

Patterned molds fabrication

Patterned molds were fabricated with poly-lactic acid (PLA) using a FDM 3D printer (BCN3D Technologies). Concave, flat and convex molds were printed using a concentric circle pattern. Due to the intrinsic properties of the layer by layer printing of the molds, different heights were given to the different surfaces using a 0.4 mm nozzle, mainly providing LH or printing resolutions of 300, 200 and 50 µm (Figure 3.2.). As a control, an unpatterned surface was used. In order to fabricate the unpatterned surfaced molds, the 50 µm LH molds were treated with acetone for 3 minutes and its surface was smoothed with the help of a microbrush. PLA molds were sterilized with 70% ethanol and UV irradiation for at least 30 minutes. Subsequently, molds were rinsed twice with 1X PBS.

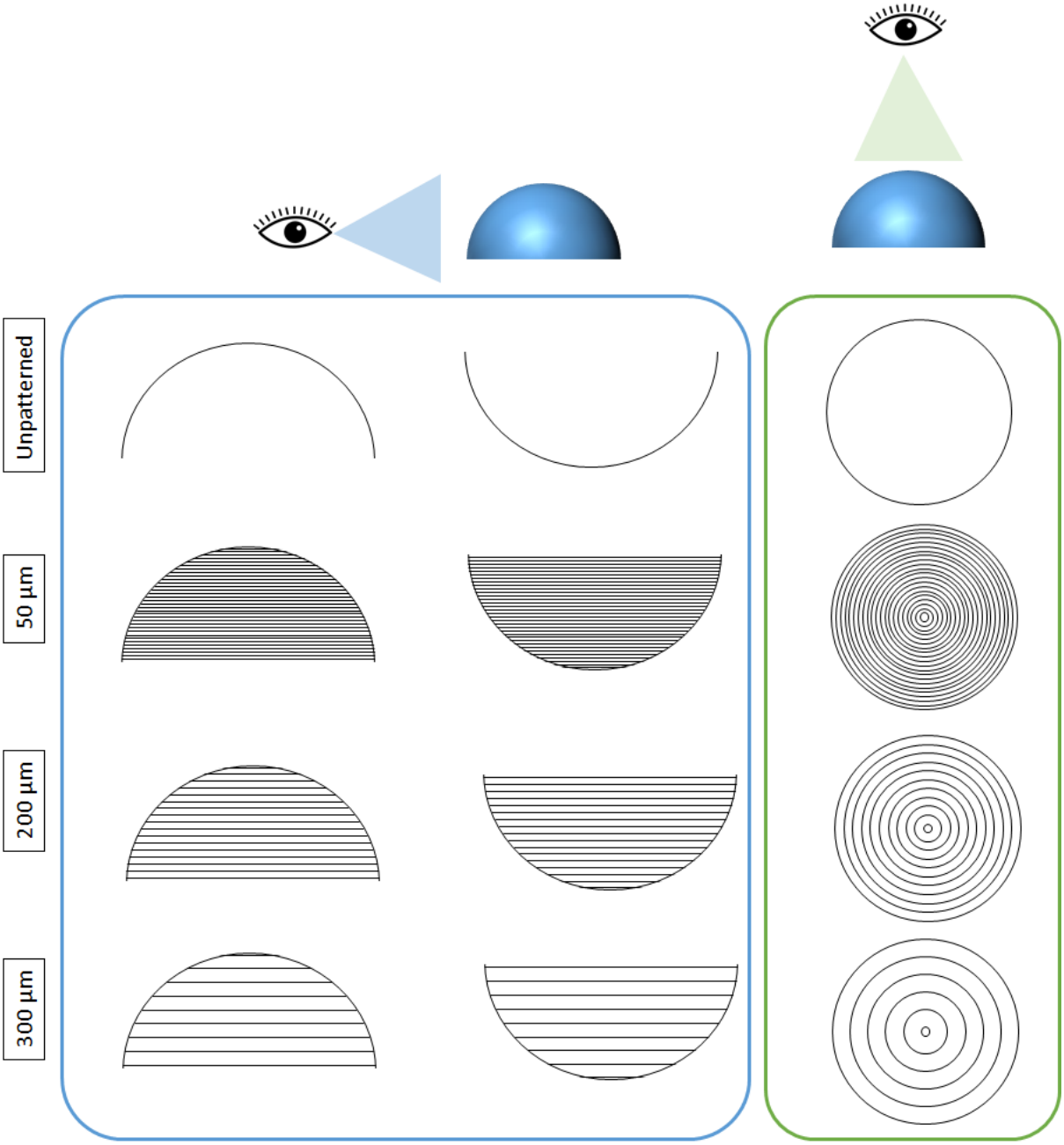

Figure 3.2. Molds printed by a FDM 3D printer using concentric directionality. The cross-sectional (blue) and top view (green) of unpatterned molds and with different printing resolutions (50, 200 and 300 µm).

Hydrogel characterization

The LH and distance between peaks was measured in order to analyze the platforms used for human corneal endothelial cells (HCEC) culture. Since the molds will be used as the substrates onto which the collagen will be placed, analyzing the pattern imprinted into the collagen hydrogels is of great importance (Figure 3.3).

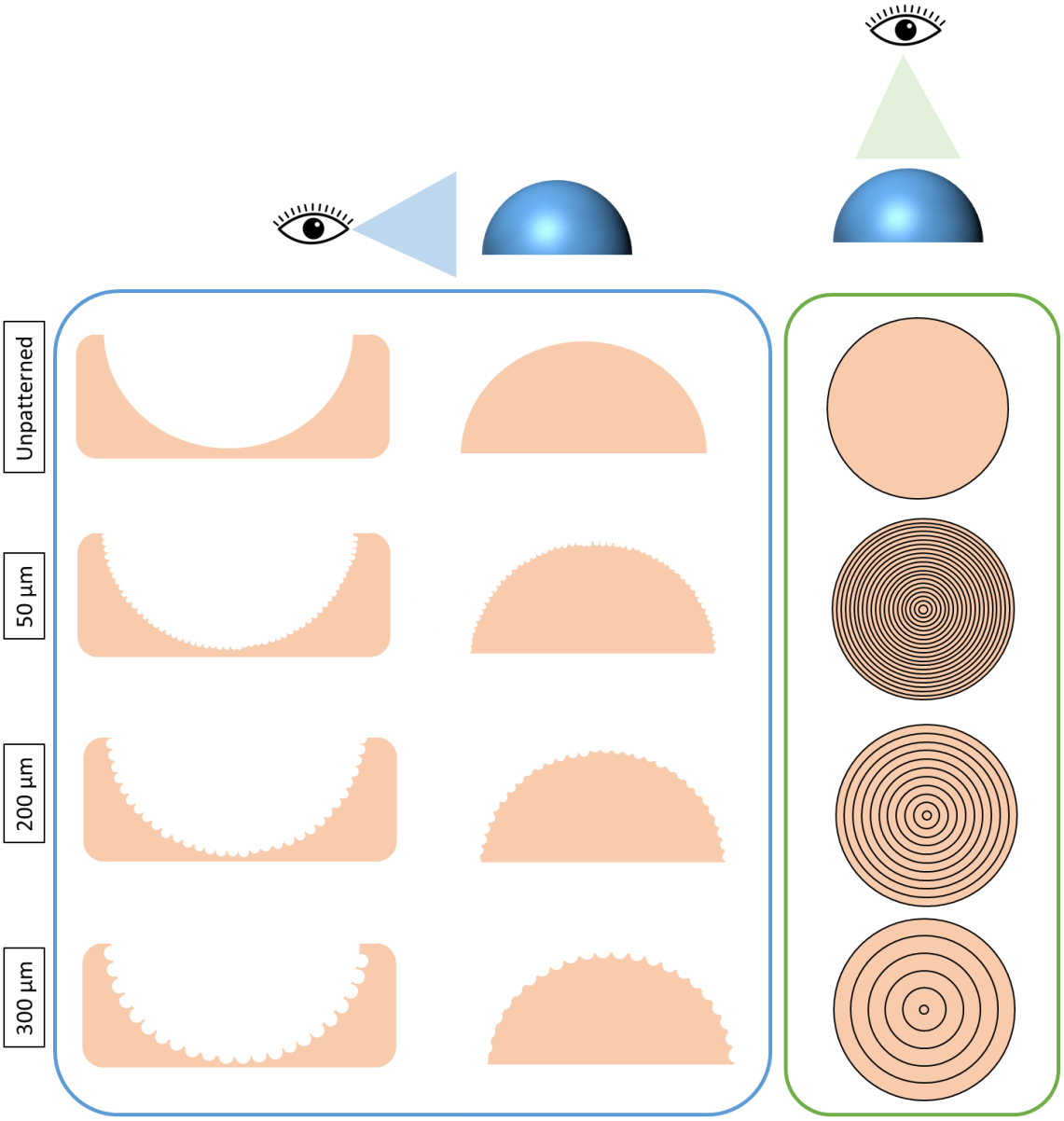

Figure 3.3. Imprinted pattern on hydrogels. The cross-sectional (blue) and top view (green) of unpatterned hydrogels and with different printing resolutions (50, 200 and 300 µm).

Merely for imaging and analysis purposes, silicon was used a modeling material to allow analyzing the obtained patterns. Silicon was placed onto the molds with the different LH and was left overnight until complete drying. Complete drying was performed to ensure an easy demolding from the mold. No volume contraction was observed in the samples, which guaranteed similar behavior to that of collagen hydrogels. The silicon was then carefully sectioned with a scalpel obtaining sections of 1 mm of thickness. The obtained thin layers were similar to those schematically represented in Figure 3.4. Then, optical microscope

images were taken (Olympus CKX41, Nikon) and characterization of curved patterned samples was performed using ImageJ.

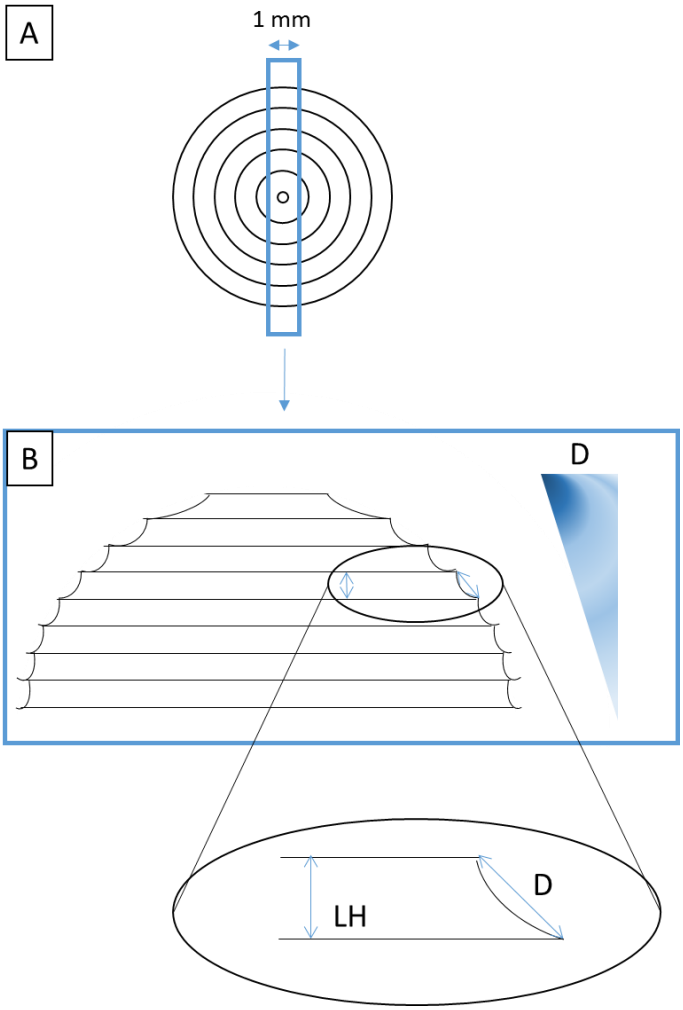

Figure 3. 4. Molds characterization. A) Silicon patterned substrates were sectioned for its characterization. B) The layer height (LH) and distance between peaks (D) were measured using ImageJ.

3. 2. 1. 2. Collagen isolation and characterization

Collagen isolation

Tendons from sixteen-month bovine were collected from a local abattoir. Type I collagen isolation protocol was performed as previously reported [32]. Shortly, tendons were separated manually from its surrounding fascia, muscle or blood, and washed with 1X phosphate buffered saline (PBS) (Sigma-Aldrich) solution. Tendons were kept at 4ºC during the whole extraction process. The tendon tissue was crushed with a desktop blender and

dissolved in 1M acetic acid with continuous mild stirring up to 72 hours. Then, pepsin was added at a ratio of 40 U per milligram of tendon and the solution was incubated for 72 hours under agitation. Subsequently, insoluble tendon was filtered and discarded, while soluble collagen solution was kept stirring overnight. Collagen was then purified by repeated salt precipitation using 0.9M sodium chloride (NaCl) (Sigma-Aldrich). Precipitated collagen was collected and incubated in 1M acetic acid (Sigma-Aldrich) under gentle agitation for up to 72 hours. Finally, collagen solution was dialyzed against 1 mM acetic acid using membranes with molecular weight cut-off of 12,gen000 (Sigma-Aldrich). Final collagen solution was placed in a sterile recipient and stored at 4ºC.

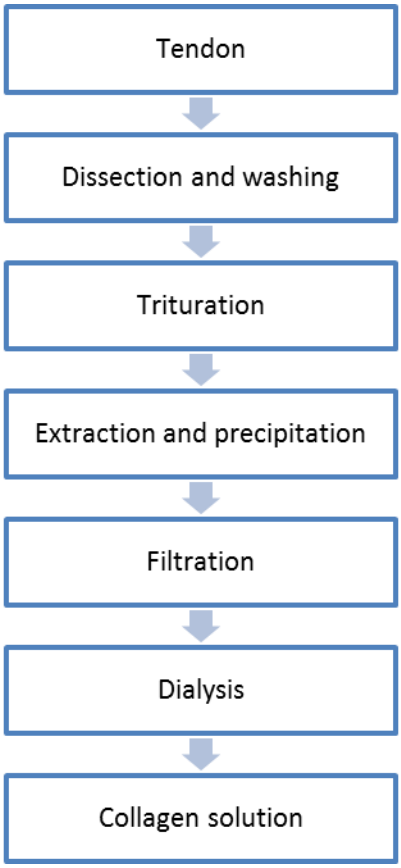

Figure 3. 5. Flow chart of the collagen isolation process.

Collagen characterization

Collagen extraction assessment

The final step prior to obtaining the collagen solution is to allow the collagen solution to decrease its acidic conditions. This is achieved by the dialysis in which the collagen molecules are maintained within the dialysis bag and the solvent is allowed to diffuse out. It also has to be taken into account that excessively reducing the pH of the solution may lead to collagen precipitation. For this reason, acid concentration was assessed using the acid-base titration in order to assure that the final acid concentration is below 0.05M.

Then, collagen concentration was determined by dry weight of collagen. For this purpose, 500 µL of the final collagen solution was kept at 60ºC overnight to dehydrate the collagen. Collagen concentration (mg/mL) was calculated according to the following formula:

$$Collagen\ concentration = \frac{Dry\ weight}{0{,}5\ mL}$$

Collagen purity assessment

Sodium dodecyl sulphate polyacrylamide gel electrophoresis (SDS-PAGE) was performed in order to confirm collagen's purity, as previously described [33,34]. Briefly, the samples were prepared at different concentrations, which were 0.5 mg/mL, 1 mg/mL and 2 mg/mL of the collagen solution. To validate the results, a 1 mg/mL collagen solution of a commercial collagen (BD Bioscience) was used as a control. Collagen solutions were neutralized in the presence of phenol red using 1M NaOH. Then, samples were denatured for 5 minutes in a termoblock at 90ºC. Finally, 30 µL of each sample was loaded in a 5% acrylamide gel using laemmli sample buffer (Bio-Rad) and Tris/glycine/SDS buffer (Bio-Rad). The gel was then stained using 0.1% w/v Coomassie brilliant blue (Sigma-Aldrich). Stained gel was imaged using a G:BOX Chemi XT imaging system (Syngene) and collagen band densitometry was analyzed by Image Studio Lite software 5.2 (LI-COR).

3. 2. 1. 3. Patterned film and hydrogel formation

Clinical scenario 1: implantable patterned films

Collagen film formation was modified from previous protocol [35]. Firstly, the final collagen solution was combined with 10X PBS, which is required to increase the ionic salt solution and trigger collagen fibrillization. Then, the pH of the collagen solution was adjusted to pH=7.2-7.4, initially with few microliters of 5M NaOH to drastically increase the pH followed by the addition of tens of microliters of 1M NaOH to more accurately adjust the pH. In order to control the pH evolution and finalize the titration at the established pH, phenol red indicator was incorporated. Phenol red presents a yellowish color at acidic pH, a reddish color at neutral pH and pinkish color at basic pH. Adjusted collagen was centrifuged to remove possible bubbles. Then, 450 µL of neutralized collagen solution was placed in 48-well plates and plates were incubated at 37ºC for 45 minutes for collagen gelation. Finally, plates were kept overnight in a flow-hood at room temperature, in order to evaporate water content. To determine its future application, consistency of collagen films, in dry and hydrated collagen, and transparency were evaluated. Consistency was assessed by its ability to form the desired shape on dry and hydrated films as well as by the hydration stability, while transparency was checked to confirm an optimal corneal clarity and visual acuity. The same protocol was performed placing the neutralized collagen solutions onto the prepared patterned molds to fabricate the curved patterned collagen films.

Clinical scenario 2: Patterned Hydrogel platform

Collagen hydrogel formation was similar to film formation. Firstly, the pH of the collagen solution was adjusted to pH=7.2-7.4 using the previously described solutions, mainly 10X PBS, 5M and 1M NaOH, and phenol red. The main difference with the film formation is the need of a cross-linking solution. When collagen is left air drying, some covalent bonds are established between the collagen chains and hence, when placed collagen in water, collagen does not dissolve. Nevertheless, fresh collagen hydrogels are not stable when placed in contact with water and its dimensional stabilization with a cross-linker is mandatory. In this case, genipin (JenKem Technology), a low toxicity cross-linker [32], was added for the formation of a more solid hydrogel. The process was then continued as previously described [32], centrifuging collagen solution to remove bubbles, followed by the addition of 450 µL

collagen solution onto the molds placed in 48-well plates, incubating them at 37ºC for 45 minutes for collagen gelation. Then, plates were sealed with parafilm and kept at room temperature overnight. Finally, hydrogels were washed with sterile PBS and cell culture medium before cell seeding.

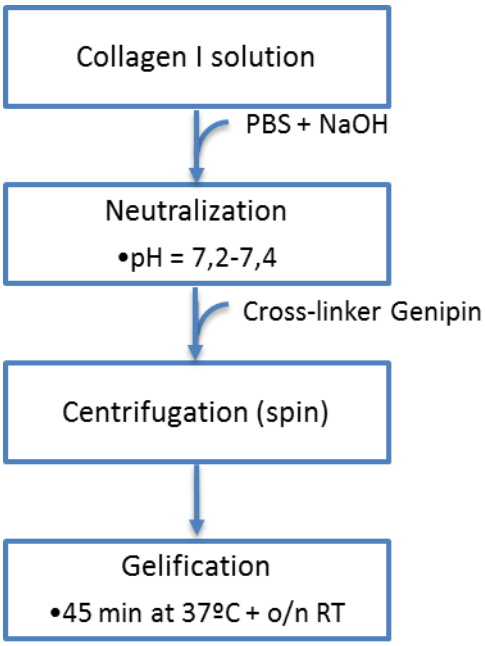

Figure 3.6. Flow chart of collagen hydrogel formation.

Cross-linking concentration

As mentioned in the previous description, genipin cross-linking solution was required for hydrogel formation. Therefore, different dilutions of the cross-linking genipin were used in order to obtain a non-cytotoxic hydrogel, but also able to maintain the patterned topography. For this purpose, a 0.625% genipin (w/v) solution was prepared in 1X PBS [32]. The genipin solution was then added on the collagen hydrogel at different volume ratios of genipin:collagen, mainly analyzing 1:100, 1:75, 1:50, 1:20 and 1:10 (Figure 3. 7). Non-cross-linked collagen was used as a control.

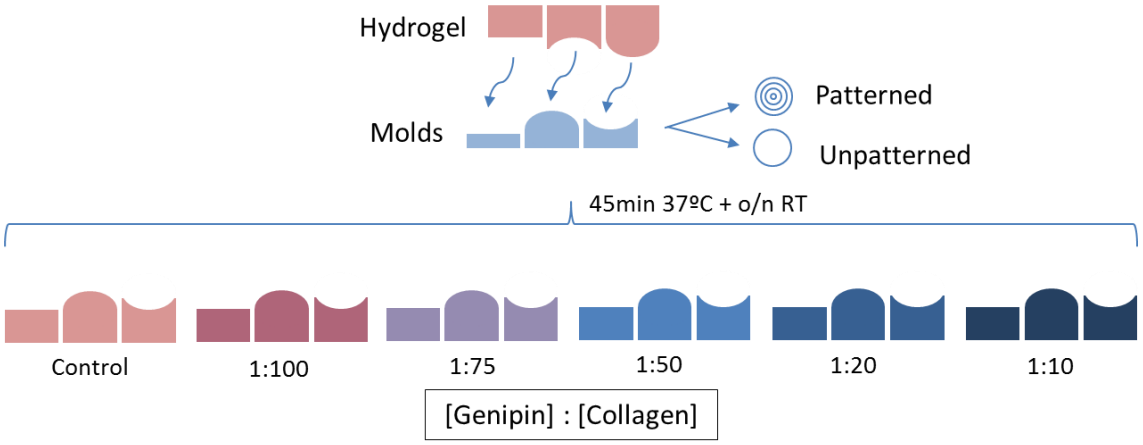

Figure 3.7. Scheme of collagen hydrogel formation using different dilutions of cross-linking (genipin). Non-cross-linked collagen hydrogel was used as a control.

3. 2. 2. Cell culture

Cell culture was performed in two different stages. Initially, in order to observe the interaction and the possible elongation of cells under the designed patterns, fibroblast cells were placed on the designed platforms as preliminary experiments. Once the optimum conditions were found, CEC were used.

3. 2. 2. 1. Fibroblasts culture

Cells were cultured in fibroblast medium which contained DMEM with 4.5 g/L glucose supplemented with 10% FBS, 1% GlutaMax and 1% Penicillin-Streptomycin. The medium was changed every 2-3 days. When the cells reached 80% confluence, they were detached using TrypLE™ Express Enzyme and re-plated on the hydrogel. Cells were cultured at a seeding density of 2.5 x 10^4 cells/ cm^2.

Three LH of patterned hydrogels were used: 300 µm, 200 µm and 50 µm. Moreover, two cell-seeding forms were tried: a drop of cells directly onto the center of the hydrogel, and culture media was added when cells were attached, or a drop of cells in the center of cell culture medium on the well plate.

After 24 hours, fibroblasts were fixed and cell morphology and density was analyzed by immunofluorescence assay.

Cell density optimization

Once the optimal LH hydrogels were selected, different cell densities were tried: 2.5 x 10^4 (low), 1 x 10^5 (medium) and 2 x 10^5 cells/cm^2 (high), which mimicked native CEC cell density. Moreover, fibroblasts were cultured for a longer period (6 days) and using the cell-seeding method with highest cell proliferation.

Therefore, cells were cultured on concave, flat and convex hydrogels and analyzed by immunofluorescence at days 3 and 6.

3. 2. 2. 2. Corneal endothelial cell culture

Human Corneal Endothelial Primary cells were purchased from Celprogen and cultured as manufacturer's indication. Shortly, frozen vial was centrifuged at 100g for 7 minutes and resuspended in CEC commercial medium (Celprogen). All cells were plated in a T25 pre-coated commercial culture flasks and incubated at 37ºC and 5% CO_2. Medium was changed every 24-48 hours. When cell confluence reached 95%, cells were detached using EDTA and centrifuged. Then, cells were re-plated at a cell density of 1 x 10^4 cells/cm^2, unless otherwise specified, or used for future experiments.

Selection of the optimum substrate for cell expansion

CEC present a characteristic polygonal morphology which has to be maintained throughout cell culture passages [36]. Therefore, prior to the culture of CEC on the collagen hydrogel, two culture coatings were evaluated for the maintenance of this morphology: the commercial coating (Celprogen), which was an ECM pre-coated flask, and a fibronectin-based (FNC) coating mix (Athena Environmental Sciences), which have been widely used for HCEC expansion [37–40].

Corneal endothelial cells on hydrogel

As mentioned before, collagen hydrogel formation requires the use of a cross-linker (genipin) to enhance its stabilization. However, the concentration of genipin depends on the cell type [41,42]. For this reason, we initially assessed the cytotoxicity of the genipin concentration used for fibroblasts and used the genipin concentration that allowed highest cell survival. Therefore, once the dilution of the cross-linker genipin was adapted to CEC and

based on our preliminary results on fibroblast culture, cells were cultured on different unpatterned and patterned hydrogels at a high seeding density which resembled native cell density (2 x 10^5 cells/cm^2). Cell morphology, cell size and total RNA were analyzed at days 3 and 6 of culture.

3. 2. 2. 3. Cell characterization

Cytotoxicity assay

Cell viability was measured using the commercially available kit Cell Counting Kit-8 (CCK-8) (Sigma-Aldrich). This assay uses a water-soluble product known as WST-8 that is reduced by cells and generates a yellow-colored product (formazan), as shown in Figure 3.8. This metabolized product is soluble in the culture medium. Therefore, the amount of the formazan dye, which has an absorbance spectrum peak at 450-460 nm, is directly proportional to the number of living cells.

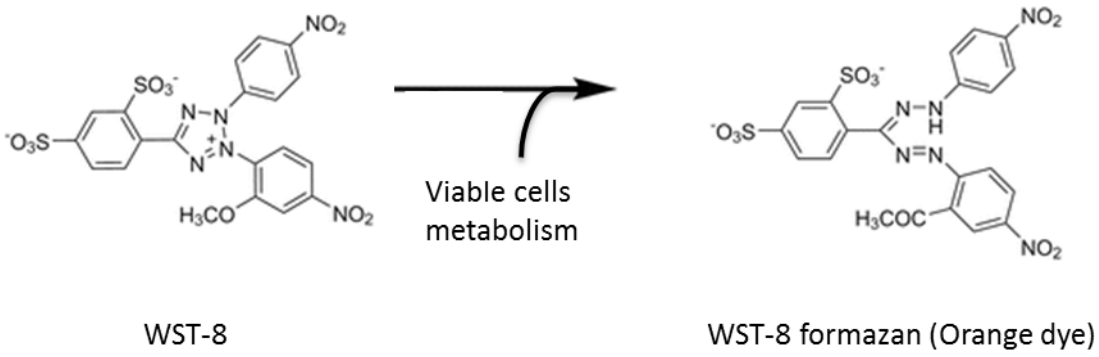

Figure 3.8. Structures of WST-8 and WST-8 formazan. Modified from manufacturer's protocol.

CCK-8 assay was performed as manufacturer's indications. Shortly, 2 x 10^5 cells/well were cultured on the hydrogel with different dilutions of genipin:collagen (1:200, 1:100 and 1:50). A non-cross-linked hydrogel was used as a control. 24 hours later, CCK-8 solution was added in every well and cells were incubated at 37 °C for 3 hours. Then, the absorbance at 450 nm was measured using a multi-detection microplate reader (Biotek, Synergy HT).

Immunofluorescence assay

Cell morphology was analyzed by immunofluorescence assay. Briefly, cells were washed with 1X PBS and fixed with 4% paraformaldehyde (Sigma-Aldrich) for 20 minutes at room temperature. Then, cells were permeabilized with 0.1% Triton X-100 for 10 minutes at room

temperature. Cells were washed and stained with 100 nM of the conjugated antibody Acti-stain 488 phalloidin (Biogen, Cat. CY-PHDG1-A) for 30 minutes in the dark at room temperature. Subsequently, cells were washed and incubated with nuclear DAPI for 5 minutes. Finally, cells were rinsed with PBS and observed using an inverted fluorescence microscope (Leica Microsystems, GMi8).

Cell circularity and cell size

Cell circularity and cell size was determined to evaluate the effect of the curvature and topography during 6 days of culture. Cell circularity was calculated according to the following formula.

$$Circularity = \frac{4\pi \times Area}{Perimeter^2}$$

Where a circularity value of 1 indicates a perfect circle, while a value of 0 corresponds to an elongated shape. Therefore, due to its characteristic polygonal shape, CEC morphology should have a circularity value close to 1 [43]. At least 100 cells per condition were analyzed.

Quantitative Real Time – Polymerase Chain Reaction (qPCR)

Gene expression was analyzed by quantitative real time – polymerase chain reaction (qPCR). Shortly, total RNA was isolated using NucleoSpin RNA kit (Macherey-Nagel) including DNAse treatment following the manufacturer's instructions. One µg of RNA with a ratio of intensities at the wavelengths of 260/280 nm between 1.8-2 was then reversed transcribed into cDNA using Transcriptor First Strand cDNA Synthesis Kit (Roche) according to the manufacturer's recommendations. CEC specific primers (Table 3.1) and FastStart Universal SYBR Green Master (Roche) were used to amplify the desired cDNA. Finally, the amplifications were performed in a CFX96 Real-Time PCR Detection System (Bio-Rad) for quantitative Real-Time PCR.

Gene	Primer	Sequence (5' -3')	Accession Number
ATP1A1	Forward	TGTGATTCTGGCTGAGAACG	NM_001160234
	Reverse	TGCTCATAGGTCCACTGCTG	
ZO-1	Forward	AGTTTGGCAGCAAGAGATGG	NM_001355015
	Reverse	GCTGTCAGAAAGATCAGGGA	
b-ACTIN	Forward	AGAGCTACGAGCTGCCTGAC	NM_001101
	Reverse	AGCACTGTGTTGGCGTACAG	

Table 3.1. List of primers used for cDNA amplification in quantitative RT-PCR.

3. 2. 3. Statistical analysis

Regarding gene expression, Mann-Whitney U-test was carried out to reveal significant differences. Differences were considered statistically significant with P value of less than 0.05. The data are presented as mean ± standard deviation.

For molds characterization, cell circularity and cell area assay, one-way analysis of variance (ANOVA) was performed to analyze differences between groups followed by Mann-Whitney U test. A P value of less than 0.001 was accepted as indicating statistical significance. The data are presented as mean ± SEM.

GraphPad Prism version 6 (GraphPad Software Inc.) was used to graph the data and statistical analyses were performed using Statistical Package for the Social Sciences (SPSS) 21 (IBM).

3. 3. Results

3. 3. 1. Mold design and fabrication

Initially, molds were designed and printed using different printing resolutions on a conventional 3D printer. Then, hydrogels were placed on the curved molds to obtain the desired patterns.

Aiming to characterize the topography of the hydrogels, the cross-sections of the different samples were analyzed. As it can be seen in Figure 3.9, unpatterned samples presented a smooth surface. On patterned models, microwells were formed between the peaks. When using the lower LH molds, the microwells significantly reduced their size compared to the higher LH molds.

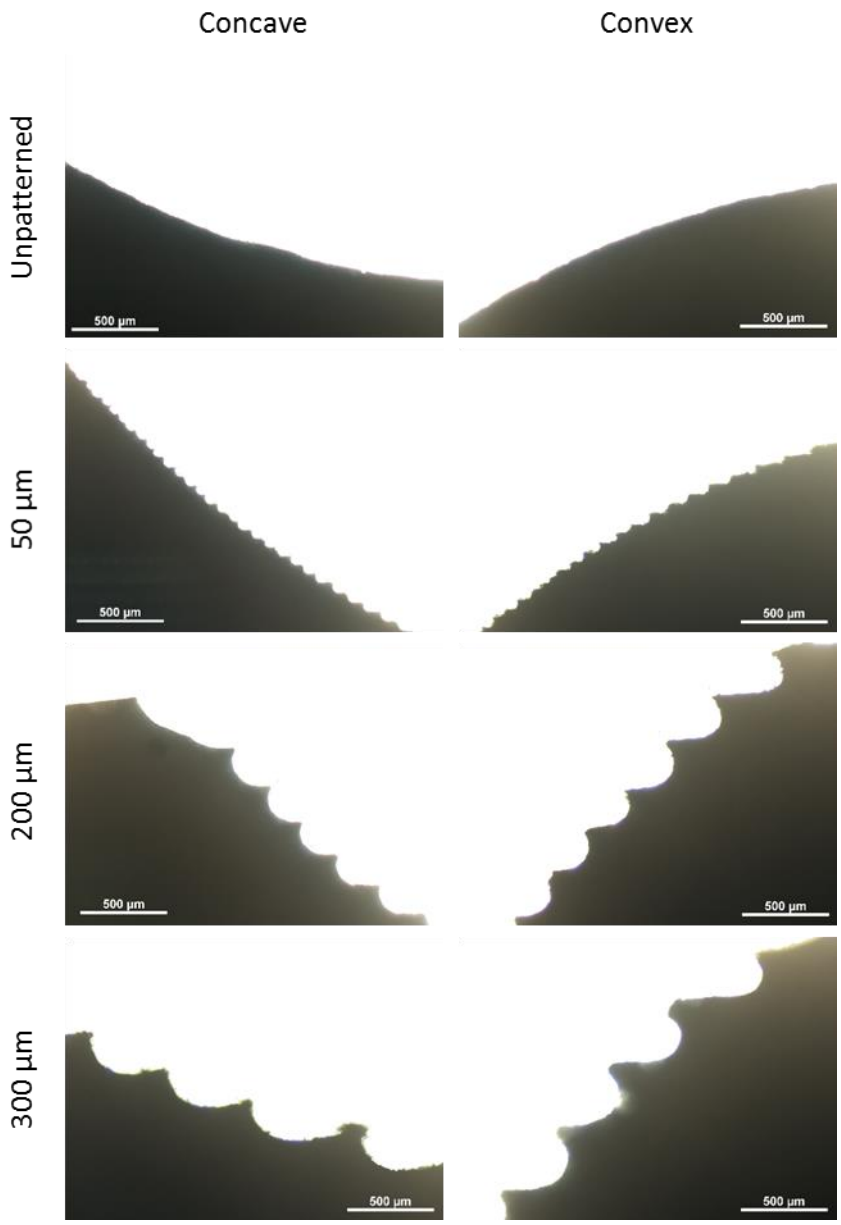

Figure 3.9. Silicon models for mold characterization. Unpatterned and patterned curved models of different printing resolutions (50, 200 and 300 µm). Scale bars: 500 µm.

Furthermore, the distance between peaks and the LH was analyzed. As shown in Figure 3.10, the distance between peaks and the LH increased as the printing resolution increased. Moreover, the values between concave and convex molds was similar, although the values were more heterogeneous as the printing resolution increased.

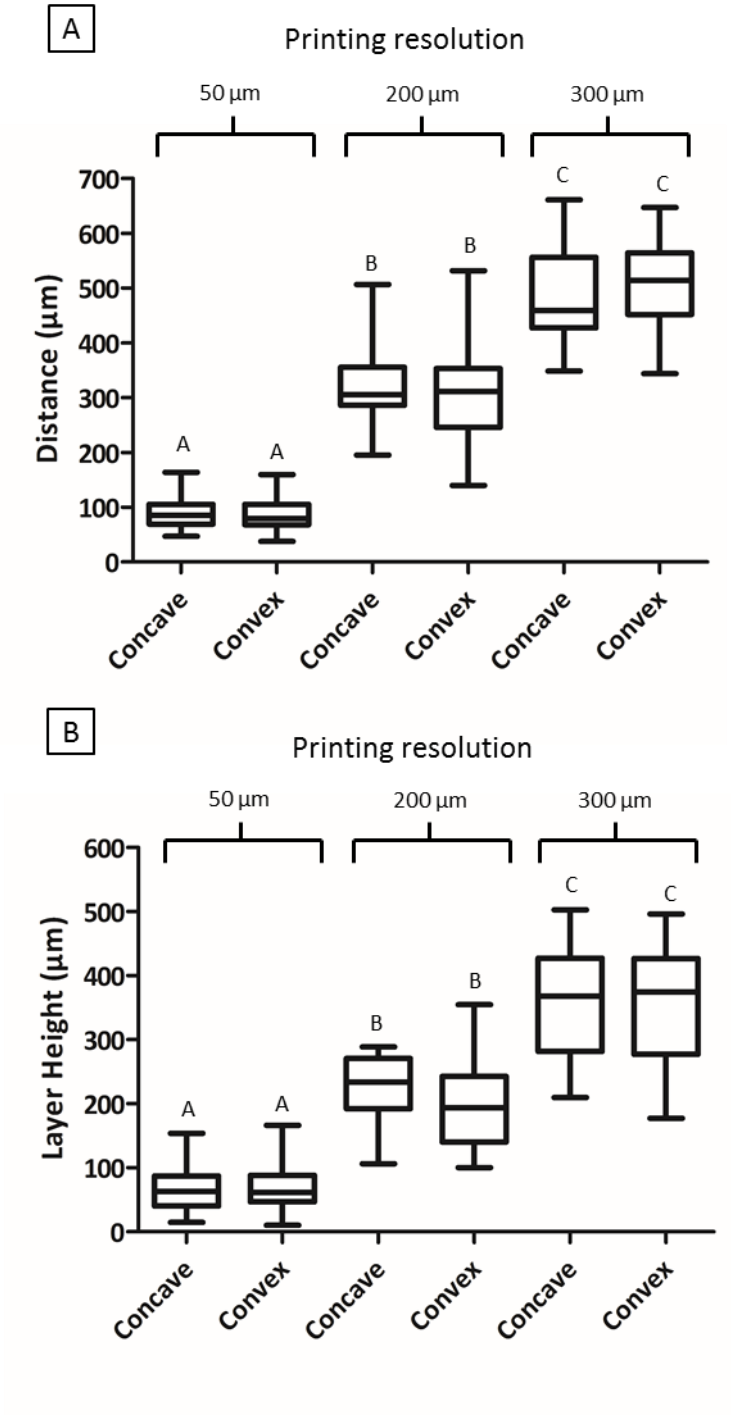

Figure 3.10. Molds characterization. Distance between peaks (A) and LH (B) in curved patterned samples with printing resolutions of 50 µm, 200 µm and 300 µm.

3. 3. 2. Collagen isolation and characterization

Collagen extraction from native tissues is a delicate and complex process since many biomacromolecules are found together. Furthermore, ensuring its proper extraction together with the proper pH conditions for its stabilization will dictate the quality of the extracted collagen. Regarding the last issue, the dialysis endpoint was established at 72 hours, after verifying that the final acid concentration was below 0.05M acetic acid. We then assessed the collagen final concentration, obtaining a final concentration of 5.4 mg/mL. Finally, in order to assess the presence of merely collagen in the solution and hence to verify its purity, an electrophoresis SDS-PAGE was performed. Due to the elevated viscosity of the extracted collagen solution, collagen solution was diluted into different concentrations, mainly 2, 1 and 0.5 mg/mL. As expected, the commercially available collagen 1 mg/mL solution showed the bands related to monomeric chains α1 and α2, dimeric chains β11 and β12, and trimeric γ chain. As can be seen in Figure 3.11., the freshly isolated collagen at three concentrations presented the same typical bands as the commercially available control, which was verified by purity quantification assessment with values over 99%.

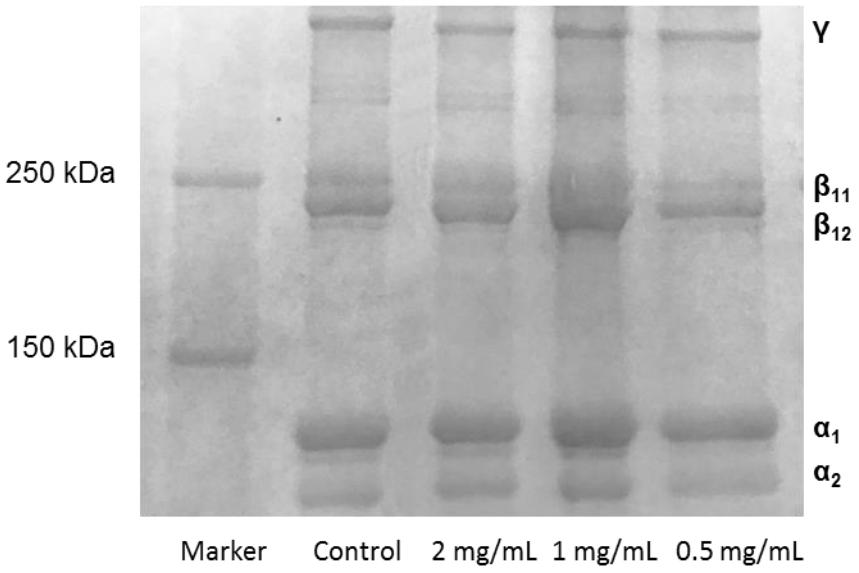

Figure 3.11. Electrophoresis gel for collagen purity assessment. Commercial collagen (1 mg/mL), and freshly collagen isolation at different concentrations (2, 1 and 0.5 mg/mL).

3. 3. 3. Patterned film and hydrogel formation

3. 3. 3. 1.Clinical scenario 1: implantable patterned films

Collagen films were formed for the culture of CEC. As described in materials and methods, three main parameters were studied to validate the viability of the designed films: the ability to maintain the shape of the mold after drying, its transparency and its hydration ability.

Initially, several drying procedures were tested in order to provide constant drying conditions and avoid excessive drying in some parts and hence bend the designed film. In general, the different drying processes led to a slight shrinkage of the film and a consequent uneven morphology together with a decreased maintenance of the curved structure (Figure 3.12 A). We then analyzed its ability to absorb water and to have enough strength to allow its manipulation showed that the films were stable even when hydrated (Figure 3.12 B). Nevertheless, when samples were hydrated some distortion of the original form was observed. Finally, the transparency of the films (Figure 3.12 C) was analyzed, showing that the films were optically transparent, which even allowed reading when placed on top of a text.

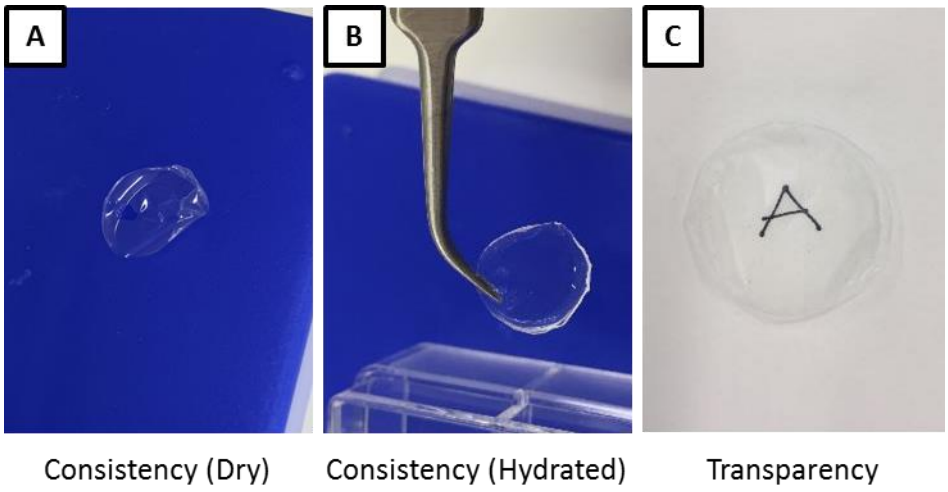

Figure 3.12. Collagen type I film formation and evaluation. Consistency evaluation in dry (A) and hydrated (B) collagen films. Transparency evaluation of the film (C).

Despite the collagen film has tremendous potential for the transplantation of corneal endothelial cells, at the current stage, we were interested in determining the effect of the curvature together with the topography. Due to the uneven drying process and the lower ability to replicate the curvature of the mold combined with a significant deformation after hydration, we arrived to the conclusion that preparing hydrogel-based platforms without having the drying step would be more beneficial at this stage.

3. 3. 3. 2. Clinical scenario 2: Patterned Hydrogel platform

Collagen hydrogels needed an exogenous cross-linker in order to form a consistent structure that did not disintegrate during its manipulation. For this purpose, 0.625% (w/v) of genipin was prepared and diverse dilutions were selected for the hydrogel formation. As expected, as the concentration of genipin rate increased (lower dilution), the hydrogel obtained a more rigid and blue-colored form. In contrast, the control (without genipin) was not able to maintain the desired pattern and rapidly lost its consistency. As shown in Figure 3.13, dilutions 1:10 and 1:20 presented a blue-grey colored hydrogel, while 1:50, 1:75, 1:100 and control hydrogels exhibited a more pinkish color.

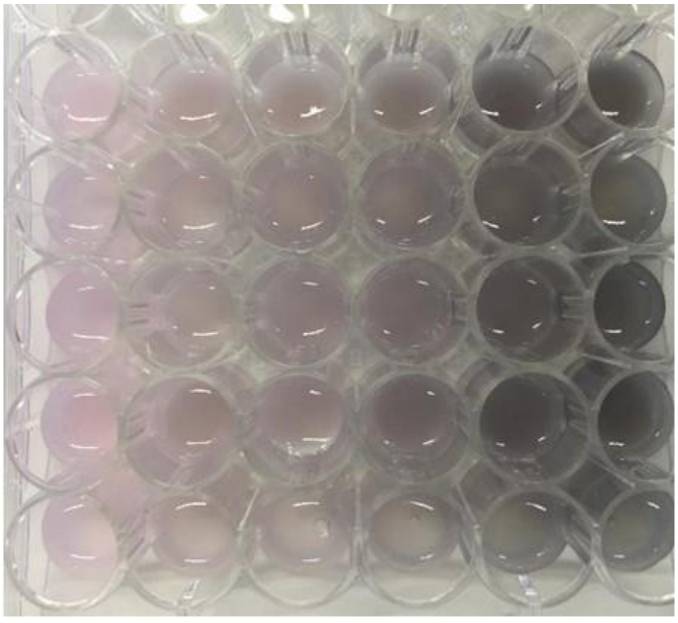

Figure 3.13. Collagen hydrogel formation. Different dilutions of cross-linking (genipin) on collagen hydrogel. Non-cross-linked collagen hydrogel was used as a control.

3. 3. 4. Cell culture

3. 3. 4. 1. Fibroblasts on hydrogel

Once the hydrogel formation was optimized, fibroblasts were cultured on different patterned hydrogels using two methods for seeding the cells: a drop of cells directly on the center of the hydrogel or on the center of the culture medium. Cell morphology was analyzed by immunofluorescence analysis.

Regarding cell morphology on high LH conditions (300 µm), there were more cells in concave hydrogels than in convex hydrogels. In fact, phalloidin staining showed that only in concave hydrogels and when seeding the drop of cells on the culture media cells presented a polygonal morphology (Figure 3.14).

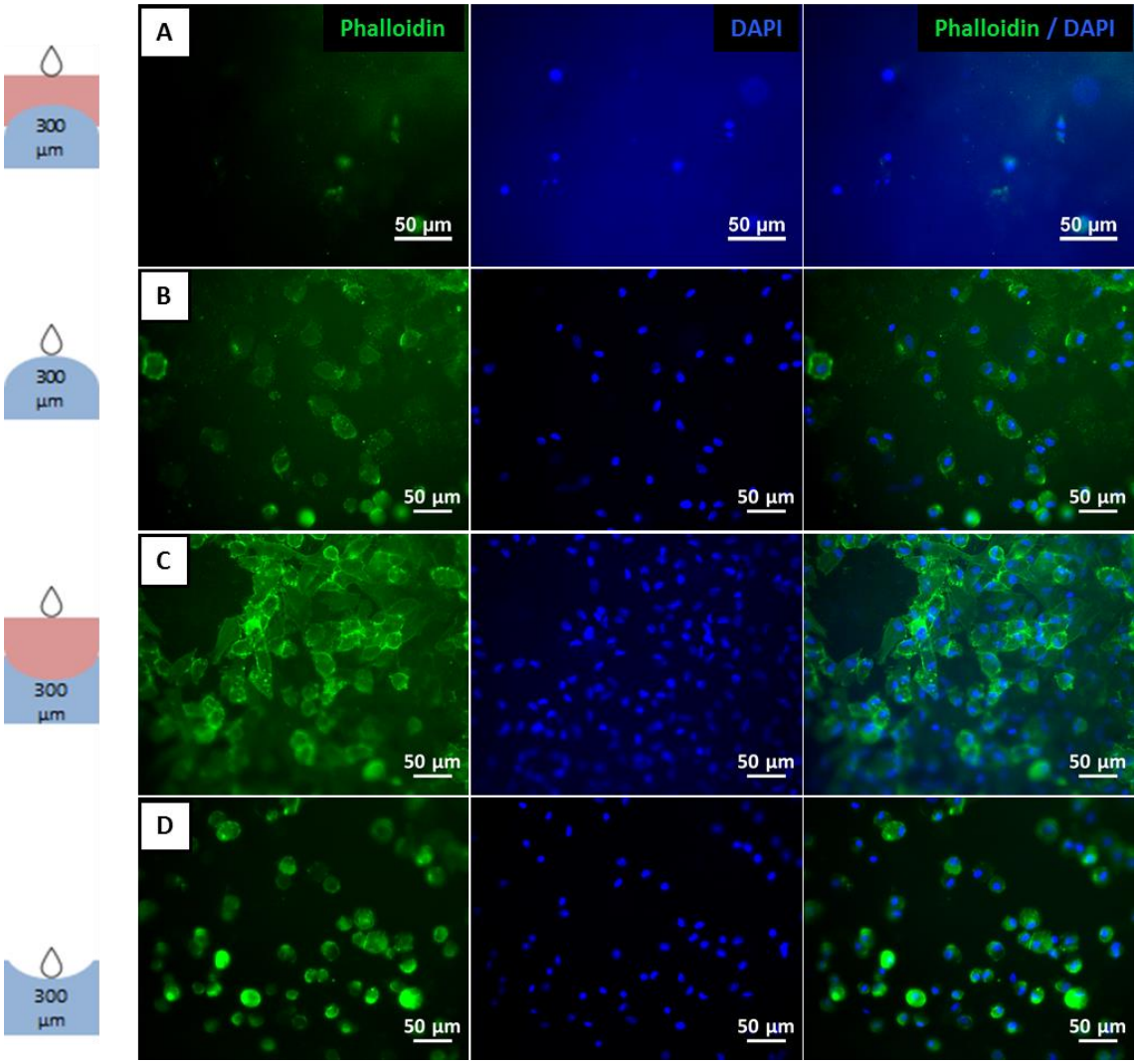

Figure 3.14. Fibroblasts cell culture on collagen hydrogels. Immunofluorescence analysis of phalloidin (green) and nuclear DAPI (blue) on patterned convex (A,B) and concave (C,D) hydrogels. Two seeding cells methods were evaluated: a drop of cells on the culture media (A,C) or directly on the hydrogel (B,D). Scale bars: 50 µm.

When cells were cultured on hydrogels with medium LH (200 µm), cells presented similar results as in the 300 µm LH conditions. Therefore, as shown in Figure 3.15, concave hydrogels exhibited a higher cell density than convex hydrogels and the seeding of the cells on the culture media presented a more polygonal morphology and higher cell number than when the cells were plated directly to the hydrogel.

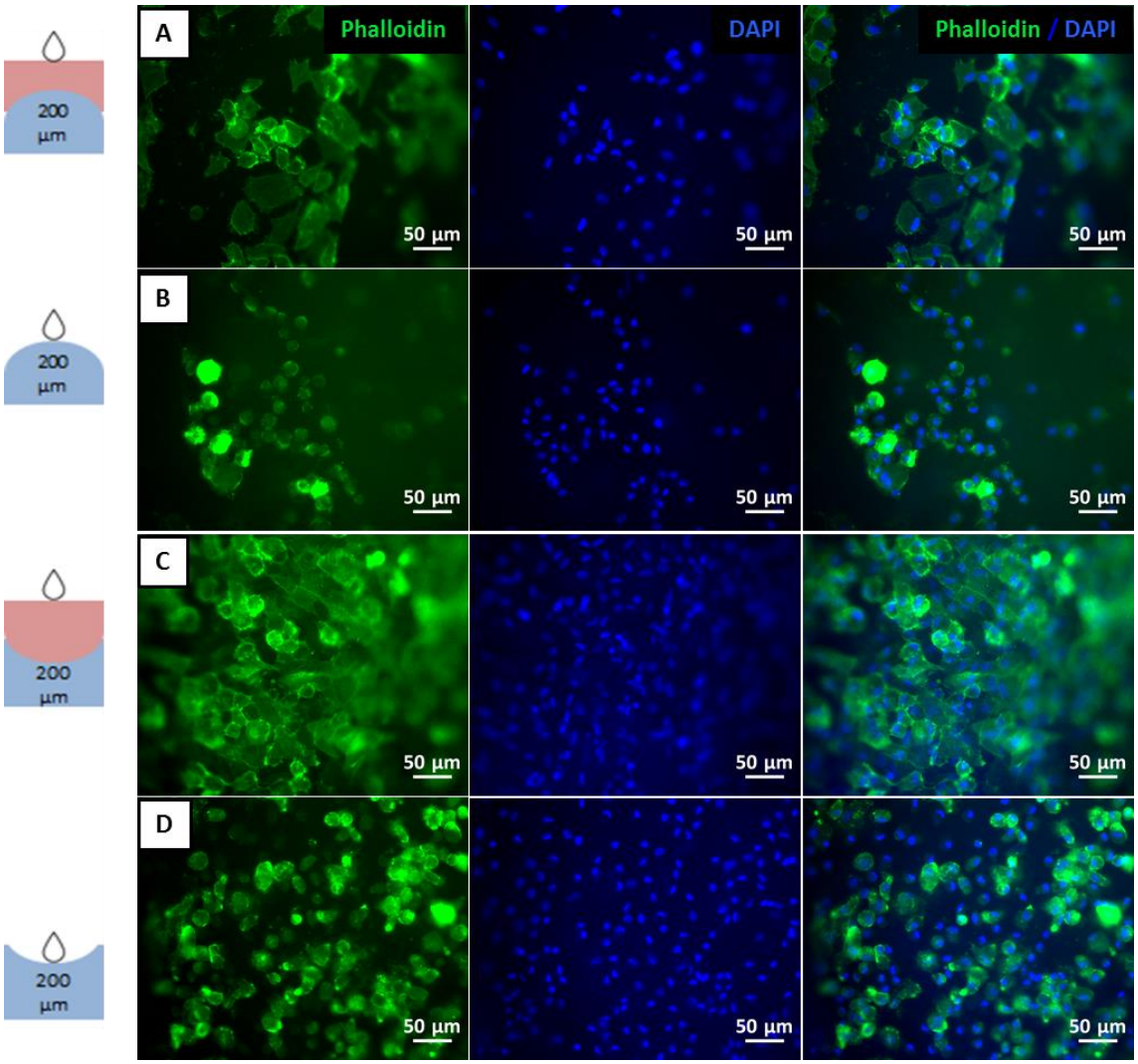

Figure 3.15. Fibroblasts cell culture on collagen hydrogels. Immunofluorescence analysis of phalloidin (green) and nuclear DAPI (blue) on patterned convex (A,B) and concave (C,D) hydrogels. Two seeding cells methods were evaluated: a drop of cells on the culture media (A,C) or directly on the hydrogel (B,D). Scale bars: 50 µm.

Focusing on the hydrogels with lowest LH (50 µm), convex and concave hydrogels presented similar number of cells. However, cells presented a more polygonal shape in concave hydrogels compared to convex hydrogels (Figure 3.16).

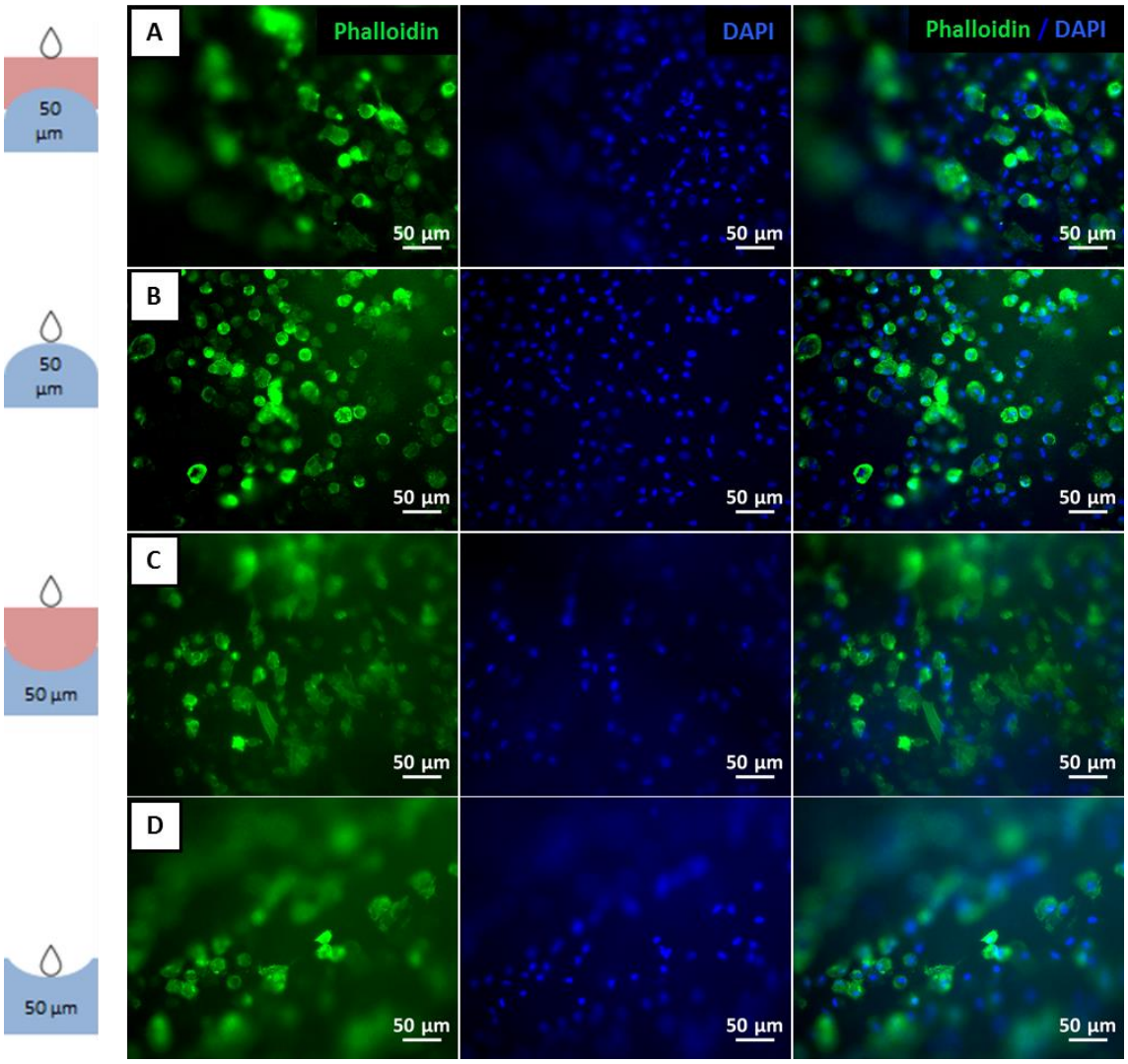

Figure 3.16. Fibroblasts cell culture on collagen hydrogels. Immunofluorescence analysis of phalloidin (green) and nuclear DAPI (blue) on patterned convex (A,B) and concave (C,D) hydrogels. Two seeding cells methods were evaluated: a drop of cells on the culture media (A,C) or directly on the hydrogel (B,D). Scale bars: 50 µm.

Cell density optimization

Aiming to further characterize cell culture on curved hydrogels, diverse cell densities (low, medium and high) were evaluated on patterned hydrogels. As preliminary results showed that after 24 hours cells were not yet al.igned, fibroblasts were cultured for 3 and 6 days on

patterned and unpatterned hydrogels. As hydrogels with 200 and 300 µm of LH did not have an effect on cell behavior, the patterned hydrogel with 50 µm of LH was used for next experiments.

As shown in Figure 3.17, phalloidin staining showed that at day 3 concave and flat hydrogel presented more aligned cells than convex hydrogel when using low cell density.

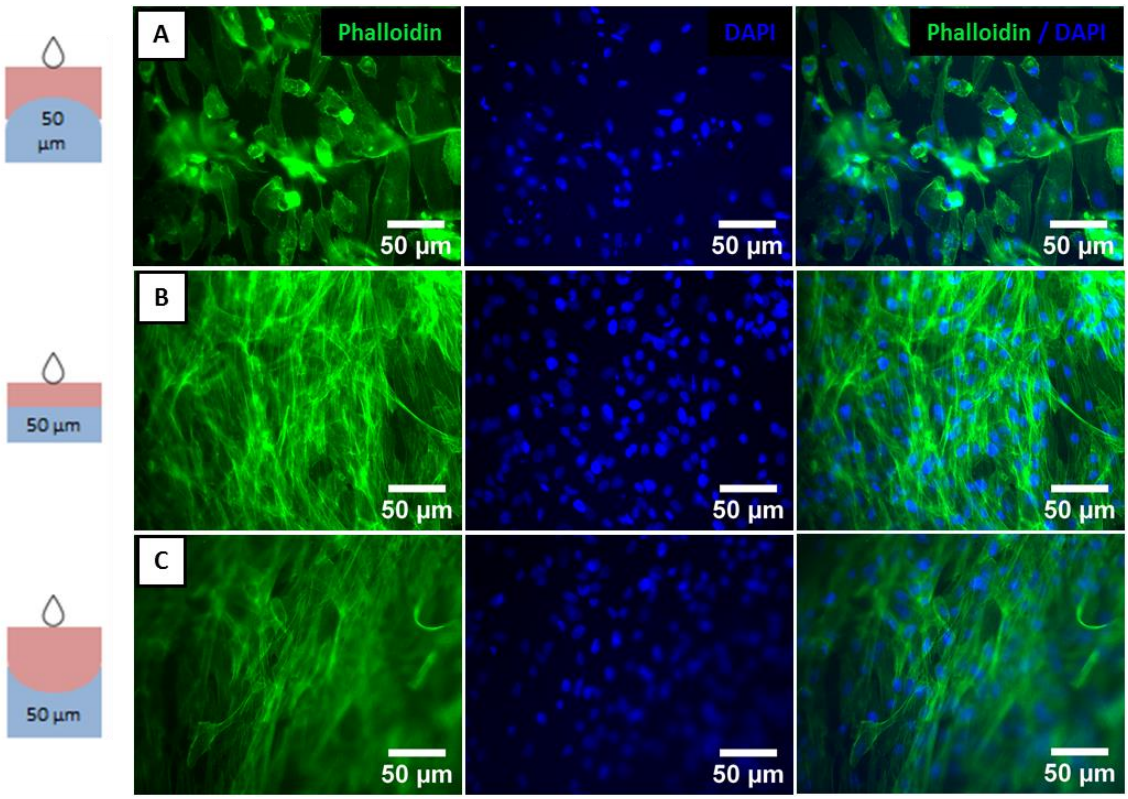

Figure 3.17. Fibroblast cell culture on collagen hydrogels. Cell morphology at patterned convex (A), flat (B) and concave (C) hydrogels at day 3 of culture using low cell density. Immunofluorescence analysis of phalloidin (green) and nuclear DAPI (blue). Scale bars: 50 µm.

However, at day 6 of culture, cells on concave hydrogel were aligned while flat and convex culture presented an irregular distribution (Figure 3.18). Further, at day 6 of culture, the number of cells decreased and its size increased.

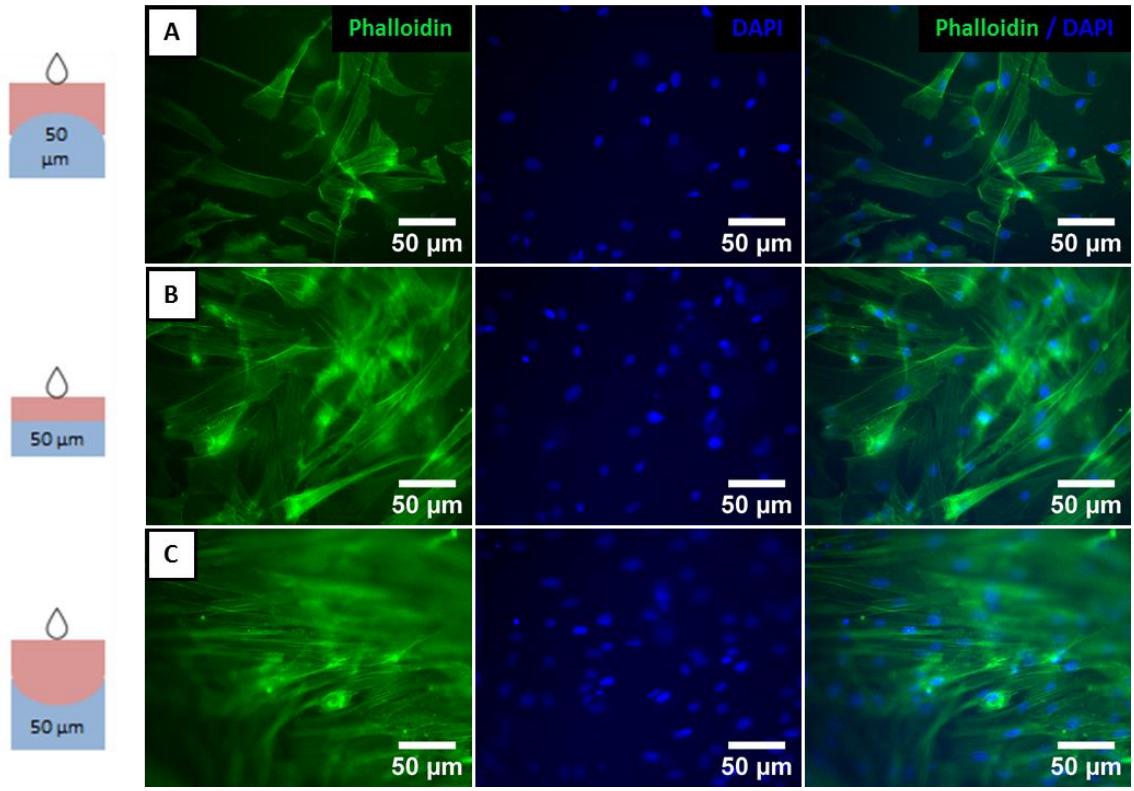

Figure 3.18. Fibroblast cell culture on collagen hydrogels. Cell morphology at patterned convex (A), flat (B) and concave (C) hydrogels at day 6 of culture using low cell density. Immunofluorescence analysis of phalloidin (green) and nuclear DAPI (blue). Scale bars: 50 µm.

Using medium cell density culture, fibroblasts were aligned at day 3 on curved hydrogels but exhibited an irregular distribution on flat hydrogels (Figure 3.19).

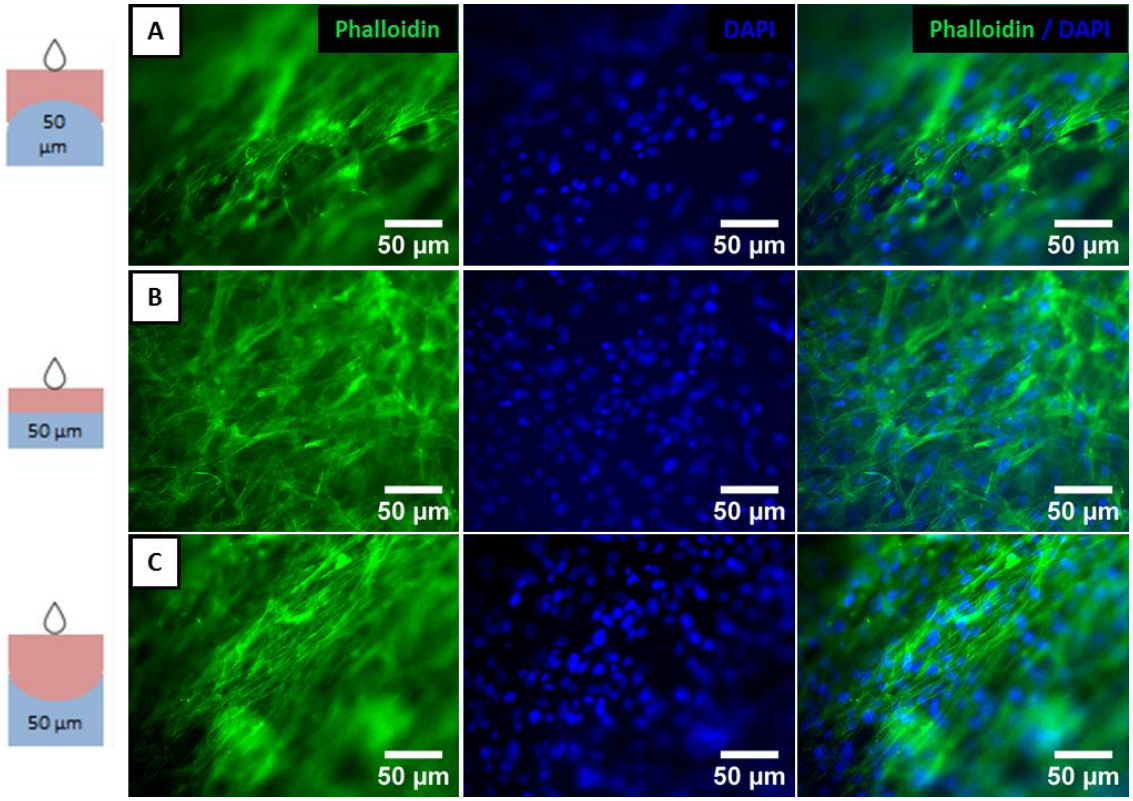

Figure 3.19. Fibroblast cell culture on collagen hydrogels. Cell morphology at patterned convex (A), flat (B) and concave (C) hydrogels at day 3 of culture using medium cell density. Immunofluorescence analysis of phalloidin (green) and nuclear DAPI (blue). Scale bars: 50 µm.

In contrast, as can be observed in Figure 3.20, all hydrogels at day 6 presented a similar distribution and orientation than day 3 although cells were more aligned on concave hydrogels.

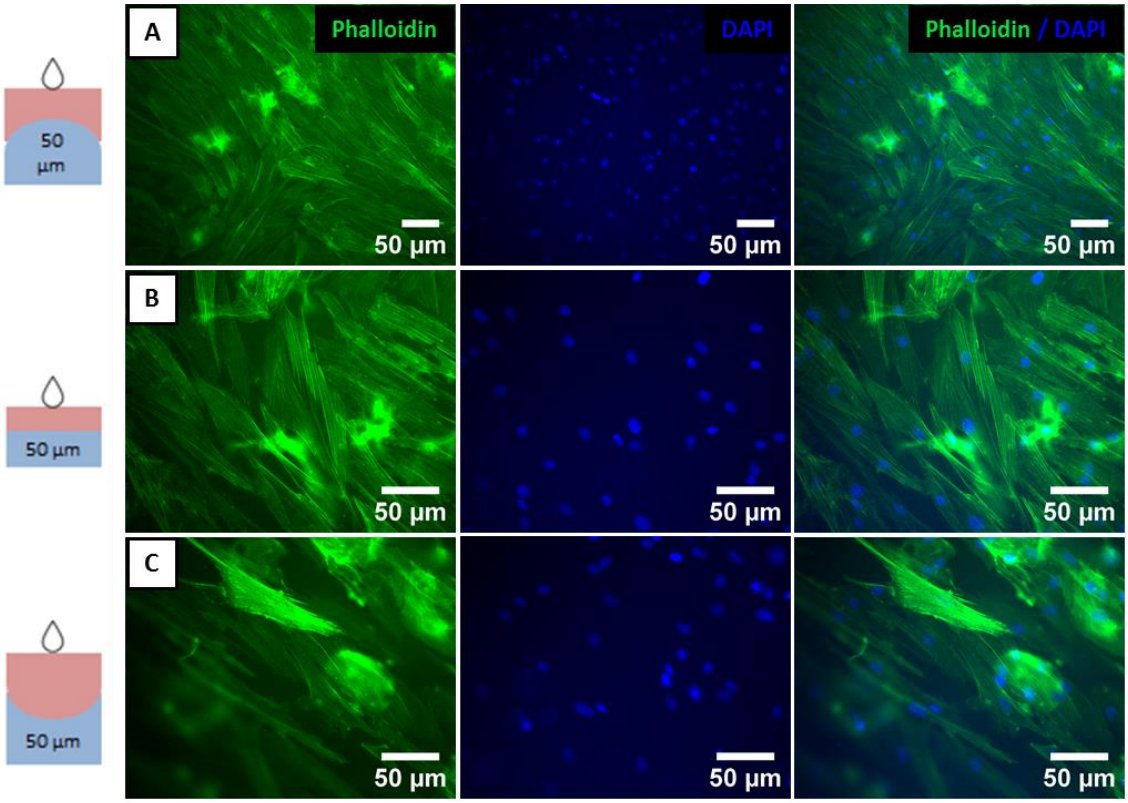

Figure 3.20. Fibroblast cell culture on collagen hydrogels. Cell morphology at patterned convex (A), flat (B) and concave (C) hydrogels at day 6 of culture using medium cell density. Immunofluorescence analysis of phalloidin (green) and nuclear DAPI (blue). Scale bars: 50 µm.

Finally, fibroblasts were cultured at a high cell density. As shown in Figure 3.21, cells were aligned on concave and convex hydrogels while cells on flat hydrogels exhibited an irregular distribution. Culturing fibroblasts at medium and high cell density presented similar results at day 3, as shown in Figure 3. 19. and 3.21.

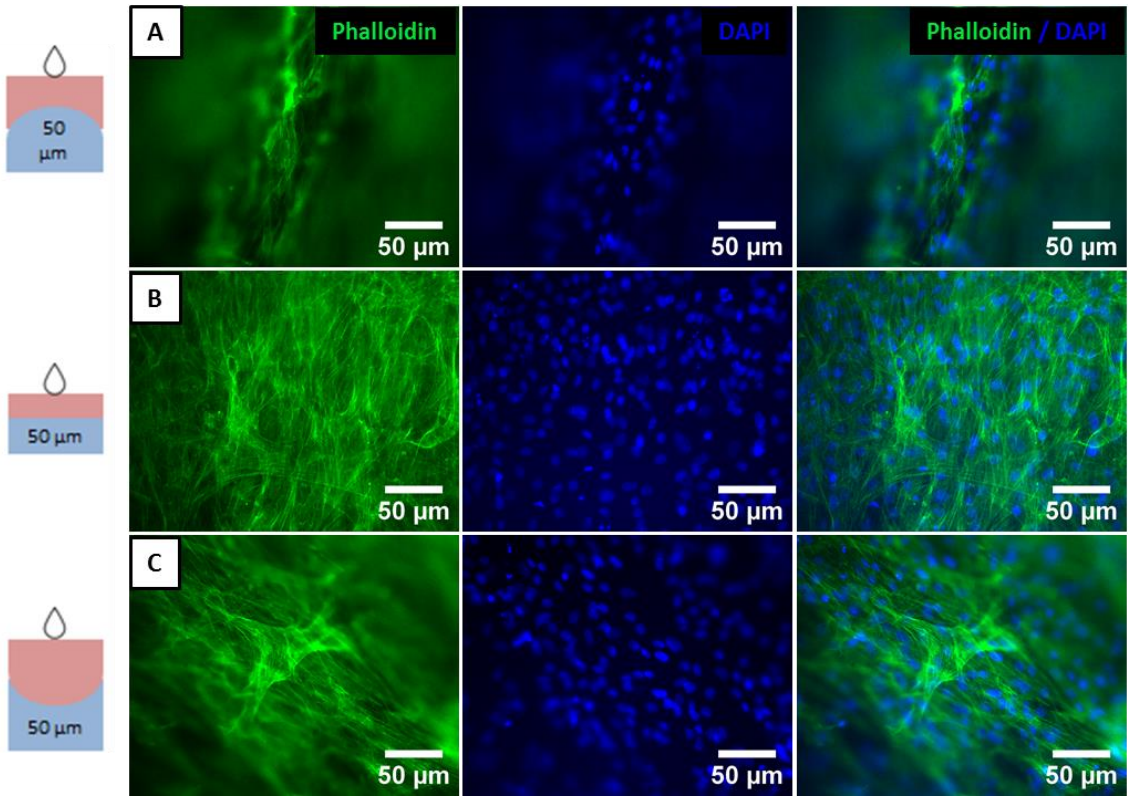

Figure 3.21. Fibroblast cell culture on collagen hydrogels. Cell morphology at patterned convex (A), flat (B) and concave (C) hydrogels at day 3 of culture using high cell density. Immunofluorescence analysis of phalloidin (green) and nuclear DAPI (blue). Scale bars: 50 µm.

Similar results were observed at day 6 (Figure 3.21), as cells presented more alignment in curved hydrogels compared to flat one. Moreover, in contrast to the other conditions, high cells density culture presented similar cell size and distribution at days 3 and 6 of culture.

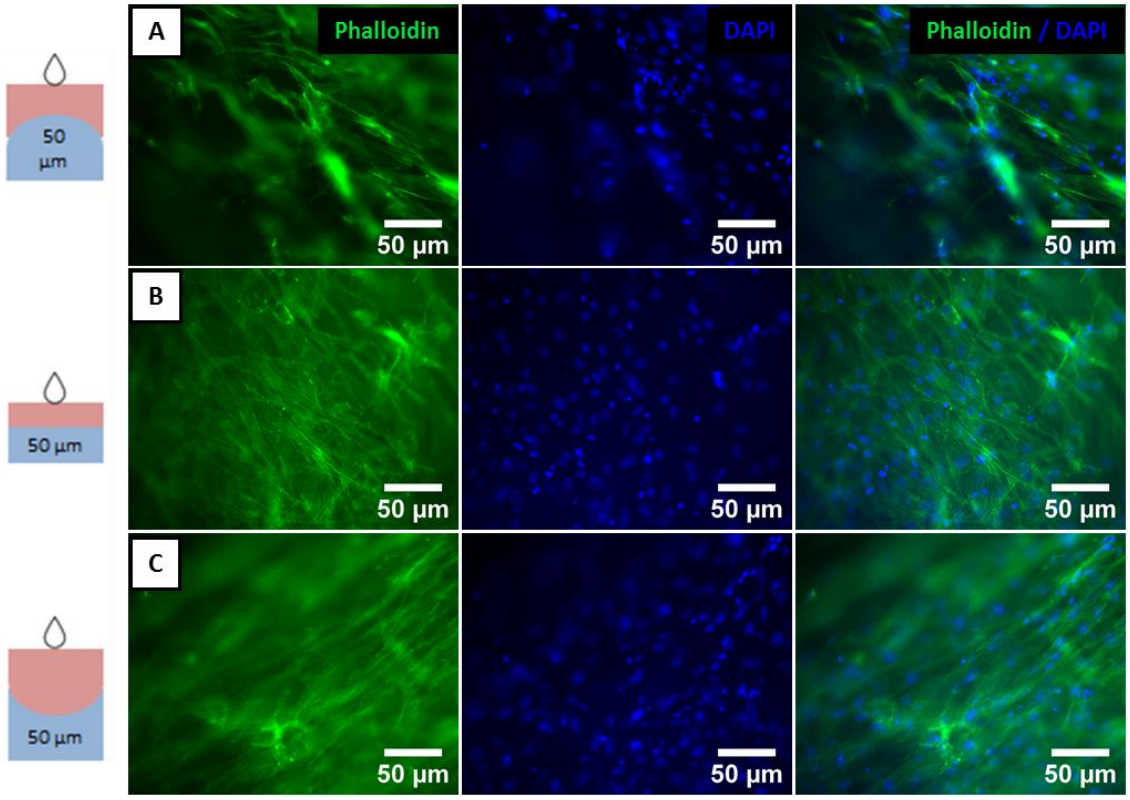

Figure 3.22. Fibroblast cell culture on collagen hydrogels. Cell morphology at patterned convex (A), flat (B) and concave (C) hydrogels at day 6 of culture using high cell density. Immunofluorescence analysis of phalloidin (green) and nuclear DAPI (blue). Scale bars: 50 µm.

3. 3. 4. 2. Corneal endothelial cell culture

Study of the corneal endothelial cell – matrix interactions: selection of the optimum substrate for expansion

Commercial CEC were cultured on ECM pre-coated tissue flasks from Celprogen. However, most of the cells were not able to exhibit its characteristic polygonal morphology. For this reason, following manufacturer's suggestion, another flask coating (FNC coating) was selected for the generation of more polygonal cells. As shown in Figure 3.23, images revealed that CEC on FNC coating presented higher cell density and more polygonal cells compared to Celprogen pre-coated flasks.

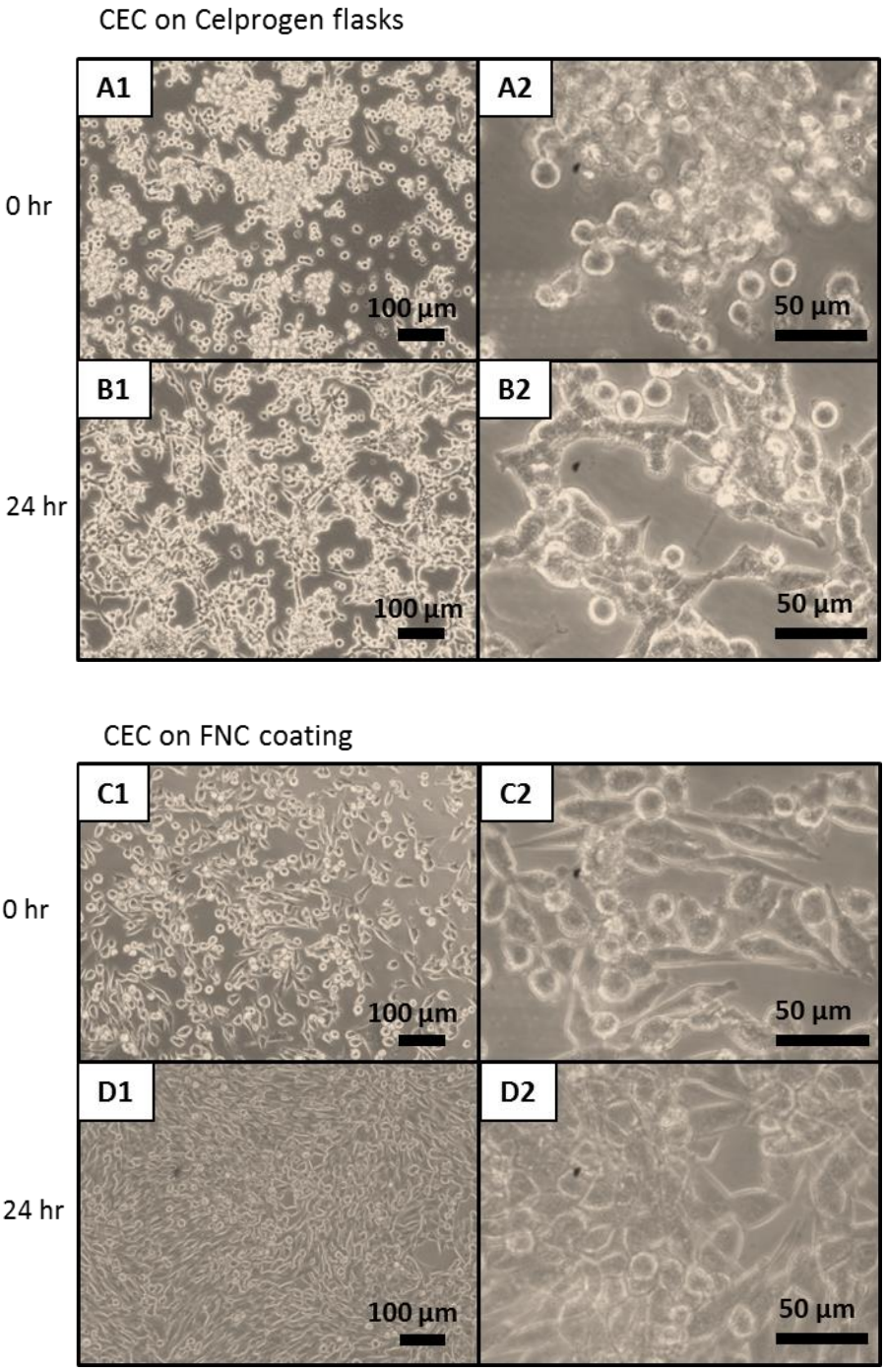

Figure 3.23. Commercial CEC cultured on different coatings. CEC were cultured on Celprogen pre-coated flasks (A,B) and on FNC coating (C,D) for 24 hours. Scale bars: 100 µm (A1-D1) and 50 µm (A2-D2).

Determining adequate genipin cross-linking concentrations

After analyzing the response of fibroblasts when cultured on hydrogels with different topographies and morphologies, similar study was performed using CEC. Nevertheless, the increased sensitivity of CEC showed that for the same cross-linking ratios as those used for the fibroblast culture, cell cytotoxicity was detected. For this reason, a new optimization of the cross-linking solution was necessary.

For this purpose, a cytotoxicity assay (CCK-8) was performed for the determination of the viable dilution of genipin. Results showed that for similar dilutions to those used for the fibroblasts culture, high cytotoxicity levels were observed. As shown in Figure 3.24, the highest concentrated genipin (dilution 1:50) presented a cell viability of less than 50%. Moreover, 1:100 dilution presented lower cytotoxicity compared to the 1:50 dilution, but still presented values below 80% viability. Nevertheless, the 1:200 dilution presented similar cell viability to that of the control (without genipin), not presenting significant differences among them. The results were shown to be significantly different compared to the 1:50 dilutions. For this reason, the dilution of 1:200 was used for further experiments.

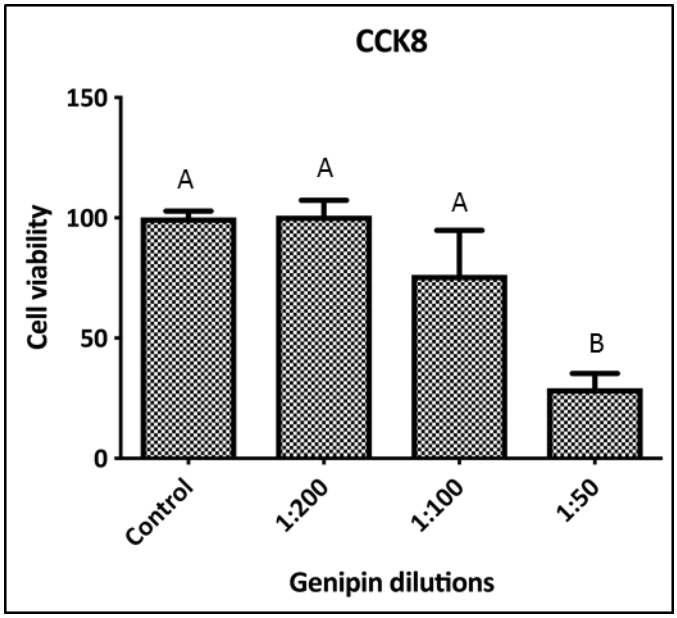

*Figure 3.24. Cell viability of CEC cultured on hydrogel. The effect of different dilutions of genipin evaluated by cell counting kit-8 (CCK-8) assay. Collagen hydrogel without genipin was used as a control. * different letter denotes significant differences. same letter denotes non-significant differences.*

Cell culture on patterned cross-linked hydrogels

Different LH hydrogels were evaluated with fibroblast culture and cells showed an alignment using the lowest LH hydrogels (50 μm). For this purpose, once the cross-linking dilution was determined for CEC culture, cells were cultured on the lowest LH using the patterned and the unpatterned curved hydrogels for 6 days.

Initially, as can be seen in Figure 3.25, confocal imaging revealed that at day 3, cells cultured in the unpatterned hydrogels showed higher cell numbers in the flat hydrogels than in the curved ones. Nevertheless, cells exhibited a polygonal shape in both the curved and the flat hydrogels.

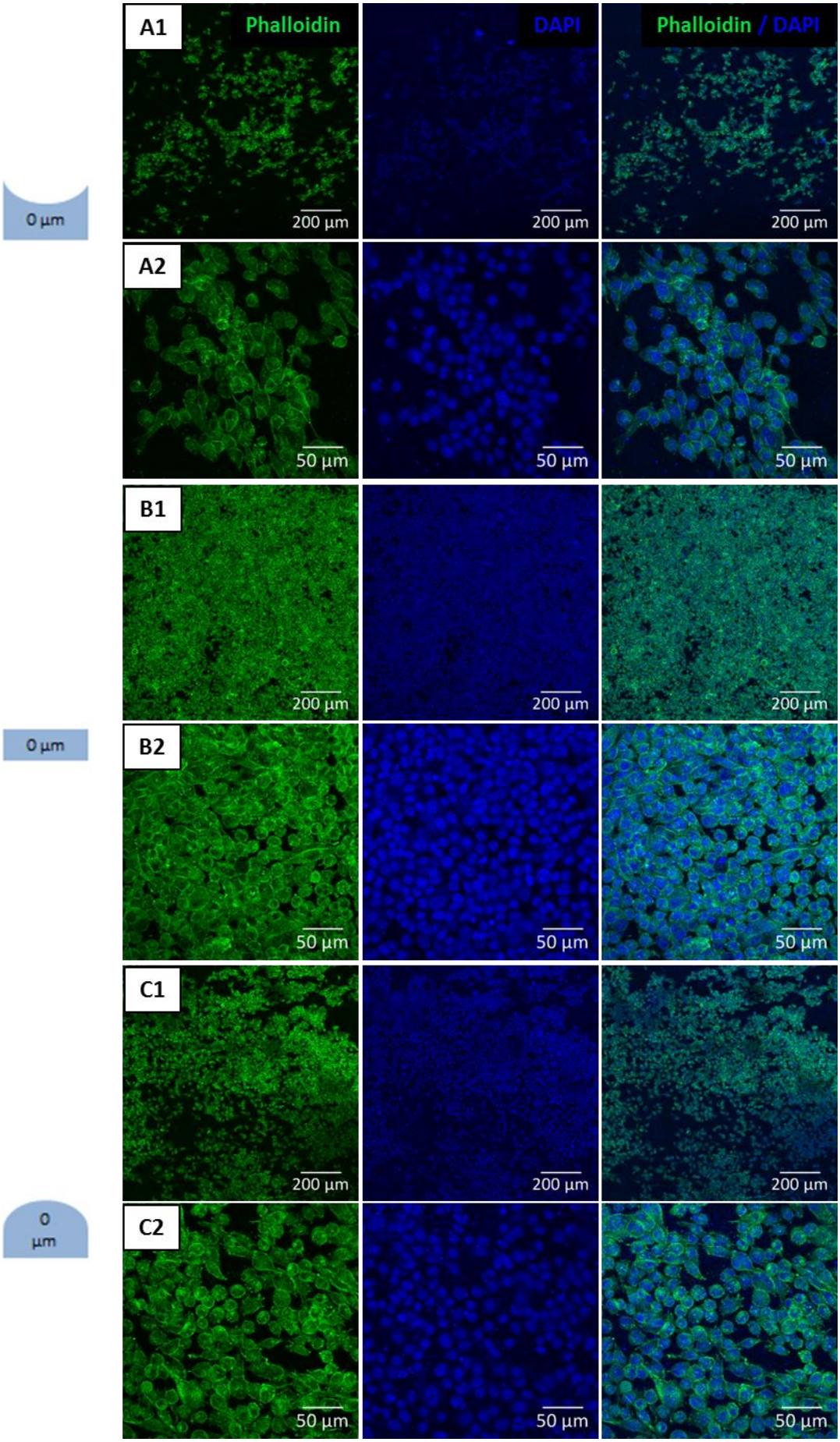
A1
Phalloidin
DAPI
Phalloidin / DAPI
0 µm
200 µm
A2
50 µm
B1
B2
C1
C2
0 µm
0 µm

Figure 3.25. CEC cultured on collagen hydrogels for 3 days. Cell morphology on convex (A), flat (B) and concave (C) unpatterned hydrogels, analyzed by immunofluorescence analysis of phalloidin (green) and nuclear DAPI (blue). Scale bars: 200 µm (A1-C1) and 50 µm (A2-C2).

We then analyzed the effect of cell behavior on CEC cultured on the same hydrogels, but presenting topographies. Regarding CEC culture with patterned hydrogels at day 3, low magnification images showed that cells tended to distribute and align along the different channels imprinted in the hydrogels. Moreover, images showed that patterned hydrogels presented high number of cells with polygonal morphology (Figure 3.26).

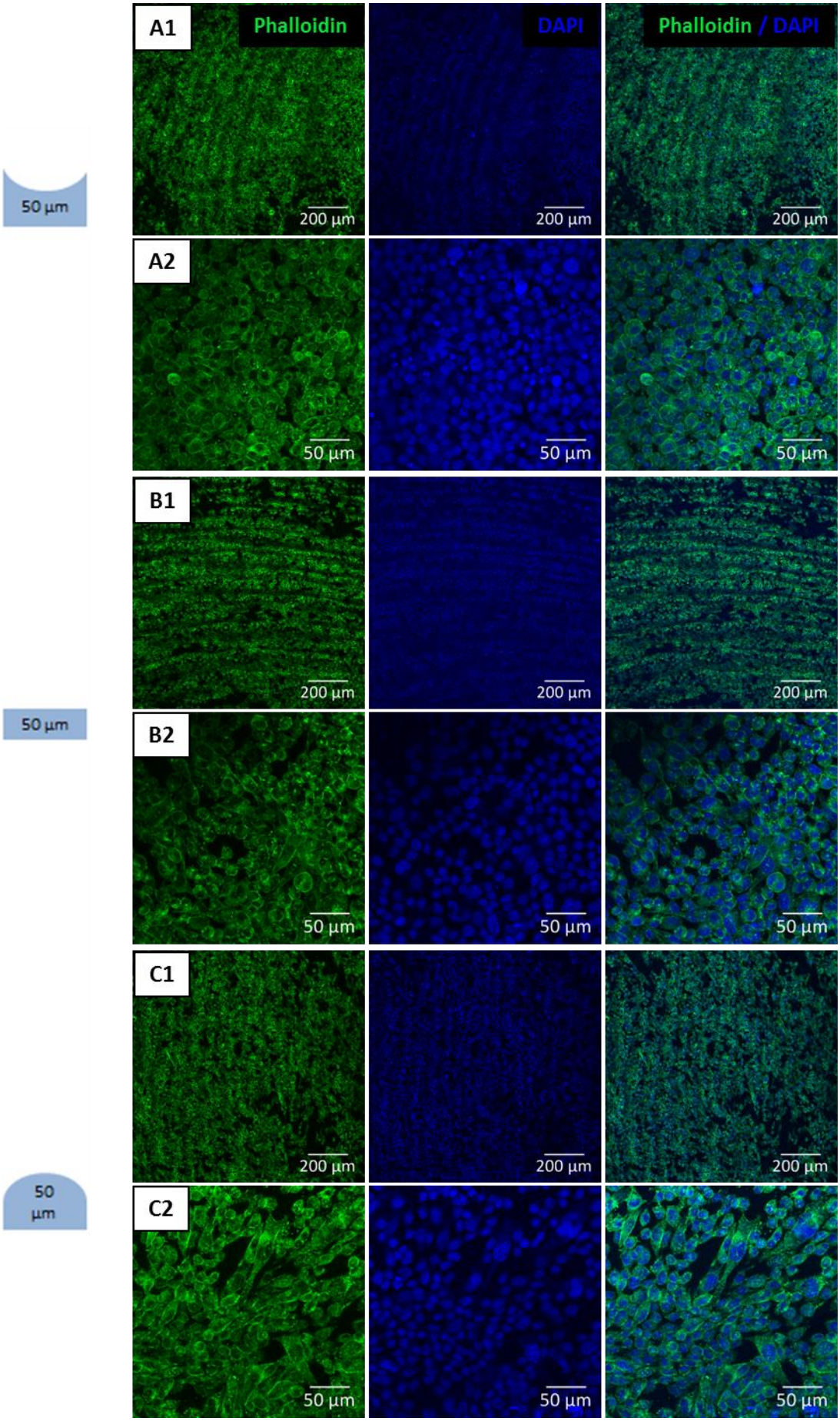
A1
Phalloidin
DAPI
Phalloidin / DAPI
200 µm
A2
50 µm
B1
B2
C1
C2
50 µm

Figure 3.26. CEC cultured on collagen hydrogels for 3 days. Cell morphology on convex (A), flat (B) and concave (C) patterned hydrogels, analyzed by immunofluorescence analysis of phalloidin (green) and nuclear DAPI (blue). Scale bars: 200 µm (A1-C1) and 50 µm (A2-C2).

We then analyzed the evolution of the different cells with time. As can be seen in Figure 3.27, immunofluorescence assay at day 6 revealed that concave and flat unpatterned hydrogels presented higher cell density than convex hydrogels. However, cells presented a more polygonal morphology on curved unpatterned hydrogels than in flat unpatterned culture, where a heterogeneous cellular morphology could be seen.

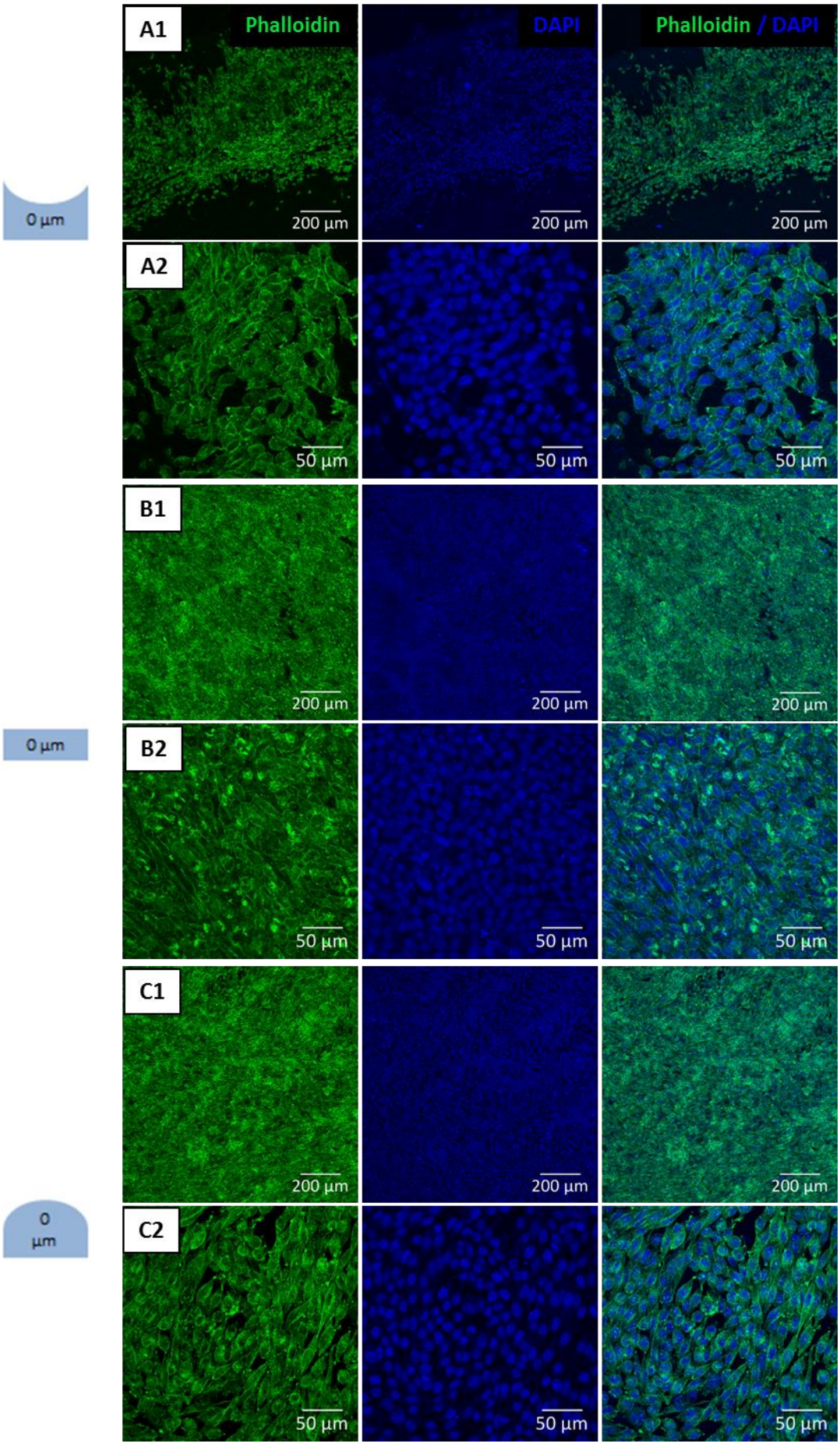
A1
Phalloidin
DAPI
Phalloidin / DAPI
0 µm
200 µm
A2
50 µm
B1
B2
C1
C2

Figure 3.27. CEC cultured on collagen hydrogels for 6 days. Cell morphology on convex (A), flat (B) and concave (C) unpatterned hydrogels, analyzed by immunofluorescence analysis of phalloidin (green) and nuclear DAPI (blue). Scale bars: 200 µm (A1-C1) and 50 µm (A2-C2).

Interestingly, significantly different results were shown when cells were left for 6 days on the patterned hydrogels. Cells were still shown to concentrate on the channels and that cells were able to present a polygonal structure that was significantly different to cells observed at 3 days for the patterned hydrogels as well as those observed on the unpatterned hydrogels at 6 days. Moreover, cell density at day 6 using patterned hydrogels was similar in all conditions (Figure 3.28).

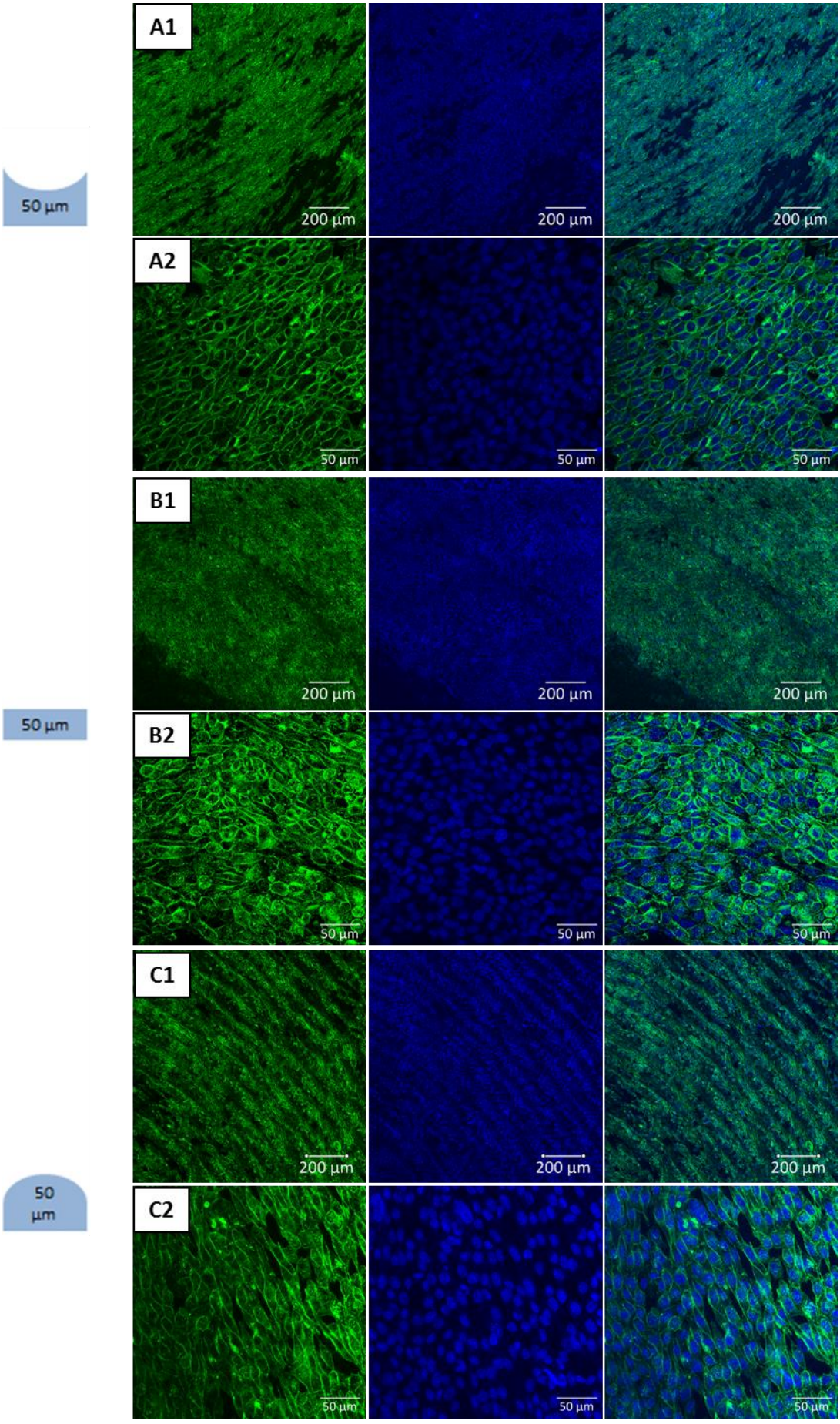
A1
A2
B1
B2
C1
C2
200 µm
50 µm
50 µm
50 µm
50 µm

Figure 3.28. CEC cultured on collagen hydrogels for 6 days. Cell morphology on convex (A), flat (B) and concave (C) patterned hydrogels, analyzed by immunofluorescence analysis of phalloidin (green) and nuclear DAPI (blue). Scale bars: 200 µm (A1-C1) and 50 µm (A2-C2).

We then studied cell circularity at days 3 and 6 (Figure 3.29). CEC exhibited an hexagonal and pentagonal morphology. A circle presents a value of 1 while an hexagon and pentagon have a circularity of 0.91 and 0.86 respectively. We should expect to obtain similar circularity results for the cultured CEC. Our results showed that at day 3, cells presented a significantly higher circularity index and more homogeneous morphology (0.870 ± 0.071) than cells at day 6 (0.719 ± 0.132). At days 6, cells tended to decrease its circularity, although their polygonal shape was increased. Furthermore, cells cultured on patterned hydrogels presented higher circularity values than unpatterned hydrogels at day 3 and 6 of culture. However, there were only significant differences between patterned and unpatterned conditions in flat molds at day 3.

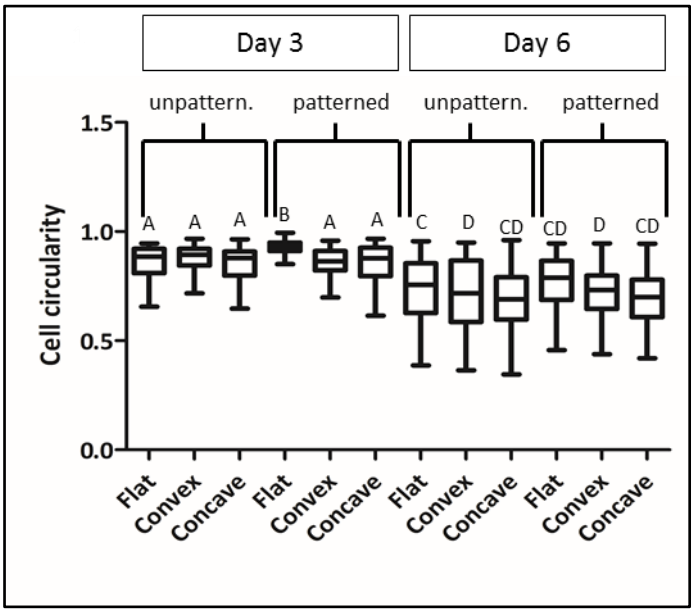

*Figure 3.29. CEC cultured on collagen hydrogels for 3 and 6 days. Morphology analysis by cell circularity values of CEC culture on unpatterned and patterned hydrogels in concave, flat and convex hydrogels. * Different letter denotes significant differences. Same letter denotes non-significant differences.*

Moreover, cell size, which was measured as cell area, indicated that at day 3 cells were significantly smaller (315.9 ± 98.48 µm) than cells at day 6 (399.5 ± 113.2 µm) as shown in Figure 3.30. However, regarding patterned and unpatterned hydrogels at day 3 and at day 6, cell size presented similar values in both conditions. In fact, as well as in cell circularity values, only flat conditions at day 3 presented significantly different values in patterned than unpatterned culture.

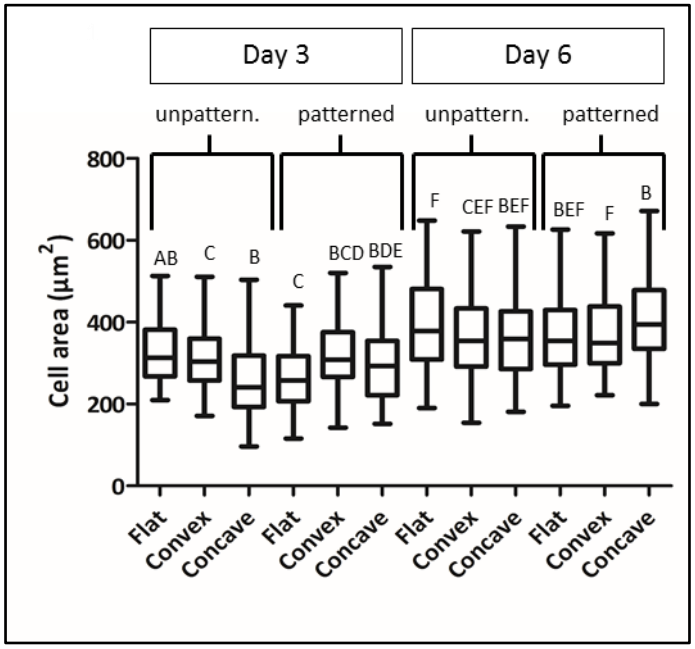

*Figure 3.30. CEC cultured on collagen hydrogels for 3 and 6 days. Morphology analysis by cell area values of CEC culture on unpatterned and patterned hydrogels in concave, flat and convex hydrogels. * Different letter denotes significant differences. Same letter denotes non-significant differences.*

Aiming to further characterize the effect of topography and curvature on CEC culture, the main cell tight junction (ZO-1) and the main pump function (ATP1A1) were analyzed by its gene expression, which is shown in Figure 3.31. Gene expression showed that at day 3, cells presented higher levels of ZO-1 in concave unpatterned hydrogels and flat patterned hydrogels. In contrast, levels of ZO-1 at day 6 were significantly increased in the flat unpatterned hydrogels.

Regarding the ATP1A1 expression at day 3, these presented significantly higher levels in curved unpatterned hydrogels than in flat hydrogels. Interestingly, patterned conditions,

concave hydrogels had significantly higher ATP1A1 expression than convex and flat conditions. Lastly, at day 6 of culture, convex unpatterned hydrogels presented the highest expression of ATP1A1, while the other conditions presented similar gene expression to the control condition.

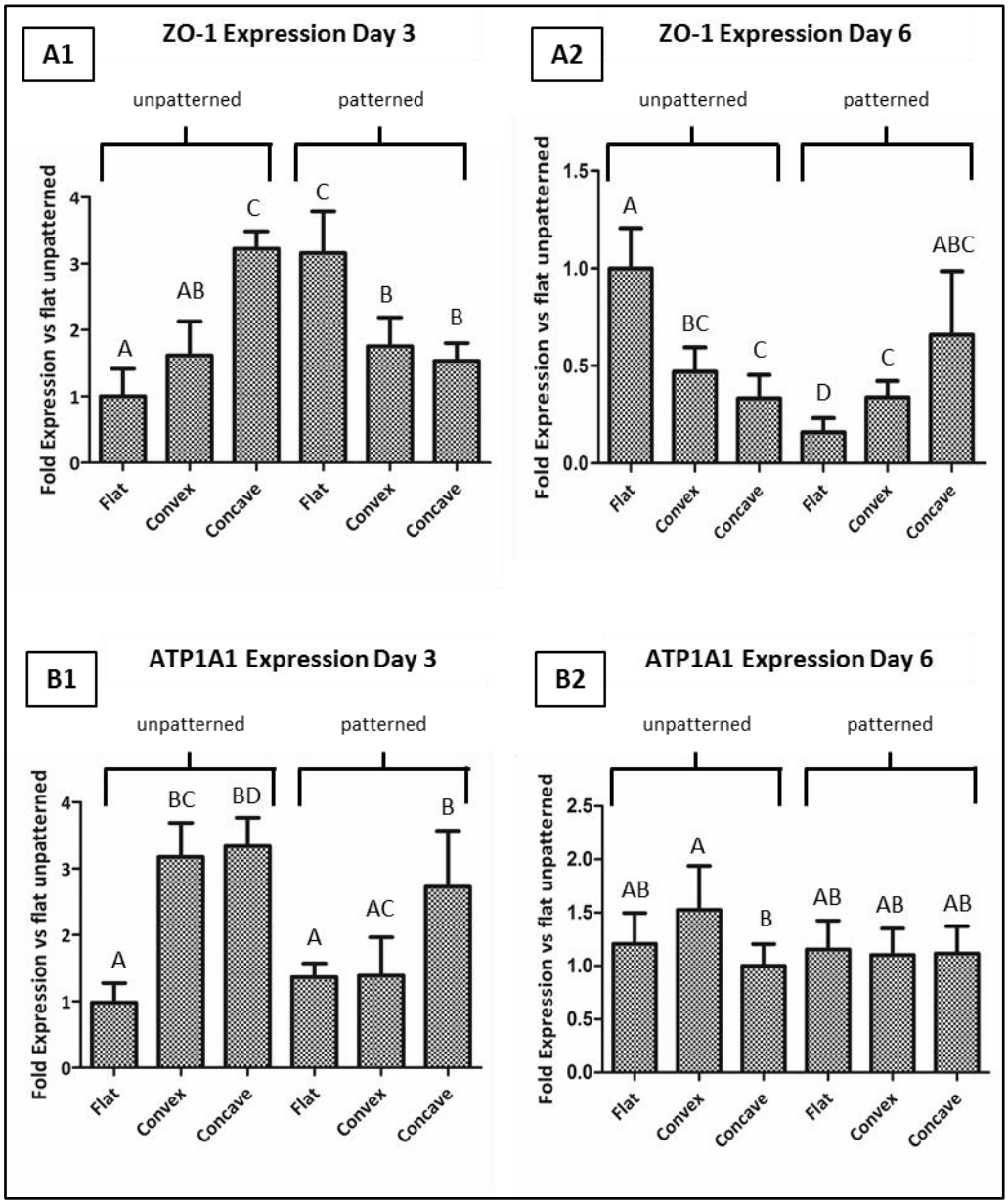

*Figure 3.31. CEC cultured on collagen hydrogels for 3 and 6 days. Fold gene expression of ZO-1 at day 3 (A1) and 6 (A2), and of ATP1A1 at day 3 (B1) and 6 (B2), analyzed by quantitative real time-polymerase chain reaction (qPCR). * Different letter denotes significant differences. Same letter denotes non-significant differences.*

3. 4. Discussion

The aim of this chapter was to study the effect of the topography and curvature on an *in vitro* culture of corneal endothelial cells (CEC). It is well known that *in vivo* cell behavior depends on their surrounding microenvironment. Therefore, many groups have studied the advantages of culturing different type of cells on surfaces that mimic the native environment [2,21,44]. More specifically, some studies have evaluated the effect of different patterned topographies in CEC culture, which ended in higher proliferation rate, maintenance of its characteristic cell morphology and improved cell function [15–17]. Ali et al. determined that Descemet's membrane, which is in contact with *in vivo* CEC, consists of fibers with elevations and pores which form an hexagonal collagen network [45,46]. Therefore, previous groups evaluated patterns that mimicked native Descemet's membrane structure like channels, wells, pillars and concentric circles [15–17]. However, the generation of these patterned molds requires the use of lithography-based techniques, which present some disadvantages as specialized equipment and difficult and expensive technique [18]. Furthermore, the use of non-implantable materials limits their applications. Therefore, we selected the concentric circled micropattern and incorporated curvature to this pattern, which can be easily and rapidly generated using a conventional 3D-printer. Moreover, this pattern has also been used in a very recent assay for the formation of corneal patient-specific molds [47].

3. 4. 1. Patterned film and hydrogel formation

We initially studied the use of a collagen film and cross-linked hydrogel, as both forms could adopt the desired printed pattern. Initially, collagen was selected as a natural biomaterial for corneal tissue engineering as it is the main component of extracellular matrixes in mammals, particularly in the cornea [48]. Therefore, many studies have previously studied the effect of collagen in CEC culture. They have determined that collagen-based substrates helped in the proliferation and maintenance of the characteristic polygonal morphology of CEC [49–52].

Collagen films were then generated and evaluated (Figure 3.12). Collagen films presented high optical properties due to its transparency and could be easily used for clinical applications, as Yoshida et al. had previously reported [53]. In fact, actual transplantation

techniques uses this method for the transplantation of corneal Descemet membrane and corneal endothelium [54]. However, they could not adopt the concentric circled pattern on aqueous medium as collagen films floated.

For this reason, we then used collagen hydrogel as an alternative scaffold for corneal tissue engineering due to its soft tissue-like properties. However, collagen hydrogels lack of sufficient strength and have high degradation rates as they present weak interactions. Therefore, hydrogels have to be modified with a cross-link reagent for the formation of stronger bonds, which ends in the formation of a stiffer substrate that adopts the desired pattern [55]. A great variety of biological, physical and chemical methods with natural and synthetic agents have been used as cross-linking strategies [56,57]. Among them, the plant extract genipin has recently become a great alternative due to its attractive properties like elevated cross-liking ability in biological tissues, natural source, slow degradation rate and low cytotoxicity compared to other chemical agents [32,58]. Furthermore, the formation of superficial blue pigmentation is an qualitatively indicator of genipin cross-linking [59]. However, high concentrations of genipin can end in cytotoxicity [41]. For this reason, different genipin dilutions in collagen hydrogel were assessed. Our preliminary results showed that the mid volume ratio (1:50) of genipin:collagen, which corresponded to 0.54 mM, presented an easy-to-handle hydrogel and a slightly pink color that was similar to the control one (Fig. 3.13). Moreover, Sundararaghavan et al. determined that the dose of genipin on fibroblast culture should not exceed 1 mM [60]. Therefore, we used this dilution for cell culture experiments.

Despite the genipin cross-linking may be of great help for the production of the collagen based hydrogels, it has to be taken into account that the cross-linking agent may be varying the stiffness of the substrate, which may ultimately guide as well cell behavior. Despite it was not the interest of this project, but perhaps future experiments could be performed on analyzing the effect of the substrate stiffness on the maintenance and differentiation of HCEC, as it has been widely reported that all cell types are able to profoundly sense the stiffness of substrates and behave similarly to cells that are found with matching stiffness values in the body [49,61].

3. 4. 2. Fibroblasts behavior on hydrogels

As an initial experiment, fibroblasts were first used as a preliminary experiment in order to optimize the culture conditions before CEC behavior characterization. We selected fibroblasts due to their numerous advantages as easy to use, well established cultured method, high proliferation rate and low cost [62].

To begin, fibroblasts were cultured for 24 hours on curved patterned hydrogels with low, medium and high LH hydrogels. Moreover, we used two methods for seeding the cells: a drop of cells directly on the hydrogel or on the culture medium. Although all conditions presented low number of cells, cells exhibited a more polygonal morphology using the seeding method of a drop of cells on the culture medium, as shown in Figures 3.14 to 3.16. Such differences could be explained as culture medium may dilute the side effect of cytotoxicity of genipin so cells seeded directly on the hydrogel were more exposed to genipin and, subsequently, had a lower survival rate. Hence, we expect that the cross-linker solution concentration presented a higher concentration in the microenvironment in which cells were not able to survive. It was previously seen that cross-linking solutions are critical and genipin has been one of the few cross-linkers that may cross-link hydrogels and allow the subsequent seeding of cells [63]. Other cross-linkers that are able to cross-link polymers in a more extensive manner, such as glutaraldehyde, has not been used to allow cell survival in the hydrogel foam and hence can only be use to cross-link composites or polymeric scaffolds [64,65].

Moreover, only when using hydrogels printed with low LH (50 µm), cells were distributed along the different concentric circles. These results may indicate that medium and high LH hydrogels were too separated for cells to notice it. It is obvious that the cell behavior on substrates will greatly depend on the cell type that is being used. In this sense, neuronal cells, which may extend up to 100 microns, generally are able to align on different sized channels, whereas smaller cells such as chondrocytes, have more limited ability to extend along channel-like structures [66,67]. In the case of fibroblasts, these cells generally have a size around few tens of microns, and hence their optimal interaction is the 50 micron sized LH. When the size of the LH was higher, cells were not able to sense the channel and behaved in a similar way to the smooth surfaces. Therefore, as shown in Figure 3.32, when

LH is lower than cell size, cells became elongated and were distributed along the circle but when LH was higher than cell size, cells morphology or distribution was not affected. This is in line with a previous report that seeded hepatocytes on different substrates concluded that spacing distances between patterns of 50 µm enhanced growth kinetics, compared to higher spacing which did not have an effect on cell growth [20]. Hepatocytes are an interesting cell source to compare with, as in their native morphology these also a present a rather circular shaped morphology similar to our CEC and hence these results are in good agreement with our results. In contrast, the topography of low LH hydrogels determined the directionality of cell adhesion, which was also reported by a previous group [16].

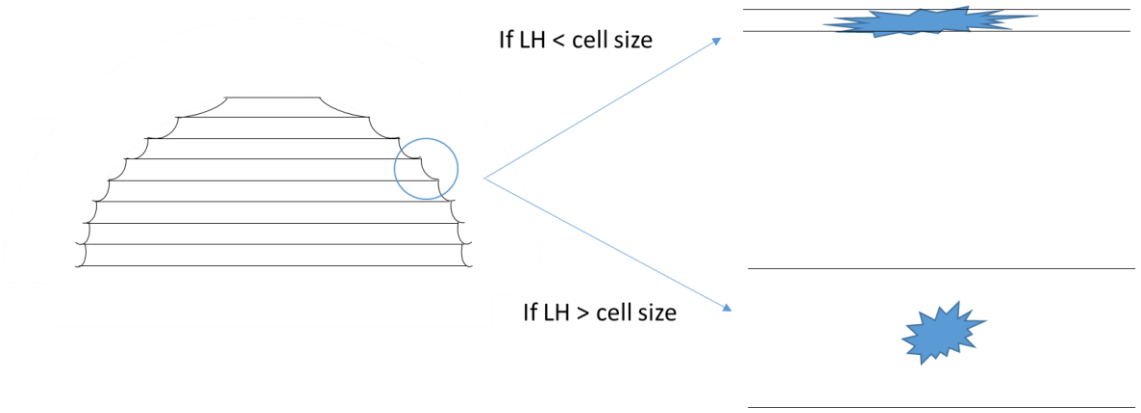

Figure 3.32. Schematic representation of cell behavior on hydrogels. When layer height (LH) is lower than the cell size cells are elongated while when LH is higher than cell size cells do not elongate.

Prior to the culture of CEC on hydrogels, fibroblasts were cultured in curved and flat patterned hydrogels, with low LH hydrogels, as our initial experiment determined that cells in low LH hydrogels seemed to distribute along the concentric circles. Moreover, cells were cultured for longer time points (3 and 6 days), to allow cells proliferate, at low, medium and high cell density, mimicking native CEC cell density. As shown in Figures 3.17 to 3.22, our results suggested that when cells were cultured at medium and high cell density on curved patterned hydrogels, particularly in concave conditions, fibroblasts were aligned along the concentric circles at days 3 and 6 of culture. These results were previously reported by different groups, who examined the effect of micro and nanotopography on fibroblasts orientation [68,69]. In contrast, in patterned flat conditions cells presented a more irregular orientation.

These preliminary results may indicate that curvature and topography have an effect on the distribution and orientation of cell culture.

3. 4. 3. Corneal endothelial cell behavior on hydrogels

Before culturing CEC on collagen hydrogels, CEC culture was optimized in order to obtain a more polygonal/hexagonal morphology, which is one of the main characteristics of CEC. For this purpose, two coatings were evaluated: the commercial ECM pre-coated flasks and fibronectin-collagen combination (FNC) coating mix (Athena Environmental Sciences), which are components of Descemet's membrane and have been widely used by different groups [37–40]. As shown in Figure 3.23, our coating assay determined that FNC coating mix presented a higher number of cells and a more polygonal morphology. Therefore, we selected FNC coating mix coating for further experiments.

We then cultured CEC on hydrogels using the same cross-linking dilution of 1:50 (genipin:collagen) than with fibroblasts culture. However, cells were not able to survive with this cross-linking concentration. Our results were in line with previous reports, which determined that the concentration of genipin depends on the cell type [41,42]. Therefore, a cytotoxicity assay with different concentrations of genipin was performed and the dilution 1:200 was elected as the optimal concentration as the mean value of cell viability was very similar to the control one.

Once cross-linking concentration was evaluated and based on our fibroblasts culture results, CEC were cultured on unpatterned and patterned, using the lowest LH, hydrogels and culturing cells at a native cell density [17]. Our results showed that the combination of topography and curvature affected on CEC behavior.

As shown in Figures 3.25 to 3.31, cells presented a more homogeneous morphology at short time (3 days), increasing its size at day 6. However, cells at day 6 presented a more polygonal morphology although cells were more elongated. To further characterize cell morphology and due to its characteristic polygonal shape, cell circularity and cell size were used for its evaluation. In fact, these parameters have been previously studied for the evaluation of *in vitro* CEC [15–17,43,70]. Previous studies that evaluated the effect of topography on CEC culture obtained cell sizes that were 3 to 10 times higher size than native cells [15,17]. However, as shown in Figures 3.29 and 3.30, our results showed that

curved patterned and unpatterned culture ended in a polygonal morphology and cell sizes similar to native cells [71]. Surprisingly, the cell circularity decreased with time, which probably indicate that cells tended to have a rather elongated morphology in some cases. This was more evident in the cases in which cell confluence was reached, such as the flat surfaces. It was previously reported that the increase as cell passage increased, CEC lost their characteristic morphology, hence showing that prolonged culture periods *in vitro* may reduce their typical morphology [49].

In order to understand in more detail the characteristic phenotype and correlate them with the cell morphology, we analyzed two main markers, mainly ZO-1 and ATP1A1. ZO-1 is mainly related with tight junctions and hence its expression is based on how these junctions are established. It was previously shown that the tight junctions in CEC have an interesting behavior, showing that despite the overall cell morphology possess a rather hexagonal shape, the philipodia tend to high surface area in order to have highest cell contact with other cells [72,73]. At 3 days, we saw that the unpatterned surfaces showed higher expression for the concave and convex surfaces compared to the flat surfaces, presenting significant differences. This could be related to the fact that when cell are presented in a curved surface, cells have to adapt to different morphologies and small stresses are created on their surfaces, probably forcing them to have higher cell to cell contact between cells and hence increase the tight junction levels [74]. Nevertheless, when the topography is present, cells start arranging in a different manner. Cells no longer have the macro architecture of curvature, but rather have pits in the size range of their own cells, forcing cells to come in close contact among them. For this reason, we expected that at this point the topography overruled the architecture and showed highest levels of expression on the flat surfaces. The fact that, in this case, the flat surfaces present higher values of ZO-1 is probably related with the fact that cells have higher chances of falling in the different pits in a more homogeneous manner that in the curved substrates, where not all the pits are identical and hence their behavior can be different. It was previously seen that a topography that forces cells to increase the tight junction connections increased as well the ZO-1 levels [15,17]. Nevertheless, after 6 days, the behavior significantly changed, showing that in the unpatterned substrate the ZO-1 levels were increased for the flat surfaces. This could be related with the fact that higher cell density is observed in this case and, hence, the chances

of having higher ZO-1 levels were increased. It was previously seen that when seeding cells at different densities, the levels of ZO-1 could be altered. Furthermore, it seemed that the curved surfaces decreased with time their effect. When analyzing the patterned substrates, we saw that in general the different substrates reduced the expression of ZO-1, especially for the flat surfaces. This could be related to the increased confluence levels showed for this condition, which forced cells to align on the pits, and despite the cell to cell contact existed, the fact that cells became elongated decreased the tight junctions between them. This could be hypothesized to be related with the EndMT, in which cells tend to reduce their endothelial la behavior and go into a more fibroblastic behavior [75]. Despite the levels of ZO-1 were also decreased for the concave and convex substrates, since these conditions did not present cells in confluence, cells did not completely adopt the fibroblastic character. We then analyzed the expression of the pump function ATP1A1, which is related with their functionality and their capacity to exchange K^+ and Na^+ from the anterior chamber to the stroma. In this case, we observed that at day 3 for the unpatterned substrates both the convex and the concave presented higher levels of ATP1A1 compared to the flat surface. This is in accordance with the fact that cells in their native environment are placed in a convex morphology and, hence, presenting this architecture enhances their functionality. This is very similar to the results obtained for ZO-1. It was previously seen that round surfaces were promising architectures for the cultured of CEC [11,53]. Similar results were observed for the patterned substrates at 3 days, showing that both the concave and the flat surfaces followed the same trend, but was not observed for the convex substrates. It seems that for the ATP1A1 expression, unlike in the case of ZO-1, the curvature of the substrates overrules the topography of the substrates. Previous results showed accordingly that ZO-1 levels were deeply influenced by the topography, whereas the ATP1A1 levels, despite they were also affected by topography, its effect was lower [15]. At day 6, the unpatterned substrates showed highest levels of expression for the convex substrates, which mimics the architecture of native cells and, hence, demonstrates that mimicking the native macro architecture had a beneficial effect on cell behavior. The flat and the concave surfaces behaved in a similar way among them, which could be related with the lower mimicking ability of their architectures and hence decreased their functionality. Finally, at day 6, the patterned substrates showed the same behavior in all three surfaces. It seems that as was previously shown, the culture of these cells may reduce their phenotypic activity with time

[75]. Hence, overall, it seems that these type of cultures are necessary for corneal endothelium tissue engineering, although the culture time points are optimum at short times in order to prevent their loss of phenotypic activity in vitro. As was mentioned earlier, this is related with the EndMT, which lead to rather fibroblastic phenotypes and hence a reduction in their functionality [75]. Therefore, short time of culture on patterned and unpatterned hydrogels may be better than longer culture.

To summarize, our results demonstrate that cross-linked collagen hydrogels can be used as a platform for CEC culture. Moreover, topography and curvature culture seems to enhance CEC cell morphology and function at short time of culture with similar sizes to that of native cell. However, further studies are needed for the generation of an easily transplantable scaffold.

3. 5. Conclusions

This chapter presents an innovative method to improve the culture of HCEC by combining for the first time a curved surface with microtopography, mimicking its native environment. For this purpose, we have used a conventional 3D printer, which is an economic, rapid an easy technique. The results show that curved patterned substrates enhanced cell function and morphology at short time of culture, as determined by the expression of characteristic markers ZO-1 and ATP1A1.

3. 6. References

[1] A.D. Theocharis, S.S. Skandalis, C. Gialeli, N.K. Karamanos, Extracellular matrix structure, Adv. Drug Deliv. Rev. 97 (2016) 4–27. doi:10.1016/j.addr.2015.11.001.

[2] M.P. Sousa, S.G. Caridade, J.F. Mano, Control of Cell Alignment and Morphology by Redesigning ECM-Mimetic Nanotopography on Multilayer Membranes, Adv. Healthc. Mater. 6 (2017). doi:10.1002/adhm.201601462.

[3] J.D. Kiang, J.H. Wen, J.C. Del Álamo, A.J. Engler, Dynamic and reversible surface topography influences cell morphology, J. Biomed. Mater. Res. - Part A. 101 A (2013) 2313–2321. doi:10.1002/jbm.a.34543.

[4] M. Paris, A. Götz, I. Hettrich, C.M. Bidan, J.W.C. Dunlop, H. Razi, I. Zizak, D.W. Hutmacher, P. Fratzl, G.N. Duda, W. Wagermaier, A. Cipitria, Scaffold curvature-mediated novel biomineralization process originates a continuous soft tissue-to-bone interface, Acta Biomater. (2017) 64–80. doi:10.1016/j.actbio.2017.07.029.

[5] G.C. Reilly, A.J. Engler, Intrinsic extracellular matrix properties regulate stem cell differentiation, J. Biomech. 43 (2010) 55–62. doi:10.1016/j.jbiomech.2009.09.009.

[6] D. Jhala, R. Vasita, A Review on Extracellular Matrix Mimicking Strategies for an Artificial Stem Cell Niche, Polym. Rev. 55 (2015) 561–595. doi:10.1080/15583724.2015.1040552.

[7] D.A. Brafman, Constructing stem cell microenvironments using bioengineering approaches, Physiol. Genomics. 45 (2013) 1123–1135. doi:10.1152/physiolgenomics.00099.2013.

[8] G.S. Hussey, J.L. Dziki, S.F. Badylak, Extracellular matrix-based materials for regenerative medicine, Nat. Rev. Mater. 3 (2018) 159–173. doi:10.1038/s41578-018-0023-x.

[9] R.A. Perez, C.R. Jung, H.W. Kim, Biomaterials and Culture Technologies for Regenerative Therapy of Liver Tissue, Adv. Healthc. Mater. 6 (2017) 1600791. doi:10.1002/adhm.201600791.

[10] L. Chu, G. Jiang, X. Le Hu, T.D. James, X.P. He, Y. Li, T. Tang, Biodegradable macroporous scaffold with nano-crystal surface microstructure for highly effective osteogenesis and vascularization, J. Mater. Chem. B. 6 (2018) 1658–1667. doi:10.1039/c7tb03353b.

[11] M. Kimoto, N. Shima, M. Yamaguchi, Y. Hiraoka, S. Amano, S. Yamagami,

Development of a bioengineered corneal endothelial cell sheet to fit the corneal curvature, Investig. Ophthalmol. Vis. Sci. 55 (2014) 2337–2343. doi:10.1167/iovs.13-13167.

[12] C.J. Bettinger, R. Langer, J.T. Borenstein, Engineering substrate topography at the Micro- and nanoscale to control cell function, Angew. Chemie - Int. Ed. 48 (2009) 5406–5415. doi:10.1002/anie.200805179.

[13] M.-C. Kim, C. Kim, L. Wood, D. Neal, R.D. Kamm, H.H. Asada, Integrating focal adhesion dynamics, cytoskeleton remodeling, and actin motor activity for predicting cell migration on 3D curved surfaces of the extracellular matrix, Integr. Biol. 4 (2012) 1386. doi:10.1039/c2ib20159c.

[14] G.M. de Peppo, H. Agheli, C. Karlsson, K. Ekström, H. Brisby, M. Lennerås, S. Gustafsson, P. Sjövall, A. Johansson, E. Olsson, J. Lausmaa, P. Thomsen, S. Petronis, Osteogenic response of human mesenchymal stem cells to well-defined nanoscale topography in vitro, Int. J. Nanomedicine. 9 (2014) 2499–2515. doi:10.2147/IJN.S58805.

[15] S. Koo, R. Muhammad, G.S.L. Peh, J.S. Mehta, E.K.F. Yim, Micro- and nanotopography with extracellular matrix coating modulate human corneal endothelial cell behavior, Acta Biomater. 10 (2014) 1975–1984. doi:10.1016/J.ACTBIO.2014.01.015.

[16] B.K.K. Teo, K.J. Goh, Z.J. Ng, S. Koo, E.K.F. Yim, Functional reconstruction of corneal endothelium using nanotopography for tissue-engineering applications, Acta Biomater. 8 (2012) 2941–2952. doi:10.1016/j.actbio.2012.04.020.

[17] R. Muhammad, G.S.L. Peh, K. Adnan, J.B.K. Law, J.S. Meh, E.K.F. Yim, Micro- and nano-topography to enhance proliferation and sustain functional markers of donor-derived primary human corneal endothelial cells, Acta Biomater. 19 (2015) 138–148. doi:10.1016/J.ACTBIO.2015.03.016.

[18] D. Qin, Y. Xia, G.M. Whitesides, Soft lithography for micro- and nanoscale patterning, Nat. Protoc. 5 (2010) 491–502. doi:10.1038/nprot.2009.234.

[19] R. Mumby, Printing for packaging, in: Packag. Technol. Fundam. Mater. Process., Woodhead Publishing (2012) 441–489. doi:10.1533/9780857095701.

[20] M. Lunova, V. Zablotskii, N.M. Dempsey, T. Devillers, M. Jirsa, E. Syková, Š. Kubinová, O. Lunov, A. Dejneka, Modulation of collective cell behaviour by geometrical constraints, Integr. Biol. (United Kingdom). 8 (2016) 1099–1110.

doi:10.1039/c6ib00125d.

[21] J. Hu, C. Hardy, C.M. Chen, S. Yang, A.S. Voloshin, Y. Liu, Enhanced cell adhesion and alignment on micro-wavy patterned surfaces, PLoS One. 9 (2014) e104502. doi:10.1371/journal.pone.0104502.

[22] H.J. Levinson, Lithography Costs, in: Princ. Lithogr., SPIE, 1000 20th Street, Bellingham, WA 98227-0010 USA (2005) 355–374. doi:10.1117/3.601520.ch11.

[23] M. Gulyas, M. Csiszer, E. Mehes, A. Czirok, Software tools for cell culture-related 3D printed structures, PLoS One. 13 (2018) e0203203. doi:10.1371/journal.pone.0203203.

[24] P. Dudek, FDM 3D printing technology in manufacturing composite elements, Arch. Metall. Mater. 58 (2013) 1415–1418. doi:10.2478/amm-2013-0186.

[25] J.L. Drury, D.J. Mooney, Hydrogels for tissue engineering: Scaffold design variables and applications, Biomaterials. 24 (2003) 4337–4351. doi:10.1016/S0142-9612(03)00340-5.

[26] M. Nitschke, S. Gramm, T. Götze, M. Valtink, J. Drichel, B. Voit, K. Engelmann, C. Werner, Thermo-responsive poly(NiPAAm-co-DEGMA) substrates for gentle harvest of human corneal endothelial cell sheets, J. Biomed. Mater. Res. - Part A. 80 (2007) 1003–1007. doi:10.1002/jbm.a.31098.

[27] J. Lai, K. Chen, G. Hsiue, Tissue-engineered Human Corneal Endothelial Cell Sheet Transplantation in a Rabbit Model Using Functional Biomaterials, Transplantation. 84 (2007) 1222–1232. doi:10.1097/01.tp.0000287336.09848.39.

[28] N. Koizumi, Y. Sakamoto, N. Okumura, N. Okahara, H. Tsuchiya, R. Torii, L.J. Cooper, Y. Ban, H. Tanioka, S. Kinoshita, Cultivated corneal endothelial cell sheet transplantation in a primate model., Invest. Ophthalmol. Vis. Sci. 48 (2007) 4519–26. doi:10.1167/iovs.07-0567.

[29] C. Shen, Q. Meng, G. Zhang, Increased curvature of hollow fiber membranes could up-regulate differential functions of renal tubular cell layers, Biotechnol. Bioeng. 110 (2013) 2173–2183. doi:10.1002/bit.24874.

[30] J. Yoshida, A. Oshikata-Miyazaki, S. Yokoo, S. Yamagami, T. Takezawa, S. Amano, Development and evaluation of porcine atelocollagen vitrigel membrane with a spherical curve and transplantable artificial corneal endothelial grafts, Investig. Ophthalmol. Vis. Sci. 55 (2014) 4975–4981. doi:10.1167/iovs.14-14211.

[31] L.F. Garner, Sagittal height of the anterior eye and contact lens fitting., Am. J. Optom. Physiol. Opt. 59 (1982) 301–5.

[32] L.M. Delgado, K. Fuller, D.I. Zeugolis, Collagen Cross-Linking: Biophysical, Biochemical, and Biological Response Analysis, Tissue Eng. Part A. 23 (2017) 1064–1077. doi:10.1089/ten.tea.2016.0415.

[33] L.M. Delgado, N. Shologu, K. Fuller, D.I. Zeugolis, Acetic acid and pepsin result in high yield, high purity and low macrophage response collagen for biomedical applications, Biomed. Mater. 12 (2017) 065009. doi:10.1088/1748-605X/aa838d.

[34] A. Satyam, P. Kumar, X. Fan, A. Gorelov, Y. Rochev, L. Joshi, H. Peinado, D. Lyden, B. Thomas, B. Rodriguez, M. Raghunath, A. Pandit, D. Zeugolis, Macromolecular Crowding Meets Tissue Engineering by Self-Assembly: A Paradigm Shift in Regenerative Medicine, Adv. Mater. 26 (2014) 3024–3034. doi:10.1002/adma.201304428.

[35] A. Satyam, G.S. Subramanian, M. Raghunath, A. Pandit, D.I. Zeugolis, *In vitro* evaluation of Ficoll-enriched and genipin-stabilised collagen scaffolds, J. Tissue Eng. Regen. Med. 8 (2014) 233–241. doi:10.1002/term.1522.

[36] A.O. Eghrari, S.A. Riazuddin, J.D. Gottsch, Overview of the Cornea: Structure, Function, and Development, in: Prog. Mol. Biol. Transl. Sci., Academic Press, 2015: pp. 7–23. doi:10.1016/bs.pmbts.2015.04.001.

[37] N. Okumura, H. Hirano, R. Numata, M. Nakahara, M. Ueno, J. Hamuro, S. Kinoshita, N. Koizumi, Cell surface markers of functional phenotypic corneal endothelial cells, Investig. Ophthalmol. Vis. Sci. 55 (2014) 7610–7618. doi:10.1167/iovs.14-14980.

[38] C. Zhu, N.C. Joyce, Proliferative response of corneal endothelial cells from young and older donors., Invest. Ophthalmol. Vis. Sci. 45 (2004) 1743–51.

[39] J.J. Zhao, N.A. Afshari, Generation of Human Corneal Endothelial Cells via In Vitro Ocular Lineage Restriction of Pluripotent Stem Cells, Investig. Ophthalmol. Vis. Sci. 57 (2016) 6878–6884. doi:10.1167/iovs.16-20024.

[40] K.L. McCabe, N.J. Kunzevitzky, B.P. Chiswell, X. Xia, J.L. Goldberg, R. Lanza, Efficient generation of human embryonic stem cell-derived corneal endothelial cells by directed differentiation, PLoS One. 10 (2015) 1–24. doi:10.1371/journal.pone.0145266.

[41] C. Wang, T.T. Lau, W.L. Loh, K. Su, D.A. Wang, Cytocompatibility study of a natural

biomaterial crosslinker-Genipin with therapeutic model cells, J. Biomed. Mater. Res. - Part B Appl. Biomater. 97 B (2011) 58–65. doi:10.1002/jbm.b.31786.

[42] E.G. Lima, A.R. Tan, T. Tai, K.G. Marra, A. DeFail, G.A. Ateshian, C.T. Hung, Genipin enhances the mechanical properties of tissue-engineered cartilage and protects against inflammatory degradation when used as a medium supplement, J. Biomed. Mater. Res. Part A. 91A (2009) 692–700. doi:10.1002/jbm.a.32305.

[43] G.S.L. Peh, K.-P. Toh, H.-P. Ang, X.-Y. Seah, B.L. George, J.S. Mehta, Optimization of human corneal endothelial cell culture: density dependency of successful cultures in vitro., BMC Res. Notes. 6 (2013). doi:10.1186/1756-0500-6-176.

[44] E.K.F. Yim, E.M. Darling, K. Kulangara, F. Guilak, K.W. Leong, Nanotopography-induced changes in focal adhesions, cytoskeletal organization, and mechanical properties of human mesenchymal stem cells, Biomaterials. 31 (2010) 1299–1306. doi:10.1016/j.biomaterials.2009.10.037.

[45] M. Ali, V. Raghunathan, J.Y. Li, C.J. Murphy, S.M. Thomasy, Biomechanical relationships between the corneal endothelium and Descemet's membrane, Exp. Eye Res. 152 (2016) 57–70. doi:10.1016/j.exer.2016.09.004.

[46] G.A. Abrams, S.S. Schaus, S.L. Goodman, P.F. Nealey, C.J. Murphy, Nanoscale topography of the corneal epithelial basement membrane and Descemet's membrane of the human., Cornea. 19 (2000) 57–64. doi:10.1097/00003226-200001000-00012.

[47] A. Isaacson, S. Swioklo, C.J. Connon, 3D bioprinting of a corneal stroma equivalent, Exp. Eye Res. 173 (2018) 188–193. doi:10.1016/j.exer.2018.05.010.

[48] S. Gandhi, S. Jain, The Anatomy and Physiology of Cornea, in: Keratoprostheses Artif. Corneas, Springer Berlin Heidelberg, Berlin, Heidelberg, 2015: pp. 19–25. doi:10.1007/978-3-642-55179-6_3.

[49] R.N. Palchesko, K.L. Lathrop, J.L. Funderburgh, A.W. Feinberg, In Vitro Expansion of Corneal Endothelial Cells on Biomimetic Substrates, Sci. Rep. 5 (2015) 7955. doi:10.1038/srep07955.

[50] T. Mimura, S. Yokoo, M. Araie, S. Amano, S. Yamagami, Treatment of rabbit bullous keratopathy with precursors derived from cultured human corneal endothelium, Investig. Ophthalmol. Vis. Sci. 46 (2005) 3637–3644. doi:10.1167/iovs.05-0462.

[51] K. Yamashita, E. Inagaki, S. Hatou, K. Higa, A. Ogawa, H. Miyashita, K. Tsubota, S.

Shimmura, Corneal endothelial regeneration using mesenchymal stem cell derived from human umbilical cord, Stem Cells Dev. 27 (2018). doi:10.1089/scd.2017.0297.

[52] E. Inagaki, S. Hatou, K. Higa, S. Yoshida, S. Shibata, H. Okano, K. Tsubota, S. Shimmura, Skin-Derived Precursors as a Source of Progenitors for Corneal Endothelial Regeneration., Stem Cells Transl. Med. 6 (2017) 788–798. doi:10.1002/sctm.16-0162.

[53] J. Yoshida, S. Yokoo, A. Oshikata-Miyazaki, S. Amano, T. Takezawa, S. Yamagami, Transplantation of Human Corneal Endothelial Cells Cultured on Bio-Engineered Collagen Vitrigel in a Rabbit Model of Corneal Endothelial Dysfunction, Curr. Eye Res. 42 (2017) 1–6. doi:10.1080/02713683.2017.1351568.

[54] M.O. Price, A.W. Giebel, K.M. Fairchild, F.W. Price, Descemet's Membrane Endothelial Keratoplasty, in: Ophthalmology, 2009: pp. 2361–2368. doi:10.1016/j.ophtha.2009.07.010.

[55] C. Echalier, S. Jebors, G. Laconde, L. Brunel, P. Verdié, L. Causse, A. Bethry, B. Legrand, H. Van Den Berghe, X. Garric, D. Noël, J. Martinez, A. Mehdi, G. Subra, Sol–gel synthesis of collagen-inspired peptide hydrogel, Mater. Today. 20 (2017) 59–66. doi:10.1016/j.mattod.2017.02.001.

[56] W.E. Hennink, C.F. van Nostrum, Novel crosslinking methods to design hydrogels, Adv. Drug Deliv. Rev. 64 (2012) 223–236. doi:10.1016/j.addr.2012.09.009.

[57] D.I. Zeugolis, P.P. Panengad, E.S.Y. Yew, C. Sheppard, T.T. Phan, M. Raghunath, An in situ and in vitro investigation for the transglutaminase potential in tissue engineering, J. Biomed. Mater. Res. - Part A. 92 (2010) 1310–1320. doi:10.1002/jbm.a.32383.

[58] L.P. Yan, Y.J. Wang, L. Ren, G. Wu, S.G. Caridade, J.B. Fan, L.Y. Wang, P.H. Ji, J.M. Oliveira, J.T. Oliveira, J.F. Mano, R.L. Reis, Genipin-cross-linked collagen/chitosan biomimetic scaffolds for articular cartilage tissue engineering applications, J. Biomed. Mater. Res. - Part A. 95 A (2010) 465–475. doi:10.1002/jbm.a.32869.

[59] S.W. Lee, J.M. Lim, S.H. Bhoo, Y.S. Paik, T.R. Hahn, Colorimetric determination of amino acids using genipin from Gardenia jasminoides, Anal. Chim. Acta. 480 (2003) 267–274. doi:10.1016/S0003-2670(03)00023-0.

[60] H.G. Sundararaghavan, G.A. Monteiro, N.A. Lapin, Y.J. Chabal, J.R. Miksan, D.I. Shreiber, Genipin-induced changes in collagen gels: Correlation of mechanical properties to fluorescence, J. Biomed. Mater. Res. - Part A. 87 (2008) 308–320. doi:10.1002/jbm.a.31715.

[61] C. Branco da Cunha, D.D. Klumpers, W.A. Li, S.T. Koshy, J.C. Weaver, O. Chaudhuri, P.L. Granja, D.J. Mooney, Influence of the stiffness of three-dimensional alginate/collagen-I interpenetrating networks on fibroblast biology, Biomaterials. 35 (2014) 8927–8936. doi:10.1016/j.biomaterials.2014.06.047.

[62] I.R. Fernandes, F.B. Russo, G.C. Pignatari, M.M. Evangelinellis, S. Tavolari, A.R. Muotri, P.C.B. Beltrão-Braga, Fibroblast sources: Where can we get them?, Cytotechnology. 68 (2016) 223. doi:10.1007/S10616-014-9771-7.

[63] R.M. Schek, A.J. Michalek, J.C. Iatridis, Genipin-crosslinked fibrin hydrogels as a potential adhesive to augment intervertebral disc annulus repair., Eur. Cell. Mater. 21 (2011) 373–83.

[64] J.Y. Lai, Biocompatibility of chemically cross-linked gelatin hydrogels for ophthalmic use, J. Mater. Sci. Mater. Med. 21 (2010) 1899–1911. doi:10.1007/s10856-010-4035-3.

[65] J.E. Gough, C.A. Scotchford, S. Downes, Cytotoxicity of glutaraldehyde crosslinked collagen/poly(vinyl alcohol) films is by the mechanism of apoptosis, J. Biomed. Mater. Res. 61 (2002) 121–130. doi:10.1002/jbm.10145.

[66] N.L. Joergensen, D.Q.S. Le, O.Z. Andersen, M. Foss, C.C. Danielsen, C.B. Foldager, M. Lind, H. Lysdahl, Topography-Guided Proliferation: Distinct Surface Microtopography Increases Proliferation of Chondrocytes *In Vitro*, Tissue Eng. Part A. 21 (2015) 2757–2765. doi:10.1089/ten.tea.2014.0697.

[67] D. Hoffman-Kim, J.A. Mitchel, R. V Bellamkonda, Topography, cell response, and nerve regeneration., Annu. Rev. Biomed. Eng. 12 (2010) 203–31. doi:10.1146/annurev-bioeng-070909-105351.

[68] J.R. Gamboa, S. Mohandes, P.L. Tran, M.J. Slepian, J.-Y. Yoon, Linear fibroblast alignment on sinusoidal wave micropatterns., Colloids Surf. B. Biointerfaces. 104 (2013) 318–25. doi:10.1016/j.colsurfb.2012.11.035.

[69] M.J. Dalby, M.O. Riehle, S.J. Yarwood, C.D.. Wilkinson, A.S.. Curtis, Nucleus alignment and cell signaling in fibroblasts: Response to a micro-grooved topography, Exp. Cell Res. 284 (2003) 272–280. doi:10.1016/S0014-4827(02)00053-8.

[70] V. Beaulieu Leclerc, O. Roy, K. Santerre, S. Proulx, TGF-β1 promotes cell barrier function upon maturation of corneal endothelial cells, Sci. Rep. 8 (2018) 4438. doi:10.1038/s41598-018-22821-9.

[71] C.H. Wörner, A. Olguín, J.L. Ruíz-García, N. Garzón-Jiménez, Cell pattern in adult human corneal endothelium, PLoS One. 6 (2011) e19483. doi:10.1371/journal.pone.0019483.

[72] H.F. Edelhauser, The Balance between Corneal Transparency and Edema The Proctor Lecture, Investig. Opthalmology Vis. Sci. 47 (2006) 1755. doi:10.1167/iovs.05-1139.

[73] Z. He, F. Forest, P. Gain, D. Rageade, A. Bernard, S. Acquart, M. Peoc 'h, D.M. Defoe, G. Thuret, 3D map of the human corneal endothelial cell, Nat. Publ. Gr. 6 (2016) 29047. doi:10.1038/srep29047.

[74] N.D. Bade, T. Xu, R.D. Kamien, R.K. Assoian, K.J. Stebe, Gaussian Curvature Directs Stress Fiber Orientation and Cell Migration, Biophys. J. 114 (2018) 1467–1476. doi:10.1016/J.BPJ.2018.01.039.

[75] O. Roy, V.B. Leclerc, J.M. Bourget, M. Thériault, S. Proulx, Understanding the process of corneal endothelial morphological change in vitro, Investig. Ophthalmol. Vis. Sci. 56 (2015) 1228–1237. doi:10.1167/iovs.14-16166.

Chapter IV: CONCLUSIONS AND FUTURE PERSPECTIVES

Chapter IV: Conclusions and future perspectives

4.1. Conclusions

Different pathway strategies for the conversion of stem cells into corneal endothelial cells

1. DPSC can be reprogrammed into iPSC with higher pluripotent expression than iPSC-derived from fibroblasts.
2. iPSC-derived from DPSC do not show chromosomal alterations.
3. DPSC in neural crest induction medium can be differentiated into NCSC expressing typical NCSC markers using suspension and adherent conditions.
4. The selected strategy for NCSC differentiation was neurospheres formation as it enhanced cell to cell communication, which ended in higher expression of characteristic NCSC markers.
5. Direct differentiation into CEC from CD73-negative DPSC using a defined medium is not able to generate CEC.
6. DPSC in a non-defined medium can be differentiated into CEC using a two-step differentiation where DPSC are differentiated into NCSC and then into CEC.
7. Conditioned medium from isolated CEC presented higher expression of typical CEC markers than from commercial CEC.

Modulating corneal endothelial cell response with corneal mimicking substrates

1. Collagen films can initially adopt the micropattern and curvature of the molds but are slightly deformed during the drying process.
2. Collagen hydrogels can replicate the curvature together with the topography but require the use of an exogenous cross-linker for its maintenance.
3. The same concentration of the cross-linker genipin used for fibroblasts, which was a ratio of 1:50 (genipin:collagen) did not permit CEC survival. However, the ratio of 1:200 can be used as it presents similar cell survival to non-cross-linked hydrogels.
4. The combination of curvature and topography enhances CEC function and morphology.

5. The expression of the tight junction ZO-1 is deeply influenced by the topography, whereas the expression of the pump function ATP1A1, despite cells are also affected by topography, its effect is lower.
6. Short time of culture on patterned and unpatterned curved hydrogels allows cells to present the characteristic polygonal morphology and cell size similar to native cells, with higher expression of characteristic CEC markers than longer time of culture.

4.2. Future perspectives

The results obtained in this thesis present an innovative method for obtaining CEC from patient-derived cells. Furthermore, results demonstrated that CEC cultured in different curvatures and topographies that mimicked native environment enhanced cell function and morphology. However, further assays should be performed to confirm their potential clinical application in corneal endothelium regeneration.

Regarding the cell differentiation process from DPSC, further characterization should be performed in differentiated cells, such as protein expression of characteristic markers. Moreover, an *in vivo* assay in an animal model with similar characteristics to human CEC, such as monkeys, should be performed to confirm that corneal thickness and transparency is restored at long term using differentiated cells.

Although this thesis presents promising results using topography and curved surfaces, we used a commercial line of CEC. Therefore, using these substrates for the differentiation process of DPSC into CEC could be an interesting strategy that should end in cells with the typical hexagonal morphology and higher expression of characteristic markers.

Nowadays, corneal endothelium regeneration usually requires a cell sheet that is implanted using a surgical procedure. However, this technique usually presents some complications due to the invasive procedure. Cell injection into the anterior chamber offers a promising alternative. However, cell attachment to the desired layer can be a limitation. Therefore, it could be interesting to study an injectable biomaterial that could attach CEC into the corneal endothelium.

Chapter V: SUPPLEMENTARY DATA

Chapter V: Supplementary data

5.1. Ethics committee approval

CER Comitè d'Ètica de Recerca | Universitat Internacional de Catalunya

Sant Cugat del Vallès, 17 d'octubre de 2017

INFORME-CERTIFICAT

Des del Comitè d'Ètica de Recerca de la UIC, hem comprovat que el Projecte de Tesi amb Codi IMR-2017-03 i títol "Aplicación de la ingeniería de tejidos a la obtención de tejido coroneal", constitueix una part del projecte amb codi BIO-ELB-2013-03 titulat "Determinación del protocolo idóneo de diferenciación osteogénica de las DPPSC para la evaluación de distintos biomateriales" ja valorat i posteriorment aprovat en data 25 de novembre de 2013, pel Comitè d'Ètica de Recerca.

En aquest cas, com el projecte del que forma part aquesta Tesi ja va ser valorat i aprovat, no es necessari que el Comitè d'Ètica de Recerca el torni a aprovar.

Davant qualsevol dubte, quedo a disposició.

Cordialment,

Fdo: Dr.Josep Argemí

President del CER

Universitat Internacional de Catalunya

5.2. Stage certificate

University of Miami Miller School of Medicine
McKnight Vision Research Center/Bascom Palmer Eye Institute
Department of Ophthalmology

Be it known that

Begoña Maria Bosch Canals, MSc, BSc

Participated in the Departments'

International Observership Program

From May 22nd, 2016 to June 23rd, 2016 and
From July 3rd, 2017 to August 31st, 2017

Certified this 31st day of August, 2017 in Miami, Florida

Eduardo C. Alfonso, MD
Professor and Chairman